Mech. Eng.

JOURNAL OF THE
AEROSPACE SCIENCES

VOLUME 27 DECEMBER, 1960 NUMBER 12

MECHANICAL ENGINEERING
DEC 14
LIBRARY
PURDUE UNIVERSITY
DEC 11 1960
LIBRARY

CONTENTS

An Appreciation ..... THE EDITORS 881

Hypersonic Viscous Flow Near the Stagnation Point in the Presence of Magnetic Field ..... CHING-SHENG WU 882

Simplified Vibration Analysis of Elastic Sandwich Plates ..... YI-YUAN YU 894

Combustion in the Boundary Layer on a Porous Surface ..... ALAN Q. ESCHENROEDER 901

Supersonic Flow at the Surface of a Circular Cone at Angle of Attack ..... JOSEPH E. WILLETT 907

The Epicycle Method for the Reduction of Flight-Test Data Using a Digital Computer ..... R. P. DANIS 913

Plastic Compressive Buckling of Simply Supported Plates on Interior Elastic Supports ..... PAUL SEIDE 921

The Divergence of Supersonic Linear Viscoelastic Lifting Surfaces Including Chordwise Bending ..... HARRY H. HILTON 926

The Flow About a Charged Body Moving in the Lower Ionosphere ..... RAUL R. HUNZIKER 935

The Buckling of Circular Cylindrical Shells Under Purely Random External Pressures ..... J. CLIFTON SAMUELS 943

Readers' Forum 951

Index to Volume 27 965

Published by
INSTITUTE OF THE AEROSPACE SCIENCES, INC.

JOURNAL OF THE AEROSPACE SCIENCES

Editor: W. R. SEARS
Director, Graduate School of Aeronautical Engineering, Cornell University

Associate Editor: ROBERT R. DEXTER *Managing Editor:* RITA J. TURINO

Editorial Assistant: CAROLINE TAYLOR

IAS Aerospace Technology Panels

Paul J. Burr, Technical Services Director, Coordinator

The members of the IAS Aerospace Technology Panels shown here are to be available, collectively or as individuals, to assist and advise IAS committees, Sections, and staff members as to currently interesting and important technical topics related to their specialties and as to people most qualified to speak or write on such topics. The panels will also stimulate thought and scientific papers of potential value for the future, and they should be sensitive to technical activity of other professional groups, seeking through joint action the enlightenment of all having professional aerospace interests. Panel chairmen are indicated with an asterisk (*).

Aerodynamics and Fluid Mechanics

Lester Lees*
Dean R. Chapman
Antonio Ferri
Paul Germain
Wayland C. Griffith
Hans W. Liepmann
C. C. Lin
W. R. Sears
John R. Sellars
R. T. Whitcomb
Hideo Yoshihara

Aeroelasticity

R. L. Bisplinghoff*
Y. C. Fung
I. E. Garrick
Martin Goland
Kurt H. Hohenemser
J. C. Houbolt
W. P. Jones
W. J. Mykytow
Robert F. Speaker

Biomedical Sciences

Brig.Gen. D. Flickinger, USAF*
W. Ross Adey
Capt. Wm. Augerson, USA
Hilding Bjurstedt
Stuart Bondurant
A. Scott Crossfield
Cdr. J. H. Ebersole, USN
W. R. Lovelace, II
Capt. Bruce Pinc, USAF
Stanley Roscoe

Communication

P. C. Sandretto*
James M. Bridges
Leonard Jaffe
David S. Little
Cdr. D. O. Mann, USN
William Sen
Claude Shannon
Arnold Shostack
Teck A. Wilson

Control, Guidance, and Navigation

C. S. Draper*
R. C. Berendsen
B. Paul Blasingame
Robert N. Brown
S. F. Eyestone
Percy Halpert
B. J. O'Connor
S. F. Schmidt
O. Hugo Schuck
H. Philip Whitaker

Energy Conversion

David Altman*
Robert Bromberg
M. U. Clauser
J. Preston Layton
Frank Marble
G. H. Markstein
A. M. Rothrock
Milton M. Slawsky
Martin Summerfield
T. Y. Toong

Flight Mechanics

H. J. Kelley*
Malcolm J. Abzug
H. Julian Allen
A. E. Bryson, Jr.
T. N. Edelbaum
William C. House
Angelo Miele
John D. Nicolaides
Charles B. Westbrook

Instrumentation

R. H. Tripp*
Paul F. Bechberger
J. M. Hungerford
Mac Lowy
Walter McKay
M. David Prince
Charles P. Sonett
George I. Toumanoff
William A. Wildhack

Meteorology

Thomas F. Malone*
Edgar M. Cortright
Robert D. Fletcher
Henry T. Harrison
Joseph Kaplan
D. S. Perkins
Herbert Riehl
Harry Wexler

Nuclear Applications

J. Donald Rauth*
Jack L. Armstrong
Robert W. Bussard
H. M. Dieckamp
Capt. R. L. Duncan, USN
Harold B. Finger
Donald J. Keirn
Frank E. Rom
Raymer E. Schreiber
D. Roy Shoults
T. B. Taylor

Operations

Benjamin S. Kelsey*
Maj. Gen. Otis Benson, USAF (MC)
Ernest A. Cutrell
Capt. E. E. Fawkes, USN
Melvin N. Gough
Franklin W. Kolk
Col. J. L. Marinelli, USA
Richard V. Rhode
W. E. Rhodes
M. B. Spaulding, Jr.
Ernest G. Stout
Maj.Gen. D. Yates, USAF

Propulsion Systems

Bruce T. Lundin*
Robert H. Boden
George W. Brady
David Cochran
Elliot Mitchell
Perry W. Pratt
C. C. Ross
John G. Wilder, Jr.
Maurice J. Zucrow

Space Physics

H. G. Stever*
John C. Evvard
Herbert Friedmann
Leo Goldberg
C. F. Hansen
Arthur Kantrowitz
Bruno Rossi
S. F. Singer
Leo Steg
Fred L. Whipple

Structures and Materials

Nicholas J. Hoff*
Samuel B. Batdorf
Bruno A. Boley
Pol Duwez
R. R. Heldenfels
Samuel Levy
George N. Mangurian
S. S. Manson
Nathan E. Promisel
Ernest E. Sechler

Vehicle Design

C. E. Pappas*
Ralph Alex
C. H. Christenson
A. J. Eggers, Jr.
E. V. Marshall
Rene H. Miller
John R. Ragazzini
George S. Trimble, Jr.

SUBSCRIPTION RATES

JOURNAL OF THE AEROSPACE SCIENCES, Published Monthly. United States and Possessions: 1 Year, $15.00; Single Copies, $1.50. Foreign Countries Including Canada (American Currency Rates): 1 Year, $16.00; Single Copies, $1.50.

AEROSPACE ENGINEERING, Published Monthly. United States and Possessions: 1 Year, $5.00; Single Copies, $0.50. Foreign Countries Including Canada (American Currency Rates): 1 Year, $6.00; Single Copies, $0.50.

Notices of change of address, which should be sent at least 30 days prior to actual change of address, and correspondence regarding subscriptions should be sent to the Circulation Department, JOURNAL OF THE AEROSPACE SCIENCES, 2 East 64th Street, New York 21, N.Y.

Manuscripts for publication, proofs, and all correspondence should be addressed to the Editorial Office of the JOURNAL.

© *Copyright, 1960, by the Institute of the Aerospace Sciences, Inc.*

Publication Office, 20th and Northampton Sts., Easton, Pa. Second-Class Mail Privileges Authorized at Easton, Pa. Acceptance for mailing at a special rate of postage provided for in Section 1103, Act of October 3, 1917, authorized April 29, 1937.

JOURNAL OF THE AEROSPACE SCIENCES

VOLUME 27 DECEMBER, 1960 NUMBER 12

An Appreciation—

ONCE AGAIN the editors of the JOURNAL in bringing Volume 27 to a close have the pleasant duty of expressing appreciation to the eminent aerospace scientists and engineers who have read and reported on manuscripts submitted for publication. Their advice has been invaluable and is most sincerely appreciated.

In the publication of Volume 27 we have based our selection on the reports submitted by the persons listed below.

W. R. SEARS
R. R. DEXTER

MALCOLM J. ABZUG
MAC C. ADAMS
H. JULIAN ALLEN
G. L. ARMSTRONG
HOLT ASHLEY
JOHN S. ATTINELLO
D. M. BADGER
HARRY BAILEY
JUDSON R. BARON
SAMUEL BATDORF
RICHARD H. BATTIN
HERBERT BECKER
MILTON BEHEIM
DWIGHT H. BENNETT
P. P. BIJLAARD
M. A. BIOT
K. D. BIRD
R. L. BISPLINGHOFF
L. BLITZER
MARTIN H. BLOOM
S. M. BOGDONOFF
BRUNO A. BOLEY
WILLIAM E. BOYCE
J. ROBERT BRANSTETTER
MAURICE A. BRULL
D. O. BRUSH
A. E. BRYSON, JR.
BERNARD BUDIANSKY
ROLF D. BUHLER
ADOLPH BURSTEIN
ADOLF BUSEMANN
WILLIAM B. BUSH
H. W. CARLSON
ANDREW F. CHARWAT
HAROLD CHEILEK
H. K. CHENG
W. L. CHOW
FRANCIS H. CLAUSER
MILTON U. CLAUSER
JOSEPH W. CLEARY
P. R. COBB
STANLEY H. COHN
JULIAN D. COLE
H. D. CONWAY
G. CORCOS
ROBERT A. CORNOG
LUIGI CROCCO
PAUL H. DENKE
D. H. DENNIS
P. R. DEPROTINE
F. W. DIEDERICH
L. H. DONNELL
WM. H. DORRANCE
JOHN E. DUBERG
E. R. G. ECKERT
ALFRED J. EGGERS
H. W. EMMONS
A. C. ERINGEN
JOHN C. EVVARD
ARTHUR A. EZRA
J. A. FAY
SAUL FELDMAN
ANTONIO FERRI
M. FINSTON
E. A. FLETCHER
WILLIAM M. FOLEY
ROY FOWLER
A. M. FREUDENTHAL
Y. C. FUNG
A. M. GARBER
B. E. GATEWOOD
GEZA S. GEDEON
GEORGE GERARD
ROBERT R. GILRUTH
I. I. GLASS
MARTIN GOLAND
N. GOODIER
THEODORE R. GOODMAN
P. E. GRAFTON
J. F. GROSS
ROBERT A. GROSS
R. L. GUSTAFSON
R. A. HARTUNIAN
HOWARD G. HATCH, JR.
WALLACE D. HAYES
MAX A. HEASLET
JOHN M. HEDGEPETH
R. RICHARD HEPPE
G. HERRMANN
HARRY H. HEYSON
H. H. HILTON
N. J. HOFF
GEORGE H. HOLDAWAY
MAURICE HOLT
G. HORVAY
JOHN C. HOUBOLT
HERBERT G. HURRELL
RICHARD HUTTON
GABRIEL ISAKSON
BRUCE G. JACKSON
W. E. JAHSMAN
PAUL G. JOHNSON
ROBERT L. JOHNSON
ROBERT T. JONES
L. L. KAVANAU
HENRY J. KELLEY
NELSON H. KEMP
JOSEPH KEMPNER
BERTRAM KLEIN
H. KORST
SAUNDERS B. KRAMER
DONALD M. KUEHN
ARNOLD M. KUETHE
W. R. LAIDLAW
EDMUND V. LAITONE
S. H. LAM
H. L. LANGHAAR
HOWARD K. LARSON
JOHN G. LEE
LESTER LEES
RICHARD H. LEVY
SAMUEL LEVY
TING YI LI
PAUL LIBBY
H. M. LIEBERSTEIN
SEYMOUR LIEBLEIN
H. W. LIEPMANN
C. C. LIN
H. E. LINDBERG
R. P. LIPKIS
JOSEPH G. LOGAN
W. H. T. LOH
H. LOMAX
A. E. LOMBARD, JR.
G. S. LUDFORD
BRUCE T. LUNDIN
PAUL S. LYKOUDIS
PAUL F. MAEDER
ARTUR MAGER
D. J. MAGLIERI
EUGENE MANGANIELLO
GEORGE N. MANGURIAN
FRANK MARBLE
J. MARIN
STEPHEN H. MASLEN
FRED W. MATTING
J. F. MELLO
R. J. MELOSH
A. MENDELSON
RUDOLPH C. MEYER
R. X. MEYER
J. W. MILES
W. F. MILLIKEN, JR.
R. D. MINDLIN
HAROLD MIRELS
L. I. MIROWITZ
W. E. MOECKEL
ERIK MOLLÖ-CHRISTENSEN
F. K. MOORE
M. MORDUCHOW
MARK V. MORKOVIN
CHARLES H. MURPHY, JR.
J. S. MURPHY
W. NACHBAR
HENRY T. NAGAMATSU
PAUL NAGHDI
S. V. NARDO
WILLIAM A. NASH
BEN A. NEFFSON
ROBERT L. NELSON
J. L. NEURINGER
F. W. NIEDENFUHR
WILLIAM J. O'DONNELL
P. J. O'LEARY
E. T. ONAT
D. E. ORDWAY
SHIH-I PAI
A. PALLONE
Y. H. PAO
C. C. PAPPAS
C. E. PAPPAS
SHARAD A. PATEL
GORDON N. PATTERSON
S. S. PENNER
KENDALL PERKINS
N. V. PETERSEN
W. PHILLIPS
F. V. POHLE
KARL POHLHAUSEN
R. F. PROBSTEIN
ROBERT G. RAGSDALE
WILMER H. REED
ERIC REISSNER
E. RESHOTKO
H. S. RIBNER
FREDERICK R. RIDDELL
CARLO RIPARBELLI
RICHARD C. ROBERTS
RUSSELL G. ROBINSON
WILLIAM P. RODDEN
PETER H. ROSE
ANATOL ROSHKO
IRA ROSS
V. J. ROSSOW
NICHOLAS ROTT
MORRIS RUBESIN
H. L. RUNYAN
JOSEPH RUTKOWSKI
PAUL E. SANDORFF
PAUL H. SAVET
S. M. SCALA
GEORGE S. SCHAIRER
GALEN B. SCHUBAUER
JOHN M. SCHULER
PAUL SEIDE
F. R. SHANLEY
A. H. SHAPIRO
S. F. SHEN
RONALD SMELT
ROBERT F. SMILEY
A. M. O. SMITH
EPHRAIM M. SPARROW
JOHN R. SPREITER
WILLIAM SQUIRE
JOHN STACK
MANUEL STEIN
JOSEPH STENOIEN
HERBERT S. SUER
G. W. SUTTON
H. S. TAN
ITIRO TANI
THEODORE THEODORSEN
FLOYD L. THOMPSON
G. A. THURSTON
LEON TRILLING
R. L. TRIMPI
M. J. TURNER
R. VAGLIO-LAURIN
E. R. VAN DRIEST
MILTON D. VAN DYKE
KERMIT E. VAN EVERY
GEORGE WALDMAN
PETER WEGENER
H. P. WHITAKER
G. WHITHAM
J. E. WILKINS, JR.
MAX L. WILLIAMS
ALBERT D. WOOD
WALTER WRIGLEY
C. S. WU
Y. A. YOLER
YI-YUAN YU
RICHARD W. ZIEMER
CHARLES ZIMMERMAN

Hypersonic Viscous Flow Near the Stagnation Point in the Presence of Magnetic Field†

CHING-SHENG WU*
Princeton University

Summary

The present study investigates the hypersonic viscous flow past blunt-nosed bodies with hydromagnetic interaction. Local-similarity solutions of flow field and temperature distribution are near the stagnation-point region. The discussions may be grouped into two parts: the two-dimensional problem (circular cylinder) and axisymmetric problem (sphere).

Numerical computations have been carried out for the sphere problem for the "viscous-layer regime," with various magnetic field strengths and electrical conductivities.

Symbols

Ω = vorticity vector
$\mathbf{v}$ = velocity vector
p = pressure
ρ = density
$\mathbf{H}$ = magnetic field intensity
$\mathbf{B}$ = magnetic induction
$\mathbf{n}$ = unit vector normal to the discontinuity surface
μ_e = magnetic permeability
ϵ = dielectric constant
$\mathbf{E}$ = electric field
$\mathbf{D}$ = electric excitation
h = enthalpy
$h_0 = h + (v^2/2)$ = total enthalpy
T = temperature
k = thermal conductivity
Φ = viscous-dissipation function
ρ_e = net charge density
$\mathfrak{R}$ = curvature tensor
r = spherical or polar radius
r_s = spherical or polar shock radius
η = dimensionless radius $(= r/r_s)$
δ = symbol used to express jump of physical quantities across the gasdynamic discontinuity

Superscripts

(m) = thermodynamic quantities associated with mechanical action
(e) = thermodynamic quantities associated with electromagnetic action

Subscripts

s = quantities immediately behind the discontinuity
∞ = quantities in front of discontinuity
n = component of vector quantities normal to the discontinuity, except when otherwise specifically noted
t = local vector component of any vector quantity in the plane
b = quantities on body surface

(I) Introduction

THE FLOW FIELD behind the shock wave which stands off a blunt-nosed body in hypersonic flow has attracted a considerable amount of attention in recent years. However, because of its mathematical complexity, the problem has not been completely solved.

A review of the literature reveals that theoretical studies have been based on essentially two fundamental approaches. The first method consists of looking for the so-called Newtonian solution and then improving it for realistic physical situations. The second method consists of finding local solutions near the stagnation point where, in many cases, the incompressibility approximation may be employed.

An interesting local solution was given by Lighthill (1957). A spherical shock was considered and a similarity solution found such that the boundary conditions immediately behind the shock wave were satisfied. Lighthill considered an incompressible and inviscid fluid in which the vorticity behind the shock is generated by the nonuniformity of shock strength. For a given shock radius, free-stream velocity, and density ratio across the shock, the body surface on which normal velocity vanishes may be found. An inviscid solution similar to Lighthill's, but for a cylindrical body, was later found independently by Hayes (1958) and by Whitham (1957).

Since these similarity solutions are quite simple and of considerable interest, it is natural to ask whether they may be extended to cover the magnetohydrodynamic case, that is, to include the hydromagnetic interaction when the fluid is electrically conducting and an external magnetic field is imposed. This study is interesting and significant because at hypersonic flight speed, the gas behind the shock wave becomes ionized and hence may be treated as a conductor. Kemp (1958) first investigated the extreme case in which the magnetic Reynolds number is considered to be vanishingly small and thus the induced magnetic field is completely ignored. This, of course, serves as only a rough approximation of the actual situation.

In addition to Kemp's work, a more complete solution has been obtained lately by Bush (1958). Bush simplifies the integration scheme by imposing the

Received October 26, 1959.

† The present work is sponsored by the Office of Scientific Research, United States Air Force, under Contract No. AF 49(638)-465.

* Formerly, Research Assistant. Now Senior Scientist, Jet Propulsion Laboratory, California Institute of Technology.

The author wishes to thank Prof. Luigi Crocco and Prof. Wallace D. Hayes for their discussions. He is also grateful to Prof. B. T. Chu at Brown University for many suggestions regarding the study of the vorticity laws.

boundary conditions of the applied magnetic field on the shock wave (not on the body surface). Thus, the problem is reduced from a two-point to a one-point boundary problem and great mathematical simplification is thus achieved.

It is the purpose of this paper to point out that local-similarity solutions are also obtainable, if both hydromagnetic interaction and viscous effects are taken into account. The following discussion can be grouped into two parts: the two-dimensional problem and the axisymmetric problem. The two-dimensional problem will concern hypersonic flow past a cylindrical body, and the axisymmetric case is essentially associated with a spherical body. It will be shown that exact solutions of the stagnation-point flow behind the detached shock wave may be obtained. These solutions are based on the "incompressible and constant property" physical model and satisfy the Navier-Stokes equations. Furthermore, it is found that solutions for the temperature distribution are obtainable even when viscous dissipation and Joule heat are taken into account.

Upon completion of the analytical part of the present study in November of 1958, it was pointed out by Prof. Wallace D. Hayes that a type of similarity solution related to that discussed in this paper had been considered for the nonhydromagnetic case by Prof. R. F. Probstein in a recent WADC report (1958). A detailed discussion of this work appears in the book, "Hypersonic Flow Theory" by Hayes and Probstein.

Mathematically, the class of similarity solutions found by Prof. Probstein takes into account variable density, viscosity, and thermal conductivity as follows:

$$\rho = \rho_0(r)$$

$$\mu = \mu_0(r) \cos\theta$$

$$k = k_0(r) \cos\theta$$

$$h = h_0(r) + h_2(r) \sin\theta$$

where h is the specific enthalpy.

However, in applying this type of solution to actual hypersonic flight problems, it should be carefully examined to see whether these postulated functional forms are realistic. This is important because in many aerodynamic problems both μ and k are temperature-dependent. In other words, we are not free to postulate the functional forms of μ, k, and the temperature, independently. The compatibility condition must be considered.

Furthermore, it is possible to consider a spinning body. The spinning effect can reduce both the viscous-layer thickness and stand-off distance of the detached shock wave. The investigation of this more complicated case will be excluded from the present paper.

(II) Some Simple Vorticity Relations in Magnetogasdynamics

(a) *A Generalization of Crocco's Vorticity Law*

In the classical hydrodynamics in which the hydromagnetic interaction is not considered, the vorticity law expresses the vorticity in terms of gradients of total enthalpy and entropy of the fluid as follows:

$$\mathbf{v} \times \boldsymbol{\Omega} = \nabla h_0 - T\nabla S \tag{2.1}$$

The vorticity law was first discovered by Crocco (1937) and has become a very important theorem in high-speed aerodynamics. As we know, in many physical problems an entropy gradient will be set up behind a curved two- or three-dimensional gasdynamic discontinuity. (If the discontinuity is nonadiabatic, a gradient of total enthalpy may also appear.) This phenomenon is mainly due to the nonuniformity of the strength of the discontinuity. Hence, according to the vorticity law (2.1), such an entropy gradient becomes a measure of the vorticity distribution behind the discontinuity.

However, since in the derivation of (2.1), no body force other than gravity is considered, a modification becomes necessary when a similar law is to be used in magnetohydrodynamics. In order to extend this vorticity law to include the presence of ponderomotive force, we shall first introduce some preliminary concepts so that the basic theory may be clarified.

Before going further, we may first focus our interest on one instructive example which concerns the entropy-balance relation in hydromagnetic theory. It is well known that the entropy balance in a moving medium may, in general, be represented by the following expression:

$$\rho(DS/Dt) = -\text{div}\ \mathbf{S}_T + S_p \tag{2.2}$$

where $\mathbf{S}_T$ is the entropy flux flowing away per unit area per unit time, and S_p is the entropy production per unit volume per unit time.

For a viscous and conducting fluid, Eq. (2.2) can be written specifically as follows:

$$\rho \frac{DS}{Dt} = -\text{div}\left(-\frac{k\nabla T}{T}\right) + k\left(\frac{\nabla T}{T}\right)^2 + \frac{\Phi}{T} + \frac{J^2}{T\sigma} \tag{2.3}$$

where k is the thermal conductivity, Φ is the viscous-dissipation function and J^2/σ is the Joule heat. The derivation of this equation is omitted here. However, the reader can find it from pertinent existing literature. From (2.3), it is seen that the viscous friction and electric resistance contribute only to the entropy production and not to the entropy transfer.

Thus, the total entropy change may be split into two parts, say,

$$\rho(DS/Dt) = \rho[(DS/Dt)]^{(m)} + \rho[(DS/Dt)]^{(e)} \tag{2.4}$$

The first term on the right represents the entropy change due to "mechanical" action only and the second part at the right indicates the entropy variation due to electromagnetic action:

$$\rho\left(\frac{DS}{Dt}\right)^{(m)} = -\nabla\cdot\left(-\frac{k\nabla T}{T}\right) + k\left(\frac{\nabla T}{T}\right)^2 + \frac{\Phi}{T} \tag{2.5}$$

$$\rho\left(\frac{DS}{Dt}\right)^{(e)} = \frac{J^2}{\sigma T} \tag{2.6}$$

From this example, two questions may naturally arise: first, whether the total entropy of a system may be considered as the sum of the entropy associated with mechanical and electromagnetic actions; and second, if the answer to the previous question is positive, whether we may extend the consideration similarly to other thermodynamic state variables.

A systematic discussion along this line has been given by Chu (1957). It is shown in his paper that, generally, thermodynamic state variables such as enthalpy, internal energy, and pressure, etc., may all be considered as the sum of a mechanical part and an electromagnetic part, as long as the free energy of the system may be written as

$$A = A^{(m)} + A^{(e)}$$

where $A = E + ST$ is the total free energy, $A^{(m)}$ is associated with mechanical action only, and $A^{(e)}$ is associated with electromagnetic action only.

This conclusion enables us to separate the general differential equation of state

$$dh = T\,dS + (1/\rho)dp + \mathbf{E}\cdot d(\mathbf{D}/\rho) + \mathbf{H}\cdot d(\mathbf{B}/\rho) \quad (2.7)$$

into two parts such that

$$dh^{(m)} = T\,dS^{(m)} + (1/\rho)dp^{(m)} \quad (2.8)$$

and

$$dh^{(e)} = T\,dS^{(e)} + (1/\rho)dp^{(e)} + \mathbf{E}\cdot d(\mathbf{D}/p) + \mathbf{H}\cdot d(\mathbf{B}/\rho) \quad (2.9)$$

Now, with this result, we may readily rederive the vorticity law. From the steady-state momentum equation, we have

$$\mathbf{v}\times\boldsymbol{\Omega} = (1/\rho)\nabla p^{(m)} + (1/2)\nabla v^2 - [(\mathbf{J}\times\mathbf{B})/\rho] \quad (2.10)$$

where $\boldsymbol{\Omega}$ is vorticity and $\mathbf{J}\times\mathbf{B}$ is ponderomotive force.

If the material of the fluid is assumed to be uniform, Eq. (2.8) may be written as a gradient equation, thus:

$$\nabla h^{(m)} = T\nabla S^{(m)} + (1/\rho)\nabla p^{(m)} \quad (2.11)$$

Combining (2.10) and (2.11), we have

$$\mathbf{v}\times\boldsymbol{\Omega} = \nabla h_0^{(m)} - T\Delta S^{(m)} - [(\mathbf{J}\times\mathbf{B})/\rho] \quad (2.12)$$

where $\nabla h_0^{(m)} = \nabla[h^{(m)} + (1/2)v^2]$

If we further decompose the vorticity vector into two components, one normal to the streamline, say $\boldsymbol{\Omega}_n$, and the other tangential to the streamline, say $\boldsymbol{\Omega}_s$, Eq. (2.12) may be rewritten as

$$v\boldsymbol{\Omega}_n = (\partial h_0^{(m)}/\partial n) - T(\partial S^{(m)}/\partial n) - [(\mathbf{J}\times\mathbf{B})_n/\rho] \quad (2.13)$$

where $\partial/\partial n$ indicates the gradient normal to the streamline and $(\mathbf{J}\times\mathbf{B})_n$ the normal component of the ponderomotive force (we assume that $\mathbf{n}\boldsymbol{\Omega}_n$, $\mathbf{v}$ and $\mathbf{n}$ form a right-hand system).

From this generalized Crocco's law we may therefore conclude that only the ponderomotive force normal to the streamline will contribute to the generation of vorticity.

(b) *Lighthill's Vorticity Expression on Magnetogasdynamics*

Lighthill (1957) provided an expression of the vorticity behind a three-dimensional curved shock in a uniform flow in terms of the density ratio, free-stream velocity and principal curvatures of the shock wave. He first showed that

$$T\,dS = [1 - (1/k)]^2\, v_{n0}dv_{n0} \quad (2.14)$$

where k is the density ratio ($= \rho_1/\rho_0$), T_1 and S_1 are temperature and entropy behind the shock wave, and v_{n0} is the local upstream velocity component normal to the shock wave. The derivation of expression (2.14) is based on Crocco's vorticity law (2.1) and three basic equations of conservation, namely,

$$\begin{aligned} \rho_0 v_{n0} &= \rho_1 v_{n1} \\ \rho_0 v_{n0}^2 + p_0 &= \rho_1 v_{n1}^2 + p_1 \\ (v_{n0}^2/2) + h_0 &= (v_{n1}^2/2) + h_1 \end{aligned} \quad (2.15)$$

where h_0 and h_1 are enthalpies in front of and right behind the shock, respectively.

Since conditions (2.15) also hold true in the present problem,* Lighthill's result (2.14) is valid in the present discussion.

From Eq. (2.12), if we write $\mathbf{v} = \mathbf{n}v_n + \mathbf{v}_t$ (where $\mathbf{n}$ is an outward-directed unit vector normal to the shock wave) we will obtain

$$\boldsymbol{\Omega}_t = \frac{1}{v_{n1}}\left[\nabla_t h_{01}^{(m)} - T\nabla_t S_1^{(m)} - \frac{\mathbf{J}\times\mathbf{B}}{\rho}\right]\times\mathbf{n} \quad (2.16)$$

The symbol ∇_t indicates that only the tangential derivative is included. Following the notations adopted by Lighthill, we again decompose Eq. (2.12) into two principal directions of curvature of the shock surface, namely, the directions a and b (the directions a, b, and n form a right-hand system). Thus, we have

$$\boldsymbol{\Omega}_{b1}v_{n1} = T_1(\partial S_1/\partial x_a) + [(\mathbf{J}\times\mathbf{B})_a/\rho_1] \quad (2.17)$$

$$-\boldsymbol{\Omega}_{a1}v_{n1} = T_1(\partial S_1/\partial x_b) + [(\mathbf{J}\times\mathbf{B})_b/\rho_1] \quad (2.18)$$

$$\boldsymbol{\Omega}_{b1} = -[(k-1)^2/k]v_{a0}\mathfrak{K}_a + [(\mathbf{J}\times\mathbf{B})_a/\rho_0 v_{n0}] \quad (2.19)$$

$$\boldsymbol{\Omega}_{a1} = [(k-1)^2/k]v_{b0}\mathfrak{K}_b - [(\mathbf{J}\times\mathbf{B})_b/\rho_0 v_{n0}] \quad (2.20)$$

where $\mathfrak{K}_a$ and $\mathfrak{K}_b$ are the principal curvatures. Eqs. (2.19) and (2.20) can also be written in vector form:

$$\boldsymbol{\Omega}_t = -\frac{(k-1)^2}{k}\,\mathbf{n}\times v_{t0}\cdot\mathfrak{K} + \frac{\mathbf{n}\times(\mathbf{J}\times\mathbf{B})_t}{\rho_0 v_{n0}} \quad (2.21)$$

Again, it is instructive to show that this result may also be obtained by utilizing a method given by Hayes (1957) without recourse to the thermodynamic law. The details of this will be omitted here.

* We consider the gas has finite conductivity and the magnetic field has no discontinuity across the gasdynamic shock wave.

(III) The Local-Similarity Solutions

In this part, we shall consider the fluid to be incompressible, viscous and electrically conducting, and the motion to be steady. According to magnetohydrodynamic theory, we may list the governing equations as follows:

$$\text{div } \mathbf{v} = 0 \tag{3.1}$$

$$\text{curl [curl } \mathbf{v} \times \mathbf{v} - (\mu_e/4\pi\rho) \text{ curl } \mathbf{H} \times \mathbf{H}] = \nu\nabla^2 \text{ curl } \mathbf{v} \tag{3.2}$$

$$\text{div } \mathbf{H} = 0 \tag{3.3}$$

$$\text{curl [curl } \mathbf{H} - 4\pi\sigma\mu_e \mathbf{v} \times \mathbf{H}] = 0^* \tag{3.4}$$

where μ_e = magnetic permeability
σ = electric conductivity
$\mathbf{H}$ = magnetic field intensity
$\mathbf{v}$ = velocity vector
ν = kinematic viscosity
∇^2 = Laplacian operator

We have assumed that the physical properties of the fluid are constant.

(a) *Two-Dimensional Case*

(1) *Functional Forms of Solutions*—The similarity solutions under study will have the following functional forms:

$$\left.\begin{aligned} v_r &= V[f(\eta)/\eta] \cos\theta \\ v_\theta &= -V[df/d\eta] \sin\theta \\ H_r &= H_0[g(\eta)/\eta] \cos\theta \\ H_\theta &= -H_0[dg/d\eta] \cos\theta \end{aligned}\right\} \tag{3.5}$$

where V and H_0 are the free-stream velocity and reference magnetic field, respectively, and $\eta = r/r_s$ (r_s = shock radius).

Here, we have used a right-handed cylindrical coordinate system (z, r, θ). It is seen that the above similarity solutions satisfy the conditions

$$\text{div } \mathbf{v} = 0$$

$$\text{div } \mathbf{H} = 0$$

automatically. Substituting the results (3.5) into (3.2) and postulating that near the stagnation point $2\sin\theta \approx \sin 2\theta$, we have

$$\frac{d}{d\eta} f\left(\frac{f}{\eta^2} - \frac{1}{\eta}\frac{d}{d\eta}\eta\frac{df}{d\eta}\right) - 2\frac{df}{d\eta}\left(\frac{f}{\eta^2} - \frac{1}{\eta}\frac{d}{d\eta}\eta\frac{df}{d\eta}\right) - \frac{\mu_e H_0^2}{4\pi\rho V^2}\left[\frac{d}{d\eta} g\left(\frac{g}{\eta^2} - \frac{1}{\eta}\frac{d}{d\eta}\eta\frac{dg}{d\eta}\right) - 2\frac{dg}{d\eta}\left(\frac{g}{\eta^2} - \frac{1}{\eta}\frac{d}{d\eta}\eta\frac{dg}{d\eta}\right)\right] = \frac{\nu}{Vr_s}\left[\left(\frac{d}{d\eta}\eta\frac{d}{d\eta} - \frac{1}{\eta}\right)\left(\frac{f}{\eta^2} - \frac{1}{\eta}\frac{d}{d\eta}\eta\frac{df}{d\eta}\right)\right] \tag{3.6}$$

* In the present investigation, only classical continuum theory is used. Ohm's law assumes the form

$$J = \sigma(\mathbf{E} + v \times B)$$

We postulate that the net charge density ρ_e is zero, or say that the fluid is electrically neutral.

If we denote

$M_p = \mu_e H_0^2/4\pi\rho V^2$ (magnetic-pressure number)

$Re = Vr_s/\nu$ (Reynolds number)

Eq. (3.6) may be further rewritten as

$$f^2\frac{d}{d\eta}\frac{1}{f}\left(\frac{f}{\eta^2} - \frac{1}{\eta}\frac{d}{d\eta}\eta\frac{df}{d\eta}\right) - M_p g^2\frac{d}{d\eta}\frac{1}{g}\left(\frac{g}{\eta^2} - \frac{1}{\eta}\frac{d}{d\eta}\eta\frac{dg}{d\eta}\right) = \frac{1}{Re}\left[\left(\eta\frac{d^2}{d\eta^2} + \frac{d}{d\eta} - \frac{1}{\eta}\right)\left(\frac{f}{\eta^2} - \frac{1}{\eta}\frac{d}{d\eta}\eta\frac{df}{d\eta}\right)\right] \tag{3.7}$$

On the other hand, we will study the induction equation. We can write

$$\text{curl } \mathbf{H} - 4\pi\sigma\mu_e \mathbf{v} \times \mathbf{H} = \left[\frac{H_0}{r_s}\left(\frac{g}{\eta^2} - \frac{1}{\eta}\frac{d}{d\eta}\eta\frac{dg}{d\eta}\right)\sin\theta - 4\pi\sigma\mu_e V H_0\left(\frac{df}{d\eta}\frac{g}{\eta} - \frac{dg}{d\eta}\frac{f}{\eta}\right)\sin\theta\cos\theta\right]\mathbf{i}_z = \sigma E_z \mathbf{i}_z \tag{3.8}$$

Since in the present problem we do not consider any imposed electrical field, the only electrical field is induced by the motion and must be in the z-direction. However, from Maxwell's field equation,

$$\partial E_z/\partial\theta = 0 \qquad \partial E_z/\partial\eta = 0$$

we see that E_z is constant; however, if there is no electrical field at the wall, E must vanish everywhere. Utilizing the assumption that $2\sin\theta \approx \sin 2\theta$ in the stagnation point region, we may write Eq. (3.8) as follows:

$$\frac{d}{d\eta}\eta\frac{dg}{d\eta} - \frac{g}{\eta} = Rm\left(f\frac{dg}{d\eta} - g\frac{df}{d\eta}\right) \tag{3.9}$$

where $Rm = 4\pi\sigma\mu_e r_s V$ is called the magnetic Reynolds number.

Hence, we have reduced the original differential system to two simultaneous ordinary differential equations, namely, Eqs. (3.7) and (3.9).

(2) *Boundary Conditions*—In this section, we shall discuss the boundary conditions associated with different physical problems. To do this, we shall group the total boundary conditions into two sets: one at the wall and the other just behind the shock wave.

(A) *Boundary conditions immediately behind the shock wave*: In the present problem, the shock wave is postulated to have cylindrical shape. Then the velocity behind the shock wave may be written as follows:

$$v_\theta = V\sin\theta \tag{3.10}$$

$$v_r = -(V/k)\cos\theta \tag{3.11}$$

where V is the free stream velocity and k is the density ratio across the shock wave ($k = \rho/\rho_\infty$).

One additional boundary condition to be fulfilled is the vorticity condition. From the previous discussion of the vorticity law in magnetohydrodynamics, the vorticity behind the shock wave will be

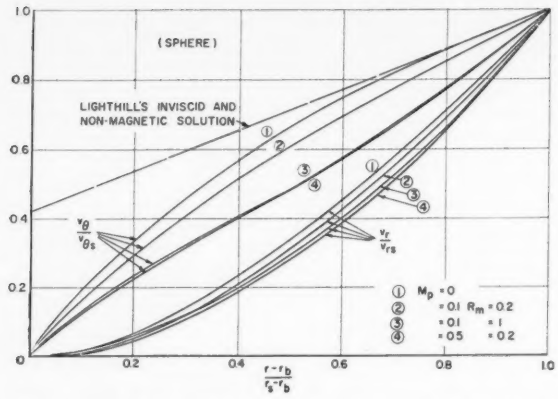

FIG. 1. Flow field in the shock layer ($Re_s = 1000$, $\rho_s/\rho_\infty = 10$).

$$[\Omega_z]_{shock} = \frac{(1-k)^2}{k}\frac{V\sin\theta}{r_s} - \left[\frac{F_\theta}{\rho_\infty V\cos\theta_s}\right]_{shock} \tag{3.12}$$

where F_θ is the θ-component of ponderomotive force:

$$\frac{F_\theta}{\rho_\infty V\cos\theta} = \frac{\mu_e}{4\pi}\frac{(\operatorname{curl}\mathbf{H}\times\mathbf{H})\cdot\mathbf{i}_\theta}{\rho_\infty V\cos\theta} = \frac{\mu_e H_0^2}{4\pi r_s\rho V}\left(\frac{g}{\eta^2} - \frac{1}{\eta}\frac{d}{d\eta}\eta\frac{dg}{d\eta}\right)\frac{g}{\eta}\sin\theta \tag{3.13}$$

Since at the shock wave $\eta = 1$,

$$[\Omega_z]_{shock} = \frac{(1-k)^2}{k}\frac{V\sin\theta}{r_s} - \frac{M\rho_p kV\sin\theta}{r_s}\frac{g}{\eta}\left[g - \frac{d}{d\eta}\eta\frac{dg}{d\eta}\right]_{\eta=1} = \frac{(1-k)^2}{k}\frac{V\sin\theta}{r_s} + \frac{M\rho kV\sin\theta Rmg}{r_s}\times\left[f\frac{dg}{d\eta} - g\frac{df}{d\eta}\right]_{\eta=1} \tag{3.14}$$

In order to write conditions (3.10), (3.11), and (3.12) in terms of the similarity functions f and g, we use (3.5). Doing this, we readily find

$$f(1) = -1/k \qquad f'(1) = -1 \tag{3.15}$$

and

$$\left(\frac{d^2f}{d\eta^2}\right)_{\eta=1} = 3 - \frac{2}{k} - k + M_p kRmg\left[\frac{1}{k}\frac{dg}{d\eta} - g\right]_{\eta=1} \tag{3.16}$$

This boundary condition is valid only when the shock layer is thicker than the viscous layer. Only then is the viscous effect on the vorticity behind the shock wave negligible. Again, if the viscous layer is as thick as the shock layer, the validity of boundary conditions (3.10) and (3.11) also breaks down. In that case, the shock wave can no longer be considered a discontinuity.

In the following discussion, we will adopt a mathematical model similar to Bush's; that is, one in which the magnetic field in the free-stream region may be described as that due to the presence of a two-dimensional dipole at the origin. The magnetic field is again postulated to be continuous across the shockwave. Since the fluid in front of the shock wave is nonconducting, the magnetic field in that region must be irrotational. Thus, the magnetic field may be written in the following analytic form:

$$\mathbf{H} = [A + (B/\eta^2)]\cos\theta\mathbf{i}_r + (B/\eta^2)\sin\theta\mathbf{i}_\theta \tag{3.17}$$

where A and B are arbitrary constants.

Hereafter, we shall exclude the $A\cos\theta$ part because the field strength should vanish at infinity; thus,

$$\mathbf{H} = (B/\eta^2)\cos\theta\mathbf{i}_r + (B/\eta^2)\sin\theta\mathbf{i}_\theta \tag{3.18}$$

Hence, if we write $B = H_0$ on the shock wave, we have

$$\left.\begin{aligned} H_r &= H_0\cos\theta \qquad g(1) = 1 \\ H_\theta &= H_0\sin\theta \qquad (dg/d\eta)_{\eta=1} = -1 \end{aligned}\right\} \tag{3.19}$$

Again, specification of the boundary conditions on the magnetic field at the shock rather than at the wall will simplify the mathematical problem considerably.

Substituting (3.19) into (3.16), we obtain

$$(d^2f/d\eta^2)_{\eta=1} = 3 - (2/k) - k - M\rho Rm(1+k) \tag{3.20}$$

(*B*) *Boundary conditions at the wall:* The boundary conditions on the velocity field at the wall may be stated as follows:

$$f'(\eta_b) = 0 \qquad f(\eta_b) = 0 \tag{3.21}$$

The first condition of (3.21) is the nonslip condition ($v_\theta = 0$ at the wall) and the second condition of (3.21) is due to $v_r = 0$ at the wall. Of course, this implies no mass injection.

(*b*) *Axisymmetric Problems*

(1) *Similarity Solutions*—With the same physical restrictions as postulated in the two-dimensional case, we may now extend our previous consideration to the spherical body. In this section, we shall investigate the similarity solutions associated with the stagnation point flow behind a detached shock wave with spherical shape.

In the present discussion, the governing equations (3.1), (3.2), (3.3), and (3.4) are still valid. However, the similarity solutions are postulated in different functional forms:

$$\begin{aligned} v_r &= V[2f(\eta)/\eta^2]\cos\theta \\ v_\theta &= V(1/\eta)(df/d\eta)\sin\theta \\ H_r &= H_0[2g(\eta)/\eta^2]\cos\theta \\ H_\theta &= -H_0(1/\eta)(dg/d\eta)\sin\theta \end{aligned} \tag{3.22}$$

where the angle θ is measured from the axis of symmetry and $\eta = (r/r_s)$.

If the right-handed spherical coordinate system (r, θ, φ) is used, we may obtain

$$f\frac{d}{d\eta}\left[\frac{1}{\eta^2}\left(\frac{2f}{\eta^2} - \frac{d^2f}{d\eta^2}\right)\right] - M_p g\frac{d}{d\eta}\left[\frac{1}{\eta^2}\left(\frac{2g}{\eta^2} - \frac{d^2g}{d\eta^2}\right)\right] = \frac{1}{2}\frac{1}{Re}\left[\left(\frac{1}{\eta}\frac{d}{d\eta}\eta^2\frac{d}{d\eta} - \frac{2}{\eta}\right)\left(\frac{2f}{\eta^3} - \frac{1}{\eta}\frac{d^2f}{d\eta^2}\right)\right] \tag{3.23}$$

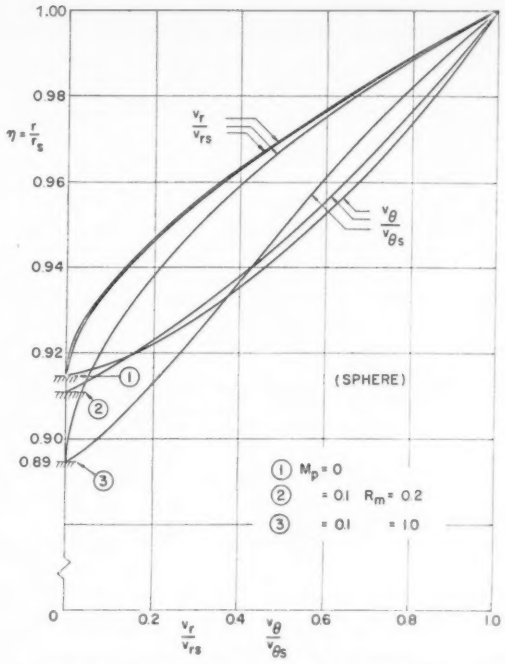

FIG. 2. Velocity distribution in the shock layer ($Re_s = 1000$, $\rho_s/\rho_\infty = 10$).

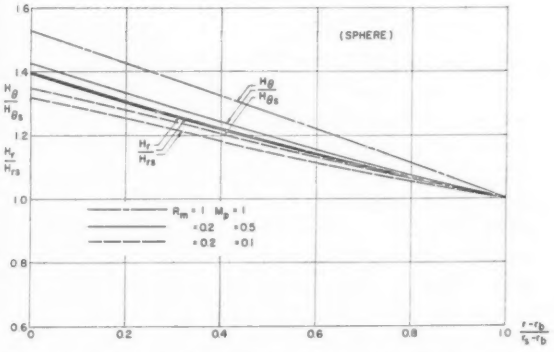

FIG. 3. Variations of magnetic field intensity across the shock layer ($Re_s = 1000$, $\rho_s/\rho_\infty = 10$).

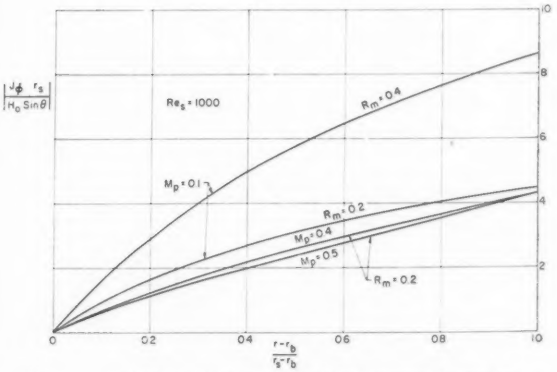

FIG. 4. Variation of induced electrical current intensity.

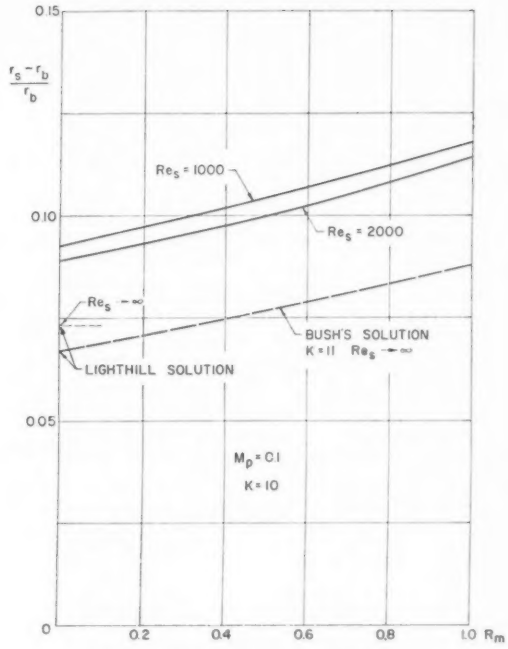

FIG. 5. Shock wave stand-off distance.

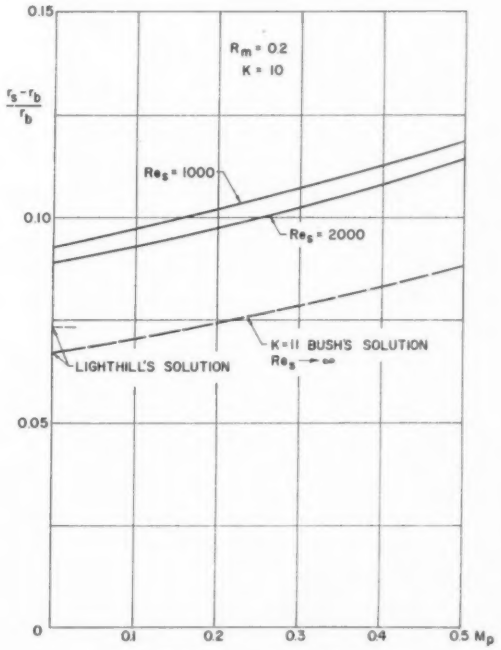

FIG. 6. Shock wave stand-off distance.

On the other hand, the induction equation may be written as

$$\left(\frac{2g}{\eta^2} - \frac{d^2g}{d\eta^2}\right) - \frac{8\pi\sigma\mu_e r_s V}{\eta^2}\left(g\frac{df}{d\eta} - f\frac{dg}{d\eta}\right) = 0 \quad (3.24)$$

For simplicity, the parameter $4\pi\sigma\mu_e r_s V$ may be denoted by Rm, the magnetic Reynolds number. Thus

$$\eta^2(d^2g/d\eta^2) - 2g = 2Rm[f(dg/d\eta) - g(df/d\eta)] \quad (3.25)$$

Again, in obtaining (3.24), we have assumed $\sin\theta \approx (1/2)\sin 2\theta$.

(2) *Boundary Conditions*—In this section, we consider the boundary conditions on the functions $f(\eta)$ and $g(\eta)$.

The velocity components immediately behind the shock wave will be

$$(v_r)_s = -(V/k)\cos\theta \quad (3.26)$$

$$(v_\theta)_s = V\sin\theta \quad (3.27)$$

where the subscript s indicates the quantity just behind the shock, k is the density ratio ($= \rho/\rho_\infty$) and V is the free-stream velocity. From the definitions given in (3.22), we obtain the following boundary conditions:

$$f(1) = -1/2k \quad (3.28)$$

$$(df/d\eta)_{\eta=0} = -1 \quad (3.29)$$

Now, since the differential equation governing $f(\eta)$ is of third order, we need one boundary condition independent of (3.28) and (3.29). To establish this third condition, we again apply the law of vorticity jump.

Accordingly, the vorticity immediately behind the shock wave may be expressed as

$$(\boldsymbol{\Omega}_\varphi)_{\eta=0} = \frac{(1-k)^2}{k}\frac{V\sin\theta}{r_s} - \frac{F_\theta}{\rho_\infty V\cos\theta} \quad (3.30)$$

where r_s is the shock radius and ρ_∞ the free-stream density. In (3.30), we have postulated that the viscous effect is negligible just behind the shock wave. However,

$$\frac{F_\theta}{\rho_\infty V\cos\theta} = \frac{4\sin\theta}{r_s\eta^5} M_p k Rm\left(g\frac{df}{d\eta} - f\frac{dg}{d\eta}\right)g \quad (3.31)$$

and

$$\boldsymbol{\Omega}_\varphi = \frac{V\sin\theta}{r_s}\left(\frac{2f}{\eta^2} - \frac{d^2f}{d\eta^2}\right) \quad (3.32)$$

$$\left(\frac{2f}{\eta^2} - \frac{d^2f}{d\eta^2}\right)_{\eta=1} = \frac{(1-k)^2}{k} - 4M_p Rmk\left(g\frac{df}{d\eta} - f\frac{dg}{d\eta}\right)_{\eta=1} g$$

Since on the shock now $\eta = 1$ and $f = -1/2k$, $df/d\eta = -1$, we therefore have

$$\left(\frac{d^2f}{d\eta^2}\right)_{\eta=1} = -\frac{2}{k} + 2 - k - 4M_p kRm \times \left[\left(g - \frac{1}{2k}\frac{dg}{d\eta}\right)g\right] \quad (3.33)$$

The velocity must satisfy the nonslip condition at the wall; thus, without mass injection,

$$f(r_b) = 0 \qquad f'(r_b) = 0$$

Again, we will specify the boundary conditions on the magnetic field at the shock wave. On the basis of assumptions similar to those made in the two-dimensional case, we can easily show that one set of permissible boundary conditions has the form

$$(\mathbf{H})_s = (2B/r_s^3)\cos\theta\mathbf{i}_r + (B/r_s^3)\sin\theta\mathbf{i}_r \quad (3.34)$$

or, if we denote $H_0 = B/r_s^3$,

$$(\mathbf{H})_s = 2H_0\cos\theta\mathbf{i}_r + H_0\sin\theta\mathbf{i}_r \quad (3.35)$$

Eq. (3.35) was first considered by Bush (1958). Thus

$$g(1) = 1 \qquad (dg/d\eta)_{\eta=1} = -1 \quad (3.36)$$

Substituting (3.36) into expression (3.33), we have

$$(d^2f/d\eta^2)_{\eta=1} = -(2/k) + 2 - k - 4M_p kRm[1 + (1/2k)] \quad (3.37)$$

(c) *Temperature Field*

In addition to the flow field and stand-off distance, the temperature field and local temperature gradient at the wall are of interest insofar as heat transfer is concerned. In order to investigate the temperature distribution, we refer back to the energy equation

$$C_v\rho\mathbf{v}\cdot\nabla T = \kappa\nabla^2 T + \Phi + (J^2/\sigma) \quad (3.38)$$

where ∇^2 is the Laplacian operator, Φ is the viscous dissipation function, and J^2/σ is Joule heating.

In realistic situations, especially hypersonic stagnation-point flow, the viscous dissipation and Joule heating are, in general, small compared to the convection and conduction terms. Therefore, by way of approximation and simplicity, the last two terms in (3.38) will be dropped. However, in the following discussion we will retain these two dissipation terms; it can be shown that a mathematically exact solution of the temperature distribution is still readily obtainable.

In order to discuss the similarity solutions of temperature distribution, we consider the energy equation in cylindrical and spherical coordinates:

$$\rho C_v\left[v_r\frac{\partial T}{\partial r} + \frac{v_\theta}{r}\frac{\partial T}{\partial\theta}\right] = \kappa\left[\frac{\partial^2 T}{\partial r^2} + \frac{1}{r}\frac{\partial T}{\partial r} + \frac{1}{r^2}\frac{\partial^2 T}{\partial\theta^2}\right] + \Phi_c + \frac{(\Delta\times\mathbf{H})^2}{(4\pi)^2\sigma} \quad \text{(cylindrical case)} \quad (3.39)$$

$$C_v\left[v_r\frac{\partial T}{\partial r} + \frac{v_\theta}{r}\frac{\partial T}{\partial\theta}\right] = \left[\frac{\partial^2 T}{\partial r^2} + \frac{2}{r}\frac{\partial T}{\partial r} + \frac{1}{r^2\sin\theta}\frac{\partial}{\partial\theta}\sin\theta\frac{\partial T}{\partial\theta}\right] + \Phi_s + \frac{(\Delta\times\mathbf{H})^2}{(4\pi)^2\sigma} \quad \text{(spherical case)} \quad (3.40)$$

where Φ_c and Φ_s are dissipation functions in cylindrical and spherical coordinates, respectively.

Hereafter, we shall introduce four dimensionless functions, namely, $R_1(\eta)$, $R_2(\eta)$, $S_1(\eta)$, $S_2(\eta)$, such that

$$T - T_0 = \frac{1}{2}\frac{V^2}{C_p}\,[R_1(\eta)\cos^2\theta + S_1(\eta)\sin^2\theta] \qquad \text{(cylindrical case)} \quad (3.41)$$

$$T - T_0 = \frac{1}{2}\frac{V^2}{C_p}\,[R_2(\eta)\cos^2\theta + S_2(\eta)\sin^2\theta] \qquad \text{(spherical case)} \quad (3.42)$$

T_0 is the stagnation temperature right behind the shock wave where the fluid may be treated as nonconducting and inviscid.

Substituting (3.41) and (3.42) into (3.39) and (3.40), respectively, we obtain two sets of equations, one for the two-dimensional case,

$$\frac{\gamma}{Pr\,Re}\left(\frac{d^2R_1}{d\eta^2} + \frac{1}{\eta}\frac{dR_1}{d\eta} - \frac{2R_1}{\eta^2} + \frac{2S_1}{\eta^2}\right) + \frac{8\gamma}{Re}\left(\frac{d}{d\eta}\frac{f}{\eta}\right)^2 - \frac{f}{\eta}\frac{dR_1}{d\eta} = 0 \quad (3.43)$$

$$Pr = \mu C_p/\theta \qquad Re = \rho V\gamma_s/\mu \qquad \gamma = C_p/C_v$$

$$\frac{\gamma}{PrRe}\left(\frac{d^2S_1}{d\eta^2} + \frac{1}{\eta}\frac{dS_1}{d\eta} - \frac{2S_1}{\eta^2} + \frac{2R_1}{\eta^2}\right) + \frac{2\gamma}{Re}\times\left(\frac{1}{\eta}\frac{df}{d\eta} - \frac{f}{\eta^2} - \frac{d^2f}{d\eta^2}\right)^2 + \frac{2M_p\gamma}{Rm}\left(\frac{g}{\eta^2} - \frac{1}{\eta}\frac{d}{d\eta}\eta\frac{dg}{d\eta}\right)^2 - \left(\frac{f}{\eta}\frac{dS_1}{d\eta} + \frac{2}{\eta}\frac{df}{d\eta}(R_1 - S_1)\right) = 0 \quad (3.44)$$

$$M_p = \mu_e H_0^2/4\pi\rho V^2 \qquad Rm = 4\pi\sigma\mu_e r_s V$$

and another for the three-dimensional case,

$$\frac{\gamma}{PrRe}\left(\frac{d^2R_2}{d\eta^2} + \frac{2}{\eta}\frac{dR_2}{d\eta} - \frac{4(R_2 - S_2)}{\eta^2}\right) + \frac{24\gamma}{Re}\left(\frac{d}{d\eta}\frac{f}{\eta^2}\right)^2 - \frac{2f}{\eta^2}\frac{dR_2}{d\eta} = 0 \quad (3.45)$$

$$\frac{\gamma}{PrRe}\left(\frac{d^2S_2}{d\eta^2} + \frac{2}{\eta}\frac{dS_2}{d\eta} - \frac{2(S_2 - R_2)}{\eta^2}\right) + \frac{24\gamma}{Re}\times\left(\eta\frac{d}{d\eta}\frac{1}{\eta^2}\frac{df}{d\eta} + \frac{2f}{\eta^3}\right)^2 + \frac{2M_p}{Rm}\gamma\left(\frac{2g}{\eta^3} - \frac{1}{\eta}\frac{d^2g}{d\eta^2}\right)^2 - \left(\frac{2}{\eta^2}\frac{df}{d\eta}(R_2 - S_2) + \frac{2f}{\eta^2}\frac{dS_2}{d\eta}\right) = 0 \quad (3.46)$$

where we have again employed the approximation $2\sin\theta \approx 2\theta$ and furthermore, consider $\cos\theta \approx 1$, the above equations reduce to four ordinary differential equations independent of θ. This verifies that (3.41) and (3.42) are possible forms of the similarity solutions of the temperature field.

The temperature and velocity fields right behind the shock wave are related according to

$$T = T_0 - (1/2C_p)(v_r^2 + v_\theta^2) \quad (3.47)$$

where C_p is the specific heat at constant pressure. Eq. (3.47) is justifiable provided that T_0 is constant in front of the shock and the viscous effect and heat conduction are negligible just behind the shock wave.

Therefore

$$(T - T_0)_{shock} = -(V^2/2C_p)[\sin^2\theta + (1/k^2)\cos^2\theta] \quad (3.48)$$

Comparing (3.41) and (3.42) with (3.48), we obtain the boundary conditions:

$$\left.\begin{aligned} R_1(1) &= -(1/k^2) \\ S_1(1) &= 1 \end{aligned}\right\} \text{ two-dimensional case} \quad (3.49)$$

$$\left.\begin{aligned} R_2(1) &= -(1/k^2) \\ S_2(1) &= -1 \end{aligned}\right\} \text{ axisymmetric case} \quad (3.50)$$

(1) Constant wall temperature:

$$R_1 = S_1 = \text{const.} \qquad \text{(cylindrical case)}$$

$$R_2 = S_2 = \text{const.} \qquad \text{(spherical case)}$$

(2) Constant wall heat transfer:

$$dR_1/d\eta = dS_1/d\eta = \text{const.} \qquad \text{(cylindrical case)}$$

$$dR_2/d\eta = dS_2/d\eta = \text{const.} \qquad \text{(spherical case)}$$

(2) is valid also for the case of an insulated wall.

(3) Variable wall temperature:

$$T = A\cos^2\theta + B\sin^2\theta$$

(4) $\partial T/\partial r = D\cos^2\theta + E\sin^2\theta$

Of course, one may consider that (1) and (2) are merely special cases of (3) and (4), respectively; but they are of utmost interest for practical reasons.

(IV) Further Consideration of the Physical Problem

In the previous analysis, constant density was assumed. It is well known that this assumption provides a good approximation near the stagnation-point region in the inviscid and nonmagnetic analysis of hypersonic flow. The justification is that since the pressure gradient across the shock layer is small, the density thus can be considered to be constant when the shock layer is thin and the temperature field is uniform. However, when the viscous friction and heat conduction are considered, this incompressibility approximation may be adopted only when the body temperature is of the same order of magnitude as the temperature right behind the shock wave. This is clearly so, since if the body is very cold, a large temperature gradient will be set up inside the viscous layer and then all temperature-dependent quantities may deviate significantly from the values immediately behind the shock wave. For this reason, in the present investigation, the body temperature is postulated to be very high, such that the temperature field in the shock layer is essentially uniform. This assumption may not be realistic, since no material at the present time can withstand that temperature. However, the main purpose of the present investigation is to study to what extent the skin friction and heat transfer rate will be reduced by the presence of hydromagnetic interaction. In fact, the present analysis has simplified the physical

model considerably. The complications due to many high-temperature phenomena, such as chemical and electronic reactions and radiation, have been ignored. Of course, neglecting these phenomena is not entirely justifiable in the study of realistic physical situations. Nevertheless, it is expected that the treatment of this idealized model should give some insight into actual physical problems.

In general magnetohydrodynamic problems, there exist two independent similarity parameters besides the conventional hydrodynamic parameters. These two parameters can be written in many different forms. Those most commonly used are:

$M_p = M_e H_0^2/\rho V_0^2$ magnetic pressure number

$Rm = \sigma\mu_e VL$ magnetic Reynolds number

or

$Qm = \sigma B_0^2 L/\rho V_0$ magnetic parameter

$Rm = \sigma\mu_e VL$ magnetic Reynolds number

Evidently, $Q_m = M_p Rm$.

In the previous discussion, we have used the parameters M_p and Rm. The reason for doing so is that M_p does not depend upon the physical properties of the fluid, but follows essentially from the imposed magnetic field intensity, H_0. Thus, by varying the values of M_p and Rm, one may easily obtain a qualitative picture of hydromagnetic effects due to the variation of electrical conductivity σ and the imposed field strength H_0. Generally, the former depends upon the flight circumstances, whereas the latter is arbitrary and controllable for certain range of H_0.

In the present investigation we are mainly interested in the "viscous layer régime" (using Probstein's (1958) terminology). In this régime, the Reynolds number for the shock radius r_s is on the order of 1000 or larger, or

$$Re_s = V_\infty r_s \rho_s/\mu \geqslant 1000$$

where V_∞ is the free-stream velocity and ρ_s the density of gas in shock layer.

In this case, we postulate that the viscous effect is insignificant right behind the shock wave. This assumption is justified from Kemp and Probstein's numerical results on nonmagnetic solutions.

In the following computation, we further consider that

$$k = \rho_s/\rho_\infty = 10 \quad \gamma = 1.22$$

and

$$Pr = 0.71$$

Numerical solutions are obtained for $M_p = 0.1$, 0.4, and 0.5, and $R_m = 0.2$, 0.4, and 1.0. They will be discussed in a later section.

(V) Method of Integration

The method of solution is straightforward. First, a value of f''' is assumed and integration then proceeds toward the body. The location of the body surface is determined by the simultaneous satisfaction of the following boundary conditions:

$$f(\eta_b) = 0$$

and

$$(df/d\eta)_{\eta=\eta_b} = 0 \qquad \eta_b = r_b/r_s$$

where r_b is the body radius. If the assumed value of f''' does not provide a solution which satisfies the above conditions at the same value of η_b, another trial value of f''' should be assumed. Thus, in order to obtain the actual solutions of $f(\eta)$ and $g(\eta)$, several trials are usually necessary.

After the solutions of $f(\eta)$ and $g(\eta)$ are known, we may further solve for $R(\eta)$ and $S(\eta)$. It is seen that the system that contains $R(\eta)$ and $S(\eta)$ is of fourth order and has two boundary conditions prescribed at the shock wave and another two at the body surface. This, at first glance, may give us difficulty if the above trial-and-error method is used.

However, this difficulty may be removed if we introduce two new formations $\Psi(\eta)$ and $\varphi(\eta)$ defined as

$$\Psi(\eta) = R_i - S_i \tag{5.1}$$

$$\varphi(\eta) = R_i + S_i \tag{5.2}$$

The energy equations then transform to the following form:

$$\frac{\gamma}{PrRe_s}\left[\frac{d^2\Psi}{d\eta^2} + \frac{1}{\eta}\frac{d\Psi}{d\eta}\right] - \frac{4\Psi}{\eta^2} - \frac{f}{\eta}\frac{d\Psi}{d\eta} + \frac{2}{\eta}\frac{df}{d\eta}\Psi + \frac{8\gamma}{Re_s}\left(\frac{d}{d\eta}\frac{f}{\eta}\right)^2 - \frac{2\gamma}{Re_s}\left(\frac{1}{\eta}\frac{df}{d\eta} - \frac{f}{\eta^2} - \frac{d^2f}{d\eta^2}\right)^2 - \frac{2M_p\gamma}{Rm}\left(\frac{g}{\eta^2} - \frac{1}{\eta}\frac{d}{d\eta}\eta\frac{dg}{d\eta}\right)^2 = 0 \tag{5.3}$$

$$\frac{\gamma}{PrRe_s}\left[\frac{d^2\varphi}{d\eta^2} + \frac{1}{\eta}\frac{d\varphi}{d\eta}\right] - \frac{f}{\eta}\frac{d\varphi}{d\eta} - \frac{2}{\eta}\frac{df}{d\eta}\Psi + \frac{8\gamma}{Re_s}\left(\frac{d}{d\eta}\frac{f}{\eta}\right)^2 + \frac{2\gamma}{Re_s}\left(\frac{1}{\eta}\frac{df}{d\eta} - \frac{f}{\eta^2} - \frac{d^2f}{d\eta^2}\right)^2 - \frac{2M_p\gamma}{Rm}\left(\frac{g}{\eta^2} - \frac{1}{\eta}\frac{d}{d\eta}\eta\frac{dg}{d\eta}\right)^2 = 0 \tag{5.4}$$

for the cylindrical case, and

$$\frac{\gamma}{PrRe_s}\left[\frac{d^2\Psi}{d\eta^2}+\frac{2}{\eta}\frac{d\Psi}{d\eta}-\frac{d\Psi}{\eta^2}\right]-\frac{2f}{\eta^2}\frac{d\Psi}{d\eta}+\frac{2}{\eta^2}\frac{df}{d\eta}\Psi-\frac{2\gamma}{Re_s}\left(\eta\frac{d}{d\eta}\frac{1}{\eta^2}\frac{df}{d\eta}-\frac{2f}{\eta^3}\right)^2-\frac{2M_p}{Rm}\gamma\left[\frac{2g}{\eta^3}-\frac{1}{\eta}\frac{d^2g}{d\eta^2}\right]^2+\frac{24\gamma}{Re_s}\left(\frac{d}{d\eta}\frac{f}{\eta^2}\right)^2=0 \quad (5.5)$$

$$\frac{\gamma}{PrRe_s}\left[\frac{d^2\varphi}{d\eta^2}+\frac{2}{\eta}\frac{d\varphi}{d\eta}-\frac{2\varphi}{\eta^2}\right]-\frac{2}{\eta^2}\frac{df}{d\eta^2}\Psi-\frac{2f}{\eta^2}\frac{d\varphi}{d\eta}+\frac{24\gamma}{Re_s}\left(\frac{d}{d\eta}\frac{f}{\eta^2}\right)^2+\frac{2\gamma}{Re_s}\left(\eta\frac{d}{d\eta}\frac{1}{\eta^2}\frac{df}{d\eta}-\frac{2f}{\eta^3}\right)^2+\frac{2M_p\gamma}{Rm}\left[\frac{2g}{\eta^3}-\frac{1}{\eta}\frac{d^2g}{d\eta^2}\right]^2=0 \quad (5.6)$$

for the spherical case. The corresponding boundary conditions are

$$\left.\begin{aligned}\varphi(1)&=-(1/k^2)-1 & \Psi(1)&=-(1/k^2)+1\\ \varphi(\eta_b)&=-2/k^2 & \Psi(\eta_b)&=0\end{aligned}\right\} \quad (5.7)$$

It is seen that Ψ now can be solved independently from φ and the integration is not difficult. After Ψ is determined, φ may be obtained successively.

(VI) Concluding Remarks

The numerical computations of the axisymmetric case are carried out at the Princeton Computation Center of Electronic Associates, Inc., with the use of the PACE 1631 fully-extended analog computer. Experience has shown that the higher the value of Reynolds number, magnetic-pressure, or magnetic Reynolds numbers, the more sensitive is the assumed value of $d^2f/d\eta^3$ on the shock wave to the solution of $f(\eta)$ and $g(\eta)$. For this reason, for Reynolds numbers up to 3000 and $M_p > 0.1$ and $Rm > 0.2$, the analog computer was not able to give satisfactory solutions essentially because of the limitation on its accuracy. Thus, the following discussions are restricted to $Re_s = 1000 \sim 2000$, $M_p \leqslant 0.05$ and $Rm \leqslant 1$. A few interesting points may be concluded from the numerical computation.

(1) The numerical results have shown that shock wave stand-off distance increases with increasing magnetic pressure number and magnetic Reynolds number for a given viscous Reynolds number. However, for given M_p and Rm, the stand-off distance decreases as the viscous Reynolds number increases. These facts may be seen from Table 1. If we take a closer look at the results shown in Table 1, which are also plotted in Figs. 5 and 6, we note the interesting fact that the stand-off distance of the shock wave depends approximately only upon the parameter $M_p \cdot Rm$. In other words, as long as the product $M_p \cdot Rm$ remains constant, the stand-off distance is almost invariant.

This conclusion may be checked with Bush's solution in which similar fact is found. From the plot in Figs. 5 and 6, we see that the above conclusion is approximately independent of viscous Reynolds number and the density ratio, k.

(2) Assuming the conclusion previously obtained is true for certain range of Rm and M_p, we then may construct a three-dimensional surface

$(r_0/r_b$ nonmagnetic case, $Rm \cdot M_p)$

as shown in Fig. 7. From this surface, the approximate values of r_b may be extrapolated for variables Rm and M_p within the ranges

$$0 \leqslant Rm \leqslant 1.0$$

$$0 \leqslant M_p \leqslant 0.5$$

(3) The induced electrical current is calculated and plotted in Fig. 4. It is seen that the maximum induced current intensity occurs near the shock wave. This is reasonable because the strongest interaction will take place in that region. The flow velocity vanishes on the body surface and there is, thus, no induced current.

(4) The induced magnetic field increases when the value of the magnetic Reynolds number and the magnetic-pressure number are increasing. In order to illustrate this, a typical plot is shown in Fig. 3. The

TABLE 1

M_p	Rm	$(r_s - r_b)/r_b$	Rm	M_p	$(r_s - r_b)/r_b$
		$Re_s = 1000$			
0.1	0	0.0929	0.2	0	0.0929
	0.2	0.0977		0.1	0.0977
	0.4	0.1022		0.4	0.1125
	1.0	0.1181		0.5	0.1186
		$Re_s = 2000$			
0.1	0	0.0893	0.2	0	0.0893
	0.2	0.0929		0.1	0.0929
	0.4	0.0977		0.4	0.1074
	1.0	0.1143		0.5	0.1147

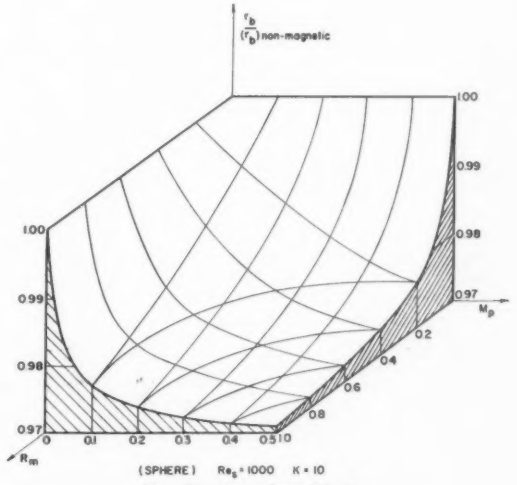

FIG. 7. Location of body.

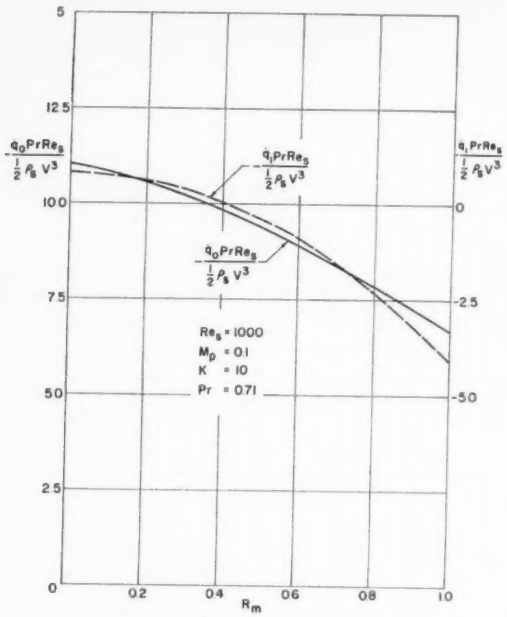

FIG. 8. Variation of heat transfer rate.

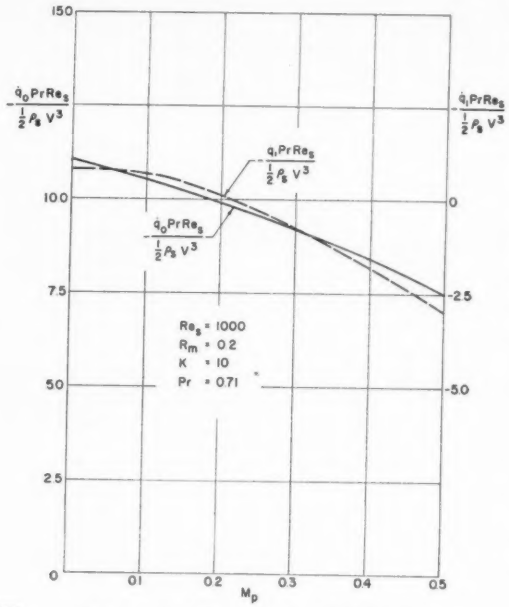

FIG. 9. Variation of heat transfer rate.

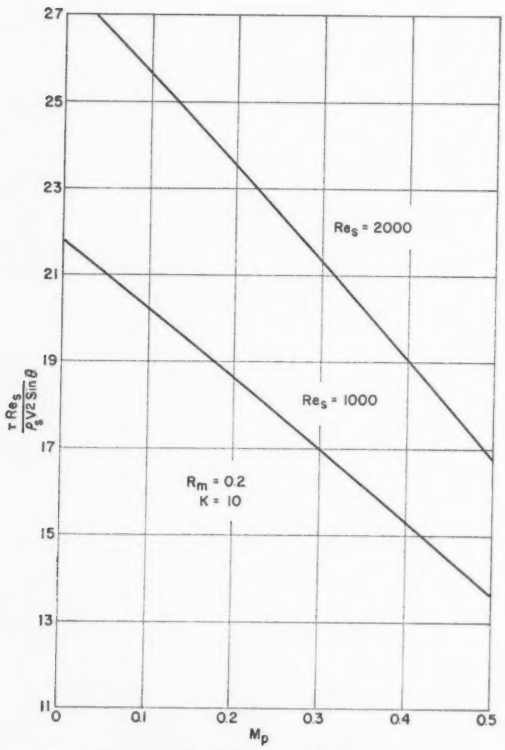

FIG. 10. Variation of skin friction.

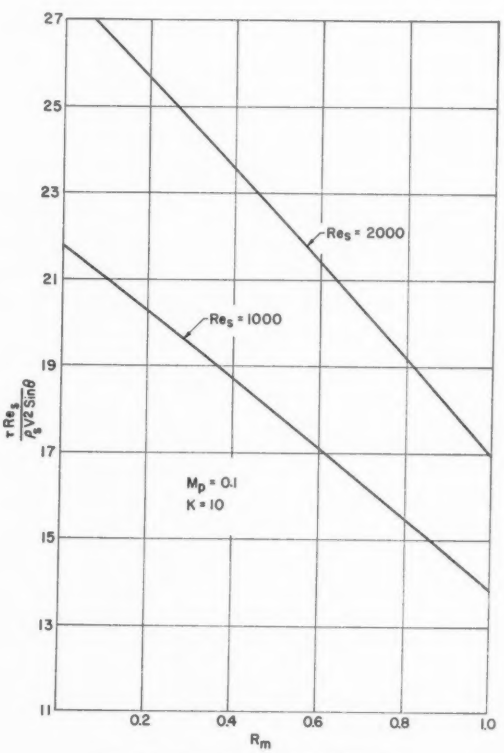

FIG. 11. Variation of skin friction.

calculated results have indicated that the induced field intensity is appreciable when $Rm > 0.2$ and $M_p > 0.1$. The ratio of the induced field intensity to the imposed field intensity is of order 1/1.4 for $Rm \approx 0.2$ and $M_p \approx 1$. That is, the induced field intensity is of the order of 30–40% of the imposed field. Therefore, the assumption that the induced field is negligible is not applicable in this case.

(5) The shape of the velocity profile of $v\theta$ changes when the fluid is highly conducting or a strong magnetic field is imposed. To illustrate this, a few typical profiles are plotted in Fig. 2. It is seen that in case $M_p = 0.1$, $Rm = 1.0$, the shape of θ/θ_{shock} changes considerably from that in the case $M_p = 0$. In addition to this, another plot of r/r_{shock} and θ/θ_{shock} against the dimensionless distance $(r - r_b)/(r_s - r_b)$ is given (Fig. 1). From this plot, we can see that the velocity components $v\theta$ and v_r are appreciably reduced in case of large Rm (= 1.0) or M_p (= 0.5). As a result of this phenomenon, the stand-off distance of the detached shock wave increases and, as we shall see later, the skin friction decreases significantly.

(6) In an attempt to discuss the skin friction situation, a dimensionless parameter

$$\frac{\tau Re_s}{\rho_s V^2 \sin\theta} = -\left(\frac{1}{\eta}\frac{d^2 f}{d\eta^2}\right)_{wall}$$

is used. The numerical results may be shown as in Table 2. It is seen that for given values of Re_s, ρ_s, and $V^2 \sin\theta$ the skin friction τ decreases with increasing values of M_p and Rm as shown in Figs. 10 and 11. The physical implication of this result is that the viscous layer is thickened and the magnitude of the velocity component v_θ is reduced across the shock layer.

(7) In addition to the skin friction parameter, another quantity we shall discuss is the heat transfer parameter, which is defined as

$$-\dot{q} Re_s Pr/(1/2)\rho_s V^3$$

Since

$$-\dot{q} = \kappa\left(\frac{\partial T}{\partial r}\right)_{r=r_b} = \kappa\frac{V^2}{2C_p}\left[\left(\frac{dR}{dr}\right)_{r_b}\cos^2\theta + \left(\frac{dS}{dr}\right)_{r_b}\sin^2\theta\right]$$

$$= \kappa\frac{V^2}{2C_p r_s}\left[\left(\frac{dR}{d\eta}\right)_{r_b} + \left(\frac{dS}{d\eta} - \frac{dR}{d\eta}\right)_{r_b}\sin^2\theta\right]$$

it is evident that

$$-\frac{\dot{q}}{\kappa(V^2/2C_p r_s)} = \left(\frac{dR}{d\eta}\right)_{r_b} + \left(\frac{dS}{d\eta} - \frac{dR}{d\eta}\right)_{r_b}\sin^2\theta = -\frac{\dot{q} Re_s Pr}{\rho_s V^3/2}$$

For simplicity, we further split this parameter into two parts, one of which is associated with the "stagnation-point" heat transfer and the other of which is θ-dependent:

$$\dot{q} = \dot{q}_0 + \dot{q}_1 \sin^2\theta$$

In that case, we have

$$(dR/d\eta)_{r_b} = -\dot{q}_0 Re_s Pr/(\rho_s V^3/2)$$

and $$(dS/d\eta)_{r_b} - (dR/d\eta)_{r_b} = -\dot{q}_1 Re_s Pr/(\rho_s V^3/2)$$

The numerical results for $Re_s = 1000$ are shown in Table 3. These results are also plotted in Figs. 8 and 9. Two interesting points can be seen:

(a) The stagnation-point heat transfer rate decreases as the magnetic-pressure number or magnetic Reynolds number increases.

(b) For nonmagnetic cases, the total heat transfer rate increases with θ, the angle measured from the stagnation-point stream line. However, the value changes from positive to negative when the electrical conductivity and imposed magnetic field strength increase. This result implies that in the latter case, the total heat transfer rate will decrease with increasing values of θ. From the plots we have obtained in Figs. 8 and 9, it is seen that for $M_p Rm > 0.04$, $\dot{q}_1$ is negative.

Lastly, it should be remarked that since the numerical computations are carried out by an analog computer, the accuracy of the results may not be sufficient. However, the qualitative pictures obtained thus far should help us to get some insight into the physical aspects of the problem.

(*Continued on page 950*)

TABLE 2

M_p	Rm	$\frac{\tau Re_s}{\rho_s V^2 \sin\theta}$	Rm	M_p	$\frac{\tau Re_s}{\rho_s V^2 \sin\theta}$
		$Re_s = 1000$			
0.1	0	21.80	0.2	0	21.80
	0.2	20.25		0.1	20.25
	0.4	18.65		0.4	15.30
	1.0	13.83		0.5	13.60
		$Re_s = 2000$			
0.1	0	27.60	0.2	0	27.60
	0.2	25.65		0.1	25.6
	0.4	23.50		0.4	19.10
	1.0	16.90		0.5	16.75

TABLE 3

M_p	Rm	$\frac{-\dot{q}_0 Re_s Pr}{\rho_s V^3/2}$	$\frac{-\dot{q}_1 Re_s Pr}{\rho_s V^3/2}$
0.1	0.0	11.06	0.81
	0 2	10 50	0 72
	0.4	9.87	±2.31
	1.0	6.69	±4.15

Rm	M_p	$\frac{-\dot{q}_0 Re_s Pr}{\rho_s V^3/2}$	$\frac{-\dot{q}_1 Re_s Pr}{\rho_s V^3/2}$
0.2	0	11.06	0.81
	0.1	0.50	0.72
	0.4	8.40	−1.80
	0.5	7.50	−3.01

Simplified Vibration Analysis of Elastic Sandwich Plates†

YI-YUAN YU*

Polytechnic Institute of Brooklyn

Summary

In a sequence of three recent papers a new flexural theory of elastic sandwich plates has been developed,[1, 2] and, on the basis of the theory, the flexural vibration of sandwich plates has been analyzed.[3] The theory is good for a very wide frequency range that is of practical interest, but vibration analysis on the basis of the theory will in general be complicated due to the high order of the equations. For low frequency ranges and for ordinary sandwich plates that have very thin face layers simplified treatment of the vibration problem becomes possible and is discussed in this paper. Simpler equations of motion of sandwich plates are introduced, and their accuracy is determined by comparing with the previous more complete equations.

Symbols

General

subscript i	= 1, 2, or 3, indicating the core, lower face, or upper face
x, y	= rectangular coordinates in plane of plate
z	= rectangular coordinate in thickness direction
prime	= differentiation with respect to x
dot	= differentiation with respect to time t

Plate Quantities

u_i, v_i, w_i	= displacements in x, y, z directions
w	= transverse deflection of plate
ψ_1, ψ_2	= changes of slope of normal to middle plane of plate in core and faces, respectively
ψ_x, ψ_y	= changes of slope of normal to middle plane of plate in core, in x and y directions
M_{xi}, M_{yi}, M_{xyi}	= bending and twisting moments
N_{xi}, N_{yi}, N_{xyi}	= membrane forces
Q_{xi}, Q_{yi}	= transverse shearing forces
Q_x	= $Q_{x1} + Q_{x2} + Q_{x3}$
Q_y	= $Q_{y1} + Q_{y2} + Q_{y3}$
h_1	= half-thickness of core
h_2	= thickness of each face
h	= $h_1 + h_2$ = total half-thickness of sandwich plate
I_{11}	= $2h_1^3/3$
I_{20}	= $2(h_2^3/12)$
I_{21}	= $2h_2h_1^2$
I_{21}'	= $2h_2[h_1 + (h_2/2)]^2$
I_{22}	= $(2/3)(h^3 - h_1^3) = I_{20} + I_{21}'$
ρ_i	= density
E_i	= Young's modulus
ν_i	= Poisson's ratio
ϵ_i	= $E_i/(1 - \nu_i^2)$
μ_i	= shear modulus
κ_i	= shear coefficient

Ratios

r_h	= h_2/h_1
r_ρ	= ρ_2/ρ_1
r_μ	= μ_2/μ_1
r_1	= $\epsilon_1/\mu_1 = 2/(1 - \nu_1)$
r_2	= $\epsilon_2/\mu_1 = [2/(1 - \nu_2)]\ r_\mu$

Vibration Quantities

ω	= circular frequency
Ω	= $(\rho_1/\mu_1)\omega^2h^2$
f	= $\sqrt{\Omega}/(1 + r_h)$
L	= wavelength
λ	= $2\pi h/L$

Received September 2, 1959.

† This research was supported by the United States Air Force under Contract AF49(638)-453 monitored by the Air Force Office of Scientific Research of the Air Research and Development Command.

* Professor, Department of Mechanical Engineering.

The author is indebted to Professor R. D. Mindlin of Columbia University, who suggested the subject of this investigation.

Introduction

IN THE NEW FLEXURAL THEORY of the elastic sandwich plate which has been developed in three recent papers,[1–3] the transverse displacement was assumed to be uniform across the plate thickness, and the displacements in the plane of the plate were assumed to be of linear variations over the thickness, with the slope in the faces taken to be different from that in the core. It was thus possible to include in the theory the effects of transverse shear deformations in the core and faces, the rotatory and translatory inertias of the core and faces, the flexural rigidity of the core, and the flexural and extensional rigidities of the faces. In addition, no restrictions were imposed upon the magnitudes of the ratios of the thicknesses, densities, and elastic constants between the core and faces. The results were therefore applicable to any symmetrically arranged three-layered plate in general. In the vibration studies of ordinary sandwich plates that have relatively thin but heavy and rigid faces, the important factors were found to be the shear effect in the core, the rotatory and translatory inertias of the core, the translatory inertia of the faces (which also has rotatory effect about the middle plane of the sandwich plate), and the joint effect of the flexural and extensional rigidities of the faces. When these factors were taken into account, the equations were shown to yield very accurate results for frequencies over a wide range that is of practical interest. This can cover up to, say, 20,000 cps or higher, as long as it is not too much higher than the first thickness-shear frequency.

The wide frequency range that can be covered by the

new theory in the case of ordinary sandwich plates also has its penalty. It was shown[3] that, while the order of the equations of motion with respect to time could be lowered through neglecting the transverse shear deformation or the rotatory inertia of the faces, which are of no importance to ordinary sandwiches, the order of the equations with respect to the space coordinate could not be reduced because of the presence of the joint effect of the rigidities of the faces, which is needed even for ordinary sandwiches. The vibration problem is thus in general complicated when solved on the basis of the new theory. The complication may be avoided, however, if we are only interested in rather low frequency ranges and/or plates with very thin faces. In such cases simplified vibration analysis of ordinary sandwich plates becomes possible and is treated in this paper.

Two sets of simpler equations of motion are presented. The first set is essentially a special degenerate version of the more complete equations given previously in the one-dimensional form,[1] and the second set is a modification of the first. The limitations of these equations are next determined, by comparing their results for the vibration of the infinite plate with those given by the previous more complete equations. The second set of simpler equations will be shown to be subject to less severe limitations and have better accuracy than the first.

(1) Previous Results

In the previous papers[1-3] as well as in this paper the sandwich plate under consideration has identical face layers. The middle plane of the plate is taken to be the xy plane. In the z direction the thicknesses of the lower face, core, and upper face extend from $-h$ to $-h_1$, $-h_1$ to h_1, and h_1 to h, respectively.

In the one-dimensional plane-strain case[1] the displacements are of the form

$$u_1 = z\psi_1, \qquad u_2, u_3 = \mp h_1(\psi_1 - \psi_2) + z\psi_2$$
$$w_1 = w_2 = w_3 = w$$

The displacement equations of motion are

$$\left.\begin{aligned}
&\epsilon_1 I_{11}\psi_1'' + \epsilon_2 I_{20}\psi_2'' + 2\epsilon_2 h_2[h_1 + (1/2)h_2][h_1\psi_1'' + (1/2)h_2\psi_2''] - 2\kappa_1\mu_1 h_1(\psi_1 + w') - \\
&\qquad 2\kappa_2\mu_2 h_2(\psi_2 + w') + hp_x = \rho_1 I_{11}\ddot{\psi}_1 + \rho_2 I_{20}\ddot{\psi}_2 + 2\rho_2 h_2[h_1 + (1/2)h_2][h_1\ddot{\psi}_1 + (1/2)h_2\ddot{\psi}_2] \\
&\epsilon_1 I_{11}\psi_1'' + 2\epsilon_2 h_2 h_1[h_1\psi_1'' + (1/2)h_2\psi_2''] - 2\kappa_1\mu_1 h_1(\psi_1 + w') + h_1 p_x = \rho_1 I_{11}\ddot{\psi}_1 + 2\rho_2 h_2 h_1[h_1\ddot{\psi}_1 + (1/2)h_2\ddot{\psi}_2] \\
&\qquad 2\kappa_1\mu_1 h_1(\psi_1' + w'') + 2\kappa_2\mu_2 h_2(\psi_2' + w'') + p_z = 2(\rho_1 h_1 + \rho_2 h_2)\ddot{w}
\end{aligned}\right\} \quad (1.1)$$

where $\epsilon_1 I_{11}$, $\epsilon_2 I_{20}$, and $2\epsilon_2 h_2$ are the flexural rigidity of the core and flexural and extensional rigidities of the faces, and $\rho_1 I_{11}$, $\rho_2 I_{20}$, $2\rho_1 h_1$, and $2\rho_2 h_2$ are similarly the rotatory and translatory inertias of the core and faces. The effect of each of these quantities may be suppressed by putting the quantity equal to zero. The transverse shear effect is, however, suppressed by putting κ_1 or κ_2 equal to infinity in the expressions of the transverse shearing forces.

The complete frequency equation of the infinite sandwich plate has been obtained[3] on the basis of Eqs. (1.1) and discussed in detail, but of particular interest here is the following simplified form:

$$\frac{1}{\kappa_1}\left(\frac{\rho_1 h_1 + \rho_2 h_2}{\rho_1 h_1}\right)\left(\frac{\rho_1 I_{11} + \rho_2 I_{21}}{\rho_1 h_1^3}\right)\Omega^2 - \left\{2\left(\frac{h^2}{h_1^2}\right)\left(\frac{\rho_1 h_1 + \rho_2 h_2}{\rho_1 h_1}\right) + \left[\left\{\frac{\rho_1 I_{11}}{\rho_1 h_1^3} + \frac{\rho_2 I_{22}}{\rho_1 h_1^3}\right\} + \right.\right.$$
$$\left.\left.\frac{1}{\kappa_1}\left(\frac{\rho_1 h_1 + \rho_2 h_2}{\rho_1 h_1}\right)\left(\frac{\epsilon_1 I_{11}}{\mu_1 h_1^3} + \frac{\epsilon_2 I_{21}}{\mu_1 h_1^3}\right)\right]\lambda^2\right\}\Omega + \left[\frac{\epsilon_1 I_{11}}{\mu_1 h_1^3} + \frac{\epsilon_2 I_{22}}{\mu_1 h_1^3}\right]\lambda^4 + \frac{1}{2\kappa_1(h^2/h_1^2)}\left(\frac{4\epsilon_1 I_{11}}{\mu_1 h_1^3} + \frac{\epsilon_2 I_{21}}{\mu_1 h_1^3}\right)\left(\frac{\epsilon_2 I_{20}}{\mu_1 h_1^3}\right)\lambda^6 = 0 \quad (1.2)$$

in which all terms have been made dimensionless. Eq. (1.2) is important in that, within the limitations that

$$r_\rho r_h^2/r_\mu, \quad (r_\rho r_h^2/r_\mu)\Omega, \quad r_h^2, \quad r_h^2\lambda^2 \ll 1 \quad (1.3)$$

it yields very accurate results for a wide frequency range for ordinary sandwich plates. As was shown in reference 3, some of these limitations may even be relaxed, and Eq. (1.2) still yields results with an accuracy comparable to those given by the exact elasticity theory. In terms of the various ratios, Eq. (1.2) may also be written as

$$\frac{1}{\kappa_1}(1 + r_\rho r_h)\left(\frac{1}{3} + r_\rho r_h\right)\Omega^2 - \left\{(1 + r_h)^2(1 + r_\rho r_h) + \left[\left\{\frac{1}{3} + r_\rho r_h(1 + r_h)\right\} + \right.\right.$$
$$\left.\left.\frac{1}{\kappa_1}(1 + r_\rho r_h)\left(\frac{1}{3}r_1 + r_2 r_h\right)\right]\lambda^2\right\}\Omega + \left[\frac{1}{3}r_1 + r_2 r_h(1 + r_h)\right]\lambda^4 + \frac{1}{12\kappa_1(1 + r_h)^2}\left(\frac{4}{3}r_1 + r_2 r_h\right)(r_2 r_h^2)\lambda^6 = 0 \quad (1.4)$$

While it is simple in Eq. (1.2) to identify the various quantities involved, Eq. (1.4) is more convenient for comparing the magnitudes of the different terms as well as for numerical calculations.

(2) First Set of Simplified Equations

By taking the displacements in the form

$$\left.\begin{aligned} u_1 &= z\psi_x, & u_2,\ u_3 &= \mp h_1\psi_x \\ v_1 &= z\psi_y, & v_2,\ v_3 &= \mp h_1\psi_y \\ w_1 &= w_2 = w_3 &&= w \end{aligned}\right\} \tag{2.1}$$

where w, ψ_x, and ψ_y are functions of x and y, and by using the same variational procedure as in reference 1, the following stress equations of motion are deduced from the three-dimensional elasticity theory:

$$\left.\begin{aligned} &(\partial/\partial x)[M_{x1} + h_1(N_{x3} - N_{x2})] + (\partial/\partial y)[M_{xy1} + h_1(N_{xy3} - N_{xy2})] - Q_{x1} + h_1 p_x = (\rho_1 I_{11} + \rho_2 I_{21})\ddot{\psi}_x \\ &(\partial/\partial x)[M_{xy1} + h_1(N_{xy3} - N_{xy2})] + (\partial/\partial y)[M_{y1} + h_1(N_{y3} - N_{y2})] - Q_{y1} + h_1 p_y = (\rho_1 I_{11} + \rho_2 I_{21})\ddot{\psi}_y \\ &(\partial Q_x/\partial x) + (\partial Q_y/\partial y) + p_z = 2(\rho_1 h_1 + \rho_2 h_2)\ddot{w} \end{aligned}\right\} \tag{2.2}$$

where

$$\begin{aligned} p_x &= (\tau_{zx3})_{z=h} + (\tau_{zx2})_{z=-h} \\ p_y &= (\tau_{zy3})_{z=h} + (\tau_{zy2})_{z=-h} \\ p_z &= (\sigma_{z3})_{z=h} - (\sigma_{z2})_{z=-h} \end{aligned}$$

The relation between the plate stresses and the plate displacements may also be derived in the manner shown in reference 1. In the isotropic case these are

$$\left.\begin{aligned} M_{x1} &= \epsilon_1 I_{11}\left(\frac{\partial\psi_x}{\partial x} + \nu_1\frac{\partial\psi_y}{\partial y}\right), & Q_{x1} &= 2\kappa_1\mu_1 h_1\left(\psi_x + \frac{\partial w}{\partial x}\right), & N_{x2} &= -N_{x3} = -\epsilon_2 h_1 h_2\left(\frac{\partial\psi_x}{\partial x} + \nu_2\frac{\partial\psi_y}{\partial y}\right) \\ M_{y1} &= \epsilon_1 I_{11}\left(\frac{\partial\psi_y}{\partial y} + \nu_1\frac{\partial\psi_x}{\partial x}\right), & Q_{y1} &= 2\kappa_1\mu_1 h_1\left(\psi_y + \frac{\partial w}{\partial y}\right), & N_{y2} &= -N_{y3} = -\epsilon_2 h_1 h_2\left(\frac{\partial\psi_y}{\partial y} + \nu_2\frac{\partial\psi_x}{\partial x}\right) \\ M_{xy1} &= \mu_1 I_{11}\left(\frac{\partial\psi_x}{\partial y} + \frac{\partial\psi_y}{\partial x}\right), & Q_{x2} &= Q_{x3} = Q_{y2} = Q_{y3} = 0, & N_{xy2} &= -N_{xy3} = -\mu_2 h_1 h_2\left(\frac{\partial\psi_x}{\partial y} + \frac{\partial\psi_y}{\partial x}\right) \end{aligned}\right\} \tag{2.3}$$

The shearing forces in the faces are zero because the faces have been taken as membranes; thus, we have

$$Q_x = Q_{x1}, \qquad Q_y = Q_{y1}$$

For sandwich plates that have isotropic faces but orthotropic cores, the plate stresses in Eqs. (2.3) for the faces remain valid, and those for the core are replaced by

$$\left.\begin{aligned} M_{x1} &= D_1\frac{\partial\psi_x}{\partial x} + D_2\frac{\partial\psi_y}{\partial y}, & Q_{x1} &= 2\kappa_1 c_{55} h_1\left(\psi_x + \frac{\partial w}{\partial x}\right) \\ M_{y1} &= D_3\frac{\partial\psi_y}{\partial y} + D_2\frac{\partial\psi_x}{\partial x}, & Q_{y1} &= 2\kappa_1 c_{44} h_1\left(\psi_y + \frac{\partial w}{\partial y}\right) \\ M_{xy1} &= D_4\left(\frac{\partial\psi_x}{\partial y} + \frac{\partial\psi_y}{\partial x}\right) \end{aligned}\right\} \tag{2.4}$$

where

$$D_1 = \left(c_{11} - \frac{c_{13}^2}{c_{33}}\right) I_{11}, \qquad D_2 = \left(c_{12} - \frac{c_{13}c_{23}}{c_{33}}\right) I_{11}$$

$$D_3 = \left(c_{22} - \frac{c_{23}^2}{c_{33}}\right) I_{11}, \qquad D_4 = c_{66} I_{11}$$

and the array of elastic constants of the core material is defined by the following stress-strain relations:

$$\begin{aligned} \sigma_{x1} &= c_{11}\epsilon_{x1} + c_{12}\epsilon_{y1} + c_{13}\epsilon_{z1} \\ \sigma_{y1} &= c_{12}\epsilon_{x1} + c_{22}\epsilon_{y1} + c_{23}\epsilon_{z1} \\ \sigma_{z1} &= c_{13}\epsilon_{x1} + c_{23}\epsilon_{y1} + c_{33}\epsilon_{z1} \\ \tau_{yz1} &= c_{44}\gamma_{yz1} \\ \tau_{zx1} &= c_{55}\gamma_{zx1} \\ \tau_{xy1} &= c_{66}\gamma_{xy1} \end{aligned}$$

The displacement equations of motion are readily obtained by substituting Eqs. (2.3) and (2.4) in Eqs. (2.2). Thus, we find for the isotropic case

$$\left.\begin{aligned}
&\left(\epsilon_1 I_{11}\frac{1-\nu_1}{2}+\epsilon_2 I_{21}\frac{1-\nu_2}{2}\right)\nabla^2\psi_x+\left(\epsilon_1 I_{11}\frac{1+\nu_1}{2}+\epsilon_2 I_{21}\frac{1+\nu_2}{2}\right)\frac{\partial e}{\partial x}-\\
&\qquad 2\kappa_1\mu_1 h_1\left(\psi_x+\frac{\partial w}{\partial x}\right)+h_1 p_x=(\rho_1 I_{11}+\rho_2 I_{21})\ddot{\psi}_x\\
&\left(\epsilon_1 I_{11}\frac{1-\nu_1}{2}+\epsilon_2 I_{21}\frac{1-\nu_2}{2}\right)\nabla^2\psi_y+\left(\epsilon_1 I_{11}\frac{1+\nu_1}{2}+\epsilon_2 I_{21}\frac{1+\nu_2}{2}\right)\frac{\partial e}{\partial y}-\\
&\qquad 2\kappa_1\mu_1 h_1\left(\psi_y+\frac{\partial w}{\partial y}\right)+h_1 p_y=(\rho_1 I_{11}+\rho_2 I_{21})\ddot{\psi}_y\\
&2\kappa_1\mu_1 h_1(\nabla^2 w+e)+p_z=2(\rho_1 h_1+\rho_2 h_2)\ddot{w}
\end{aligned}\right\}\tag{2.5}$$

where $\nabla^2=(\partial^2/\partial x^2)+(\partial^2/\partial y^2)$, $e=(\partial\psi_x/\partial x)+(\partial\psi_y/\partial y)$

For sandwich plates with orthotropic cores, we have

$$\left.\begin{aligned}
&(D_1+\epsilon_2 I_{21})\frac{\partial^2\psi_x}{\partial x^2}+(D_2+\nu_2\epsilon_2 I_{21})\frac{\partial^2\psi_y}{\partial x\partial y}+(D_4+\mu_2 I_{21})\left(\frac{\partial^2\psi_x}{\partial y^2}+\frac{\partial^2\psi_y}{\partial x\partial y}\right)-\\
&\qquad 2\kappa_1 c_{55} h_1\left(\psi_x+\frac{\partial w}{\partial x}\right)+h_1 p_x=(\rho_1 I_{11}+\rho_2 I_{21})\ddot{\psi}_x\\
&(D_2+\nu_2\epsilon_2 I_{21})\frac{\partial^2\psi_x}{\partial x\partial y}+(D_3+\epsilon_2 I_{21})\frac{\partial^2\psi_y}{\partial y^2}+(D_4+\mu_2 I_{21})\left(\frac{\partial^2\psi_x}{\partial x\partial y}+\frac{\partial^2\psi_y}{\partial x^2}\right)-\\
&\qquad 2\kappa_1 c_{44} h_1\left(\psi_y+\frac{\partial w}{\partial y}\right)+h_1 p_y=(\rho_1 I_{11}+\rho_2 I_{21})\ddot{\psi}_y\\
&2\kappa_1 c_{55} h_1\frac{\partial}{\partial x}\left(\psi_x+\frac{\partial w}{\partial x}\right)+2\kappa_1 c_{44} h_1\frac{\partial}{\partial y}\left(\psi_y+\frac{\partial w}{\partial y}\right)+p_z=2(\rho_1 h_1+\rho_2 h_2)\ddot{w}
\end{aligned}\right\}\tag{2.6}$$

The appropriate initial and boundary conditions are easily determined. The initial conditions consist in prescribing the initial values of ψ_x, ψ_y, w, $\dot{\psi}_x$, $\dot{\psi}_y$, and $\dot{w}$. The edge conditions require the specification of one member of each of the three products

$$[M_{n1}+h_1(N_{n3}-N_{n2})]\psi_n,\qquad [M_{ns1}+h_1(N_{ns3}-N_{ns2})]\psi_s,\qquad Q_{n1}w$$

and the surface conditions require the specification of one member of each of the three products

$$p_x(h_1\psi_x),\quad p_y(h_1\psi_y),\quad p_z w$$

The shear coefficient κ_1 is to be determined by the same method described in reference 2—namely, by matching the lowest frequencies obtainable from the sandwich-plate and elasticity theories for the simple thickness-shear mode of an infinite plate. We consider only the isotropic case. By setting for the thickness-shear mode

$$\psi_x=e^{i\omega t},\quad \psi_y=w=0$$

in Eqs. (2.5), it is found that

$$\kappa_1=[(1/3)+r_\rho r_h]f^2 \tag{2.7}$$

The value of f needed in Eq. (2.7) is to be calculated from Eq. (13) of reference 2—i.e.,

$$f\tan f=1/r_\rho r_h \tag{2.8}$$

which was derived from the theory of elasticity for the simple thickness-shear mode of ordinary sandwich plates. Since Eq. (2.7) is the same as Eq. (14) of reference 2, the other conclusions deduced for such plates in that reference become valid. For instance, it has been shown that

$$\left.\begin{aligned}
&\kappa_1=\pi^2/12 && \text{when } r_\rho r_h=0\\
&\kappa_1=1 \text{ approximately} && \text{when } r_\rho r_h>2
\end{aligned}\right\}\tag{2.9}$$

which are consequences of Eqs. (2.7) and (2.8).

In the one-dimensional isotropic case, the three displacement equations of motion reduce to the following two:

$$\left.\begin{aligned}
&(\epsilon_1 I_{11}+\epsilon_2 I_{21})\psi_x''-2\kappa_1\mu_1 h_1(\psi_x+w')+\\
&\qquad h_1 p_x=(\rho_1 I_{11}+\rho_2 I_{21})\ddot{\psi}_x\\
&2\kappa_1\mu_1 h_1(\psi_x'+w'')+p_z=2(\rho_1 h_1+\rho_2 h_2)\ddot{w}
\end{aligned}\right\}\tag{2.10}$$

These may be deduced from Eqs. (1.1) of the more complete theory by assuming

$$(1/2)h_2\ll h_1,\qquad \epsilon_2 I_{20}\psi_2\ll\epsilon_1 I_{11}\psi_1$$
$$(1/2)h_2\psi_2\ll h_1\psi_1,\qquad 2\kappa_2\mu_2 h_2(\psi_2+w')\ll 2\kappa_1\mu_1 h_1(\psi_1+w')$$

which are approximately true for plates with very thin faces. In this case, the first two Eqs. (1.1) become the same, and, on substituting ψ_x for ψ_1, both reduce to the first of Eqs. (2.10). The first set of simpler equations thus constitutes a special degenerate case of the previous more complete equations.

It is noted that Eqs. (2.5) of sandwich plates are analogous to the equations of motion of homogeneous plates which take into account the effects of shear and rotatory inertia—for instance, Eqs. (16) of reference 4.* Similarly, Eqs. (2.10) of the one-dimensional case are

* Such analogy between equilibrium equations of sandwich and homogeneous plates has been depicted in reference 5.

analogous to the Timoshenko beam equations. Existing solutions of such equations of homogeneous beams and plates may therefore be applied to sandwich beams and plates immediately. However, there is an important difference between the two cases—namely, while the equations of homogeneous plates always yield very accurate results for the lowest branch of the frequency curve (in the case of an infinite plate in plane strain) up to and even beyond the value of the cutoff frequency of the next higher branch, satisfactory results for the lowest branch are obtainable from Eqs. (2.5) and others in the sandwich case only if certain conditions of restriction are fulfilled, as will be shown in a later section.

Eqs. (2.5) and (2.6) of sandwich plates may be further simplified if the second branch of the frequency curve (in the case of an infinite plate in plane strain) is not to be considered, in which case terms involving rotatory inertias $\rho_1 I_{11}$ and $\rho_2 I_{21}$ may be disregarded. The flexural rigidity of the core is often much smaller than the contribution of the faces, and in such a case the terms involving $\epsilon_1 I_{11}, D_1, \ldots, D_4$ may be neglected. These additional simplifications, however, in general will not reduce significantly the amount of computation work involved in the vibration analysis of finite sandwich plates.

(3) Second Set of Simplified Equations

Another set of simpler equations may be derived by assuming the displacements in the form

$$\left.\begin{aligned} u_1 &= z\psi_x, \quad u_2, u_3 = \mp [h_1 + (h_2/2)]\psi_x \\ v_1 &= z\psi_y, \quad v_2, v_3 = \mp [h_1 + (h_2/2)]\psi_y \\ w_1 &= w_2 = w_3 = w \end{aligned}\right\} \tag{3.1}$$

The core of the sandwich plate could further be assumed to be arbitrarily extended slightly so that it would be joined to the faces at the middle planes $z = \pm [h_1 + (h_2/2)]$ of the latter instead of at the interfaces $z = \pm h_1$. By the method used in reference 1 and also in Section (2) of this paper it may be shown that this would lead to a set of equations very similar to Eqs. (2.2) to (2.6) of the first set, with the only difference that all h_1's in the latter equations were to be replaced by $h_1 + (h_2/2)$.

Now that the above proposed extension of the core from $z = \pm h_1$ to $z = \pm [h_1 + (h_2/2)]$ is only imaginary, any replacement of h_1 by $h_1 + (h_2/2)$ associated with the core itself would not seem justified. The replacement will therefore be made only when it concerns the faces.* This involves the replacement of h_1 either contained in or directly connected with N_x, N_y, N_{xy}, p_x, p_y, and I_{21} in Eqs. (2.2) and (2.3). No change need be made in Eqs. (2.4). In the displacement equations of motion (2.5) and (2.6) it finally involves the replacement of I_{21} by I_{21}', $h_1 p_x$ by $[h_1 + (h_2/2)]p_x$, and $h_1 p_y$ by $[h_1 + (h_2/2)]p_y$. The equations thus obtained constitute the second set and will be referred to as Eqs. (3.2) to (3.6).

The initial conditions for the first set of equations given in the last section remain valid for the second set, but the previous edge and surface conditions must be modified by replacing h_1 by $h_1 + (h_2/2)$. Similarly, the shear coefficient is now also different. For the simple thickness-shear mode Eqs. (3.5) yield

$$\kappa_1' = [(1/3) + r_\rho r_h(1 + r_h)]f^2 \tag{3.7}$$

where a third term $r_h^2/4$ has been omitted from inside the factor $(1 + r_h)$, which was not present in Eq. (2.7). To distinguish the two different shear coefficients, a prime has been inserted in Eq. (3.7). Eq. (2.8) may still be used, but the second of Eqs. (2.9) is no longer true.

An analogy between the equations of sandwich plates and homogeneous plates still exists, also within certain limitations of the former, which are to be depicted in the next section. The limitations of the second set of equations are, however, not entirely the same as those of the first set. The second set may also be further simplified in the same manner as was described at the end of Section (2).

(4) Limitations of Equations

We shall now determine what limitations must be imposed upon the equations derived in the last two sections when they are applied to vibration problems of ordinary sandwich plates. For this purpose we derive on the basis of these equations the frequency equation of flexural vibration of the infinite sandwich plate, and compare the result with the frequency equation (1.2) or (1.4) based on the previous more complete equations. It is sufficient to consider the isotropic plane-strain case, as was done in reference 3. We start with Eqs. (2.5) of the first set. By putting in these equations

$$\begin{aligned} p_x &= p_y = p_z = 0 \\ w &= W \sin(\lambda x/h) \sin \omega t \\ \psi_x &= \Psi_x \cos(\lambda x/h) \sin \omega t \\ \psi_y &= 0 \end{aligned}$$

the frequency equation is easily found to be

$$\frac{1}{\kappa_1}\left(\frac{\rho_1 h_1 + \rho_2 h_2}{\rho_1 h_1}\right)\left(\frac{\rho_1 I_{11} + \rho_2 I_{21}}{\rho_1 h_1^3}\right)\Omega^2 - \left\{2\left(\frac{h^2}{h_1^2}\right)\left(\frac{\rho_1 h_1 + \rho_2 h_2}{\rho_1 h_1}\right) + \left[\left(\frac{\rho_1 I_{11}}{\rho_1 h_1^3} + \frac{\rho_2 I_{21}}{\rho_1 h_1^3}\right) + \frac{1}{\kappa_1}\left(\frac{\rho_1 h_1 + \rho_2 h_2}{\rho_1 h_1}\right)\left(\frac{\epsilon_1 I_{11}}{\mu_1 h_1^3} + \frac{\epsilon_2 I_{21}}{\mu_1 h_1^3}\right)\right]\lambda^2\right\}\Omega - \left[\frac{\epsilon_1 I_{11}}{\mu_1 h_1^3} + \frac{\epsilon_2 I_{21}}{\mu_1 h_1^3}\right]\lambda^4 = 0 \tag{4.1}$$

* In this respect the present model of sandwich construction differs from that used in reference 6.

or

$$\frac{1}{\kappa_1}(1 + r_\rho r_h)\left(\frac{1}{3} + r_\rho r_h\right)\Omega^2 - \left\{(1 + r_h)^2(1 + r_\rho r_h) + \left[\left(\frac{1}{3} + r_\rho r_h\right) + \frac{1}{\kappa_1}(1 + r_\rho r_h)\left(\frac{1}{3} r_1 + r_2 r_h\right)\right]\lambda^2\right\}\Omega + \left[\frac{1}{3} r_1 + r_2 r_h\right]\lambda^4 = 0 \quad (4.2)$$

The similarity between Eqs. (4.1) and (1.2), or (4.2) and (1.4), is noted. There are however three differences: (a) $\rho_2 I_{22}$ in Eq. (1.2) has been replaced by $\rho_2 I_{21}$ in Eq. (4.1), (b) $\epsilon_2 I_{22}$ has similarly been replaced by $\epsilon_2 I_{21}$, and (c) the λ^6 term which reflects the effect of the flexural rigidity of the faces is missing in Eqs. (4.1) and (4.2). Since the terms $(1/3) + r_\rho r_h(1 + r_h)$ in Eq. (1.4) and $(1/3) + r_\rho r_h$ in Eq. (4.2) are much smaller than the terms containing $r_2 r_h$ immediately next to them, the replacement of $\rho_2 I_{22}$ by $\rho_2 I_{21}$ will not have much effect. As was observed in reference 3 and may be readily and explicitly shown to be true in the simpler case of the quadratic Eq. (4.2), the second root of Ω is approximately equal to the quotient between the coefficient of the Ω term and that of the Ω^2 term. Its value given by Eq. (4.1) or (4.2) is therefore very nearly equal to that given by Eq. (1.2) or (1.4).

The other two items (b) and (c) affect mainly the lower root of Ω, which may be computed approximately by dividing the constant term by the coefficient of the Ω term, as may also be explicitly shown to be true for Eq. (4.2). Since the coefficient of the Ω term is essentially the same in Eqs. (4.2) and (1.4), the difference between the lower roots of these equations will be approximately proportional to the difference between their constant terms. Since r_1 for ordinary sandwich plates is much smaller than $r_2 r_h$, the difference between the constant terms is seen to be negligible if

$$r_h \ll 1, \qquad \frac{r_2 r_h^3}{12\kappa_1(1 + r_h)^2}\lambda^2 \ll 1 \quad (4.3)$$

which result from the above items (b) and (c), respectively. In addition to the conditions in (1.3), therefore, those in (4.3) must be further imposed if the first set of equations presented in this paper is to yield accurate results for the lower branch of the frequency curve. When the conditions in (4.3) are not satisfied, the approximate error in the lower frequency calculated from Eq. (4.2) as compared with that from Eq. (1.4) is equal to

$$\frac{\sqrt{\Omega} - \sqrt{\Omega'}}{\sqrt{\Omega}} \approx 1 - \left[1 + r_h + \frac{r_2 r_h^2}{12\kappa_1(1 + r_h)^2}\lambda^2\right]^{-1/2} \quad (4.4)$$

where Ω and Ω' are the lower roots of Eqs. (1.4) and (4.2), respectively. The error does not vanish even for very long waves, that is, for very low frequencies. For $r_h = 1/10$, the minimum error is about 5 per cent. The error increases with r_h (thicker faces), and also with λ (higher frequencies).

The frequency equation may similarly be derived from Eqs. (3.5) of the second set. The result is of the same form as Eq. (4.1), the only difference being that I_{21} in the latter equation is now replaced by I_{21}'. In terms of the ratios, it takes the form

$$\frac{1}{\kappa_1'}(1 + r_\rho r_h)\left[\frac{1}{3} + r_\rho r_h(1 + r_h)\right]\Omega^2 - \left\{(1 + r_h)^2(1 + r_\rho r_h) + \left[\left\{\frac{1}{3} + r_\rho r_h(1 + r_h)\right\} + \frac{1}{\kappa_1'}(1 + r_\rho r_h)\left\{\frac{1}{3} r_1 + r_2 r_h(1 + r_h)\right\}\right]\lambda^2\right\}\Omega + \left[\frac{1}{3} r_1 + r_2 r_h(1 + r_h)\right]\lambda^4 = 0 \quad (4.5)$$

where a third term $r_h^2/4$ has been dropped from inside each of the additional factors $(1 + r_h)$ which were not present in Eq. (4.2). Eq. (4.5) is again different from Eq. (1.4). However, the limitations of Eq. (4.5) may be shown to be less restrictive than those of Eq. (4.2), as follows. The respective lower roots of Eqs. (1.4) and (4.5) are approximately

$$\Omega \approx \frac{r_2 r_h \lambda^4}{1 + r_\rho r_h} \frac{(1 + r_h) + \frac{r_2 r_h^3}{12\kappa_1(1 + r_h)^2}\lambda^2}{(1 + r_h)^2 + \frac{r_2 r_h}{\kappa_1}\lambda^2}, \qquad \Omega' \approx \frac{r_2 r_h \lambda^4}{1 + r_\rho r_h} \frac{(1 + r_h)}{(1 + r_h)^2 + \frac{r_2 r_h(1 + r_h)}{\kappa_1'}\lambda^2}$$

The difference between the lower frequencies is therefore given by

$$\frac{\sqrt{\Omega} - \sqrt{\Omega'}}{\sqrt{\Omega}} \approx 1 - \left[\frac{(1 + r_h)}{(1 + r_h) + \frac{r_2 r_h^3}{12\kappa_1(1 + r_h)^2}\lambda^2} \frac{(1 + r_h)^2 + \frac{\kappa_1'}{\kappa_1(1 + r_h)}\frac{r_2 r_h(1 + r_h)}{\kappa_1'}\lambda^2}{(1 + r_h)^2 + \frac{r_2 r_h(1 + r_h)}{\kappa_1'}\lambda^2}\right]^{1/2}$$

TABLE 1

λ	$\frac{r_2 r_h^3 \lambda^2}{12\kappa_1(1+r_h)^2}$	Lower Value of $\sqrt{\Omega}$					Higher Value of $\sqrt{\Omega}$		
		(a) Eq. (1.4)	(b) Eq. (4.5)	(c) Eq. (4.2)	% diff. (a) & (b)	% diff. (a) & (c)	Eq. (1.4)	Eq. (4.5)	Eq. (4.2)
0	0	0	0	0	0	0	0.565	0.565	0.565
0.05	0.000828	0.01754	0.01754	0.01675	0	3.93	0.800	0.800	0.800
0.1	0.00331	0.0445	0.0443	0.0424	0.45	4.72	1.262	1.267	1.262
0.5	0.0828	0.257	0.247	0.236	3.89	8.17	5.66	5.69	5.66
1.0	0.331	0.567	0.496	0.474	12.54	16.40	11.28	11.35	11.28

which is easily seen to be always positive as it is in Eq. (4.4) and is seen to approach zero if

$$\left.\begin{aligned} \frac{r_2 r_h^3}{12\kappa_1(1+r_h)^2}\lambda^2 &\ll 1 \\ 1 - \frac{\kappa_1'}{\kappa_1(1+r_h)} &\ll 1 \end{aligned}\right\} \tag{4.6}$$

The second of these conditions, according to Eqs. (2.7) and (3.7), leads to

$$\frac{r_h}{(1+3r_\rho r_h)(1+r_h)} \ll 1 \tag{4.7}$$

While condition (4.6) is the same as the second of (4.3), condition (4.7) is certainly less restrictive than the first of (4.3). The second set of equations in Section (3) therefore yield more accurate results for the lower branch of the frequency curve than the first set in Section (2). The second set is somewhat less accurate for the higher branch, but this need not concern us, because the present simplified treatment aims at low frequency ranges.

To illustrate the above discussion, we present the numerical results calculated from Eqs. (1.4), (4.2), and (4.5) for one of the cases that has been treated in reference 3, in which the core material is cellular cellulose acetate and the face material aluminum. The various ratios are

$$r_h = 1/10, \quad r_\rho = 34.4, \quad r_\mu = 1683, \quad r_1 = 2.20, \quad r_2 = 4790$$

Eqs. (2.7) and (3.7) yield

$$\kappa_1 = 0.997, \quad \kappa_1' = 1.086$$

The results for $\sqrt{\Omega}$ together with the percentage differences for the lower $\sqrt{\Omega}$ are listed in Table 1 for several values of λ. The ratio

$$r_2 r_h^3 \lambda^2 / 12\kappa_1(1+r_h)^2$$

is also included for reference.

Since

$$\frac{r_h}{(1+3r_\rho r_h)(1+r_h)} = 0.00803$$

condition (4.7) is satisfied. Condition (4.6) is likewise satisfied for $\lambda = 0.05$ and 0.1, for which Eq. (4.5) is therefore very accurate, and its results for lower $\sqrt{\Omega}$ differ only very slightly from those of Eq. (1.4). On the other hand, since $r_h = 1/10$ does not quite fulfill the first condition in (4.3), Eq. (4.2) is not very accurate even for $\lambda < 0.05$. The cutoff value $\sqrt{\Omega} = 0.565$ of the higher branch corresponds to a frequency of $\omega = 10{,}600$ cps when $h = 0.3$ in. The frequency corresponding to $\sqrt{\Omega} = 0.0445$ for $\lambda = 0.1$ is 836 cps, which gives an idea of the approximate frequency range that can be covered adequately by the equations presented in this paper.

References

[1] Yu, Yi-Yuan, *A New Theory of Elastic Sandwich Plates—One-Dimensional Case*, J. Appl. Mech., Vol. 26, pp. 415–421, 1959.

[2] Yu, Yi-Yuan, *Simple Thickness-Shear Modes of Vibration of Infinite Sandwich Plates*, J. Appl. Mech., Vol. 26, pp. 679–681, 1959.

[3] Yu, Yi-Yuan, *Flexural Vibrations of Elastic Sandwich Plates*, Journal of the Aero/Space Sciences, Vol. 27, No. 4, pp. 272–282, April, 1960.

[4] Mindlin, R. D., *Influence of Rotatory Inertia and Shear on Flexural Motions of Isotropic, Elastic Plates*, J. Appl. Mech., Vol. 18, pp. 31–38, 1951.

[5] Reissner, E., *On Bending of Elastic Plates*, Quart. Appl. Math., Vol. 5, pp. 55–68, 1947.

[6] Reissner, E., *Small Bending and Stretching of Sandwich-Type Shells*, NACA Report 975, 1950.

✦ ✦ ✦

Microcards for Volumes 1–5 Available

Microcards for Volumes 3–5 of the JOURNAL are now available (Vols. 1 and 2 were republished in this form earlier). All five volumes are priced at $5.50 each, and are obtainable through:

J. S. Canner & Company, Inc.
Boston, Roxbury 20, Mass.

Combustion in the Boundary Layer on a Porous Surface

ALAN Q. ESCHENROEDER*
Cornell University

Summary

The position of the diffusion flame in a boundary layer with uniform mixture injection from a porous wall parallel to a uniform air stream is determined under the conditions of laminar, steady flow with zero streamwise pressure gradient. Under the assumption of fast forward reaction rate, solutions of the boundary layer forms of the conservation laws of aerothermochemistry are obtained leading to a formula for the downstream velocity at the flame in terms of composition and flow variables. The rates of change of conditions at the wall in the streamwise direction are assumed to be relatively small. Methods of treating complex reaction systems are described, and a generalized form of the Reynolds analogy is developed.

Symbols

c_f = friction coefficient
$\bar{c}_p$ = constant pressure specific heat at constant composition
$\mathfrak{D}$ = diffusion coefficient
H = constant pressure heating value
h = specific enthalpy (defined in Eq. 5)
k = thermal conductivity
Le = Lewis-Semenov number, $\rho\mathfrak{D}\bar{c}_p/k$
m = mass concentration
n = total number of species present
$\overline{Pr}$ = "frozen" Prandtl number, $\bar{c}_p\mu/k$
Q_v = volumetric rate of energy production due to chemical reaction
q = heat flux
r = stoichiometric constant of proportionality
T = absolute temperature
U_1 = free stream velocity
u = local downstream velocity
$\bar{u}$ = nondimensional local downstream velocity, u/U_1
v = local normal velocity
w_K = volumetric rate of production of species K
$\bar{x}, x$ = downstream distance from the leading edge
y = normal distance
β = blowing ratio, $\rho_0 v_0/\rho_1 U_1$
μ = absolute viscosity
ξ = nondimensional distance, $\beta^2\rho_1 U_1 x/\mu_1$
ρ = density
τ = shear stress
Φ_m = mass equivalence ratio

Subscripts

a = region between flame and wall
b = region between flame and free stream
e = conditions at entrance of porous wall
f = fuel species
K = species index
M = mixture
o = conditions at porous wall surface
ϕ = oxygen species
$+$ = conditions at diffusion flame
1 = conditions at free stream

Received September 21, 1959.

* Presently Associate Aeronautical Engineer, Aerodynamic Research Department, Cornell Aeronautical Laboratory, Inc.

The author wishes to acknowledge the guidance and interest of Profs. D. G. Shepherd and D. E. Ordway at Cornell University. The reading and discussing of the analysis by Dr. Theodore von Kármán is also sincerely appreciated.

Introduction

RECENT INTEREST in the areas of mass transfer cooling, liquid fuel combustion, and erosive burning of solid propellants has stimulated several investigations of transfer and combustion rates in boundary layers with mass addition.[1–5] In addition to these applications, the proposed use of external burning for lift augmentation of supersonic and hypersonic vehicles[6] provides impetus for the present study of flame behavior. All previous work has been done for the injection rate varying inversely with the square root of distance from the leading edge and for a pure injected species. Such assumptions are usually adequate for describing an interphase boundary, but the injection of gas through a porous wall and the need for optimum combustion conditions suggest the adoption of a new model in which the flame receives oxygen both from the free stream and from the initial mixture. Then, the new model differs from the old one in two respects:

(1) The injected mass flux is assumed constant because the flow of gas supplied to the porous wall, rather than a phase-change mechanism, controls the total injection rate.

(2) A fuel-air mixture, rather than pure fuel, is assumed to flow through the pores. Therefore, the mass and heat transfer potentials must be allowed to vary in the streamwise direction to fulfill the new boundary conditions.

The position of the diffusion flame in the boundary layer is determined, and a generalized form of the Reynolds analogy is developed as a means of calculating heat transfer rates. In the present work, burning is assumed to begin at the leading edge. In reality, excess heat and mass transfer from the flame cause quenching in this region, so that some distance may exist between the leading edge and the ignition point. Then, completely premixed combustion would occur at the beginning of the flame, and chemical kinetics, rather than diffusion, would be the local rate-controlling process. An experimental investigation of flame stabilization has been carried out in order to study this

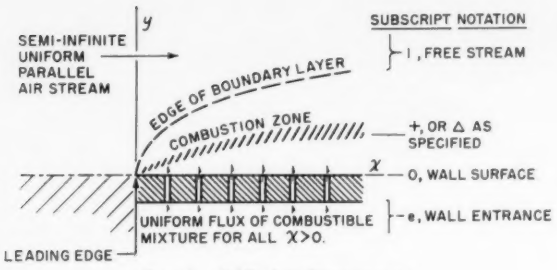

FIG. 1. Diffusion flame model.

aspect of the problem. Reference 7 contains the results of the measurements.

Diffusion Flame Analysis

The location of a diffusion flame in the boundary layer will first be determined. The method of analysis is based upon the conservation laws of aerothermochemistry subject to the following assumptions: (1) all the physical simplifications of boundary layer theory are valid; (2) there is steady laminar flow with zero external pressure gradient; (3) energy production and transport due to combustion exceeds that due to viscous dissipation by a considerable amount; (4) the kinetic energy associated with thermal molecular motion is large compared with that arising from macroscopic fluid velocity; (5) radiative energy transport is practically negligible; (6) diffusion due to temperature and pressure gradients is small compared with that due to concentration gradients, which is assumed to obey Fick's law; and (7) the physical situation is described by the diagram shown in Fig. 1.

The governing conservation equations of mass, momentum, energy, and chemical species are, respectively,

Global Conservation of Mass:

$$\frac{\partial(\rho u)}{\partial x} + \frac{\partial(\rho v)}{\partial y} = 0 \tag{1}$$

Conservation of Momentum:

$$\rho\left(u\frac{\partial u}{\partial x} + v\frac{\partial u}{\partial y}\right) = \frac{\partial}{\partial y}\left(\mu\frac{\partial u}{\partial y}\right) \tag{2}$$

Conservation of Energy:

$$\rho\left(u\frac{\partial h}{\partial x} + v\frac{\partial h}{\partial y}\right) = \frac{\partial}{\partial y}\left[\left(k\frac{\partial T}{\partial y}\right) + \sum_{K=1}^{n}\rho\mathfrak{D}_{KM}h_K\frac{\partial m_K}{\partial y}\right] + Q_v \tag{3}$$

Conservation of the Kth Species:

$$\rho\left(u\frac{\partial m_K}{\partial x} + v\frac{\partial m_K}{\partial y}\right) = \frac{\partial}{\partial y}\left(\rho\mathfrak{D}_{KM}\frac{\partial m_K}{\partial y}\right) + w_K \tag{4}$$

where $\mathfrak{D}_{KM}$ is the diffusion coefficient of the Kth species into the mixture, h_K is the sensible enthalpy associated with the Kth species, m_K is the mass concentration of the Kth species, and Q_v is the volumetric rate of energy release due to chemical reaction. The enthalpy h is defined in differential form by

$$dh = \bar{c}_p dT + \sum_{K=1}^{n} h_K dm_K \tag{5}$$

in which $\bar{c}_p$ is the specific heat of the mixture at constant pressure and composition, i.e.,

$$\bar{c}_p = \sum_{K=1}^{n} m_K c_{pK} \tag{6}$$

Alternatively, the "frozen" specific heat and the enthalpy of the Kth species are expressed by

$$\bar{c}_p = \frac{\partial h}{\partial T}\Big]_{p,\ m_1,\ m_2,\ \cdots,\ m_n}; \qquad h_K = \frac{\partial h}{\partial m_K}\Big]_{p,\ T}$$

w_K is the volumetric rate of production of the Kth species.

From Eq. (5), the conductive heat flux is given by

$$k\frac{\partial T}{\partial y} = \frac{k}{\bar{c}_p}\left[\frac{\partial h}{\partial y} - \sum_{K=1}^{n} h_K\frac{\partial m_K}{\partial y}\right] \tag{7}$$

which can be substituted in Eq. (3) to yield

$$\rho\left(u\frac{\partial h}{\partial x} + v\frac{\partial h}{\partial y}\right) = \frac{\partial}{\partial y}\left[\frac{\mu}{\overline{Pr}}\left(\frac{\partial h}{\partial y}\right) + \sum_{K=1}^{n}\rho\mathfrak{D}_{KM}\left(1 - \frac{1}{Le_K}\right)h_K\frac{\partial m_K}{\partial y}\right] + Q_v \tag{8}$$

The Prandtl number $\overline{Pr}$ is defined as $\bar{c}_p\mu/k$ and the Lewis number Le_K of the Kth species is defined as $\rho\mathfrak{D}_{KM}\bar{c}_p/k$.

The molecular capability of the gas to transport the Kth species by diffusion will now be equated to its capability to conduct heat; that is, $Le_K = 1$ will be adopted as an *additional assumption*. Eq. (8) then becomes

$$\rho\left(u\frac{\partial h}{\partial x} + v\frac{\partial h}{\partial y}\right) = \frac{\partial}{\partial y}\left[\frac{\mu}{\overline{Pr}}\left(\frac{\partial h}{\partial y}\right)\right] + Q_v \tag{9}$$

and Eq. (4) becomes

$$\rho\left(u\frac{\partial m_K}{\partial x} + v\frac{\partial m_K}{\partial y}\right) = \frac{\partial}{\partial y}\left[\frac{\mu}{\overline{Pr}}\left(\frac{\partial m_K}{\partial y}\right)\right] + w_K \tag{10}$$

As Cohen *et al.*[3] have demonstrated, certain features of the basic equations are clarified by changing the independent variables from (x, y) to $(\bar{x}, u)$, according to the method of Crocco,[8] where $\bar{x}$ is the downstream distance along the plate. Eqs. (9) and (10), after application of this transformation, become, respectively,

$$\frac{\partial h}{\partial \bar{x}} = \frac{\tau}{\rho u\mu}\frac{\partial \tau}{\partial u}\left(\frac{1 - \overline{Pr}}{\overline{Pr}}\right) + \frac{\tau^2}{\rho u\mu}\frac{1}{\overline{Pr}}\frac{\partial^2 h}{\partial u^2} + \frac{Q_v}{\rho u} \tag{11}$$

and

$$\frac{\partial m_K}{\partial \bar{x}} = \frac{\tau}{\rho u\mu}\frac{\partial \tau}{\partial u}\left(\frac{1 - \overline{Pr}}{\overline{Pr}}\right) + \frac{\tau^2}{\rho u\mu}\frac{1}{\overline{Pr}}\frac{\partial^2 m_K}{\partial u^2} + \frac{w_K}{\rho u} \tag{12}$$

where

$$\tau = \mu(\partial u/\partial y) \tag{13}$$

If the "frozen" Prandtl number is considered to be unity, these equations further reduce to

$$\frac{\partial h}{\partial \xi} = \frac{\tau^2}{\rho u \mu}\frac{\partial^2 h}{\partial u^2} + \frac{Q_v}{\rho u} \tag{14}$$

and

$$\frac{\partial m_K}{\partial \xi} = \frac{\tau^2}{\rho u \mu}\frac{\partial^2 m_K}{\partial u^2} + \frac{w_K}{\rho u} \tag{15}$$

In principle, the model of Fig. 1 can be achieved by injecting any fuel-air mixture which is richer than stoichiometric, i.e., so that oxygen must diffuse from the free stream to the combustion zone in order to complete the combustion. The transformed conservation equations will be employed to investigate the diffusion flame under these conditions. As a simplifying approximation, a kind of local similarity is assumed; in particular, the rate of change of either enthalpy or concentration with downstream distance along any given velocity contour is neglected at each station where profile calculations are made. Such an assumption breaks down near the leading edge, but it is no worse than boundary layer simplifications in that respect, for the configuration considered here. Eqs. (14) and (15) then become

$$\tau^2(\partial^2 h/\partial u^2) + \mu Q_v = 0 \tag{16}$$

and

$$\tau^2(\partial^2 m_K/\partial u^2) + \mu w_K = 0 \tag{17}$$

Because the flame is controlled by diffusion, it is reasonable to consider that $Q_v, w_K = 0$ everywhere in the flow except at a thin sheet of chemical reaction if the Kth species is a reactant or product. In other words, fast forward reaction rates are assumed. A method which does not require any restrictions on the reaction rate or chemical mechanism is described in a later portion of this section. The present method, however, emphasizes the essential physical features of the problem, perhaps with an attendant sacrifice of quantitative precision. Eqs. (16) and (17) are solved most easily in a piecewise fashion, that is, over regions bounded on at least one side by a flame sheet. Within such regions and for $\tau \neq 0$, Eqs. (16) and (17) reduce to

$$d^2h/du^2 = 0 \tag{18}$$

and

$$d^2m_K/du^2 = 0 \tag{19}$$

implying that h and m_K can be found uniquely as linear functions of u if there exist appropriate relationships governing their boundary values. The energy and species equations are, therefore, effectively decoupled from the global continuity and momentum equations over each region.

The boundary value relationship at the wall is obtained by equating the total mass flux fed to the porous slab to the sum of convective and diffusive transport rates of fuel species from the surface, or

$$m_{fe}\rho_e v_e = m_{fo}\rho_o v_o - \rho_o \mathfrak{D}_{fM}\frac{\partial m_f}{\partial y}\Big]_o \tag{20}$$

The chemical subscripts f and M denote, respectively, fuel and mixture. As illustrated in Fig. 1, the local subscripts e and o refer to conditions at the entrance

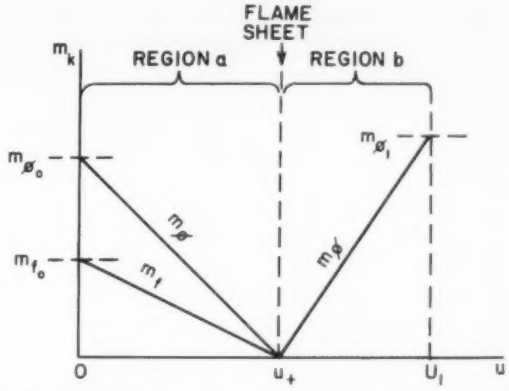

FIG. 2. Variation of species concentrations with downstream velocity for $Le_K = Pr = 1$, and $\bar{x}$ = constant.

of the pores and at the external surface of the wall, respectively. In deriving Eq. (20), it is assumed that no chemical reactions occur before the mixture enters the external flow and that mass transfer parallel to the wall surface is negligible within the wall. The quantities m_{fe} and $\rho_e v_e$ are independent variables, but m_{fo} and the diffusion term are controlled by flow conditions. But by global conservation of mass $\rho_o v_o = \rho_e v_e$, so Eq. (20) may be rewritten as

$$m_{fe}\rho_o v_o = m_{fo}\rho_o v_o - \rho_o \mathfrak{D}_{fM}\frac{\partial m_f}{\partial y}\Big]_o \tag{21}$$

The mass balance at the flame is based on the following conditions: (1) fuel and oxygen fluxes enter the flame in stoichiometric proportions; (2) fuel and oxygen concentrations vanish at the flame; and (3) the normal diffusive mass fluxes to the flame are large in comparison with any other components of mass flux. Condition (3) is consistent because of the relatively small inclination of the flame to the wall, arising from boundary layer simplifications. Mathematically expressed, the mass balance at the flame is

$$-\left[\rho\mathfrak{D}_{fM}\frac{\partial m_f}{\partial y}\right]_{+a} = r\left\{\left[\rho\mathfrak{D}_{\phi M}\frac{\partial m_\phi}{\partial y}\right]_{+b} - \left[\rho\mathfrak{D}_{\phi M}\frac{\partial m_\phi}{\partial y}\right]_{+a}\right\} \tag{22}$$

Each quantity in brackets is evaluated at the flame sheet approaching either from region a or b as indicated by the subscript following the $+$ sign. Figure 2 shows the respective regions. The stoichiometric constant of proportionality is denoted by r and the oxygen species by the subscript ϕ.

Manipulation of the linear forms of the profiles of m_K versus u in Fig. 2 is the key to solving Eqs. (21) and (22) in order to find the value of u at the flame. The solution of the velocity boundary layer $u(x, y)$ by the methods of reference 9 can then be used if the y coordinate of the flame is desired. In the present work, however, only the u coordinate is found. Two additional definitions are useful in the remainder of the analysis:

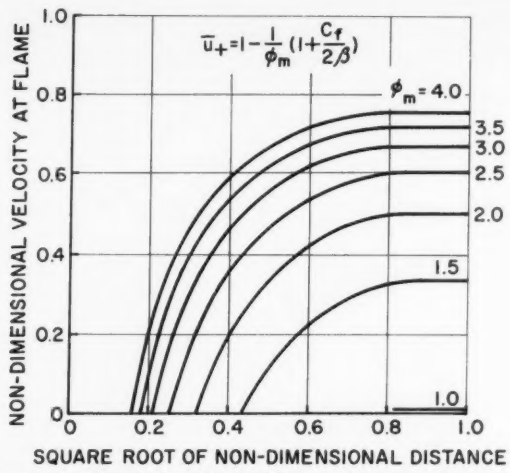

FIG. 3. Position of the diffusion flame as determined by mixture and flow parameters.

$$\beta = \rho_o v_o / \rho_1 U_1 \tag{23}$$

and

$$c_f = \tau_o / (1/2)\rho_1 U_1^2 \tag{24}$$

Incorporation of Eqs. (13), (23), (24) and the conditions $\overline{Pr} = Le_K = 1$ into Eq. (21) yields

$$m_{fe} = m_{fo} - \frac{c_f}{2\beta} U_1 \frac{dm_f}{du}\bigg]_o \tag{25}$$

The slope $dm_f/du]_o$ is seen to be $-m_{fo}/u_+$ from inspection of Fig. 2. u_+ is the downstream velocity at the flame. Thus, Eq. (25) becomes

$$m_{fo} = \frac{m_{fe}}{1 + (c_f/2\beta\bar{u}_+)} \tag{26}$$

Similar operations on Eq. (22) give

$$-\tau_+ \frac{dm_f}{du}\bigg]_{+a} = r\left\{\tau_+ \frac{dm_\phi}{du}\bigg]_{+b} - \tau_+ \frac{dm_\phi}{du}\bigg]_{+a}\right\} \tag{27}$$

Dividing each side of Eq. (27) by τ_+, which is single-valued, and substituting the slopes obtained from Fig. 2, the following expression is found for the non-dimensional downstream velocity at the flame:

$$\bar{u}_+ = \frac{m_{fo} - r m_{\phi o}}{m_{fo} - r(m_{\phi o} - m_{\phi 1})} \tag{28}$$

Substitution in Eq. (28) of m_{fo} from Eq. (26) and of $m_{\phi o}$ from an analogous formula gives an equation for $\bar{u}_+$ as a function of flow parameters and known concentrations. Eq. (28) thus becomes

$$\bar{u}_+ = \frac{m_{fe} - r[m_{\phi e} + (c_f/2\beta)m_{\phi 1}]}{m_{fe} - r(m_{\phi e} - m_{\phi 1})} \tag{29}$$

For the particular model chosen, Eq. (29) can be further simplified. Because the composition of air can be considered uniform, the oxygen concentration in the injected mixture is related to that in the free stream by

$$m_{\phi e} = (1 - m_{fe})m_{\phi 1} \tag{30}$$

Substitution of Eq. (30) into Eq. (29) gives

$$\bar{u}_+ = 1 - \frac{r m_{\phi 1}[1 + (c_f/2\beta)]}{m_{fe}(1 + r m_{\phi 1})} \tag{31}$$

From the definition of r, the expression $r m_{\phi 1}/(1 + r m_{\phi 1})$ is the stoichiometric mass concentration of fuel in a fuel-air mixture. If an equivalence ratio Φ_m is defined as the ratio of m_{fe} to the stoichiometric concentration, Eq. (31) can be rewritten as

$$\bar{u}_+ = 1 - \frac{1}{\Phi_m}\left(1 + \frac{c_f}{2\beta}\right) \tag{32}$$

$\bar{u}_+$ is thereby a function of $c_f/2\beta$ with Φ_m as a parameter. In order to evaluate $c_f/2\beta$, only Eqs. (1) and (2) need be solved subject to the boundary condition $\rho_o v_o$ = constant, since these equations have been decoupled from the energy and species equations. The desired solution[9, 10] yields the friction parameter $c_f(\rho_1 U_1 x/\mu_1)^{1/2}$ as a function of the square root of a nondimensional distance $\sqrt{\xi}$ defined by

$$\sqrt{\xi} = \beta\sqrt{\rho_1 U_1 x/\mu_1} \tag{33}$$

Thus, from Eq. (32) and the boundary layer solution, $\bar{u}_+$ is ultimately a function of $\sqrt{\xi}$ with Φ_m as a parameter. Figure 3 shows the function in graphical form. The intersection of the flame with the wall ($\bar{u}_+ = 0$) is the boundary between the surface combustion regime and the diffusion flame regime. At the stoichiometric concentration, surface combustion would occur over the entire plate. As the parameter $c_f/2\beta$ approaches zero because of vanishing shear stress at the wall, the flame position is controlled mainly by the equivalence ratio Φ_m. The model cannot be a good approximation near the leading edge unless thermal and chemical conditions permit burning at the surface regardless of local concentration.

With methods exactly parallel to those just employed, the heat transfer problem can be handled. Two balance equations—one at the surface and one at the flame—are used in conjunction with Eq. (18) to determine the enthalpy at the flame in terms of $\bar{u}_+$. The method can be checked for consistency by substituting Eq. (32) for $\bar{u}_+$ into the enthalpy formula and thereby obtaining the adiabatic combustion enthalpy for stoichiometric burning. The steps are detailed in reference 7.

Two Generalizations of the Analysis

Cohen, *et al.*[3] have indicated that multiple flame sheets can also be analyzed with the boundary layer conservation equations in the Crocco variables. The double-branched or bifurcated flame, therefore, can be treated with a simple extension of the above theory. Physically, the bifurcated flame is interesting because rich hydrocarbon-air mixtures give rise to an inner flame yielding partially combustible products which, in turn, burn in an outer flame with oxygen from external air. Water vapor and carbon monoxide exist in concentrations approximating a "water gas" equilib-

rium with hydrogen and carbon dioxide in the gas between the branches of the bifurcated flame. Both this and the double-cone Bunsen flame are manifestations of the phenomena described by Browne and Powell[11] as the "first and second stoichiometric," corresponding to the two oxidation states of carbon.

Since the bifurcated flame analysis is very similar to the single flame analysis already given, only the results will be stated here. The nondimensional downstream velocity at the outer branch is independent of the location of the inner branch and is theoretically equal to the value for the single flame given by Eq. (32). The position of the inner branch is determined largely by chemical kinetics rather than by diffusion. A more complete discussion of these points is presented elsewhere.[7]

A generalization still broader than that of multiple flame sheets can be introduced. Only a verbal explanation will be given here because only a synthesis of existing techniques is necessary. Basically, the need for specifying discrete flame sheets is eliminated by using redefined dependent variables in conjunction with recent inhomogeneous combustion theory. Thus, this refinement of the present method does not require any sort of chemical flame model.

Enthalpy and concentrations can be redefined following the boundary layer analyses of Denison and Dooley[2] and Lees.[4] A similar redefinition of concentration was used earlier by Spalding[12] for investigating combustion of a liquid surface. The inhomogeneous combustion approach proposed by Browne and Powell[11] can be employed instead of the Burke and Schumann[13] diffusion flame model used in the previous analysis. The new form of enthalpy is taken to include flow kinetic energy and chemical formation energy in addition to thermal energy, and mass concentrations of chemical elements are used rather than those of species. Of course, the concentration of an element includes all of the atoms of that particular element whether they be free or combined in radicals or compounds. The net effects of the redefinitions are the removal of assumptions (3) and (4) and the appearance of atomic conservation equations in place of species conservation equations. No production term appears in the energy equation because the heats of reactions are all absorbed in the heats of formation now included in the enthalpy. Moreover, no production terms appear in the atomic equations because the atoms merely change partners in chemical reactions and thus do not lose their intrinsic identities. A single differential operator can be defined such that its application to the downstream velocity, to the total enthalpy, and to the atom concentrations gives the momentum equation, the energy equation and the atomic equations, respectively. If boundary conditions are compatible, i.e., if the total enthalpy and the atom fractions at the surface vary slowly enough with downstream distance, the similarity can be invoked to solve combustion problems over a single region without any stipulations as to reaction rates. The Browne and Powell method of calculating concentration profiles can, therefore, be extended to boundary layer flows. Where those authors employed "a hydrodynamic correction factor" to an equation involving purely diffusive transport and no convection, the method here suggested makes use of a velocity boundary layer solution which can be applied with the Crocco forms of the energy and atom conservation equations. Thus, the transfer of momentum and energy are accounted for directly, in addition to the transfer of mass. This generalized approach should be used for the boundary layer problem if an improvement in accuracy is sought or if a reasonably good reaction model is not known, but the previous calculations based on the simple model suffice for the purposes of the present work.

Reynolds Analogy for Mass and Heat Transfer

A relationship between the heat flux, the mass flux, and the shear stress at the wall is useful for estimating heat transfer rates. The analysis turns now to the assumption of a combustion model slightly more general than the previous one. A one-step reaction is assumed so that the generation of sensible heat is directly dependent upon the disappearance of fuel, and the thin flame limitation is no longer necessary. A Reynolds analogy for the film combustion of a liquid fuel was developed by Emmons[1] and was based on such a reaction scheme.

The negative product of the constant-pressure heating value H and the fuel species production w_f is substituted for the energy production Q_v in Eq. (16) to give

$$\frac{\tau^2}{\mu}\frac{\partial^2 h}{\partial u^2} - Hw_f = 0 \tag{34}$$

Multiplication of Eq. (17) by H, which is considered constant, results in

$$\frac{\tau^2}{\mu}\frac{\partial^2 (Hm_f)}{\partial u^2} + Hw_f = 0 \tag{35}$$

The sum of Eqs. (34) and (35) is

$$\frac{\tau^2}{\mu}\frac{\partial^2}{\partial u^2}(h + Hm_f) = 0 \tag{36}$$

Since a slow surface variation of either h or m_f with downstream distance was assumed by the previous local similarity simplification, there is for nonzero shear a linear relationship between $(h + Hm_f)$ and $\bar{u}$, which holds for $0 \leqslant \bar{u} \leqslant 1$. Effectively, the addition of Eqs. (34) and (35) combines the heat and mass transfer aspects of the problem. If the free stream gas contains no fuel, the linear relationship assumes the form

$$h + Hm_f = (h_o + Hm_{fo})(1 - \bar{u}) + h_1\bar{u} \tag{37}$$

Differentiation of Eq. (37) with respect to y and evaluation of the result at the wall is indicated by

$$\left.\frac{\partial h}{\partial y}\right]_o + H\left.\frac{\partial m_f}{\partial y}\right]_o = -\frac{(h_o - h_1 + Hm_{fo})}{U_1}\left.\frac{\partial u}{\partial y}\right]_o \quad (38)$$

The Reynolds analogy follows directly from Eq. (38) with substitutions for the gradients normal to the wall. The concentration derivative is replaced by solving for it from Eq. (21), and the velocity derivative is found from Eq. (13). Both Eq. (13) and Eq. (21) are boundary conditions. It remains to solve for the enthalpy derivative in terms of the heat flux, which is the sum of conductive and diffusive contributions. The heat flux to the wall is written as

$$q_o = k\left.\frac{\partial T}{\partial y}\right]_o + \left.\sum_{K=1}^{n} \rho \mathfrak{D}_{KM} h_K \frac{\partial m_K}{\partial y}\right]_o \quad (39)$$

Substituting of Eq. (7) for the conductive term into Eq. (39) and setting $Le_K = 1$ gives

$$q_o = \frac{k}{\bar{c}_p}\left.\frac{\partial h}{\partial y}\right]_o \quad (40)$$

Now, all the derivatives in Eq. (38) can be replaced to give the Reynolds analogy as

$$q_o = -\frac{(h_0 + Hm_{fo} - h_1)}{U_1}\tau_o + H(m_{fe} - m_{fo})\rho_o v_o \quad (41)$$

Note that as m_{fo} and $\rho_o v_o$ approach zero, Eq. (41) becomes the usual expression of the analogy for boundary layer flow over an impermeable wall. At the boundary layer blowoff condition described in the literature,[10, 14] $\tau_o \rightarrow 0$, and from Eqs. (24) and (26) $m_{fo} \rightarrow m_{fe}$; therefore, $q_o \rightarrow 0$.

Conclusions

Certain features of the behavior of a flame in the boundary layer on a porous flat plate with uniform mixture injection have been investigated theoretically. In the analytical approach, the effects of varying the injected mixture composition have been considered, as well as those arising from the flow conditions. The distance over which surface combustion predominates increases with decreasing equivalence ratio for rich injected mixtures. In the limit of stoichiometric concentration, surface combustion occurs over the entire plate. Although the simple diffusion flame criteria should suffice for examining basic trends, analyses of complicated chemical systems can be carried out by incorporating more advanced combustion concepts in the boundary layer theory. Some insight into the influence of injection and combustion on the heat transfer rate is gained by the development of a generalized Reynolds analogy.

References

[1] Emmons, H. W., *Film Combustion of a Liquid Fuel*, Harvard University, Combustion Aerodynamics Laboratory, Interim Technical Report No. 6, June, 1953.

[2] Denison, M. R., and Dooley, D. A., *Combustion in the Laminar Boundary Layer of Chemically Active Sublimators*, Aeronutronic Systems Inc., Publication U-110, September, 1957.

[3] Cohen, C. B., Bromberg, R., and Lipkis, R. P., *Boundary Layers with Chemical Reactions Due to Mass Additions*, Ramo-Wooldridge Corp., Guided Missiles Research Division, GM-TR-268, October, 1957.

[4] Lees, L., *Convective Heat Transfer with Mass Addition and Chemical Reactions*, Third Combustion and Propulsion Colloquium, AGARD, NATO, March, 1958.

[5] Hartnett, J. P., and Eckert, E. R. G., *Mass Transfer Cooling with Combustion in a Laminar Boundary Layer*, Heat Transfer and Fluid Mechanics Institute of 1958, Preprint, pp. 54–68, Stanford University Press, Stanford, 1958.

[6] Dorsch, R. G., Serafini, J. S., Fletcher, E. A., and Pinkel, I. I., *Experimental Investigation of Aerodynamic Effects of External Combustion in Airstream below Two-Dimensional Supersonic Wing at Mach 2.5 and 3.0*, N.A.S.A Memo 1-11-59E, March, 1959.

[7] Eschenroeder, A. Q., *Flame Stabilization in the Boundary Layer of a Porous Flat Plate*, Doctoral Thesis, Cornell University, 1959.

[8] Crocco, L., *Una Caratteristica Trasformazione delle Equazioni dello Strato Limite nei Gas*, Atti di Guidonia, N. 7, pp. 105–120, May 10, 1939.

[9] Eschenroeder, A. Q., *The Compressible Laminar Boundary Layer With Constant Injected Mass Flux at the Surface*, Readers Forum, Journal of the Aero/Space Sciences, Vol. 26, No., 11, p. 762, November, 1959.

[10] Lew, H. G., and Fanucci, J. B., *An Exact Solution of the Laminar Boundary Layer with Zero Pressure Gradient and Homogeneous Injection*, Pennsylvania State University, Technical Report No. 6, July, 1955.

[11] Browne, W. G., and Powell, H. N., *A Principle of Mixing Similarity and its Application to Inhomogeneous Combustion*, Sixth Symposium on Combustion, pp. 37–60, Reinhold Publishing Co., New York, 1957.

[12] Spalding, D. B., *The Combustion of Liquid Fuels*, Fourth Symposium on Combustion, pp. 847–864, Williams and Wilkins, Baltimore, 1953.

[13] Burke, S. P., and Schumann, T. E. W., *Diffusion Flames*, Industrial and Engineering Chemistry, Vol. 20, No. 10, pp 998–1004, October, 1928.

[14] Emmons, H. W., and Leigh, D. C., *Tabulation of the Blasius Function with Blowing and Suction*, Aeronautical Research Council Report No. 15,996, June, 1953.

Change of Address

Since the Post Office Department does not as a rule forward magazines to forwarding addresses, it is important that the Institute be notified of changes in address 30 days in advance of publishing date to ensure receipt of every issue of the JOURNAL and AEROSPACE ENGINEERING. Notices should be printed legibly and sent to:

Circulation Department
Institute of the Aerospace Sciences, Inc.
2 East 64th Street, New York 21, N.Y.

Supersonic Flow at the Surface of a Circular Cone at Angle of Attack†

JOSEPH E. WILLETT*
McDonnell Aircraft Corporation

Summary

Formulas for the inviscid flow properties on the surface of a cone at angle of attack are derived for use in conjunction with the M.I.T. cone tables. These formulas are based upon an entropy distribution on the cone surface which is uniform and equal to that of the shocked fluid in the windward meridian plane. They predict values for the flow variables which may differ significantly from the corresponding values obtained directly from the cone tables. The differences in the magnitudes of the flow variables computed by the two methods tend to increase with increasing free-stream Mach number, cone angle and angle of attack.

Symbols‡

a = sound speed
a_1 = free-stream sound speed
$\bar{a}$ = sound speed at zero angle of attack
c = limit speed
c_v = specific heat at constant volume
K_i = coefficients defined by Eqs. (35) through (39) for $i = 1, 2, 3, 4, 5$
M = Mach number
p = pressure
$\bar{p}$ = pressure at zero angle of attack
p_0 = parameter given in third volume of M.I.T. cone tables
p_1 = free-stream pressure
p_2 = parameter given in third volume of M.I.T. cone tables
P_i = functions of θ introduced in Eq. (11) for $i = 1, 2, 3$
q = velocity
Q_i = parameters introduced in Eqs. (47) through (51) for $i = 1, 2, 3, 4, 5$
r = spherical coordinate denoting distance from origin
R_i = functions of θ introduced in Eq. (12) for $i = 1, 2, 3$
S = specific entropy
S_0 = constant reference value of specific entropy
$\bar{S}$ = specific entropy at zero angle of attack
S_i = parameters defined by Eqs. (14), (15), and (16) for $i = 1, 2, 3$
t = time
u = radial component of velocity
$\bar{u}$ = radial component of velocity at zero angle of attack
$\bar{u}_i$ = coefficient of α^i for $i = 1, 2, 3, \ldots$ in power series representation of radial component of velocity on cone surface
U = free-stream velocity
U_i = functions of θ introduced in Eq. (8) for $i = 1, 2, 3$
v = component of velocity in direction of increasing θ
$\bar{v}$ = component of velocity in direction of increasing θ at zero angle of attack
V_i = functions of θ introduced in Eq. (9) for $i = 1, 2, 3$
w = component of velocity in direction of increasing ϕ
W_i = functions of θ introduced in Eq. (10) for $i = 1, 2$
α = angle of attack
γ = ratio of specific heats
ϵ = angle of yaw (defined in the M.I.T. cone tables as the negative of the angle of attack α used herein)
η = parameter given in second volume of M.I.T. cone tables
θ = polar angle of spherical coordinate system
θ_2 = half-angle of solid cone
ξ = parameter given in second volume of M.I.T. cone tables
ρ = density
ρ_0 = parameter given in the third volume of the M.I.T. cone tables
ρ_1 = free-stream density
ρ_2 = parameter given in the third volume of the M.I.T. cone tables
ϕ = azimuth angle of spherical coordinate system

Received October 12, 1959. Revised and received February 18, 1960.

† This paper is a condensation of reference 12.

* Research Scientist.

‡ In Sections (4) and (5), all symbols which represent functions of position are specialized to the cone surface.

(1) Introduction

THE INVISCID SUPERSONIC FLOW past circular cones at zero angle of attack is given by the analysis of Taylor and Maccoll.[1, 2] For finite angles of attack, a perturbation solution which expresses the flow variables as power series in the angle of attack has been developed explicitly to second order by A. H. Stone.[3–5] An extensive set of tables has been prepared at Massachusetts Institute of Technology[6–8] using the solutions of Taylor and Maccoll and of Stone. Unfortunately, the Stone formulation does not in general permit adequate representation of the inviscid flow near the cone surface. Antonio Ferri[9] demonstrated mathematically that the formulation fails in a thin layer at the cone surface. He introduced the concept of a vortical layer of negligible thickness across which the flow variables other than the pressure and the normal component of velocity vary discontinuously from the Stone values to values at the cone surface which may in general be significantly different. Using this concept he derived correction formulas which yield the proper distributions of entropy and velocity at the cone surface to first order in the angle of attack.

In the present paper the vortical-layer corrections for the inviscid flow variables at the cone surface are developed to second order in the angle of attack. A procedure is presented for computing the inviscid values of the pressure, density, magnitude of the velocity, radial and circumferential velocity components, temperature, and Mach number at the cone surface at angle of attack using the M.I.T. cone tables in conjunction with the formulas developed herein.

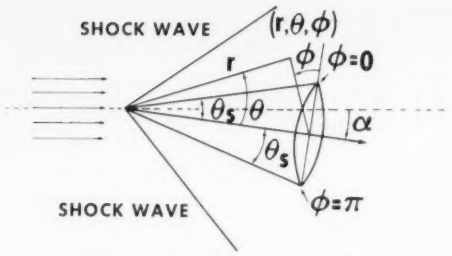

FIG. 1. Body coordinate system.

In view of the possible dispersion of the vortical layer by viscous effects, it is recommended that the properties at the outer edge of the boundary layer be obtained both with and without the vortical-layer corrections to obtain upper and lower limits.

(2) Theoretical Formulation

The problem under consideration consists of the steady inviscid flow near the surface of a circular cone at angle of attack in a supersonic stream. It will be assumed that the cone is not too blunt, so that a shock wave will be attached to the cone apex. It is convenient to formulate the problem in spherical polar coordinates (r, θ, ϕ) with the origin at the cone apex and the polar axis coincident with the axis of the cone (i.e., body coordinates). The azimuth angle ϕ has been chosen so that $\phi = 0, \pi$ corresponds to the plane of symmetry, with $\phi = 0$ representing the leeward meridian plane and $\phi = \pi$ representing the windward meridian plane (see Fig. 1). Let the velocity components at the point (r, θ, ϕ) in the direction of increasing r, θ, and ϕ be denoted by u, v, and w, respectively. Since the flow is conical (i.e., the flow variables are independent of radial coordinate r) and steady (i.e., independent of time t) the differential equations for inviscid flow assume the form

$$2\rho u \sin\theta + \frac{\partial}{\partial\theta}(\rho v \sin\theta) + \frac{\partial}{\partial\phi}(\rho w) = 0 \qquad (1)$$

$$v\frac{\partial u}{\partial\theta} + w\csc\theta\frac{\partial u}{\partial\phi} - v^2 - w^2 = 0 \qquad (2)$$

$$v\frac{\partial v}{\partial\theta} + w\csc\theta\frac{\partial v}{\partial\phi} + \frac{1}{\rho}\frac{\partial p}{\partial\theta} + uv - w^2\cot\theta = 0 \qquad (3)$$

$$v\frac{\partial w}{\partial\theta} + w\csc\theta\frac{\partial w}{\partial\phi} + \frac{\csc\theta}{\rho}\frac{\partial p}{\partial\phi} + uw + vw\cot\theta = 0 \qquad (4)$$

$$v\frac{\partial S}{\partial\theta} + \frac{w}{\sin\theta}\frac{\partial S}{\partial\phi} = 0 \qquad (5)$$

where p, ρ, and S denote pressure, density, and specific entropy, respectively. Eq. (1) expresses the conservation of mass, Eqs. (2), (3), and (4) comprise the conservation of momentum, and Eq. (5) specifies that the flow is adiabatic and reversible. If, in addition, the equation of state for a perfect gas

$$p\rho^{-\gamma}/(\gamma - 1) = e^{(S-S_0)/c_v} \qquad (6)$$

is included, the number of equations equals the number of dependent variables. The solution of this set of equations consistent with the appropriate boundary conditions at the shock and the cone surface completely determines the flow. The symbols γ, c_v, and S_0 denote the ratio of specific heats, the specific heat at constant volume, and a constant reference value of the specific entropy, respectively. The appropriate form of the Bernoulli equation is

$$(q^2/2) + \gamma p/(\gamma - 1)\rho = (U^2/2) + \gamma p_1/(\gamma - 1)\rho_1 = c^2/2 \qquad (7)$$

where q is the velocity at an arbitrary point in the flow, $c^2/2$ is the Bernoulli constant which is completely independent of position and time, and p_1, ρ_1, and U are the free-stream pressure, density, and velocity, respectively.

The perturbation solution of A. H. Stone[3–5] expresses the flow variables in powers of the angle of attack α. The independent variables are θ and ϕ and the ϕ-dependence of each coefficient of α and α^2 is represented by a Fourier series which reduces to one or two terms in each case. The solution which has been developed explicitly to second order only is of the form

$$u = \bar{u} + \alpha U_1\cos\phi + \alpha^2(U_2 + U_3\cos 2\phi) \qquad (8)$$

$$v = \bar{v} + \alpha V_1\cos\phi + \alpha^2(V_2 + V_3\cos 2\phi) \qquad (9)$$

$$w = \alpha W_1\sin\phi + \alpha^2 W_2\sin 2\phi \qquad (10)$$

$$p/\bar{p} = 1 + \alpha P_1\cos\phi + \alpha^2(P_2 + P_3\cos 2\phi) \qquad (11)$$

$$\rho/\bar{\rho} = 1 + \alpha R_1\cos\phi + \alpha^2(R_2 + R_3\cos 2\phi) \qquad (12)$$

where $\bar{u}$, $\bar{v}$, ..., $\bar{\rho}$ are the flow variables at zero angle of attack; these quantities and U_1, U_2, ..., R_3 are functions of the polar angle θ only. The solution retains this form in an alternate spherical polar coordinate system in which the polar axis lies in the direction of the free stream (i.e., wind coordinates). The corresponding functions of the polar angle for wind coordinates have been tabulated under the direction of Z. Kopal[6–8] for various combinations of free-stream Mach number and cone angle. These tabulations may be used in conjunction with the transformation formulas of Roberts and Riley[10] to obtain the functions of θ in Eqs. (8) through (12). Unfortunately, the Stone theory does not comprise the correct inviscid solution within a thin layer adjacent to the cone surface. This difficulty is considered in detail in the next two sections and correction formulas for the flow at the cone surface are developed.

(3) Characteristics of the Vortical Layer

The validity of the Stone theory in a thin layer at the cone surface was first challenged by Antonio Ferri[9] who noted that the entropy distribution predicted by the theory does not satisfy the differential equations for inviscid flow. At the cone surface the

normal velocity component v equals zero and the circumferential velocity component w does not equal zero (except in the plane of symmetry). Consequently, Eq. (5) requires that $\partial S/\partial\phi$ vanish on the cone surface, i.e., that S be constant there. By use of Eqs. (6), (11), and (12) the entropy distribution of the Stone theory can be expressed in the form

$$S = \bar{S} + \alpha S_1 \cos\phi + \alpha^2 (S_2 + S_3 \cos 2\phi) \quad (13)$$

where

$$S_1 = c_v[P_1 - \gamma R_1] \quad (14)$$

$$S_2 = c_v[(\gamma R_1^2/4) - (P_1^2/4) + P_2 - \gamma R_2] \quad (15)$$

$$S_3 = c_v[(\gamma R_1^2/4) - (P_1^2/4) + P_3 - \gamma R_3] \quad (16)$$

In view of the presence of the cosine terms in Eq. (13), the Stone formulation does not yield the constant entropy on the cone surface required by Eq. (5). The analysis of Ferri has shown that all streamlines which are in contact with the cone surface, except those which originate in either the leeward or windward meridian plane, when traced in the flow direction approach asymptotically the leeward generator and when traced in the reverse direction approach asymptotically the windward generator. Since the entropy of each particle is conserved after passage through the shock and the particles whose streamlines are in contact with the surface all pass through the shock at the windward meridian plane, the entropy on the cone surface must equal the (constant) value in the windward meridian plane.

Eqs. (5), (9), (10), and (13) can be combined to obtain

$$\frac{\partial S}{\partial\theta} = \frac{\alpha^2 W_1 S_1 (\sin\phi)^2}{\bar{v}\sin\theta} + 0(\alpha^3) \quad (17)$$

where $\bar{v}$ is the velocity component in the direction of increasing θ at zero angle of attack. Taking the derivative of Eq. (13) with respect to θ, substituting the resulting expression for $\partial S/\partial\theta$ into Eq. (17), using the trigonometric identity

$$(\sin\phi)^2 = (1/2) - (\cos 2\phi)/2 \quad (18)$$

to eliminate $(\sin\phi)^2$, and equating coefficients of like terms of the power series and Fourier cosine series, yields

$$\partial\bar{S}/\partial\theta = 0 \quad (19)$$

$$\partial S_1/\partial\theta = 0 \quad (20)$$

$$\partial S_2/\partial\theta = W_1 S_1/2\bar{v}\sin\theta \quad (21)$$

$$\partial S_3/\partial\theta = -(W_1 S_1/2\bar{v}\sin\theta) \quad (22)$$

The Stone theory assumes that derivatives of the Fourier terms are of the same order as the Fourier terms themselves; e.g., $\alpha^2\partial S_2/\partial\theta$ and $\alpha^2\partial S_3/\partial\theta$ are regarded as being of second order. It is clear, however, that $\bar{v}$ must approach zero near the cone surface and the right member of Eqs. (21) and (22) must approach infinity. Consequently, the Stone theory is expected to fail near the cone surface.

From Eq. (1) specialized to the case of zero angle of attack, $\partial\bar{v}/\partial\theta$ can be shown to be $-2\bar{u}$ at the cone surface, since $\bar{v}$ is zero there. Thus

$$\bar{v} = -2\bar{u}\Delta\theta + 0[(\Delta\theta)^2] \quad (23)$$

where $\Delta\theta$ equals $\theta - \theta_s$, θ_s is the cone half-angle, and the radial velocity component $\bar{u}$ is to be evaluated at θ equals θ_s. Consequently, near the cone surface $\bar{v}$ is of the order of $\Delta\theta$. It follows from Eqs. (21), (22), and (23) that $\alpha^2\partial S_2/\partial\theta$ and $\alpha^2\partial S_3/\partial\theta$, which are assumed in the Stone solution to be of second order, become first-order at an angular distance α from the surface. This conical layer of thickness α at the cone surface has been referred to by Ferri[9] as the vortical layer.

Actually, the layer in which the Stone solution yields incorrect values for the flow variables is not conical. Eqs. (17) and (23) indicate that $\partial S/\partial\theta$ (which the theory regards as being of the order of α^2) becomes of the order of α in a layer of thickness $\alpha(\sin\phi)^2$ and thus at ϕ equals zero or π this layer is of zero thickness. According to Eqs. (19)–(22), $\bar{S}$ and S_1 are independent of θ and although S_2 and S_3 vary with θ the sum $S_1 + S_2$ remains constant. Therefore, S as given by Eq. (13) is independent of θ when ϕ equals zero or π and remains constant all the way to the surface. Since symmetry requires that the w be zero at $\phi = 0$ or π, Eq. (5) requires that S be constant in the windward and leeward meridian planes. Thus the Stone theory is valid even at the cone surface in these two planes. It should be noted that all streamlines except those confined to the windward meridian plane ultimately approach asymptotically the leeward generator of the cone surface, and thus it comprises a singular line.

Consider next the pressure distribution at the surface of cones at angles of attack. Comparison of experimental data with pressure values calculated by the second-order Stone theory shows good agreement despite the failure of the theory to yield the correct entropy distribution.[10, 11] The validity of the second-order Stone expression for the pressure distribution can be established theoretically by consideration of the order of magnitude of the pressure gradient in the vortical layer. From Eq. (3) $\partial p/\partial\theta$ can be seen to be given by

$$\partial p/\partial\theta = -\bar{\rho}\bar{u}\bar{v} + 0(\alpha^2) \quad (24)$$

at an angular distance $\Delta\theta = \alpha$, in view of Eqs. (8), (9), (10), and (12) and the fact that v is of the same order as $\bar{v}$. Since $\bar{v}$ is of the order of $\Delta\theta$, $\partial p/\partial\theta$ is of the order of α at $\Delta\theta = \alpha$ and decreases to zero at the surface. The pressure variation across the vortical layer is of the order of $(\partial p/\partial\theta)\Delta\theta$, which is α^2. The error in the Stone entropy distribution does not effect terms corresponding to zero angle of attack (e.g., $\bar{\rho}$, $\bar{u}$, and $\bar{v}$); thus the resulting error in $\partial p/\partial\theta$ is in terms of the order of α^2, and the error in the pressure at the cone surface is of the order of α^3.

(4) Corrections to the Stone Theory at the Cone Surface

Although the Stone theory yields specious results at and very near the cone surface, formulas can be derived which may be used in conjunction with the Stone solution to obtain the correct inviscid solution. The formulas are based on the following theorems discussed in the preceding section: (i) the entropy at the cone surface is constant and equal to the entropy of the shocked fluid in the windward meridian plane;* (ii) the pressure at the cone surface is given correctly to second order by the Stone theory. In addition, the following boundary condition is applicable: (iii) the normal component of velocity at the cone surface is zero. These three conditions, Eqs. (2) and (7), and appropriate equations of state are sufficient to completely determine the flow variables at the cone surface in terms of the Stone solution parameters. These parameters are obtainable from the M.I.T. cone tables and are expressible in body coordinates by means of the transformation formulas of Roberts and Riley.[10] The body coordinate system of Fig. 1 will be assumed in deriving the correction formulas. In the subsequent discussion all quantities which are, in general, functions of position will be specialized to the flow at the cone surface.

The correct inviscid entropy at the cone surface must be constant and equal to the value at $\phi = \pi$ which, according to Eq. (13) is

$$S = \bar{S} - \alpha S_1 + \alpha^2(S_2 + S_3) \tag{25}$$

The inviscid pressure distribution at the cone is given by Eq. (11). Since the entropy and pressure are thereby known at any point on the cone surface, the thermodynamic state is uniquely determined. Thus any other thermodynamic state variable can be evaluated using the perfect-gas equation of state relating that variable and the pressure and entropy. The correct inviscid density distribution on the cone surface, for example, can be obtained by applying Eq. (6) to the cone surface at angle of attack and, alternately, at zero angle of attack, dividing the former expression by the latter, eliminating $p/\bar{p}$ and $S - \bar{S}$ by means of Eqs. (11) and (25), and expanding each member of the equation in powers of the angle of attack. This procedure yields

$$\begin{aligned}\rho/\bar{\rho} = 1 &+ \alpha[(P_1/\gamma) - R_1] + \alpha\cos\phi[P_1/\gamma] + \\ &\alpha^2[R_2 + (3+\gamma)(P_1^2/4\gamma^2) - (P_1R_1/\gamma) - \\ &(P_3/\gamma) + R_3] + \alpha^2\cos\phi[(P_1^2/\gamma^2) - (P_1R_1/\gamma)] + \\ &\alpha^2\cos 2\phi[(P_3/\gamma) - (\gamma-1)P_1^2/4\gamma^2]\end{aligned} \tag{26}$$

where terms of higher order than the second have been neglected.

Consider next the velocity of the gas at the cone surface. For given free-stream conditions, the Bernoulli equation expresses the square of the velocity as a known function of the enthalpy (which in turn can be expressed as a function of the pressure and density using the appropriate equation of state). Thus the magnitude of the velocity can be evaluated since expressions for the pressure and density are known. Applying Eq. (7) to the cone surface at angle of attack and, alternately, at zero angle of attack, eliminating the Bernoulli constant between the two resulting equations, and solving for q^2 yields

$$q^2 = \bar{u}^2 + \frac{2\gamma\bar{p}}{(\gamma-1)\bar{\rho}} - \frac{2\gamma p}{(\gamma-1)\rho} \tag{27}$$

By introducing the square of the sound speed at zero angle of attack, $\bar{a}^2$, into this equation with the aid of the relation

$$\bar{a}^2 = \gamma\bar{p}/\bar{\rho} \tag{28}$$

and expanding the resulting equation in powers of α by use of Eqs. (11), (26), and (28), q^2 can be expressed in the form

$$\begin{aligned}q^2 = \bar{u}^2 + \frac{2\bar{a}^2}{\gamma-1}\{&\alpha[(P_1/\gamma) - R_1] + \\ &\alpha\cos\phi\,[(1-\gamma)P_1/\gamma] + \\ &\alpha^2[3(\gamma-1)(P_1^2/4\gamma^2) + (P_1R_1/\gamma) - \\ &R_1^2 - P_2 - (P_3/\gamma) + R_2 + R_3] + \\ &\alpha^2\cos\phi[(\gamma-1)(P_1^2/\gamma^2) + (1-\gamma)(P_1R_1/\gamma)] + \\ &\alpha^2\cos 2\phi[(\gamma-1)(P_1^2/4\gamma^2) + (1-\gamma)(P_3/\gamma)]\}\end{aligned} \tag{29}$$

The magnitude of the velocity at the cone surface can be obtained from this equation.

A differential equation for the radial velocity component u can be derived as follows. The normal component of the velocity on the cone surface is zero and the coordinate system is orthogonal; therefore

$$q^2 = u^2 + w^2 \tag{30}$$

On the cone surface Eq. (2) reduces to

$$w = (1/\sin\theta_s)(du/d\phi) \tag{31}$$

where $\theta = \theta_s$ is regarded as a constant parameter and the partial derivative becomes a total derivative. Introducing Eq. (31) into Eq. (30) yields

$$q^2 = u^2 + (\sin\theta_s)^{-2}(du/d\phi)^2 \tag{32}$$

or, alternately,

$$\begin{aligned}q^2 = (u-\bar{u})^2 + (\sin\theta_s)^{-2}[d(u-\bar{u})/d\phi]^2 + \bar{u}^2 + \\ 2\bar{u}(u-\bar{u})\end{aligned} \tag{33}$$

By using Eq. (29) to eliminate q^2, this differential equation assumes the form

$$\begin{aligned}(\sin\theta_s)^{-2}[d(u-\bar{u})/d\phi]^2 + (u-\bar{u})^2 + 2\bar{u}(u-\bar{u}) = \\ \alpha K_1 + \alpha K_2\cos\phi + \alpha^2 K_3 + \alpha^2 K_4\cos\phi + \\ \alpha^2 K_5\cos 2\phi\end{aligned} \tag{34}$$

where

* It will be convenient to express this entropy value as the second-order Stone entropy expression evaluated at the windward generator of the cone.

$$K_1 = \frac{2\bar{a}^2}{(\gamma - 1)\gamma}(P_1 - \gamma R_1) \tag{35}$$

$$K_2 = -2\bar{a}^2 P_1/\gamma \tag{36}$$

$$K_3 = \frac{2\bar{a}^2}{(\gamma - 1)}\{[3(\gamma - 1)P_1^2/4\gamma^2] + [P_1R_1/\gamma] - R_1^2 - P_2 - (P_3/\gamma) + R_2 + R_3\} \tag{37}$$

$$K_4 = 2\bar{a}^2[(P_1^2/\gamma^2) - (P_1R_1/\gamma)] \tag{38}$$

$$K_5 = 2\bar{a}^2[(P_1^2/4\gamma^2) - (P_3/\gamma)] \tag{39}$$

The solution of Eq. (34) can be obtained as follows. Let u be represented by

$$u = \bar{u} + \sum_{i=1}^{\infty} \alpha^i \bar{u}_i \tag{40}$$

where the $\bar{u}_i$ are functions of ϕ only for fixed values of the free-stream conditions and cone angle. Substituting this expression into Eq. (34) and neglecting terms of higher order than α^2 result in

$$\alpha^2(\sin\theta_s)^{-2}(d\bar{u}_1/d\phi)^2 + \alpha^2\bar{u}_1^2 + 2\alpha\bar{u}\bar{u}_1 + 2\alpha^2\bar{u}\bar{u}_2 = \alpha K_1 + \alpha K_2\cos\phi + \alpha^2 K_3 + \alpha^2 K_4\cos\phi + \alpha^2 K_5\cos 2\phi \tag{41}$$

Equating coefficients of like powers of α yields

$$2\bar{u}\bar{u}_1 = K_1 + K_2\cos\phi \tag{42}$$

$$(\sin\theta_s)^{-2}(d\bar{u}_1/d\phi)^2 + \bar{u}_1^2 + 2\bar{u}\bar{u}_2 = K_3 + K_4\cos\phi + K_5\cos 2\phi \tag{43}$$

Thus,

$$\bar{u}_1 = (K_1/2\bar{u}) + (K_2/2\bar{u})\cos\phi \tag{44}$$

and

$$\bar{u}_2 = \left\{\frac{K_3}{2\bar{u}} - \frac{K_1^2}{8\bar{u}^3} - \frac{K_2^2}{16\bar{u}^3}[1 + (\sin\theta_s)^{-2}]\right\} + \left\{\frac{K_4}{2\bar{u}} - \frac{K_1K_2}{4\bar{u}^3}\right\}\cos\phi + \left\{\frac{K_5}{2\bar{u}} + \frac{K_2^2}{16\bar{u}^3}[(\sin\theta_s)^{-2} - 1]\right\}\cos 2\phi \tag{45}$$

By using Eqs. (35) through (39) to eliminate K_1, K_2, ..., K_5 in Eqs. (44) and (45) and using the resulting expressions to eliminate $\bar{u}_1$ and $\bar{u}_2$ in Eq. (40), an expression for the radial component of velocity at the cone surface may be obtained to second order in the form

$$u/\bar{u} = 1 + \alpha(Q_1 + Q_2\cos\phi) + \alpha^2(Q_3 + Q_4\cos\phi + Q_5\cos 2\phi) \tag{46}$$

where

$$Q_1 = \frac{\bar{a}^2(P_1 - \gamma R_1)}{(\gamma - 1)\gamma\bar{u}^2} \tag{47}$$

$$Q_2 = -\frac{\bar{a}^2 P_1}{\gamma\bar{u}^2} \tag{48}$$

$$Q_3 = \frac{3\bar{a}^2P_1^2}{4\gamma^2\bar{u}^2}\{1 - (\bar{a}^2/3\bar{u}^2) \times [1 + 2/(\gamma - 1)^2 + (\sin\theta_s)^{-2}]\} + \frac{P_1R_1\bar{a}^2}{(\gamma - 1)\gamma\bar{u}^2}\{1 + [\bar{a}^2/\bar{u}^2(\gamma - 1)]\} - \frac{R_1^2\bar{a}^2}{(\gamma - 1)\bar{u}^2}\{1 + [\bar{a}^2/2\bar{u}^2(\gamma - 1)]\} + [\bar{a}^2/(\gamma - 1)\bar{u}^2]\{R_2 + R_3 - P_2 - (P_3/\gamma)\} \tag{49}$$

$$Q_4 = [P_1^2 - \gamma P_1R_1]\left[\frac{\bar{a}^2}{\bar{u}^2\gamma^2}\right]\left[1 + \frac{\bar{a}^2}{\bar{u}^2(\gamma - 1)}\right] \tag{50}$$

$$Q_5 = \frac{\bar{a}^2P_1^2}{4\gamma^2\bar{u}^2}\{1 + (\bar{a}^2/\bar{u}^2)[(\sin\theta_s)^{-2} - 1]\} - \frac{\bar{a}^2P_3}{\gamma\bar{u}^2} \tag{51}$$

By substituting Eq. (46) into Eq. (31), an expression for the circumferential component of velocity can be obtained in the form

$$w/\bar{u} = -\frac{\alpha Q_2\sin\phi}{\sin\theta_s} - \frac{\alpha^2(Q_4\sin\phi + 2Q_5\sin 2\phi)}{\sin\theta_s} \tag{52}$$

(5) Procedure for Computing the Inviscid Flow Properties at the Cone Surface

The inviscid flow variables evaluated at the surface of a cone in a supersonic stream at angle of attack are expected to be useful in approximating the conditions at the outer edge of the boundary layer. The following procedure may be employed to compute the pressure, density, magnitude of the velocity, radial and circumferential velocity components, temperature, and Mach number at the surface of the cone using the inviscid flow equations of Section (4) in conjunction with the M.I.T. cone tables.[6-8] The procedure will yield the flow properties in the body coordinate system illustrated in Fig. 1. The azimuth angle ϕ is measured from the leeward meridian plane around the axis of the cone. The angle of attack α is equal to the negative value of the angle of yaw ϵ defined in the cone tables.

For the desired free-stream Mach number (i.e., M with no subscript in the cone tables*) and cone half-angle θ_s, the following quantities are to be taken directly from the tables at the value of θ equal to θ_s:

(i) $\bar{u}$ and $\bar{a}^2$ from the first volume[6] of the tables;**

(ii) $\eta/\bar{p}$ and $\xi/\bar{p}$ from the second volume[7] of the tables;

* The symbol (S) following the M denoting Mach number in the table headings indicates a "second" solution which is believed to be unstable to a high degree; the reliability of the theory for such solutions is questionable.

** Although these two symbols do not have bars over them in the first volume of the cone tables, they do in the second and third volumes. The desired value of the velocity at the cone surface at zero angle of attack is also given in the headings of the second volume and denoted by $\bar{u}_s$.

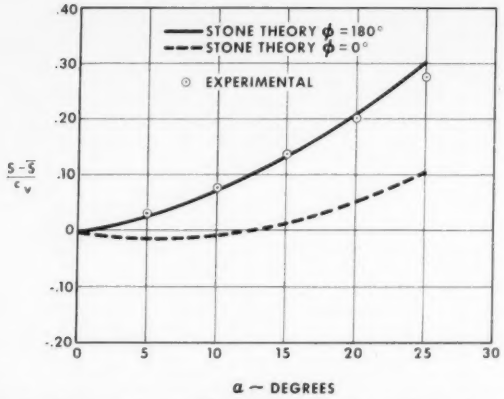

FIG. 2. Increase in specific entropy on the surface of a 15-degree cone at Mach 3.53 due to angle of attack.

(iii) $p_0/\bar{p}$, $p_2/\bar{p}$, $\rho_0/\bar{\rho}$, and $\rho_2/\bar{\rho}$ from the third volume[8] of the tables.

From these values, the quantities P_1, P_2, P_3, R_1, R_2, and R_3 can be evaluated using the equations*

$$\left.\begin{aligned} P_1 &= -\eta/\bar{p} \\ R_1 &= -\xi/\bar{\rho} \\ P_2 &= (p_0/\bar{p}) + (\gamma\bar{u}^2/2\bar{a}^2) + (\eta/2\bar{p})\cot\theta_s \\ P_3 &= (p_2/\bar{p}) + (\gamma\bar{u}^2/2\bar{a}^2) - (\eta/2\bar{p})\cot\theta_s \\ R_2 &= (\rho_0/\bar{\rho}) + (\bar{u}^2/2\bar{a}^2) + (\xi/2\bar{\rho})\cot\theta_s \\ R_3 &= (\rho_2/\bar{\rho}) + (\bar{u}^2/2\bar{a}^2) - (\xi/2\bar{\rho})\cot\theta_s \end{aligned}\right\} \quad (53)$$

with the ratio of specific heats γ equal to 1.405 for air.

The pressure at the cone surface at angle of attack divided by the pressure at the cone surface at zero angle of attack may be computed by means of Eq. (11). The increase in specific entropy due to angle of attack divided by the specific heat at constant volume, $(S - \bar{S})/c_v$, may be computed using Eqs. (14), (15), (16), (25), and (53). Then the density and temperature at the cone surface at angle of attack divided by the corresponding values at zero angle of attack may be computed from the equations of state

$$\rho/\bar{\rho} = (p/\bar{p})^{1/\gamma} e^{-(S-\bar{S})/\gamma c^v} \quad (54)$$

and

$$T/\bar{T} = (p/\bar{p})(\rho/\bar{\rho})^{-1} \quad (55)$$

For zero angle of attack the values of pressure $\bar{p}$, density $\bar{\rho}$, and temperature $\bar{T}$ at the cone surface are obtainable from the free-stream conditions using the first volume of the cone tables.

The limit speed c is given by

$$c^2 = U^2 + 2a_1^2/(\gamma - 1) \quad (56)$$

where U and a_1 are the velocity and sound speed, respectively, of the free stream. The magnitude of the velocity at the cone surface at angle of attack may be computed by means of the Bernoulli equation

$$q^2 + 2\gamma p/(\gamma - 1)\rho = c^2 \quad (57)$$

The square of the Mach number at the cone surface is given by

$$M^2 = (q^2/\bar{a}^2)(T/\bar{T})^{-1} \quad (58)$$

where q and $\bar{a}$ must be expressed in the same units. The sound speed $\bar{a}$ at the cone surface at zero angle of attack is given in the first volume of the cone tables in units of the limit speed c and, consequently, must be multiplied by c to convert to proper units for use in this equation.

The radial velocity component and the circumferential velocity component at the cone surface at angle of attack, each divided by the velocity at zero angle of attack, may be computed using Eqs. (46) through (52). The velocity $\bar{u}$ at the surface of the cone at zero angle of attack is also given in the first volume of the cone tables in units of the limit speed c and must be multiplied by c to convert to proper units.

The flow variables at the edge of the boundary layer can be computed from experimental measurement of the pressure distribution on the cone surface and the angle of the attacked shock in the windward meridian plane for given free-stream conditions and cone angle. The free-stream conditions and the angle of the shock are sufficient to determine the specific entropy in the windward meridian plane and this value may be taken as the approximate value of the specific entropy of the entire outer surface of the boundary layer. The measured pressure and the computed entropy together with the appropriate equations of state determine all other variables of state (e.g., density and temperature). The magnitude of the velocity may then be computed using the Bernoulli equation and the velocity components u and w may be computed using Eqs. (32) and (31). The determination of u and w requires the solution of a second-order differential equation.

(6) Concluding Remarks

The Stone theory, which describes the supersonic flow over cones at angle of attack, does not, in general, yield the correct inviscid-flow variables (except pressure) on and very near the cone surface. Fig. 2 shows the increase in entropy on the cone surface due to angle of attack for a 15-degree cone at free-stream Mach 3.53. Note that the second-order Stone theory values at 180 degrees are in good agreement with values computed from the shock photographs of reference 11 for angles of attack up to nearly 25 degrees. The uncorrected Stone theory predicts a continuous variation of entropy around the cone surface from the value given by the solid line to that given by the broken line. The entropy correction is clearly needed in this case. The importance of the correction increases with increase in the cone angle, Mach number, and angle of attack.

(*Continued on page 920*)

* These equations transform the wind-coordinate parameters of the cone tables to the body-coordinate parameters of this paper. They are obtained by direct comparison of Eqs. (29) and (30) of reference 10 with Eqs. (11) and (12) of the present paper.

The Epicycle Method for the Reduction of Flight-Test Data Using a Digital Computer†

R. P. DANIS*

Avco Research and Advanced Development Division

Summary

The problem of determining aerodynamic characteristics of ICBM re-entry vehicles from flight-test programs is made more difficult because available instrumentation is limited to measuring linear accelerations and angular rates. Therefore, the angle of attack and certain aerodynamic coefficients must be determined by reducing these measurements of the motion in conjunction with trajectory and atmospheric data.

The data reduction method presented in this paper uses rate gyro data, and is based on the assumption that the solution of the equation of the pitching and yawing motions is in the form of the sum of two rotating vectors. The basis for this approach lies in the fact that the solution of the differential equation of motion (in a body-axis system) is the sum of two rotating vectors, that is, an epicycle for both the angle of attack and the angular rate. The solution requires the usual assumptions that the aerodynamic forces and moments are linear independent functions of the angle of attack and that the angles are small. The method of computing the magnitude and frequency of the two rotating vectors involves an iteration on a digital computer and is presented in detail.

Symbols

A, B, C, D	= constants appearing in Eq. (9)
A	= reference area
F	= applied forces
I	= moment of inertia
M	= applied moment
V	= velocity of body relative to free stream
C_1, C_2	= initial magnitude of epicycle vectors for angle of attack
C_3	= initial trim position due to vehicle asymmetry
K_1, K_2	= initial magnitude of epicycle vectors for angular rate
D	= reference length
u, v, w	= velocity of X, Y, Z axes
p, q, r	= angular rate of X, Y, Z axes
$u_1, u_2, \theta_1, \theta_2$	= epicycle parameters
m	= mass of vehicle
C_{m_α}	= rate of change of aerodynamic moment coefficient with respect to angle of attack
C_{m_q}	= rate of change of moment coefficient with angular rate
C_{n_α}	= rate of change of normal force with respect to angle of attack
ω	= angular rate of vehicle $(q + ir)$ in plane normal to x-axis
ϕ_1, ϕ_2	= initial phase angles of epicycle vectors
Φ_1, Φ_2	= total angle turned through by epicycle vectors
ω_1, ω_2	= angular velocity of epicycle vectors
ρ, μ, λ	= constants appearing in Eqs. (1)–(4)
α	= $\tan^{-1}(w/u)$ = angle of attack
β	= $\tan^{-1}(v/u)$ = angle of sideslip
α'	= $\cos^{-1}(u/V)$ = total angle of attack
$\dot{\alpha}'$	= rate of change of angle of attack with respect to body axes
$\dot{\alpha}_s'$	= rate of change of α' with respect to nonrolling (space) axes referred to body axes (equal to $\dot{\alpha}' + p \times \alpha'$)
$\dot{\alpha}_{ss}'$	= $\dot{\alpha}_s'$ referred to space axes (equal to $\dot{\alpha}_s' e^{ipt}$)

Received October 14, 1959. Revised and received May 13, 1960.

† This work was supported by the U. S. Air Force, Ballistic Missile Division, under Contract No. AF 04(647)-305.

* Assistant Manager, Titan/Atlas Re-entry Vehicle R&D Project Office.

Introduction

BECAUSE THE PERFORMANCE of a re-entry vehicle depends considerably on its aerodynamic characteristics, the objectives of a re-entry vehicle flight-test program include the determination of the vehicle's stability characteristics. The conventional methods used to reduce aerodynamic test data require precise measurements of the vehicle's trajectory, attitude, angle of attack, angular rate and, in static tests, direct measurements of the force and moments involved. However, in re-entry flight tests, the airborne instrumentation is usually limited to internal measurement of the vehicle motions. The problem facing the analyst, then, is to determine the angle-of-attack envelope and the stability characteristics of a re-entry vehicle (in terms of the moment and force coefficients), given only telemetered measurements of the angular rates and linear accelerations of the re-entry vehicle.

The approach suggested in this paper makes use of the fact that the solution of the equations of motion for the angular velocity can be represented as the sum of two rotating vectors (epicyclic motion), the magnitudes of which are time-varying functions of the moment and force coefficients, atmospheric density, roll rate, and the vehicle free-stream velocity. The test data are then "fitted" with an epicyclic equation, whereby they are smoothed and numerical values are obtained for the magnitude and frequency of the two vectors from which, the density and velocity being known, the stability derivatives may be derived. The presentation of the numerical technique with which the parameters of the epicycle (magnitude and frequency) may be determined from test data is the main intent of the following sections.

The Epicyclic Solution of the Equations of Motion

The equations of motion for a rolling, axisymmetric vehicle can be solved by making certain assumptions,

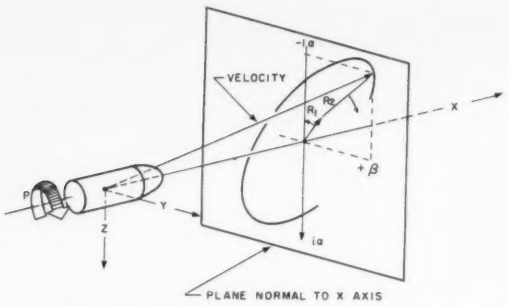

FIG. 1. Schematic of epicyclic pitching and yawing motion.

the principal one being that the moment and force coefficients are linear functions of the angle of attack. In many cases, it is convenient to study the pitching and yawing motions for short intervals of time (or altitude) so that the density, velocity, and roll rate may be considered constant, whereas in other applications requiring greater accuracy, the rates of change of density and velocity must be considered.[1–5] However, in all cases the oscillatory motion of the vehicle can be approximated by an epicycle. Fig. 1 is a schematic representation of this type of motion which can be written in a body-axis reference system as follows:

$$\alpha' = C_1 e^{u_1(t) + i\theta_1(t)} + C_2 e^{u_2(t) + i\theta_2(t)} + C_3$$
$$\alpha' = \beta + i\alpha$$

where u_1, u_2, θ_1, θ_2 are functions of the aerodynamic coefficients, density, velocity, and roll rate. C_3, a function of asymmetry, which is quite small for most missiles in comparison to C_2 and C_1, will be ignored in subsequent discussion although it can readily be handled if it appears. Note, however, that in a space-fixed system this term would cause the motion to appear tricyclic.

Since the available data do not include direct measurements of the angle of attack, it is expeditious to express the solution of the equations of motion in terms of the angular rates, since well-developed rate-measuring instruments are available. This is usually not difficult, since ω appears as an independent variable similar to α'. In other words, aerodynamic forces determine the angular rates of a vehicle as uniquely as they do its attitude or angle of attack. This is illustrated in Appendix A where a solution for the equations of motion, applicable for short time intervals, is presented. Although this may not be the best form of the solution for final coefficient analysis, it does illustrate, among other things, that the desired aerodynamic coefficients appear in terms of the epicycle parameters. In general, the epicycle method has two main advantages; first, it provides optimum filtering of the rate data even if the data contain considerable noise, and second, the aerodynamic coefficients are easily determined from the solution of the epicycle equation. The main limitations are that it can be applied only when the motion is harmonic and when the moment and forces are linear functions of the angle of attack. However, within certain limits, the approach can be applied when the system is operating in the nonlinear range, but the coefficients determined will represent "average" values. This limits their interpretation, but not necessarily their usefulness.

The Determination of the Epicycle Parameters

The determination of the stability derivatives was shown in the previous section to depend on determining the parameters of the epicycle. Since the flight-test vehicle motions are most frequently recorded by rate gyros, the method will be developed in notation that represents angular rate data. It should be noted, however, that missile attitude or angular accelerations may also be used as an input.

Of the many possible methods for determining the best-fitting epicycle through a series of data points, the most desirable is, of course, one which is rapid, automatic, and readily applicable to modern high-speed digital computers. The straightforward numerical procedures found in most texts,[6] however, are extremely sensitive to the accuracy of the data. This limitation was overcome by use of an approach suggested by the Naval Ordnance Test Station (NOTS), China Lake, California, for a different application but one which could be adapted to the flight-test problem. This approach utilizes an iteration procedure that converges rapidly. It begins with an initial input of the angular rates of the rotating vectors. Successive passes improve on the initial values and also determine the other parameters of the epicycle, by use of the criterion that the square of the deviations from the mean must be a minimum.

The basic problem is to fit the motions of the two vectors (see Fig. 2) to a series of time-dependent data points. This motion is described by

$$\omega = q + ir = e^{u_1 + i\theta_1} + e^{u_2 + i\theta_2} \tag{1}$$

where
$$u_1(t) = \rho_1 + \lambda_1 t + \mu_1 t^2 = \log K_1 \tag{2a}$$
$$u_2(t) = \rho_2 + \lambda_2 t + \mu_2 t^2 = \log K_2 \tag{2b}$$
$$\theta_1(t) = a_1 + b_1 t + c_1 t^2 + d_1 t^3 \tag{3}$$
$$\theta_2(t) = a_2 + b_2 t + c_2 t^2 + d_2 t^3 \tag{4}$$

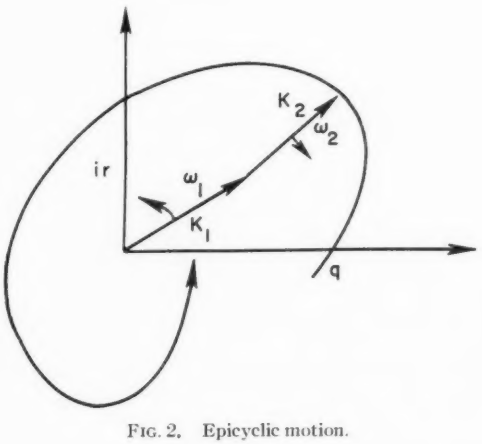

FIG. 2. Epicyclic motion.

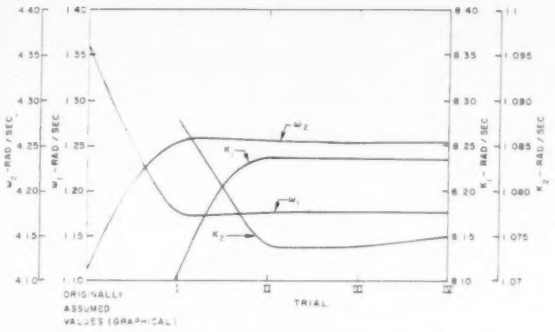

FIG. 3. Examples of convergence of test data.

Eq. (1) may be rewritten

$$q = K_1 \cos \theta_1 + K_2 \cos \theta_2 \tag{5}$$

$$r = K_1 \sin \theta_1 + K_2 \sin \theta_2 \tag{6}$$

where q and r are the pitch and yaw angular rates referred to a body-axis system.

By breaking up the data into small time groups, the influence of damping and second- and third-order derivatives of θ may be ignored. Thus, Eqs. (5) and (6) become

$$q = K_1 \cos (\omega_1 t + \phi_1) + K_2 \cos (\omega_2 t + \phi_2) \tag{7}$$

$$r = K_1 \sin (\omega_1 t + \phi_1) + K_2 \sin (\omega_2 t + \phi_2) \tag{8a}$$

where K_1, and K_2 are constants, and $\phi = a$ and $\omega = b$. Further, by letting

$$\left.\begin{aligned} A &= K_1 \cos \phi_1 \qquad B = K_1 \sin \phi_1 \\ C &= K_2 \cos \phi_2 \qquad D = K_2 \sin \phi_2 \end{aligned}\right\} \tag{8b}$$

Eqs. (7) and (8a) become

$$\left.\begin{aligned} q &= A \cos \omega_1 t - B \sin \omega_1 t + \\ &\qquad C \cos \omega_2 t - D \sin \omega_2 t \\ r &= A \sin \omega_1 t + B \cos \omega_1 t + \\ &\qquad C \sin \omega_2 t + D \cos \omega_2 t \end{aligned}\right\} \tag{9}$$

The problem is now to find A, B, C, D, ω_1 and ω_2. If straightforward numerical fits were employed at this point to solve for all six unknowns, the difficulty mentioned earlier would appear. Instead, therefore, values of ω_1 and ω_2 are determined approximately from plots of rate gyro data, and these values are used in the first calculations. The normal equations for the least-squares fit of Eqs. (9) are derived in the usual manner.[6]

Once A, B, C and D are determined, K_1, K_2, θ_1 and θ_2 are calculated for each group from Eqs. (8b). Next, from the ϕ's of each group, the total angle turned through for each vector from $t = 0$ can be calculated. Then by taking the derivative of this function, new values of ω_1 and ω_2 are obtained for the next trial. Likewise, the variation in K from group to group may be used to compute the complete damping function. The trials are repeated until the function converges and/or the fit of the analytical solution and the data points is acceptable. The mathematical details are covered in Appendix C.

A computer routine which accomplishes the above calculations has been programmed for a DATATRON digital computer. Examples of the convergence taken from test data are presented in Fig. 3. It should be noted that had the rate data contained any indication of an off-center "trim" position due to vehicle asymmetry, the effect could have been removed prior to the fitting of the epicycle by transforming the rate data to the trim position with appropriate numerical procedures. This procedure is identical with removing a "bias" introduced by an off-center gyro calibration.

Determination of Angle of Attack

Of the several methods investigated for determining angle of attack, the technique presented here is potentially the most accurate for those cases where the angles of attack are relatively small.

The basis for this method is the fact that if the vehicle is not plunging (that is, if the lift is small) the rate of change of angle of attack is equivalent to the angular rate of the body. This can be seen if the force equation with the gravity term omitted (derived in Appendix B) is examined:

$$\dot{\alpha}' + ip\alpha' = i(q + ir) + \{[\Sigma(F_y + iF_z)]/mV\} \tag{10}$$

The left-hand side can be recognized as the rate of change of angle of attack with respect to the nonrolling, space-fixed axes resolved along the body axes. Now if the vehicle configuration is such that the lateral forces are small or the trajectory altitude sufficiently high, the equation reduces to

$$\dot{\alpha}' + ip\alpha' = i(q + ir) = i\omega \tag{11}$$

It is further shown in Appendix B that ω is epicyclic in form, and that the relationship between the magnitude of angle of attack and the parameters of the epicycle of the rate data is

$$\left.\begin{aligned} |\alpha'|_{max} &= \left|\frac{K_1}{\omega_1 + p}\right| + \left|\frac{K_2}{\omega_2 + p}\right| \\ |\alpha'|_{min} &= \left|\left|\frac{K_1}{\omega_1 + p}\right| - \left|\frac{K_2}{\omega_2 + p}\right|\right| \end{aligned}\right\} \tag{12}$$

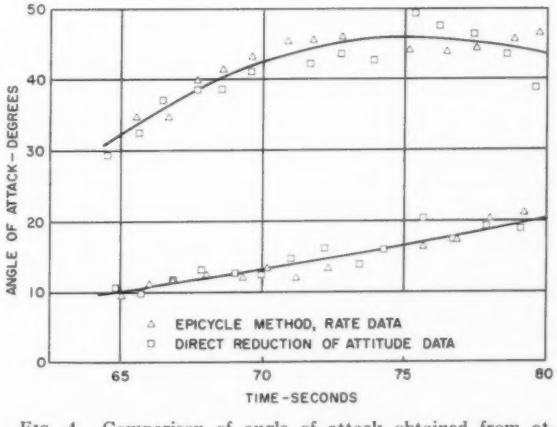

FIG. 4. Comparison of angle of attack obtained from attitude measurements and rate gyro data, using the epicycle method.

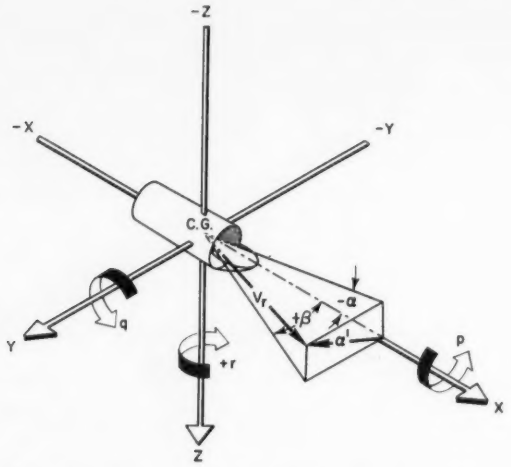

FIG. 5. Schematic view of the body-axis coordinate system.

The consequences of the assumptions made as to the magnitude of the right-hand terms of Eq. (10) have been examined in detail and shown to be quite valid for almost all re-entry vehicle configurations.

A comparison of the angle-of-attack envelope obtained from flight-test rate data through the use of Eq. (12) with that obtained from attitude measurements is presented in Fig. 4. It can be seen that the agreement is excellent even in the extended range of 40°, primarily because the small-angle assumptions produced errors which are obscured by the accuracy of the data.

Appendix A: The Epicycle Solution of the Equation of Motion

In the coordinate system shown in Fig. 5, the equations of motion may be written, assuming rotational symmetry,

$$\left.\begin{aligned} ma_x - mgf(\theta,\phi) &= \Sigma F_x \\ m(\dot{v} - wp + ur) - mgf(\theta,\phi) &= \Sigma F_y \\ m(\dot{w} - uq + vp) - mgf(\theta,\phi) &= \Sigma F_z \\ I_x\dot{p} + (I_z - I_y)qr &= \Sigma M_x \\ I_y\dot{q} + (I_x - I_z)pr &= \Sigma M_y \\ I_z\dot{r} + (I_y - I_x)pq &= \Sigma M_z \end{aligned}\right\} \quad \text{(A-1)}$$

The trajectory of the missile may be decomposed into straight-line segments with $\dot{v} = 0$ and $\dot{p} = 0$. Further, the gravity term is negligible compared with the other terms and the following simplifications may be made by letting

$$I_y \cong I_z \cong I \qquad u/V \cong 1$$
$$v/V \cong \beta \qquad w/V \cong \alpha$$

Eqs. (A-1) then become

$$O = F_x$$

$$mV(\dot{\beta} - \alpha p + r) = \Sigma F_y \quad \text{(A-2)}$$

$$mV(\dot{\alpha} - q + \beta p) = \Sigma F_z \quad \text{(A-3)}$$

$$p = \text{constant}$$

$$\dot{q} + [(I_x/I) - 1]pr = (\Sigma M_y)/I \quad \text{(A-4)}$$

$$\dot{r} + [(1 - (I_x/I)]pq = (\Sigma M_z)/I \quad \text{(A-5)}$$

At this point, it is convenient to make the plane normal to the missile's x-axis a complex plane with y as the real and z as the imaginary axis. This results in two new variables:

$$\alpha' = \beta + i\alpha$$
$$\omega = q + ir$$

Eqs. (A-2) through (A-5) can thus be reduced by multiplying (A-3) and (A-5) by i and adding to the previous equations:

$$\left.\begin{aligned} \dot{\alpha}' + ip\alpha' - i\omega &= [\Sigma(F_y + iF_z)]/mV \\ \dot{\omega} + ip[1 - (I_x/I)]\omega &= [\Sigma(M_y + iM_z)]/I \end{aligned}\right\} \quad \text{(A-6)}$$

Assuming that the moments and forces are linear functions of angle of attack and angular rate, then

$$[\Sigma(F_y + iF_z)]/mV = -(qtAC_{n\alpha'}/mV)(\alpha')$$

$$[\Sigma(M_y + iM_z)]/I = -(iq_tAD/I)\ [C_{m\alpha}(\alpha') + iC_{m_q}(\omega)]$$

Substituting in (A-6) and rearranging yields

$$\dot{\alpha}' + \left[ip + \frac{q_tAC_{n\alpha}}{mV}\right]\alpha' - i\omega = 0$$

$$\dot{\omega} + \left[ip\left(1 - \frac{I_x}{I}\right) - \frac{q_tADC_{m_q}}{I}\right]\omega + \left[\frac{iq_tADC_{m\alpha}}{I}\right]\alpha' = 0$$

With $D = d/dt$, this reduces to

$$(D^2 + BD + C)\alpha' = 0$$
$$(D^2 + BD + C)\omega = 0$$

which has the solution for the angular rate

$$\omega = K_1e^{r_1t} + K_2e^{r_2t}$$

where

$$r_{1,2} = -(B \pm \sqrt{B^2 - 4C})/2$$

K_1 and K_2 are set by initial conditions, and

$$B = ip\left(2 - \frac{I_x}{I}\right) + \frac{q_tAC_{n\alpha}}{mV} - \frac{q_tADC_{m_q}}{I}$$

$$C = -p^2\left(1 - \frac{I_x}{I}\right) + ip\left(1 - \frac{I_x}{I}\right)\frac{q_tAC_{n\alpha}}{mV} - ip\frac{q_tAD\,C_{m_q}}{I} - \frac{q_tAD\,C_{m\alpha}}{I} - \frac{C_{m_q}C_{n\alpha}q_t^2A^2D}{mVI}$$

Note that the solution for the angle of attack is identical except for the initial conditions:

$$\alpha' = C_1e^{r_1t} + C_2e^{r_2t}$$

The roots can be separated into real and imaginary parts, and the solutions rewritten

$$\alpha' = C_1 e^{u_1(t) + i\theta_1(t)} + C_2 e^{u_2(t) + i\theta_2(t)}$$

$$\omega = K_1 e^{u_1(t) + i\theta_1(t)} + K_2 e^{u_2(t) + i\theta_2(t)}$$

Neglecting the influence of damping terms on frequency results in the following approximation for the imaginary parts of the solution:

$$\theta_{1,2} \cong p\left(1 - \frac{I_x}{2I}\right) \pm \sqrt{\frac{p^2 I_x^2}{4I^2} - \frac{q_t A D C_{m\alpha}}{I}} \quad \text{(A-7)}$$

Following the method of Nelson[2] the real parts are found as

$$u_{1,2} = -\frac{1}{2}\left[\frac{q_t A C_{n\alpha}}{mV} - \frac{q_t A D C_{mq}}{I}\right] \pm \frac{pI_x}{\omega_0 I}\left[\frac{q_t A C_{n\alpha}}{mV} + \frac{q_t A D C_{mq}}{I}\right]$$

where

$$\omega_0 \cong \sqrt{\frac{p^2 I_x^2}{4I^2} - \frac{q_t A D C_{m\alpha}}{I}} = \frac{\theta_1 - \theta_2}{2}$$

Appendix B: Determination of the Angle of Attack From Rate Data

From the basic equations of motion listed in Eq. (A-1), Appendix A, the force equations may be written:

$$(\dot{v} + i\dot{w}) + ip(v + iw) - iu(q + ir) = [\Sigma(F_y + iF_z)]/mV \quad \text{(B-1)}$$

This equation is a result of writing the basic vector equation with respect to a fixed axis and then converting it to the body axis by the well-known transformation

$$\left(\frac{d\mathbf{V}}{dt}\right)_{\text{space}} = \left(\frac{d\mathbf{V}}{dt}\right)_{\text{body}} + \boldsymbol{\omega} \times \mathbf{V}$$

Thus, if the aerodynamic forces were zero and the following approximations were made:

$$\frac{v + iw}{\mathbf{V}} \cong \alpha', \qquad \frac{\dot{v} + i\dot{w}}{\mathbf{V}} \cong \dot{\alpha}', \qquad \frac{u}{\mathbf{V}} \cong 1$$

Eq. (B-1) would say that the rate of change of α' in the nonrolling body axes is equivalent to the angular rate of the vehicle, $q + ir$. In other words, Eq. (B-1) would be

$$\dot{\alpha}' + ip\alpha' = i(q + ir) \quad \text{(B-2)}$$

The left-hand side can be recognized as

$$\left(\frac{d\alpha'}{dt}\right)_{\text{space}} = \left(\frac{d\alpha'}{dt}\right)_{\text{body}} + p \times \alpha'$$

Thus, it can be seen that if the lift forces are small, that is, if

$$[\Sigma(F_y + iF_z)]/Vm = 0$$

Eq. (B-2) may be very useful, since it is $(q + ir)$ that is measured by rate gyros.

The solutions of Appendix A for α' and ω are not contradictory to Eq. (B-2). This can be shown as follows: From Appendix A, neglecting damping terms and $\dot{\omega}$,

$$\alpha' = C_1 e^{i\omega_1 t} + C_2 e^{i\omega_2 t} \quad \text{(B-3)}$$

Upon differentiation this is

$$\dot{\alpha}' = iC_1\omega_1 e^{i\omega_1 t} + iC_2\omega_2 e^{i\omega_2 t} \quad \text{(B-4)}$$

Now Eq. (B-2) states that

$$\alpha' + ip\alpha' = i\omega \quad \text{(B-5)}$$

Substituting (B-3) and (B-4) in (B-5) yields

$$C_1(\omega_1 + p)e^{i\omega_1 t} + C_2(\omega_2 + p)e^{i\omega_2 t} = \omega \quad \text{(B-6)}$$

This can be rewritten

$$K_1 e^{i\omega_1 t} + K_2 e^{i\omega_2 t} = \omega = q + ir \quad \text{(B-7)}$$

which is identical in form to the solution found in Appendix A.

It can be further shown that Eq. (B-6) is consistent with classical approaches by the following: The relationship between angular rates (p, q, r), and the Euler system (ψ, θ, ϕ) is

$$p = \dot{\phi} - \dot{\psi}\sin\theta$$

$$q = \dot{\theta}\cos\phi + \dot{\psi}\cos\theta\sin\phi$$

$$r = \dot{\theta}\sin\phi + \dot{\psi}\cos\theta\cos\phi$$

For small θ and ψ, these can be reduced to

$$p \cong \dot{\phi}, \qquad q \cong \theta\cos\phi + \dot{\psi}\sin\phi$$

$$r \cong -\dot{\theta}\sin\phi + \dot{\psi}\cos\phi, \qquad \phi \cong pt$$

$$\omega = q + ir \cong (\dot{\theta} + i\dot{\psi})e^{-ipt}$$

or, if ω is resolved in to the space-fixed coordinates,

$$\omega e^{ipt} = \theta + i\psi \approx \dot{\alpha}_{ss}'$$

where $\dot{\alpha}_{ss}' = \dot{\alpha}_s'$ resolved into space system coordinates. Now let

$$\alpha_{ss}' = \alpha_s' e^{ipt}$$

then

$$\dot{\alpha}_{ss}' = \dot{\alpha}' e^{ipt} + \dot{\alpha}' e^{ipt}$$

Substituting (B-3) and (B-4) yields

$$\dot{\alpha}_{ss}' = iC_1(\omega_1 + p)e^{i(\omega_1 + p)t} + iC_2(\omega_2 + p)e^{i(\omega_2 + p)t}$$

or, since

$$i\omega \cong \dot{\alpha}_{ss}' e^{-ipt}$$

therefore

$$\omega \cong C_1(\omega_1 + p)e^{i\omega_1 t} + C_2(\omega_2 + p)e^{i\omega_2 t} \quad \text{(B-8)}$$

From the preceding sections, it follows that

$$|\alpha'| = |C_1 e^{i\omega_1 t}| + |C_2 e^{i\omega_2 t}|$$

$$|\alpha'|_{max} = |C_1| + |C_2| \qquad |\alpha'|_{min} = ||C_1| - |C_2||$$

Thus, if the values of the initial magnitudes C_1 and C_2 can be found, the oscillation envelope will be determined.

Eq. (B-8) can be written in the following form:

$$\omega = q + ir = K_1 e^{i\omega_1 t} + K_2 e^{i\omega_2 t} \qquad \text{(B-9)}$$

Now by fitting an epicycle to Eq. (B-9), K_1, ω_1, K_2, and ω_2 are determined. Thus, by using Eq. (B-8) and comparing (B-9) and (B-7), the oscillation envelope is found to be

$$\left.\begin{aligned} |\alpha'|_{max} &= \left|\frac{K_1}{\omega_1 + p}\right| + \left|\frac{K_2}{\omega_2 + p}\right| \\ |\alpha'|_{min} &= \left|\left|\frac{K_1}{\omega_1 + p}\right| - \left|\frac{K_2}{\omega_2 + p}\right|\right| \end{aligned}\right\} \qquad \text{(B-10)}$$

Appendix C: Description of Datatron-Routine, Best-Fit Epicycle

The first step is to examine the data to select the amount of data which can be processed at once. This can be estimated from plots of q versus r from which rough measurements of the frequency and vector magnitudes may be obtained. The sections are chosen so that a cubic can represent the variations in ω and an exponential quadradic the variations of the magnitudes. The routine is also limited to 1000 input data points. The number of data points in each short group is from 5 to 15, with a nominal value of 10. Thus, the following input constants will be provided for each run:

(1) Block address and lane number of first time group of data to be taken from magnetic tape;

(2) Word positions of input q and r in each time group;

(3) N, the number of groups in the section of data to be taken;

(4) n, the number of data points for each group;

(5) ω_{1j} and ω_{2j} for each group;*

(6) Beginning block address and lane number for output q, r, Δq, Δr;

(7) Word positions for output data q', r', Δq, Δr, in each time group. There are three parts to the procedure as specified below:

Part I

Calculation of vector magnitudes, K_{1j} and K_{2j}, and total angles turned through, Φ_{1j} and Φ_{2j}, for each group.

(1) Calculation of the midpoint time of each group:

$$\bar{t}_j = \frac{1}{n}\sum_{i=1}^{n} t_i$$

where i = data point index
i = 1, 2, 3, . . . , n
j = group index
j = 1, 2, 3, . . . , N
n = number of data points in each group
N = number of groups in the section

(2) Calculation of A, B, C, and D:

$$\begin{vmatrix} n & 0 & x_j & 0 \\ 0 & n & 0 & x_j \\ x_j & 0 & n & 0 \\ 0 & x_j & 0 & n \end{vmatrix} \begin{vmatrix} A_j \\ B_j \\ C_j \\ D_j \end{vmatrix} = \begin{vmatrix} \sum_{i=1}^{n} [q_i \cos \omega_{1j}(t_i - \bar{t}_j) + r_i \sin \omega_{1j}(t_i - \bar{t}_j)] \\ \sum_{i=1}^{n} [-q_i \sin \omega_{1j}(t_i - \bar{t}_j) + r_i \cos \omega_{1j}(t_i - \bar{t}_j)] \\ \sum_{i=1}^{n} [q_i \cos \omega_{2j}(t_i - \bar{t}_j) + r_i \sin \omega_{2j}(t_i - \bar{t}_j)] \\ \sum_{i=1}^{n} [-q_i \sin \omega_{2j}(t_i - \bar{t}_j) + r_i \cos \omega_{2j}(t_i - \bar{t}_j)] \end{vmatrix}$$

where $x_j = \sum_{i=1}^{n} \cos\,(\omega_{1j} - \omega_{2j})(t_i - \bar{t}_j)$

(3) Calculation of ϕ_{1j}, ϕ_{2j}, K_{1j}, and K_{2j}:

$$\phi_{1j} = \tan^{-1}(B_j/A_j) \qquad K_{1j} = \sqrt{A_j^2 + B_j^2}$$

$$\phi_{2j} = \tan^{-1}(D_j/C_j) \qquad K_{2j} = \sqrt{C_j^2 + D_j^2}$$

$$0° \le \phi_{1j} \le 360° \qquad 0° \le \phi_{2j} \le 360°$$

where the quadrant determination is made in the standard manner with B and D as ordinates, and A and C as abscissas.

(4) Calculation of $\dot{\Phi}_{1,j-1}$ and $\dot{\Phi}_{2,j-1}$ $(1 < j \le N)$:

$$\dot{\Phi}_{1,j-1} = (\Phi_{1,j-1} - \Phi_{j-2})/(\bar{t}_{1,j-1} - \bar{t}_{j-2})$$

$$\dot{\Phi}_{2,j-1} = (\Phi_{2,j-1} - \Phi_{2,j-2})/(\bar{t}_{j-1} - \bar{t}_{j-2})$$

where $\dot{\Phi}_{1,1} = \omega_{1,1}$ $\dot{\Phi}_{2,1} = \omega_{2,1}$

(5) Calculation of β_{1j} and β_{2j}:

$$\beta_{1j} = \frac{\Phi_{1,j-1} + (\bar{t}_j - \bar{t}_{j-1})\dot{\Phi}_{1,j-1} - \phi_{1j}}{360°}$$

$$\beta_{2j} = \frac{\Phi_{2,j-1} + (\bar{t}_j - \bar{t}_{j-1})\dot{\Phi}_{2,j-1} - \phi_{2j}}{360°}$$

where β_{1j} and β_{2j} are to be rounded off to nearest integer.

(6) Calculation of Φ_{1j} and Φ_{2j}:

$$\dot{\Phi}_{1j} = \beta_{1j}(360°) + \phi_{1j}$$

$$\dot{\Phi}_{2j} = \beta_{2j}(360°) + \phi_{2j}$$

where $\dot{\Phi}_{1,1} = \phi_{1,1}$ $\Phi_{2,1} = \phi_{2,1}$

* For the first pass, the values of ω_{1j} and ω_{2j} are estimated from plots of q versus r. Subsequent passes use outputs of the previous run.

The outputs of this part (to be tabulated in fixed or floating point) are K_{1j}, K_{2j}, Φ_{1j}, Φ_{2j}, A_j, B_j, C_j, and D_j for each group.

Note: The values of ω_{1j} and ω_{2j} for the first trial are supplied, and for all successive trials are those calculated in Part II.

Part II

Fit a cubic or quadratic through the Φ's and a quadratic or straight line through the K's of the section.

(1) Calculation of a_1, b_1, c_1, d_1, a_2, b_2, c_2, and d_2:

$$|M_1| \begin{vmatrix} a_1 \\ b_1 \\ c_1 \\ d_1 \end{vmatrix} = \begin{vmatrix} \sum_{j=1}^{N} \Phi_{1j} \\ \sum_{j=1}^{N} [\Phi_{1j}, t_j'] \\ \sum_{j=1}^{N} [\Phi_{1j}, (t_j')^2] \\ \sum_{j=1}^{N} [\Phi_{1j}, (t_j')^3] \end{vmatrix} \qquad |M_1| \begin{vmatrix} a_2 \\ b_2 \\ c_2 \\ d_2 \end{vmatrix} = \begin{vmatrix} \sum_{j=1}^{N} \Phi_{2j} \\ \sum_{j=1}^{N} [\Phi_{2j}, t_j'] \\ \sum_{j=1}^{N} [\Phi_{2j}, (t_j')^2] \\ \sum_{j=1}^{N} [\Phi_{2j}, (t_j')^3] \end{vmatrix}$$

where

$$|M_1| = \begin{vmatrix} N & \sum_{j=1}^{N} (t_j') & \sum_{j=1}^{N} (t_j')^2 & \sum_{j=1}^{N} (t_j')^3 \\ \sum_{j=1}^{N} (t_j') & \sum_{j=1}^{N} (t_j')^2 & \sum_{j=1}^{N} (t_j')^3 & \sum_{j=1}^{N} (t_j')^4 \\ \sum_{j=1}^{N} (t_j')^2 & \sum_{j=1}^{N} (t_j')^3 & \sum_{j=1}^{N} (t_j')^4 & \sum_{j=1}^{N} (t_j')^5 \\ \sum_{j=1}^{N} (t_j')^3 & \sum_{j=1}^{N} (t_j')^4 & \sum_{j=1}^{N} (t_j')^5 & \sum_{j=1}^{N} (t_j')^6 \end{vmatrix}$$

and

$$t_j' = \bar{t}_j - \bar{t}_{j-1}$$

Note: Inclusion of the d_1 and d_2 terms is optional.

(2) Calculation of ω_{1j} and ω_{2j} which will be used in calculations of the next trial for all j's.

$$\omega_{1j} = b_1 + 2c_1 t_j' + 3d_1 (t_j')^2, \qquad \omega_{2j} = b_2 + 2c_2 t_j' + 3d_2 (t_j')^2$$

(3) Calculation of ρ_1, λ_1, μ_1, ρ_2, λ_2, and μ_2:

$$|M_2| \begin{vmatrix} \rho_1 \\ \lambda_1 \\ \mu_1 \end{vmatrix} = \begin{vmatrix} \sum_{j=1}^{N} \ln K_{1j} \\ \sum_{j=1}^{N} [(\ln K_{1j}) t_j'] \\ \sum_{j=1}^{N} [(\ln K_{1j})(t_j')^2] \end{vmatrix} \qquad |M_2| \begin{vmatrix} \rho_2 \\ \lambda_2 \\ \mu_2 \end{vmatrix} = \begin{vmatrix} \sum_{j=1}^{N} \ln K_{2j} \\ \sum_{j=1}^{N} [(\ln K_{2j}) t_j'] \\ \sum_{j=1}^{N} [(\ln K_{2j})(t_j')^2] \end{vmatrix}$$

where

$$|M_2| = \begin{vmatrix} N & \sum_{j=1}^{N} (t_j') & \sum_{j=1}^{N} (t_j')^2 \\ \sum_{j=1}^{N} (t_j') & \sum_{j=1}^{N} (t_j')^2 & \sum_{j=1}^{N} (t_j')^3 \\ \sum_{j=1}^{N} (t_j')^2 & \sum_{j=1}^{N} (t_j')^3 & \sum_{=1}^{N} (t_j')^4 \end{vmatrix}$$

Note: Inclusion of the μ_1 and μ_2 terms is optional.

The tabulated outputs (in either fixed or floating decimal form) are a_1, b_1, c_1, d_1, a_2, b_2, c_2, d_2, ρ_1, λ_1, μ_1, ρ_2, λ_2, and μ_2 for each j.

Part III

Smoothed rates and resulting deviations.

(1) Calculational q_i' and r_i':

$$q_i' = K_1 \cos \theta_1 + K_2 \cos \theta_2$$

$$r_i' = K_1 \sin \theta_1 + K_2 \sin \theta_2$$

where

$$K_1 = e^{\alpha_1 + \lambda_1 t_i' + \mu_1 t_i'^2}$$

$$K_2 = e^{\alpha_2 + \lambda_2 t_i' + \mu_2 t_i'^2}$$

$$\theta_1 = a_1 + b_1 t_i' + c_1(t_i')^2 + d_1(t_i')^3$$

$$\theta_2 = a_2 + b_2 t_i' + c_2(t_i')^2 + d_2(t_1')^3$$

$$t_i' = t_i - \bar{t}_{j=1}$$

Note: Throughout Part III i is the index for all data points of the section ($i = 1, 2, \ldots, n \times N$).

(2) Calculation of Δq_i and Δr_i:

$$\Delta q_i = q_i - q_i'$$

$$\Delta r_i = r_i - r_i'$$

Note: Inclusion of the μ_1, μ_2, d_1, and d_2 terms should be optional.

The outputs of this part (to be tabulated and stored in fixed decimal form on magnetic tape) are q_i', r_i', Δq_i, and Δr_i. The results of each run can be examined and when a new run is required the values of ω_{1j} and ω_{2j} from the previous run will be used for the input to Part I.

The pertinent units employed are as follows: time, sec; q, r, degrees/sec; ϕ, degrees; ω, degrees/sec; Φ, degrees; Φ, degrees/sec.

References

[1] Nicolaides, John D., and MacAllister, Leonard C., *A Review of Aeroballistic Range Research on Winged and/or Finned Missiles*, Ballistic Technical Note No. 5, Bureau of Ordnance, Department of the Navy, Washington, D. C., 1955.

[2] Nelson, Robert L., *The Motions of Rolling Symmetrical Missiles Referred to a Body-Axis System*, NACA TN 3737, November, 1956.

[3] Murphy, Charles H., Jr., *The Prediction of Nonlinear Pitching and Yawing Motion of Symmetric Missiles*, Journal of the Aeronautical Sciences, Vol. 24, No. 7, p. 473, July, 1957.

[4] Charters, A. C., *The Linearized Equations of Motion Underlying the Dynamic Stability of Aircraft, Spinning Projectiles, and Symmetrical Missiles*, NACA TN 3350, January, 1955.

[5] Murphy, C. H., *Data Reduction for the Free-Flight Spark Ranges*, Rep. No. 900, Ballistics Research Laboratory, Aberdeen Proving Ground, Md., February, 1954.

[6] Hildebrand, F. B., *Introduction to Numerical Analysis*, McGraw-Hill Book Co., Inc., New York, 1956.

✦ ✦ ✦

Supersonic Flow at Surface of a Circular Cone (*Continued from page 912*)

Analysis of the experimental data of reference 11 suggests that the range of angles of attack for which Stone theory provides useful approximations for the pressure on the cone surface and the entropy in the windward plane of symmetry may significantly exceed that for which the second-order correction formulas of Section (4) are valid approximations. Consequently, it may be desirable to solve Eqs. (31) and (32) numerically at angles of attack beyond the range of validity of Eqs. (46) and (52).

Recently, H. K. Cheng[14] obtained a perturbation solution for the hypersonic flow over yawed cones. He has shown in the hypersonic approximation (i.e., for small $\gamma - 1$ and large free-stream Mach number) that despite the breakdown of the perturbation solution near the cone surface, the expression for the pressure on the cone surface remains valid to second order. This is a special case of the present work in which it was assumed on the basis of experimental evidence and order-of-magnitude considerations that Stone's perturbation solution for supersonic flow yields in useful approximation the pressure distribution on the cone surface to second order in the angle of attack.

References

[1] Taylor, G. I., *Air Pressure on a Cone Moving at High Speeds*, Proc. Roy. Soc., A139, pp. 278–311, 1933.

[2] Maccoll, J. W., *The Conical Shock Wave Formed by a Cone Moving at High Speed*, Proc. Roy. Soc., A159, pp. 459–472, 1937.

[3] Stone, A. H., *On Supersonic Flow Past a Slightly Yawing Cone*, Jour. Math. and Phys., Vol. 27, No. 1, pp. 67–81, April, 1948.

[4] Stone, A. H., *On Supersonic Flow Past a Slightly Yawing Cone. II*, Jour. Math. and Phys., Vol. 30, No. 4, pp. 200–213, January, 1952.

[5] Stone, A. H., *Corrections to the Paper "On Supersonic Flow Past a Slightly Yawing Cone. II,"* Jour. Math. and Phys., Vol. 31, No. 4, p. 300, January, 1953.

[6] Staff of the Computing Section, Center of Analysis (under direction of Zdeněk Kopal), *Tables of Supersonic Flow Around Cones*, Tech. Report No. 1, M.I.T., 1947.

[7] Staff of the Computing Section, Center of Analysis (under direction of Zdeněk Kopal), *Tables of Supersonic Flow Around Yawing Cones*, Tech. Report No. 3, M.I.T., 1947.

[8] Staff of the Computing Section, Center of Analysis (under direction of Zdeněk Kopal), *Tables of Supersonic Flow Around Cones of Large Yaw*, Tech. Report No. 5, M.I.T., 1949.

[9] Ferri, Antonio, *Supersonic Flow Around Circular Cones at Angles of Attack*, NACA Report No. 1045, 1951.

[10] Roberts, Richard C., and Riley, James D., *A Guide to the Use of the M.I.T. Cone Tables*, Journal of the Aeronautical Sciences, Vol. 21, pp. 336–342, 1954.

[11] Holt, Maurice, and Blackie, John, *Experiments on Circular Cones at Yaw in Supersonic Flow*, Journal of the Aeronautical Sciences, Vol. 23, No. 10, p. 931, October, 1956.

[12] Willett, Joseph E., *Vortical Layer Effects on the Supersonic Flow Around Circular Cones at Angles of Attack*, McDonnell Aircraft Corporation Report No. 6765, March, 1959.

[13] Moore, Franklin K., *Laminar Boundary Layer on a Circular Cone in Supersonic Flow at a Small Angle of Attack*, NACA TN 2521, October, 1951.

[14] Cheng, Hsien K., *Hypersonic Shock-Layer Theory of a Yawed Cone and Other Three-Dimensional Pointed Bodies*, WADC TN 59–335, October, 1959.

Plastic Compressive Buckling of Simply Supported Plates on Interior Elastic Supports

PAUL SEIDE*

Space Technology Laboratories, Inc.

Summary

The plastic compressive buckling of rectangular plates on elastic foundations is treated by means of the Bijlaard-Stowell theory of plastic stability. Four specific cases of interior elastic support are considered for simply supported plates: a uniform foundation, equally spaced longitudinal or transverse line supports, and uniformly distributed point supports. All solutions are similar to those for the corresponding elastic problems.

Symbols

$\bar{A}, \bar{B}, \bar{C}, \bar{F}$ = functions of material properties given by Eqs. (3)
a = plate length
a_{mn} = deflection function coefficients
b = plate width
C_1 = $(1/4) + (3/4)(E_t/E_s)$
c_1 = foundation modulus, lb. per in. per sq.in.
c_2, c_3 = longitudinal and transverse line support constants, respectively, lb. per in. per in.
c_4 = point support constant, lb. per in.
D = elastic plate flexural stiffness, $[D = Et^3/12\ (1 - \nu^2)]$
E = Young's modulus of plate material
E_s = secant modulus of plate material
E_t = tangent modulus of plate material
k_{el}, k_{pl} = elastic and plastic buckling stress coefficients, respectively
k_1, k_3 = buckling stress coefficient for plate supported by foundation and transverse line supports respectively $(b^2\sigma_{cr}t/\pi^2D)$
k_2, k_4 = buckling stress coefficient for plate supported by longitudinal line and point supports, respectively $(l^2\sigma_{cr}t/\pi^2D)$
L = distance between transverse supports; longitudinal distance between point supports
l = distance between longitudinal supports; transverse distance between point supports
M = number of longitudinal bays
N = number of transverse bays
p, q = number of buckles in transverse and longitudinal directions, respectively
t = plate thickness
V = potential energy
V_p = potential energy of plate
V_s = potential energy of supports
w = plate deflection
x, y = coordinates in plate
β_1 = plate aspect ratio (a/b)
β_2 = bay aspect ratio between longitudinal stiffeners (a/l)
β_3 = bay aspect ratio between transverse stiffeners (L/b)
β_4 = bay aspect ratio between point supports (L/l)
γ_1 = foundation stiffness parameter (b^4c_1/π^4D)
γ_2 = longitudinal line support stiffness parameter (l^3c_2/π^4D)
γ_3 = transverse line support stiffness parameter (b^3c_3/π^4D)
γ_4 = point support stiffness parameter (l^2c_4/π^4D)
ϵ = strain
η = k_{pl}/k_{el}, plastically effectiveness ratio
ν = Poisson's ratio
σ = stress
σ_{cr} = critical compressive load
σ_y = secant yield stress defined by the intersection of the stress-strain curve and a line through the origin having a slope of $0.7\ E$

Subscripts

1, 2, 3, 4 = pertaining to problems investigated in the present paper

Received October 26, 1959.

* Member of the Technical Staff, Engineering Mechanics Department.

Introduction

THE ELASTIC STABILITY of stiffened plates has been treated in detail in numerous papers. No such investigations have been presented, however, for stiffened plates that buckle in the plastic range. In the present paper, four problems in the theory of plastic buckling of elastically supported plates are solved in a manner similar to that for the corresponding elastic stability solutions. The cases treated are the plastic buckling under uniform axial compression of simply supported plates stiffened in the interior by a uniform foundation, by longitudinal or transverse line supports, or by point supports or posts (see Fig. 1).

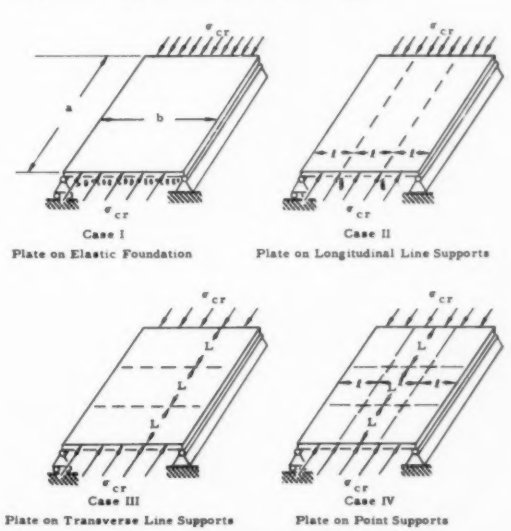

FIG. 1. Problems treated in this paper.

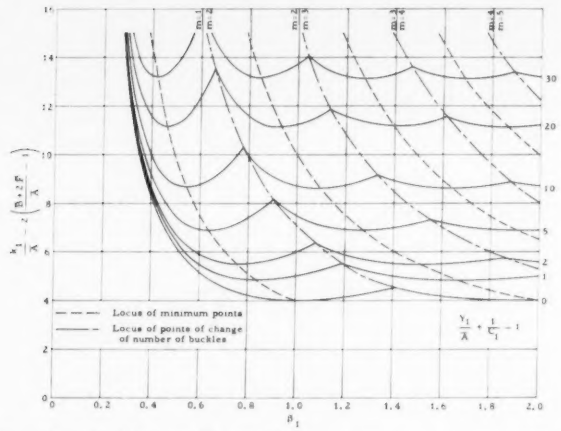

FIG. 2. Buckling coefficients for plate on elastic foundation.

The plastic stability theory used is the Bijlaard-Stowell deformation theory (references 1 and 2). Although a deformation theory of plasticity can be shown to lead to inconsistencies in certain cases, the results obtained from its application to plastic stability problems appear to be in much better agreement with experiment than those given by flow theories. Various arguments have been advanced to account for this paradoxical situation, including the introduction of the effects of initial imperfections, but the evidence in favor of flow theory over deformation theory for buckling remains inconclusive at the present time.

Theory

The plastic compressive buckling load is given by the minimization of the following expression, based on the work of references 1 and 2:

$$V = V_p + V_s \tag{1}$$

where

$$V_p = \frac{D}{2}\int_0^a\int_0^b \left[\bar{A}\left(\frac{\partial^2 w}{\partial x^2}\right)^2 + 2\bar{B}\frac{\partial^2 w}{\partial x^2}\frac{\partial^2 w}{\partial y^2} + \bar{C}\left(\frac{\partial^2 w}{\partial y^2}\right)^2 + 4\bar{F}\left(\frac{\partial^2 w}{\partial x \partial y}\right)^2 - \frac{\sigma_{cr} t}{D}\left(\frac{\partial w}{\partial x}\right)^2\right] dx\, dy \tag{2a}$$

V_s = strain energy stored in elastic supports (2b)

and

$$\bar{A} = \frac{4}{3}\frac{E_s}{E} C_1 \frac{1-\nu^2}{1 + \frac{2}{3}(1-2\nu)\frac{E_s}{E} - \frac{1}{3}(1-2\nu)^2 \frac{E_t}{E}\frac{E_s}{E}} \tag{3a}$$

$$\bar{B} = \frac{1}{2}\frac{1-(1-2\nu)(E_t/E)}{C_1}\bar{A} \tag{3b}$$

$$\bar{C} = (1/C_1)\bar{A} \tag{3c}$$

$$\bar{F} = \frac{1}{3}\frac{E_s}{E}\frac{1-\nu^2}{1-(1/3)(1-2\nu)(E_s/E)} \tag{3d}$$

$$C_1 = \frac{1}{4} + \frac{3}{4}\frac{E_t/E}{E_s/E} \tag{3e}$$

Note that Eqs. (1) to (3) reduce to Eq. (18) of reference 2 when ν is equal to 1/2 and to the elastic equations when $E_t/E = E_s/E = 1$.

A suitable deflection function for the simply supported plate is given by

$$w = \sum_{m=1}^{\infty}\sum_{n=1}^{\infty} a_{mn} \sin\frac{m\pi x}{a}\sin\frac{n\pi y}{b} \tag{4}$$

Substitution of Eq. (4) into Eq. (2a) then yields

$$V_p = \frac{\pi^4 Db}{8a^3}\sum_{m=1}^{\infty}\sum_{n=1}^{\infty}\left[\bar{A}m^4 + 2(\bar{B}+2\bar{F})m^2n^2\frac{a^2}{b^2} + \bar{C}n^4\frac{a^4}{b^4} - \frac{b^2\sigma_{cr}t}{\pi^2 D}m^2\frac{a^2}{b^2}\right]a_{mn}^2 \tag{5}$$

The form of the expression for the strain energy stored in the interior elastic support varies with the type of support. Therefore, each case will be treated separately in the following sections.

Case I—Uniform Foundation

The energy stored in the uniform Winkler foundation is given by

$$V_{s_1} = \frac{1}{2}c_1\int_0^a\int_0^b w^2\, dx\, dy = \frac{\pi^4 Db}{8a^3}\sum_{m=1}^{\infty}\sum_{n=1}^{\infty}\gamma_1\beta_1^4 a_{mn}^2 \tag{6}$$

Then

$$\partial(V_p + V_{s_1})/\partial a_{mn} = 0 = \bar{A}m^4 + 2(\bar{B}+2\bar{F})m^2n^2\beta_1^2 + (\bar{C}n^4+\gamma_1)\beta_1^4 - k_1m^2\beta_1^2, \quad m = 1, 2, \ldots \quad n = 1, 2, \ldots \tag{7a}$$

from which

$$k_1 = \bar{A}(m^2/\beta_1^2) + 2(\bar{B}+2\bar{F}) + (\bar{C}+\gamma_1)(\beta_1^2/m^2), \quad m = 1, 2, \ldots \tag{7b}$$

since, for minimum k_1, n is taken as unity. The value of m used is also that which minimizes k_1.

Eq. (7b) may be put into the form of that for the elastic plate on an elastic foundation; thus,

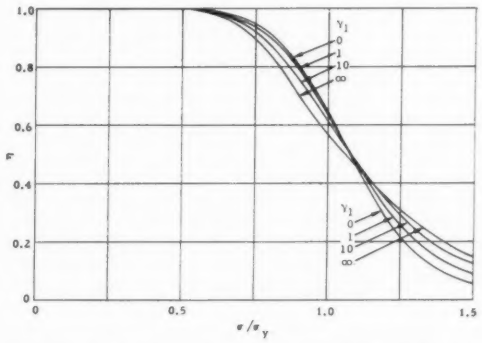

FIG. 3. Reduction factors for buckling of infinite simply supported plate on elastic foundation ($\nu = 0.3$).

$$\frac{k_1}{\bar{A}} - 2\left(\frac{\bar{B} + 2\bar{F}}{\bar{A}} - 1\right) = \left(\frac{m}{\beta_1} + \frac{\beta_1}{m}\right)^2 + \left(\frac{\gamma_1}{\bar{A}} + \frac{1}{C_1} - 1\right)\frac{\beta_1^2}{m^2} \quad (8)$$

Thus, if we plot the quantity

$$\left[\frac{k_1}{\bar{A}} - 2\left(\frac{\bar{B} + 2\bar{F}}{\bar{A}} - 1\right)\right]$$

versus β_1 for different values of

$$\left(\frac{\gamma_1}{\bar{A}} + \frac{1}{C_1} - 1\right)$$

we obtain curves that are applicable for any stress-strain curve. The use of these curves, shown in Fig. 2, for analysis or design is subject to a trial and error procedure in most cases. For instance, if we are given the material, length, and width of the plate, the desired buckling stress, and the foundation modulus, we may enter Fig. 2 with the given value of β_1 and obtain corresponding values of k_1 and γ_1, which are plotted. With the desired buckling stress and the given foundation modulus we may now assign various values of the plate thickness t and obtain other corresponding values of k_1 and γ_1, which when plotted will yield a straight line that will intersect the theoretical curve of k_1 versus γ_1 and will thus determine the plate thickness. As another example in the realm of analysis, if we are given the plate dimensions and material, and the foundation modulus, Fig. 2 will define a theoretical curve of

$$\frac{k_1}{\bar{A}} - 2\left(\frac{\bar{B} + 2\bar{F}}{\bar{A}} - 1\right)$$

versus

$$\frac{\gamma_1}{\bar{A}} + \frac{1}{C_1} - 1$$

If now we choose various values of buckling stress, we obtain, from the plate dimensions and the foundation modulus, corresponding values of

$$\frac{k_1}{\bar{A}} - 2\left(\frac{\bar{B} + 2\bar{F}}{\bar{A}} - 1\right) \quad \text{and} \quad \frac{\gamma_1}{\bar{A}} + \frac{1}{C_1} - 1$$

which yield a curve intersecting the theoretical curve to determine the buckling stress.

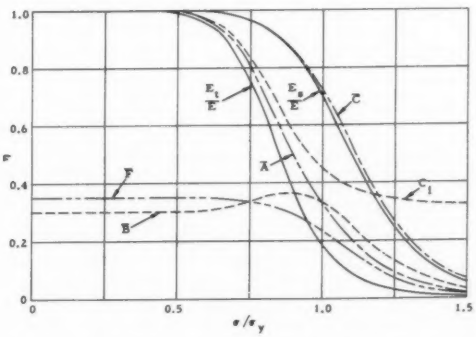

FIG. 4. Material constants for stress-strain curve ($\nu = 0.3$).

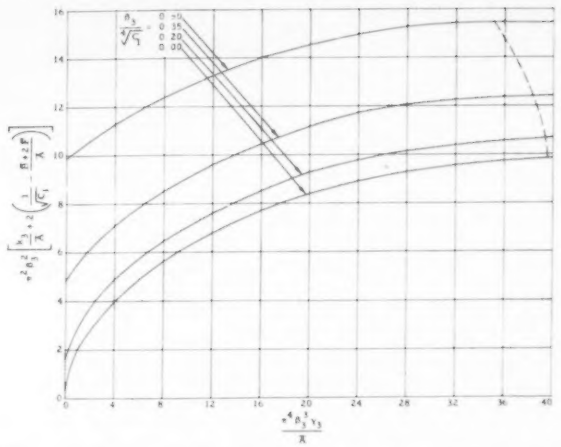

FIG. 5. Buckling stress coefficients for infinitely long plate on transverse line supports.

It is also customary to express plastic buckling results as

$$k_{pl} = \eta k_{el} \quad (9)$$

Then, since the buckling load of an elastic plate on an elastic foundation is given by

$$k_1 = [(m/\beta_1) + (\beta_1/m)]^2 + \gamma_1(\beta_1^2/m^2), \qquad m = 1, 2, \ldots \quad (10a)$$

we have

$$\eta = \frac{\bar{A}(m^2/\beta_1^2) + 2(\bar{B} + 2\bar{F}) + (\bar{C} + \gamma_1)(\beta_1^2/m^2)}{[(\bar{m}/\beta_1) + (\beta_1/\bar{m})]^2 + \gamma_1(\beta_1^2/\bar{m}^2)}, \qquad m = 1, 2, \ldots \quad \bar{m} = 1, 2, \ldots \quad (10b)$$

where the notation $\bar{m}$ has been introduced to indicate that m and $\bar{m}$ may not have the same value for given values of β_1 and γ_1.

For the infinitely long plate, β_1/m varies continuously, so that Eq. (7b) can be minimized analytically. Then

$$\partial k_1/\partial(\beta_1^2/m^2) = 0 = (\bar{C} + \gamma_1) - \bar{A}(m^4/\beta_1^4) \quad (11a)$$

or

$$\beta_1/m = \sqrt[4]{\bar{A}/(\bar{C} + \gamma_1)} \quad (11b)$$

and

$$k_1 = 2[\sqrt{\bar{A}(\bar{C} + \gamma_1)} + \bar{B} + 2\bar{F}] \quad (11c)$$

From this, for the infinitely long plate, we have

$$\eta = \frac{\sqrt{\bar{A}(\bar{C} + \gamma_1)} + \bar{B} + 2\bar{F}}{\sqrt{1 + \gamma_1} + 1} \quad (11d)$$

Reduction factors for the infinitely long plate are illustrated in Fig. 3 for the Ramberg-Osgood stress-strain curve described by

$$\frac{E_t}{\sigma_y} = \frac{\sigma}{\sigma_y} + \frac{3}{7}\left(\frac{\sigma}{\sigma_y}\right)^{10} \quad (12)$$

The derived quantities E_t/E, E_s/E, C_1, $\bar{A}$, $\bar{B}$, $\bar{C}$, and $\bar{F}$ (for $\nu = 0.3$) are plotted in Fig. 4.

Case II—Equally Spaced, Longitudinal Line Supports

The energy stored in the longitudinal line supports is

$$V_{s_2} = \frac{1}{2} c_2 \int_0^a \sum_{p=1}^{N-1} (w_y = pl)^2 dx = \frac{\pi^4 Db}{8a^3} \gamma_2 \beta_2^4 \frac{2}{N} \sum_{p=1}^{N-1} \sum_{m=1}^{\infty} \left(\sum_{n=1}^{\infty} a_{mn} \sin n\pi \frac{p}{N} \right)^2 \tag{13}$$

Then

$$\frac{\partial(V_p + V_{s_2})}{\partial a_{mn}} = 0 = \left[\bar{A} m^4 + 2(\bar{B} + 2\bar{F}) m^2 n^2 \frac{\beta_2^2}{N^2} + \bar{C} n^4 \frac{\beta_2^4}{N^4} - k_2 m^2 \beta_2^2 \right] a_{mn} + \gamma_2 \beta_2^4 \sum_{j=1}^{\infty} a_{mj} \sum_{p=1}^{N-1} \sin n\pi \frac{p}{N} \sin j\pi \frac{p}{N} \qquad \begin{matrix} m = 1, 2, 3, \ldots \\ n = 1, 2, 3, \ldots \end{matrix} \tag{14}$$

Eq. (14) are analogous to Eq. (A4) of reference 3, and the stability criteria may be written immediately as

$$\frac{1}{\gamma_2} + \sum_{j=-\infty}^{\infty} \frac{1}{\bar{A}(m^4/\beta_2^4) + 2(\bar{B} + 2\bar{F})(m^2/\beta_2^2)[2j + (p/N)]^2 + \bar{C}[2j + (p/N)]^4 - k_2(m^2/\beta_2^2)} = 0, \qquad \begin{matrix} m = 1, 2, 3, \ldots \\ p = 1, 2, \ldots (N-1) \end{matrix} \tag{15a}$$

and

$$k_2 = \bar{A}(m^2/\beta_2^2) + 2(\bar{B} + 2\bar{F}) + \bar{C}(\beta_2^2/m^2) \qquad m = 1, 2, 3, \ldots \tag{15b}$$

whichever yields the lower value of k. Eq. (15a) can also be expressed in the closed form

$$\frac{1}{\gamma_2} = \frac{\pi^4}{2\bar{C}(\theta_1^2 + \theta_2^2)} \left(\frac{(\sinh \theta_1)/\theta_1}{\cosh \theta_1 - \cos \pi(p/N)} - \frac{(\sin \theta_2)/\theta_2}{\cos \theta_2 - \cos \pi(p/N)} \right) \tag{16a}$$

where

$$\theta_{1,2} = \pi(m/\beta^2)\sqrt{(1/\bar{C})\left\{\sqrt{(\bar{B} + 2\bar{F})^2 + \bar{C}[k_2(\beta_2^2/m^2) - \bar{A}]} \pm (\bar{B} + 2\bar{F})\right\}} \qquad \begin{matrix} m = 1, 2, 3, \ldots \\ p = 1, 2, \ldots (N-1) \end{matrix} \tag{16b}$$

Eqs. (16) coincide with Eqs. (A21) of reference 4 if the following substitutions are made:

$$\left.\begin{aligned} k_2/(\bar{B} + 2\bar{F}) &= (k)_{\text{ref. 4}} - \left\{1 - [\bar{A}\bar{C}/(\bar{B} + 2\bar{F})^2]\right\}(m/\beta)^2_{\text{ref. 4}} \\ \beta_2/m &= \sqrt{(\bar{B} + 2\bar{F})/\bar{C}}(\beta/m)_{\text{ref. 4}} \\ \gamma_2 &= \bar{C}(\psi b^3/\pi^4 D)_{\text{ref. 4}} \end{aligned}\right\} \tag{17}$$

With these definitions, we can utilize the results of reference 4 to find plastic buckling coefficients. For a given value of σ/σ_y, the curve of k_2 versus β_2/m for a given value of γ_2 and for a given value of buckling stress may be obtained by subtracting the quantities

$$\left\{1 - [\bar{A}\bar{C}/(\bar{B} + 2\bar{F})^2]\right\}(m/\beta)^2_{\text{ref. 4}}$$

from the ordinates of the curve of reference 4 for $\psi b^3/\pi^4 D$ equal to $\gamma_2/\bar{C}$. This procedure yields the curve of $k_2/(\bar{B} + 2\bar{F})$ versus $(\beta_2/m)\sqrt{\bar{C}/(\bar{B} + 2\bar{F})}$ for plastic buckling, from which the curve of k_2 versus β_2/m is obtained by multiplying the ordinate by $\bar{B} + 2\bar{F}$ and the abscissa by $\sqrt{(\bar{B} + 2\bar{F})/\bar{C}}$. When this is repeated for other values of buckling stress we obtain a complete series of curves for a given value of γ_2.

Case III—Equally Spaced, Transverse Line Supports

For transverse line supports the stored energy is given by

$$V_{s_3} = \frac{1}{2} c_3 \sum_{q=1}^{M-1} \int_0^b w^2_{x=qL}\, dy = \frac{\pi^4 Db}{8a^3} \gamma_3 \beta_3^3 (2M^3) \sum_{i=1}^{M-1} \left(\sum_{M=1}^{\infty} a_{mn} \sin \frac{m\pi i}{M} \right)^2 \tag{18}$$

Then

$$\frac{\partial(V_p + V_{s_3})}{\partial a_{mn}} = 0 = [\bar{A} m^4 + 2(\bar{B} + 2\bar{F}) m^2 n^2 M^2 \beta_3^2 + \bar{C} n^4 M^4 \beta_3^4 - k_3 m^2 M^2 \beta_3^2] a_{mn} + 2M^3 \beta_3^3 \gamma_3 \sum_{k=1}^{\infty} a_{kn} \sum_{i=1}^{M-1} \sin \frac{m\pi q}{M} \sin \frac{k\pi q}{M} = 0, \qquad \begin{matrix} m = 1, 2, 3, \ldots \\ n = 1, 2, 3, \ldots \end{matrix} \tag{19}$$

Eqs. (19) are similar to Eqs. (8) of reference 5, and the stability criteria may then be written immediately as

$$\frac{1}{\beta_3^3 \gamma_3} + \sum_{k=-\infty}^{\infty} \frac{1}{\bar{A}[2k + (q/M)]^4 + 2(\bar{B} + 2\bar{F})\beta_3^2[2k + (q/M)]^2 + \bar{C}\beta_3^4 - k_3\beta_3^2[2k + (q/M)]^2} = 0, \qquad q = 1, 2, \ldots (M-1) \tag{20a}$$

where n has been taken equal to unity for minimum γ_3, and

$$k_3 = \bar{A}(m^2/\beta_3^2) + 2(\bar{B} + 2\bar{F}) + \bar{C}(\beta_3^2/m^2), \qquad m = 1, 2, 3, \ldots \tag{20b}$$

whichever yields the lower value of k_3. Eq. (20a) may also be expressed in the closed form

$$\frac{1}{\gamma_3} + \frac{\pi^4\beta_3^3}{2\bar{A}(\phi_1^2 - \phi_2^2)}\left[\frac{(\sin\phi_1)/\phi_1}{\cos\phi_1 - \cos\pi(q/M)} - \frac{(\sin\phi_2)/\phi_2}{\cos\phi_2 - \cos\pi(q/M)}\right] = 0, \qquad q = 1, 2, \ldots (M-1) \tag{21a}$$

where

$$\phi_{1,2} = \pi\beta_3\sqrt{(1/\bar{A})[(k_3/2) - \bar{B} - 2\bar{F} \pm \sqrt{[(k_3/2) - \bar{B} - 2\bar{F}]^2 - \bar{A}\bar{C}}]} \tag{21b}$$

When there are an infinite number of transverse bays, q/M varies continuously, and minimization of γ_3 with respect to q/M yields

$$\cos\pi\frac{q}{M} = \frac{1}{2}\left[\cos\phi_1 + \cos\phi_2 - (\cos\phi_1 - \cos\phi_2)\frac{\sqrt{(\sin\phi_1)/\phi_1} + \sqrt{(\sin\phi_2)/\phi_2}}{\sqrt{(\sin\phi_1)/\phi_1} - \sqrt{(\sin\phi_2)/\phi_2}}\right], \qquad -1 \le \cos\pi\frac{q}{M} \le 1 \tag{22a}$$

and

$$\gamma_3 = -\frac{2\bar{A}(\phi_1^2 - \phi_2^2)}{\pi^4\beta_3^3}\frac{\cos\phi_1 - \cos\phi_2}{[\sqrt{(\sin\phi_1)/\phi_1} - \sqrt{(\sin\phi_2)/\phi_2}]^2} \tag{22b}$$

It can be shown that Eqs. (21) and (22) of the present paper are identical with Eqs. (12) and (16) of reference 5 for $\alpha = 0$ if we make the substitutions

$$k_3 = \sqrt{\bar{A}\bar{C}}\left[k_{\text{ref. 5}} - 2\left(1 - \frac{\bar{B} + 2\bar{F}}{\sqrt{\bar{A}\bar{C}}}\right)\right], \qquad \beta_3 = \beta_{\text{ref. 5}}\sqrt[4]{\bar{A}/\bar{C}}, \qquad \gamma_3 = \gamma_{\text{ref. 5}}\sqrt[4]{\bar{C}^3\bar{A}} \tag{23}$$

which indicates that the results of reference 5 may be used to obtain plastic buckling coefficients with little difficulty. The transformed results of reference 5 for an infinitely long plate are shown in Fig. 5.

Case IV—Point Supports or Posts

When the interior support is provided by elastic point supports or posts, the stored energy is expressed by

$$\left.\begin{aligned} V_{s_4} &= \frac{1}{2}c_4\sum_{q=1}^{M-1}\sum_{p=1}^{N-1}(w_{x=qL,\,y=pl})^2 \\ &= \frac{\pi^4 Db}{8a^3}4\gamma_4\frac{M^3}{N}\beta_4^3\sum_{q=1}^{M-1}\sum_{p=1}^{N-1}\left(\sum_{m=1}^{\infty}\sum_{n=1}^{\infty}a_{mn}\sin\frac{m\pi q}{M}\sin n\pi\frac{p}{N}\right)^2 \end{aligned}\right\} \tag{24}$$

Then

$$\frac{\partial(V_p + V_{s4})}{\partial a_{mn}} = 0 = \left[\bar{A}m^4 + 2(\bar{B} + 2\bar{F})m^2n^2\frac{M^2}{N^2}\beta_4^2 + \bar{C}n^4\frac{M^4}{N^4}\beta_4^4 - k_4m^2M^2\beta_4^2\right]a_{mn} + 4\gamma_4\beta_4^3\frac{M^3}{N}\sum_{j=1}^{\infty}\sum_{k=1}^{\infty}a_{jk}\left(\sum_{q=1}^{M-1}\sin m\pi\frac{q}{M}\sin j\pi\frac{q}{M}\right)\left(\sum_{p=1}^{N-1}\sin n\pi\frac{p}{N}\sin k\pi\frac{p}{N}\right), \qquad \begin{matrix} m = 1, 2, 3, \ldots \\ n = 1, 2, 3, \ldots \end{matrix} \tag{25}$$

Eqs. (25) are similar to Eqs. (7) of reference 6, and the stability criteria may be written upon inspection as

$$\frac{1}{\beta_4^3\gamma_4} + \sum_{j=-\infty}^{\infty}\sum_{k=-\infty}^{\infty}\frac{1}{\left[\bar{A}\left(2j + \frac{q}{M}\right)^4 + 2(\bar{B} + 2\bar{F})\left(2j + \frac{q}{M}\right)^2\left(2k + \frac{p}{N}\right)^2\beta_4^2 + \bar{C}\left(2k + \frac{p}{N}\right)^4\beta_4^4 - k_4\left(2j + \frac{q}{M}\right)^2\beta_4^2\right]} = 0, \qquad \begin{matrix} q = 1, 2, \ldots (M-1) \\ p = 1, 2, \ldots (N-) \end{matrix} \tag{26}$$

together with

$$k_t = \bar{A}(m^2/\beta_t^2) + 2(\bar{B} + 2\bar{F}) + \bar{C}(\beta_t^2/m^2) \tag{27}$$

whichever of Eqs. (26) or (27) yields the lowest buckling stress. There does not appear to be any simple correspondence between Eqs. (26) and Eqs. (11) of reference 6, so that new calculations for plastic buckling of post stiffened plates are necessary.

Concluding Remarks

Solutions for the plastic compressive buckling of simply supported plates on four different types of interior elastic supports have been presented. It has shown that the numerical results for three of the prob-

(*Continued on page 950*)

The Divergence of Supersonic Linear Viscoelastic Lifting Surfaces Including Chordwise Bending†

HARRY H. HILTON*

University of Illinois and Hughes Aircraft Company

Summary

An elastic-viscoelastic analogy is developed for the creep deformations of lifting surfaces. It is applicable to chordwise bending and torsional divergence analyses. The general linear viscoelastic stress-strain relationships are used and the analogy is derived in terms of Fourier and Laplace transforms. An illustrative example for the case of torsional divergence is included and the contributions of the various parameters influencing creep deformations are discussed. It is further shown that analyses based on linear viscoelastic stress-strain relations will not lead to divergence of the lifting surface in a finite time. However, the deformations can become exceedingly large in a relatively short time and alternate methods for the determination of maximum lifetimes are presented.

An expression is derived for the effective polar moment of inertia for an arbitrary cross section. It is shown that for a homogeneous linear viscoelastic body it is identical to the expression for an equivalent homogeneous elastic body.

Symbols

a = speed of sound
A = area
a_n, b_n = viscoelastic material properties
b = half span
B = see Eq. (12)
B_{2n} = Euler's number
c = chord
c_1 = distance from leading edge to point of maximum thickness
C = see Eq. (45)
D = ratio of aerodynamic to elastic stiffness
e = distance from axis of twist to center of pressure
G = shear modulus
$\overline{G}$ = complex shear modulus, see Eq. (20)
h = thickness
I = moment of inertia
J_e = effective polar moment of inertia
K = bulk modulus
$L_n(t)$ = Laguerre polynomial
M = Mach number
M_B = bending moment
M_T = torque
P, Q = differential operators
p = complex variable in Laplace transform
q = aerodynamic pressure
R_M = amplification factor
t = time
t^* = nondimensional time
T = temperature
w = deflection
x, y, z = coordinates
α = slope of chord line
α^r = rigid-body angle of attack
ϵ_x = strain
η = coefficient of viscosity
θ = angle of twist
ξ = nondimensional form of x
ρ = density of air
σ_x = bending stress
σ_s = shear stress
τ = relaxation time
ω = complex variable in Fourier transform

Received October 2, 1959.

† The analysis described in this paper was performed under the sponsorship of the Systems Development Laboratories, Hughes Aircraft Company, and the author is grateful to them for permission to publish this article.

* Professor of Aeronautical Engineering, University of Illinois; and Consultant, Hughes Aircraft Company.

Introduction

THE PROBLEM OF DIVERGENCE of supersonic, elastic wings has been studied extensively by Biot.[1,‡] He has demonstrated the tendency of the leading edge to "curl up" and he has also investigated the influence of chordwise bending on torsional divergence. The elastic leading edge problem has been further discussed by Fung.[2]

Due to high speeds, the structure of a flying vehicle will be exposed to aerodynamic heating and, at the resulting elevated temperatures, the material properties will change radically. The material will become inelastic, exhibit creep characteristics, experience reductions in strength and stiffness properties, and be subjected to thermal stresses. Since the aerodynamic moments are, as a first approximation, directly proportional to the slope of the deflected chord line, and since the resisting bending and torsional moments are dependent upon the nature of the stress-strain relationship, it is evident that the inelastic behavior will change the aeroelastic problem into an aeroinelastic one.

A relatively large number of empirical and theoretical expressions describing inelasticity are available in the literature.[3] From the mathematical point of view, the simplest of these are the linear viscoelastic stress-strain laws, by means of which inelasticity is represented by linear relations between stresses, strains, and their time derivatives. It was first shown by Alfrey[4,5] and by subsequent extensions of his work[6–13] that in many static, thermal stress, and

‡ Reference 1 is a comprehensive summary of six of Biot's papers.

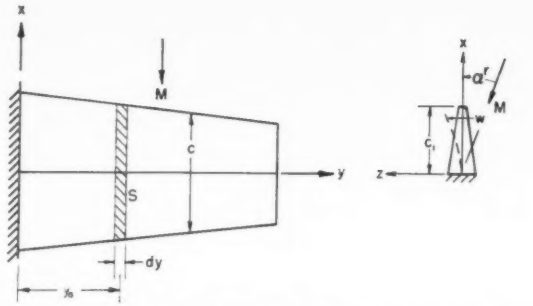

FIG. 1. Effect of chordwise bending on chord of fore portion of strip "S."

buckling problems, viscoelastic solutions are obtainable by analogy from equivalent elastic solutions.

Very few papers have been published on aeroinelastic phenomena. Allen et al.[12] have investigated the vibration of viscoelastic beams loaded by steady aerodynamic forces. Bozajian[14] has studied the divergence of nonlinear viscoelastic surfaces. Divergence and flutter of rigid surfaces on linear and nonlinear viscoelastic supports has been investigated by the author.[15]

Admittedly, for large stresses the actual inelastic behavior of most materials is nonlinear and the linear viscoelastic laws do not account for such phenomena. However, Allen et al.[12] have demonstrated that some linear viscoelastic stress-strain relationships, such as those of the Maxwell-Kelvin body, can be used to represent actual creep properties under constant stress and temperature. It has further been shown[16] that under constant stress and temperature a Maxwell-Kelvin linear viscoelastic body is analogous to the experimentally determined nonlinear creep law for QQ-M-44 magnesium alloy of Baer.[17]

In view of the foregoing and because of the relative ease with which the general linear viscoelastic stress-strain laws can be handled analytically, the present study was undertaken to gain fundamental insight into the creep divergence problem. This paper generally follows Biot's work with the exception that viscoelastic rather than elastic material behavior is taken into account. Both torsional divergence and the increase in stresses with time due to chordwise bending and creep are considered. The present analysis is a generalization and extension to many dimensions of the previously treated one-dimensional creep divergence problem.[15]

Leading Edge Instability and Stress Magnification Due to Chordwise Bending

General Analysis

Consider a unit chordwise strip of a lifting surface at $y = y_0$ (Fig. 1). Since there is a zero chordwise slope at the point of maximum thickness one can assume that the wedge is effectively clamped at this point. One can further assume that there is no spanwise bending or twisting, since the strip is of small width. As a first approximation transient effects in the aerodynamic force and the inertia of the wedge are neglected and the lift and moment are assumed to be directly proportional to the slope of the deflected chord line. These assumptions are the same as those of Biot[1] in the elastic case and are justified in the viscoelastic case since the creep rates are relatively small.

For equilibrium in bending it is necessary that

$$\int_{A(x)} \sigma_x dA = 0 \tag{1}$$

$$\int_{A(x)} \sigma_x z \, dA = M_B(x, y_0, t) \tag{2}$$

where $\sigma_x = \sigma_x(x, y_0, t)$ is the bending stress normal to the cross section.

If one limits the temperature to a function of time only, then the stress field remains one-dimensional, provided that the lifting surface is not made of dissimilar materials and is not restrained at more than one edge. Such conditions will be assumed to prevail. The general one-dimensional, compressible, viscoelastic stress-strain relation is [3, 5, 8]

$$\{P + Q(1/K)\}\sigma_x = 3Q\{\epsilon_x - \alpha T\} \tag{3}$$

with the differential operators defined as

$$P = \sum_{n=0}^{r} a_n(T) \frac{\partial^n}{\partial t^n} \tag{4}$$

$$Q = \sum_{n=0}^{s} b_n(T) \frac{\partial^n}{\partial t^n} \tag{5}$$

If the usual assumption is made that plane sections remain plane, then

$$\epsilon_x = z\psi(x, y_0, t) + \alpha T \tag{6}$$

and Eq. (1) is identically satisfied since the x-axis is taken to pass through the centroid of all sections of the undeformed wedge. Substitution of Eqs. (3) and (6) into Eq. (2) yields

$$3I\,Q\{\psi\} = \{P + Q(1/K)\}\{M_B\} \tag{7}$$

and, from the usual geometric relations of a deflected beam based on plane sections remaining plane, one can show that

$$\psi = \partial^2 w/\partial x^2 \tag{8}$$

if the nonlinear terms are neglected in the expression for the radius of curvature.

Then from Eqs. (7) and (8) one obtains the governing differential equation

$$3I\,Q\{\partial^2 w/\partial x^2\} = \{P + Q(1/K)\}\,M_B \tag{9}$$

which can be modified to read

$$3Q\{(\partial^2/\partial x^2)[I(\partial^2 w/\partial x^2)]\} = \{P + Q(1/K)\}q \tag{10}$$

if the material properties a_n and b_n [Eqs. (4) and (5)] are independent of x.

For a wedge at a rigid-body angle of attack α^r, the aerodynamic load per unit area is

$$q = (2M^2/\sqrt{M^2 - 1})\rho a^2[(\partial w/\partial x) + \alpha^r] \tag{11}$$

For temperatures which are time-dependent only, the material properties a_n and b_n are functions of time only. In order to take into account the Mach number, altitude, and angle of attack history during a given flight or over the entire life of the vehicle, Eq. (11) may be written as

$$q = B(t)[(\partial w/\partial x) + \alpha^r(t)] \tag{12}$$

It is convenient at this stage to introduce the following nondimensional variables

$$\xi = 1 - (x/c_1) \tag{13}$$

$$\alpha^v = \partial w/\partial x \tag{14}$$

Then Eq. (10) becomes

$$-3Q\{(\partial^2/\partial\xi^2)[I(\partial\alpha^v/\partial\xi)]\} = c_1{}^3\{P + Q(1/K)\}\{B(t)[\alpha^v + \alpha^r(t)]\} \tag{15}$$

Eq. (15) is a partial differential equation with variable coefficients. The solution to the viscoelastic divergence problem can be obtained in a manner similar to that given in references 6 and 8.

In particular, as a first case, let the wedge be examined under conditions of time-independent temperature, Mach number, and altitude.

Let

$$\bar{\alpha}^v(\xi, \omega) = \frac{1}{\sqrt{2\pi}} \int_{-\infty}^{\infty} \alpha^v(\xi,t)e^{i\omega t}\, dt \tag{16}$$

be the Fourier transform[18] of $\alpha^v(\xi, t)$. Then, the differential time operators can be transformed as follows[8]:

$$\bar{P}(\omega)\bar{\alpha}^v(\xi, \omega) = \frac{1}{\sqrt{2\pi}} \int_{-\infty}^{\infty} P\{\alpha^v(\xi, t)\}e^{-i\omega t}dt \tag{17}$$

$$\bar{Q}(\omega)\bar{\alpha}^v(\xi, \omega) = \frac{1}{\sqrt{2\pi}} \int_{-\infty}^{\infty} Q\{\alpha^v(\xi, t)\}e^{-i\omega t}dt \tag{18}$$

Operating on Eq. (15) with the Fourier transform yields

$$\frac{\partial^2}{\partial\xi^2}\left[I\frac{\partial\bar{\alpha}^v}{\partial\xi}\right] = \begin{cases} -\dfrac{Bc_1{}^3}{3}(\bar{G}^{-1} + K^{-1})(\bar{\alpha}^v + \bar{\alpha}^r) & \text{for } \alpha^r = \alpha^r(t) \quad (19) \\ -\dfrac{Bc_1{}^3}{3}(\bar{G}^{-1} + K^{-1})\left[\bar{\alpha}^v + \dfrac{\overline{[a_0 + (b_0/K)]\alpha^r}}{\bar{Q}(\bar{G}^{-1} + K^{-1})}\right] & \text{for } \alpha^r = \text{const.} \end{cases}$$

with

$$\bar{G} = \bar{G}(\omega) = \bar{Q}(\omega)/\bar{P}(\omega) = \left[\sum_{n=0}^{s}(i\omega)^n b_n\right]\left[\sum_{n=0}^{r}(i\omega)^n a_n\right]^{-1} \tag{20}$$

The initial conditions are dependent upon the particular viscoelastic stress-strain relation. The boundary conditions for chordwise bending with a clamped edge at the point of maximum thickness are

$$\alpha^v(1, t) = Q\left\{\frac{\partial\alpha^v(0, t)}{\partial\xi}\right\} = Q\left\{\frac{\partial}{\partial\xi}\left[I(0)\frac{\partial\alpha^v(0, t)}{\partial\xi}\right]\right\} = 0 \tag{21}$$

which, in order to be used in conjunction with Eq. (19), are transformed to

$$\bar{\alpha}^v(1, \omega) = \bar{Q}\frac{\partial\bar{\alpha}^v(0, \omega)}{\partial\xi} = \bar{Q}\frac{\partial}{\partial\xi}\left[I(0)\frac{\partial\bar{\alpha}^v(0, \omega)}{\partial\xi}\right] = 0 \tag{22}$$

It is evident from Eqs. (19) and (22) that for constant temperature, Mach number, and altitude conditions, the Fourier transform of the viscoelastic chordline slope is equal to that of an equivalent elastic wedge of shear modulus $\bar{G}(\omega)$ and equivalent rigid-body angle of attack $\bar{\alpha}^r$ or $\overline{[a_0 + (b_0/K)]\alpha^r}/\bar{Q}(\bar{G}^{-1} + K^{-1})$. This analogy may be thought of as a further extension of Alfrey's analogy[4] to this aeroviscoelastic problem and is similar in nature to the analogy for the general thermal stress problem in media with temperature-dependent properties.[8]

Therefore, it is only necessary to know the elastic solution corresponding to shear modulus $\bar{G}$ and an equivalent rigid-body angle of attack. In general, such elastic solutions must be known in any case, since most viscoelastic bodies have initial values corresponding to elastic solutions. If

$$\alpha^{*e} = \begin{cases} \alpha^{*e}[\xi, \bar{G}, \bar{\alpha}^r, \omega] & \text{for } \alpha^r = \alpha^r(t) \\ \alpha^{*e}[\xi, \omega, \bar{G}, \overline{[a_0 + (b_0/K)]\alpha^r}/\bar{Q}(\bar{G}^{-1} + K^{-1})] & \text{for } \alpha^r = \text{const.} \end{cases} \tag{23}$$

is the equivalent elastic solution of Eq. (19) corresponding to some boundary conditions, such as those of Eq. (22) for instance, then the viscoelastic deflections may be obtained from the inverse Fourier transform[18]

$$\alpha^v(\xi, t) = \frac{1}{\sqrt{2\pi}} \int_{-\infty}^{\infty} \alpha^{*e}e^{-i\omega t}\, d\omega \tag{24}$$

In the foregoing, it has, of course, been tacitly assumed that the Fourier transforms and their inverse of all the functions involved as defined by Eq. (16) exist, i.e., that all the functions are absolutely integrable over the entire infinite range. If this condition is not fulfilled, then one can make use of Fourier sine or cosine transforms or Laplace transforms with appropriate modifications in Eq. (19).

In the more general case where the temperature, Mach number, and altitude vary in time, it is possible to construct a stepwise analogy such as the one developed in reference 8 for thermal stresses in viscoelastic bodies. The time scale is divided into a number of intervals and the coefficients of Eq. (15) are approximated by step functions such that

$$\hat{a}_n(t) = \begin{cases} a_n(\hat{t}_m), & t_m \le t < t_{m+1} \\ 0, & \text{elsewhere} \end{cases} \tag{25}$$

etc., where m is an integer and

$$\hat{t}_m = (t_m + t_{m+1})/2 \tag{26}$$

Then, for the interval $t_m \leq t < t_{m+1}$, the Fourier transform is defined as previously and Eq. (19) is valid in each interval with the understanding that the equivalent shear modulus and rigid-body angle of attack vary from interval to interval. Thus, from Eq. (24),

$$\alpha_m{}^v(\xi, t) = \frac{1}{\sqrt{2\pi}} \int_{-\infty}^{\infty} \alpha_m{}^{*e}[\xi, \omega, \bar{G}_m, \bar{\alpha}_m{}^r]\, e^{-i\omega t}\, d\omega \tag{27}$$
$$t_m \leq t < t_{m+1}$$

A detailed discussion of the boundary and initial conditions for each interval may be found in reference 8. Hence, the analogy is applied in each time interval.

Stress Amplification Due to Flexibility

The bending moment at the point of maximum thickness of the wedge will certainly be larger for a flexible wedge than for a rigid one. The amplication factor $R_M{}^v$ is defined as

$$R_M{}^v = 2M_B{}^v(1, t)/B(t)c_1{}^2\alpha^r \tag{28}$$

where the moment $M_B{}^v$ is defined by Eq. (9). The stress at the maximum thickness section of the wedge is obtained from Eqs. (3), (6), and (8),

$$c_1 \left\{P + Q\left(\frac{1}{K}\right)\right\} \sigma_x(1, t) = -3Q \left\{\frac{\partial \alpha^v(1, t)}{\partial \xi}\right\} z \tag{29}$$

or from Eq. (9),

$$\left\{P + Q\left(\frac{1}{K}\right)\right\}\left\{\sigma_x(1, t) - \frac{zM_B{}^v(1, t)}{I(1)}\right\} = 0 \tag{30}$$

It is evident from Eq. (30) that large bending stresses may develop in the wedge long before leading edge instability appears. If the viscoelastic moment exceeds the corresponding elastic moment, which is to be expected, owing to creep (since creep deformations will increase the slope of the chord, which, in turn, increases the aerodynamic pressure [Eq. (11)] and, hence the bending moment), then the viscoelastic stress will be larger than the elastic stress and the latter will give unconservative strength estimates.

Stability Considerations

The system described by Eq. (15) becomes unstable, that is, leading edge "curl-up" takes place, whenever the deflection, w, increases without bound. The deflection is obtained from Eq. (14) by integration, with the boundary condition

$$w(1, t) = 0 \tag{31}$$

such that

$$w(\xi, t) = -c_1 \int_1^{\xi} \alpha^v(\xi, t)\, d\xi \tag{32}$$

Due to the type of aerodynamic loading applied to the cantilever wedge, the maximum deflection will always occur at the leading edge, $\xi = 0$.

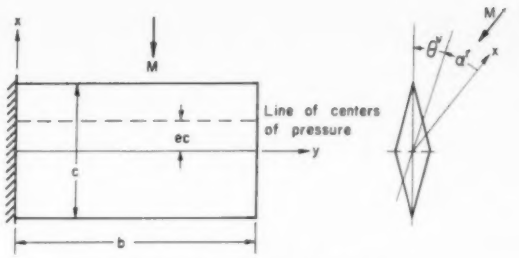

FIG. 2. Effect of torsional twist.

Let $t_{L.E.}$ be the time corresponding to the onset of leading edge instability, defined by

$$\lim_{t \to t_{L.E.}} w(0, t) \to \infty \tag{33}$$

The value of $t_{L.E.}$ will depend upon the cross section, the particular viscoelastic stress-strain relation, and the temperature, Mach number, and altitude conditions. It is quite possible that under a given set of conditions the deflection will remain finite. In such a case, linear viscoelastic leading-edge instability will not occur.

As was pointed out previously, many viscoelastic media have for their initial conditions the corresponding elastic values. Consequently, even if the analysis of Biot[1] indicates no leading edge instability, it is still possible for the viscoelastic wedge to become instable after some time. (If there is elastic instability, then $t_{L.E.} = 0$ and no further viscoelastic analysis is necessary.)

It is not possible to list regions of stability, because of the large number of variables involved; each case must be examined individually.

It was shown in reference 15 that for a rigid lifting surface on a linear viscoelastic support no finite divergence time exists. In those cases where linear viscoelasticity is unable to predict a finite $t_{L.E.}$, Eq. (33) can be modified to predict an ultimate time, t_u, which instead of being based on a stability criteria such as $t_{L.E.}$ is defined as the time corresponding to a preassigned maximum deflection or stress. Under such a definition, an ultimate time always exists for a linear viscoelastic body.

Torsional Divergence

Case 1. Chordwise Bending Neglected

Consider next a linear viscoelastic lifting surface, rigid in bending but able to twist. For the sake of simplicity, it will be assumed that the shear centers are on a straight line (Fig. 2), although the analysis can be easily modified for a more general case. The problem is, therefore, to determine the torsional stability of the surface subjected to a torque proportional to the rigid-body angle of attack and to the angle of twist θ^v.

It will be assumed that the usual assumptions of the

linear elastic theory hold equally well for the viscoelastic case.

The displacements in the x, y, z directions are respectively assumed to be

$$\left.\begin{aligned} u &= -\theta^v(y, t)z \\ v &= (\partial\theta^v/\partial y)\phi(x, z, t) \\ w &= \theta^v x \end{aligned}\right\} \tag{34}$$

Then the shear strains are

$$\gamma_{xy} = \frac{1}{2}\left(\frac{\partial v}{\partial x} + \frac{\partial u}{\partial y}\right) = \frac{1}{2}\left(\frac{\partial v}{\partial x} - \frac{\partial \theta^v}{\partial y}\, z\right) \tag{35}$$

$$\gamma_{yz} = \frac{1}{2}\left(\frac{\partial w}{\partial y} + \frac{\partial v}{\partial z}\right) = \frac{1}{2}\left(\frac{\partial \theta^v}{\partial y}\, x + \frac{\partial v}{\partial z}\right) \tag{36}$$

The general viscoelastic stress-strain relations in shear are

$$P\{\sigma_{xy}\} = 2Q\{\gamma_{xy}\} \tag{37}$$

etc., with the differential operators defined by Eqs. (4) and (5).

Let the line integral of the resultant shear stress, σ_s, be evaluated along the boundary of the cross section at constant time.

$$\oint_{t,y=\text{const.}} \sigma_s ds = \oint_{t,y=\text{const.}} \left[\sigma_{xy}\frac{dx}{ds} + \sigma_{yz}\frac{dz}{ds}\right] ds \tag{38}$$

Substituting into Eq. (38) from Eqs. (34)–(37) one obtains

$$\oint_{t,y=\text{const.}} P\{\sigma_s\} ds = \oint_{t,y=\text{const.}} Q\left\{\frac{\partial v}{\partial x}\, dx + \frac{\partial v}{\partial z}\, dz\right\} - \oint_{t,y=\text{const.}} Q\left\{\frac{\partial \theta^v}{\partial y}\,(z dx - x dz)\right\} \tag{39}$$

For a_n's and b_n's which are independent of x and z, the first integral on the right of Eq. (39) vanishes since v is single-valued and the integration is along a closed curve. Then Eq. (39) reduces to

$$P\left\{\oint_{t,y=\text{const.}} \sigma_s ds\right\} = 2A(y)\, Q\left\{\frac{\partial \theta^v}{\partial y}\right\} \tag{40}$$

where $A(y)$ is the entire cross-sectional area.

From geometric and equilibrium considerations, which are independent of material properties, one obtains the usual relation for the shear stress of a hollow section,[19]

$$2A(y)h\sigma_s = \int_{\substack{y \\ t=\text{const.}}}^{b} M_T(y', t)dy' \tag{41}$$

where M_T is torque per unit span.

Substitution of Eq. (41) into (40) and differentiation with respect to y yields

$$(\partial/\partial y)[J_e(y)\, Q\{\partial\theta^v/\partial y\}] = -P\{M_T\} \tag{42}$$

where

$$J_e(y) = 4[A(y)]^2 \Big/ \oint_{y=\text{const.}} [ds/h(s, y)] \tag{43}$$

It is interesting to note that the effective polar moment of inertia, $J_e(y)$, for time-dependent viscoelastic material properties is the same as in the usual homogeneous elastic case. The foregoing analysis can be readily extended to multicelled cross sections.

For the wing of Fig. 2, when inertia effects are neglected, Eq. (42) reduces to

$$(\partial/\partial y)[J_e(y)Q\{\partial\theta^v/\partial y\}] = -C(y)P\{\theta^v + \alpha^r(t)\} \tag{44}$$

with

$$C(y) = 2\rho a^2 M^2 e(y)[c(y)]^2/\sqrt{M^2 - 1} \tag{45}$$

It is assumed that inertia effects can be neglected because the creep rates are essentially small. However, if desired, they can be readily included by the proper definition of the a_2 term on the right-hand side of Eq. (44).

If the a_n's and b_n's are constants, then one can again use the Fourier transforms as defined in Eqs. (16)–(18), and (20) and obtain from Eq. (44).

$$\frac{\partial}{\partial y}\left[J_e\frac{\partial \bar{\theta}^v}{\partial y}\right] = \begin{cases} -C(y)(\bar{\theta}^v + \bar{\alpha}^r)/\bar{G}, & \alpha^r = \alpha^r(t) \\ -C(y)[(\bar{\theta}^v/\bar{G}) + (\overline{a_0\alpha^r}/\bar{Q})], & \alpha^r = \text{const.} \end{cases} \tag{46}$$

For a cantilever wing, the boundary conditions on the transforms are

$$\bar{\theta}^v(0, \omega) = \bar{Q}[\partial\bar{\theta}^v(b, \omega)/\partial y] = 0 \tag{47}$$

It is evident from the discussion in the previous section that Eqs. (46) and (47) again represent an analogy between the Fourier transform of the angle of twist of a viscoelastic surface and the twist of an equivalent elastic lifting surface of shear modulus $\bar{G}$ and equivalent rigid-body angle of attack $\bar{\alpha}^r$. The initial conditions are, of course, dependent on the particular viscoelastic stress-strain relation.

In the more complex problem where the a_n's and b_n's are time-dependent because of temperature variations, one can again resort to the stepwise analogy outlined in the previous section and in reference 8.

Case 2. Three-Dimensional Problem

Biot[1] has treated the three-dimensional divergence problem by approximating the lifting surface by a plate. Hilton and Benjamin[10] have derived the governing differential equation for an incompressible viscoelastic plate in bending and compression. For a plate of constant thickness, with the deflection $w = w(x, y, t)$ measured from the initial deflection $w_0 = w_0(x, y)$, the governing equation for the aeroviscoelastic problem is

$$h^3 Q\{\nabla^4 w\} = 3P\{B(t)[(\partial w/\partial x) + \alpha^r(t)]\} \tag{48}$$

It is apparent that the discussion of analogies in the previous two sections applies to this case as well. Consider as a first example the case of constant $B(t)$; temperature application of the Fourier transform as before reduces Eq. (48) to

$$h^3\bar{G}\nabla^4\bar{w} = \begin{cases} 3B[(\partial\bar{w}/\partial x) + \bar{\alpha}^r], & \alpha^r = \alpha^r(t) \\ 3B[(\partial\bar{w}/\partial x) + \bar{a}_0\alpha^r/\bar{P}] & \alpha^r = \text{const.} \end{cases} \quad (49)$$

The boundary conditions can also be transformed and the analogy is complete. For time-dependent temperatures and/or $B(t)$, the stepwise procedures outlined previously can again be used.

Case 3. Approximate Treatment of the Three-Dimensional Problem

Instead of using plate theory as outlined in the previous section, it is possible to use a modified strip method suggested by Biot[1] for the elastic problem. Basically the lifting surface is assumed to consist of the fore and aft parts of a strip as shown in Fig. 3. The bending moments at the points where the portions of the strip are joined are designated respectively by $M_{B_F}{}^v(1, y, t)$ and $M_{B_A}{}^v(1, y, t)$. The torque $M_T{}^v(y, t)$ which is acting on this strip is the difference between these two bending moments. Then the governing differential equation of the strip are obtained from Eq. (42), that is,

$$(\partial/\partial y)[J_e(y)Q\{\partial\theta^v/\partial y\}] = -P\{M_{B_F}{}^v(1, y, t) - M_{B_A}{}^v(1, y, t)\} = -P\{M_T{}^v(y, t)\} \quad (50)$$

and is subject to the boundary conditions expressed by Eq. (47). The bending moments are defined by Eq. (9).

The application of the Fourier transform to Eq. (50) for constant a_n and b_n results in

$$(\partial/\partial y)[J_e(y)\bar{G}(\partial\bar{\theta}^v/\partial y)] = -\bar{M}_T{}^v(y, \omega) \quad (51)$$

It will be noted that the Fourier transform of the viscoelastic angle of twist obeys a differential equation which is analogous to the elastic problem for shear modulus $\bar{G}$ and action by a torque $\bar{M}_T{}^v(y, \omega)$.

Since the viscoelastic bending moments are larger than the corresponding elastic ones, it follows that the viscoelastic torque $M_T{}^v$ is larger than the equivalent elastic one. Consequently, one may expect that the viscoelastic angle of twist will be larger than that for an elastic lifting surface having the same geometric and aerodynamic properties.

Stability Considerations

If at any time t_D the deflections are such that the internal, resisting torsional moments are exceeded by the applied torques, the deflections will increase without bound. Then for $t_D = 0$, the lifting surface is said to be elastically torsionally divergent and for $t_D > 0$ it is inelastically torsionally divergent. In the elastic case, divergence occurs instantaneously when the divergence Mach number ($M_D{}^e$) is reached. In the inelastic case, for any Mach number less than $M_D{}^e$, the deflections, and consequently the applied torques, increase with time until an unstable condition is reached at time t_D.

Let the time t_D be called the divergence time, that is, the time at which a lifting surface for a given stiffness,

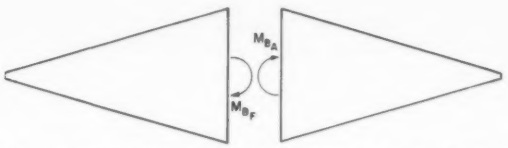

FIG. 3. Moments due to chordwise bending on fore and aft portions of strip.

Mach number, altitude, and temperature will diverge torsionally due to creep. For the two cases considered in this section, the time t_D is defined as

$$\lim_{t \to t_D} \theta^v(y, t) \to \infty \quad (52)$$

and

$$\lim_{t \to t_D} w(x, y, t) \to \infty \quad (53)$$

Again it is also possible to define an ultimate time, t_u, as the time necessary to reach some preassigned value of θ^v or w other than infinity.

Illustrative Example

In order to illustrate the results of the present analysis a simple, fundamental example will be considered. It consists of a rectangular lifting surface of span $2b$ having viscoelastic properties of the Maxwell-body type. All material and aerodynamic properties are taken constant along the span. This problem is chosen because under time-independent flight conditions it leads to an analytic solution.

For these conditions, Eq. (44) is specialized to read

$$\partial^3\theta^v/\partial t^*\partial y^{*2} = -D[(\partial\theta^v/\partial t^*) + \theta^v + \alpha^r] \quad (54)$$

with initial conditions

$$\theta^v(y^*, 0) = \theta^e(y^*) \quad (55)$$

and where

$$D = Cb^2/GJ_e, \quad t^* = t/\tau, \quad y^* = y/b \quad (56)$$

The nondimensional quantity D is the ratio of the aerodynamic to elastic torsional stiffness.

In this problem, the Laplace rather than the Fourier transform is chosen because the former is simpler to handle in this particular case. Let $\bar{\theta}^v(y^*, p)$ be the Laplace transform of $\theta^v(y^*, t^*)$, and note that the governing differential equation for the equivalent elastic problem can be obtained from Eq. (44) by setting $P = 1$ and $Q = G$, which yields

$$(d^2\theta^e/dy^{*2}) + D(\theta^e + \alpha^r) = 0 \quad (57)$$

Taking the Laplace transform of Eq. (54) results in

$$(\partial^2\bar{\theta}^v/\partial y^{*2}) + \varphi^2[\bar{\theta}^v + (\alpha^r/p)] = 0 \quad (58)$$

where

$$\varphi^2 = D[1 + (1/p)] \quad (59)$$

Comparison of Eqs. (57) and (58) leads one to observe again the previously discussed analogy, i.e., that the Laplace transform of the viscoelastic angle of twist, $\bar{\theta}^v$, is equal to the angle of twist θ^e in an equivalent

elastic problem where the shear modulus is $G(1 + 1/p)^{-1}$ and the rigid-body angle of attack is α^r/p. (Note that the equivalent shear modulus is the ratio of transforms of the operators Q and P and that the equivalent rigid-body angle of attack is the Laplace transform of the viscoelastic α^r.) Consequently, the viscoelastic angle of twist, $\theta^v(y^*, t^*)$, is the inverse transform of the equivalent elastic angle of twist, since $\bar{\theta}^v(y, p) = \theta^e(y, \varphi, \alpha^r/p)$.

The solution of Eq. (58) or an equivalent Eq. (57) subject to the boundary condition (44) is

$$\bar{\theta}^v(y, p) = (\alpha^r/p)\left[\frac{\cos\varphi(1 - y^*)}{\cos\varphi} - 1\right] \tag{60}$$

To invert the Laplace transform, one expands this expression in an infinite series as follows:

$$\bar{\theta}^v = \alpha^r \sum_{n=0}^{\infty}\sum_{l=0}^{n} \frac{(-1)^l(1 - y^*)^{2l}}{(2l)!}\frac{B_{2(n-l)}D^n}{[2(n - l)]!} \times \frac{(p + 1)^n}{p^{n+1}} - \frac{\alpha^r}{p} \tag{61}$$

where the $B_{2(n-l)}$ are Euler's numbers. The inverse transform of Eq. (61) may be obtained from reference 20.

$$\theta^v = \alpha^r \sum_{n=0}^{\infty}\sum_{l=0}^{n} \frac{(-1)^l(1 - y^*)^{2l} B_{2(n-l)}D^n L_n(-t^*)}{(2l)![2(n - l)]!} - \alpha^r \tag{62}$$

where the $L_n(-t^*)$ are Laguerre polynomials which are expressible in the form

$$L_n(-t^*) = \sum_{k=0}^{n} \frac{n!(t^*)^k}{[k!]^2(n - k)!} \tag{63}$$

The largest angle of twist necessarily occurs at the tip of the cantilevered lifting surface ($y^* = 1$) and for the purposes of stability considerations it will be sufficient to investigate this point. The resulting angle of twist is found from Eq. (62),

$$\theta^v(1, t^*) = \alpha^r \sum_{n=0}^{\infty} \frac{B_{2n}D^n L_n(-t^*)}{(2n)!} - \alpha^r \tag{64}$$

It is shown in the appendix that the series (64) converges for all $t^* < \infty$; consequently, no finite divergence time is obtained for this linear viscoelastic body. Similar results have been observed in cases of creep buckling of columns[9, 21] and plates,[10] and creep divergence of lumped-mass viscoelastic systems.[15]

The resultant shear stress, σ_s^v, can be determined by substituting Eq. (41) into (40), which yields

$$P\{\sigma_s^v\} = [J_e/2hA(y)b]Q\{\partial\theta^v/\partial y^*\} \tag{65}$$

For the particular case of the Maxwell-body type of stress-strain relation used in this illustrative example, the substitution of the proper values of the differential operators P and Q into Eq. (65) yields, with the help of Eq. (62),

$$\left\{\frac{\partial}{\partial t^*} + 1\right\}\sigma_s^v = F\sum_{n=0}^{\infty} f_n(y^*)\frac{dL_n(-t^*)}{dt^*} \tag{66}$$

where

$$f_n(y^*) = \sum_{l=0}^{n} \frac{(-1)^{l+1}(1 - y^*)^{2l-1} B_{2(n-l)}D^n}{(2l - 1)!\,[2(n - l)]!} \tag{67}$$

$$F = (J_e G\alpha^r)/(2hAb) \tag{68}$$

The solution of the differential equation (66) subject to the initial conditions $\sigma_s^v(y^*, 0) = \sigma_s^e(y^*)$, can be written in the following nondimensional form:

$$(\sigma_s^v/F) = (e^{t^*} - 1)f_1(y^*) + (\sigma_s^e/F) + \sum_{n=2}^{\infty}\left[-e^{-t^*} + L_n(-t^*) - \frac{t^* L^1_{n-1}(-t^*)}{n(n + 1)}\right]f_n(y^*) \tag{69}$$

where σ_s^e is the shear stress of the equivalent elastic problem, given by

$$\sigma_s^e = F\sum_{n=0}^{\infty} f_n(y^*) \tag{70}$$

and where the Laguerre polynomials are defined by

$$L^1_{n-1}(-t^*) = \sum_{k=0}^{n-1} \frac{n!(t^*)^k}{(n - k - 1)!(k + 1)!k!} \tag{71}$$

The results of a numerical example* for typical parametric variations are presented in Figs. 4 to 7. Both the maximum angle of twist (at the tip) and the maximum stress (at the root) are presented. Figs. 4 and 5 show the magnification with time of the maximum angle of twist due to creep over the rigid-body angle of attack and the maximum elastic angle of twist, respectively. It should be noted that the magnification of $\theta_{max.}^v$ is more pronounced with increase in the nondimensional parameter D [Eq. (56)]. It should be further noted that D increases with increasing Mach number, decreasing altitude, increasing area of lifting surface [see Eq. (45) for functional dependence of C], decreasing effective polar moment of inertia, and increasing temperature (since the shear modulus decreases).

Fig. 6 is a cross plot of the preceding figure. It indicates, for any value of D, the length of time needed to reach a preassigned value of the ratio of the maximum viscoelastic to elastic angle of twist. In the absence of a finite divergence time, such as the one defined by Eq. (52), the results of Fig. 6 can be used essentially to predict the lifetime of the lifting surface by limiting the maximum deflection. Once the configuration is fixed, the only unknown in the quantity D is the Mach number and an altitude combination. It should be remembered that for the configuration of the illustrative example, D must be less than $\pi^2/4$ in order to avoid elastic divergence.

In Fig. 7 the magnification of the maximum viscoelastic shear stress with time is shown. It is, of course, possible to cross-plot the results of Fig. 7 to

* The author is indebted to W. A. Madsen for carrying out the numerical computations.

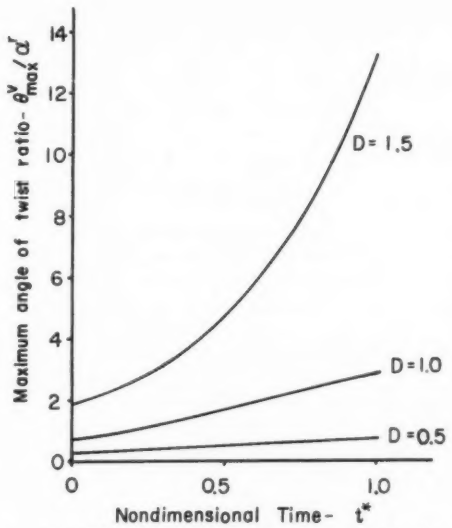

FIG. 4. Magnification with time of maximum angle of twist.

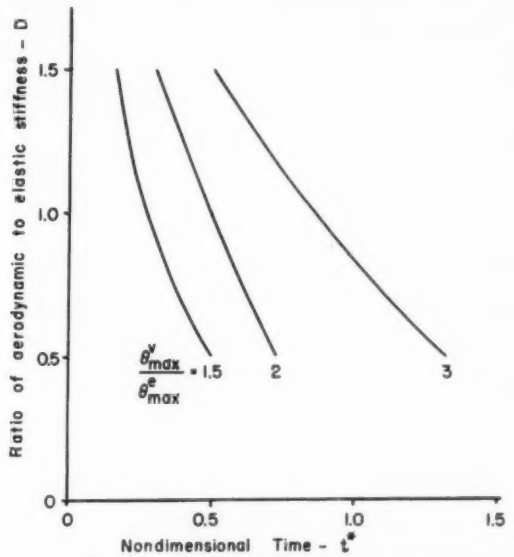

FIG. 6. Time to reach a given angle of twist magnification.

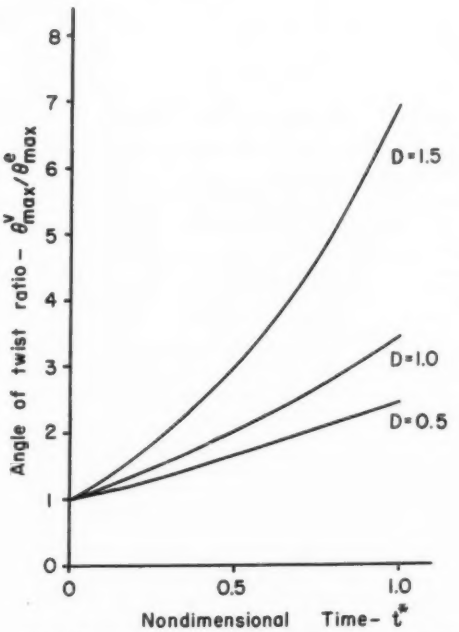

FIG. 5. Magnification with time of the ratio of maximum viscoelastic to elastic angle of twist.

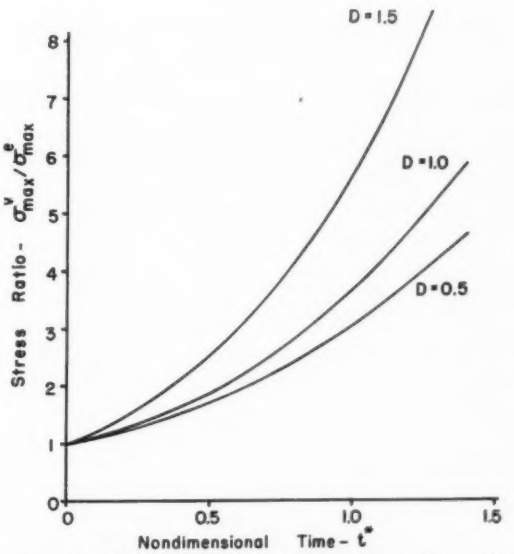

FIG. 7. Magnification with time of ratio of maximum viscoelastic to elastic shear stress.

produce graphs, similar to Fig. 6, that would indicate the length of time needed to reach a prescribed stress magnification.

In all these plots the nondimensional time t^* has been used as the abscissa. It is very sensitive to temperature variations, since it is the ratio of the real time to the relaxation time. Typical values for the relaxation time vary from 6×10^{36} sec. at room temperature to 7×10^{-4} sec. at 800°F. for "Puron" iron.[22, 23] This indicates that for a given real time the angle of twist will increase appreciably with temperature.

Appendix: Convergence of Series in Illustrative Example

Consider the series (64) defining $\theta^r(1, t^*)$. As a first test of convergence one must show that the Laguerre polynomials remain finite. Let the usual ratio test be applied to the series (63) representing $L_n(-t^*)$:

$$R_1 = \lim_{k \to n \to \infty} |(k+1)^2| \to \infty \tag{72}$$

Therefore, the Laguerre polynomials converge uniformly and absolutely for all finite t^*.

Next, let the ratio test be applied to the series (64), or

$$R_2 = \lim_{n \to \infty} \left| \frac{B_{2(n+1)}(2n)!\, DL_{n+1}(-t^*)}{B_{2n}[2(n+1)]!\, L_n(-t^*)} \right| \tag{73}$$

From the properties of Euler's numbers, it is known that

$$\lim_{n \to \infty} \left| \frac{B_{2(n+1)}(2n)!}{B_{2n}[2(n+1)]!} \right| \to \frac{4}{\pi^2} \tag{74}$$

Substitution of (74) into Eq. (73) yields

$$R_2 = \frac{4D}{\pi^2} \lim_{n \to \infty} \left| \frac{L_{n+1}(-t^*)}{L_n(-t^*)} \right| \tag{75}$$

But D must be less than $\pi^2/4$ in order to avoid elastic torsional divergence [see Equation (57)]. The limit of the ratio of the Laguerre polynomials may be evaluated from the recurrence relation

$$(n+1)L_{n+1}(-t^*) - (2n+1+t^*)L_n(-t^*) + nL_{n-1}(-t^*) = 0 \tag{76}$$

Dividing Eq. (76) by $(n+1)L_n(-t^*)$, taking the limit as $n \to \infty$, and letting

$$\lim_{n \to 0} \left| \frac{L_{n+1}(-t^*)}{L_n(-t^*)} \right| = U(t^*) \tag{77}$$

one obtains from Eq. (76)

$$U = 2 - (1/U) \qquad (t^* < \infty) \tag{78}$$

since U is finite by virtue of the convergence of the Laguerre polynomials as seen by Eq. (72). From (78) it follows that U is unity, and therefore from (75) it follows that $R_2 < 1$, which means that the series (64) convergences uniformly and absolutely for all $t^* < \infty$.

References

[1] Biot, M. A., *The Divergence of Supersonic Wings Including Chordwise Bending*, Journal of the Aeronautical Sciences, Vol. 23, No. 3, pp. 237–251, 1956.

[2] Fung, V. C., *On the Behavior of a Sharp Leading Edge*, Journal of the Aeronautical Sciences, Vol. 20, No. 9, pp. 644–645, 1953.

[3] Freudenthal, A. M., *The Inelastic Behavior of Engineering Materials and Structures*, John Wiley & Sons, Inc., New York, 1950.

[4] Alfrey, T., *Nonhomogeneous Stress in Viscoelastic Media*, Quarterly of Applied Mathematics, Vol. 2, pp. 113–119, 1944.

[5] Alfrey, T., *Mechanical Behavior of High Polymers*, Interscience Publishers, Inc., New York, 1948.

[6] Read, W. T., *Stress Analysis for Compressible Viscoelastic Materials*, Journal of Applied Physics, Vol. 21, pp. 671–674, 1950.

[7] Tsien, H. S., *A Generalization of Alfrey's Theorem for Viscoelastic Media*, Quarterly of Applied Mathematics, Vol. 8, pp. 104–106, 1950.

[8] Hilton, H. H., Hassan, H. A., and Russell, H. G., *Analytical Studies of Thermal Stresses in Media Possessing Temperature-Dependent Viscoelastic Properties*, WADC TR 53-322, 1953.

[9] Hilton, H. H., *Creep Collapse of Viscoelastic Columns with Initial Curvatures*, Journal of the Aeronautical Sciences, Vol. 19, No. 12, pp. 844–846, 1952.

[10] Hilton, H. H., and Benjamin, R. B., *Small and Large Deflection Theories for Initially Curved Viscoelastic Plates in Edge Compression*, paper submitted to Journal of the Aero/Space Sciences for publication.

[11] Lorsch, H. G., and Freudenthal, A. M., *On Mixed Boundary Value Problems of Linear Viscoelastic Solids*, Proceedings of the Second U.S. National Congress of Applied Mechanics, pp. 539–545, 1954.

[12] Allen, H. F., Brull, M. A., and Wilkie, W. J., *A Study of the Stress Analysis and Structural Testing Procedures Applicable to Aircraft Structures at Elevated Temperatures*, WADC TR 54-499, 1954.

[13] Hoff, N. J., *Approximate Analysis of Structures in the Presence of Moderately Large Creep Deformations*, Quarterly of Applied Mathematics, Vol. 12, No. 1, p. 49–55, 1954.

[14] Bozajian, J. M., private communication, August, 1956.

[15] Hilton, H. H., *Pitching Instability of Rigid Lifting Surfaces on Viscoelastic Supports in Subsonic or Supersonic Potential Flow*, Proceedings of the Third Midwestern Conference on Solid Mechanics, pp. 1–19, 1957.

[16] Hilton, H. H., *On the Representation of Nonlinear Creep by a Linear Viscoelastic Model*, Journal of the Aero/Space Sciences, Vol. 26, No. 5, pp. 311–312, May, 1959.

[17] Baer, H. W., *Prediction of Very Short Time Creep Buckling from Very Short Time Tensile-Creep Properties*, Proceedings of the Second U.S. National Congress on Applied Mechanics, pp. 569–576, 1954.

[18] Churchill, R. W., *Modern Operational Mathematics in Engineering*, McGraw-Hill Book Company, Inc., New York, 1944.

[19] Bruhn, E. F., *Analysis and Design of Airplane Structures*, Tri-State Offset Company, Cincinnati, p. A.5.3, 1949.

[20] Erdélyi, A., (Ed.), *Tables of Integral Transforms*, Vol. I, p. 175; McGraw-Hill Book Company, Inc., 1954.

[21] Kempner, J., and Pohle, F. V., *On the Nonexistence of a Finite Critical Time for Linear Viscoelastic Columns*, Journal of the Aeronautical Sciences, Vol. 20, No. 8, pp. 572–573, August, 1953.

[22] Kê, T. S., *Anelastic Properties of Iron*, Metals Technology, T.P. No. 2370, 1948.

[23] Everett, F. L., and Miklowitz, J., *Poisson's Ratio at High Temperature*, Journal of Applied Physics, Vol. 15, pp. 592–598, 1944.

The Flow About a Charged Body Moving in the Lower Ionosphere†

RAUL R. HUNZIKER*

Convair, San Diego, A Division of General Dynamics Corporation

Summary

The flow about an electrically charged body traveling at high speeds through the lower ionosphere is analyzed. A simple gas model composed of electrons, ions, and neutral particles is used and the hydrodynamic description given is based on Maxwell's transfer equations for a mixture.

The conditions under which local statistical equilibrium can be assumed are discussed, and different approaches to determine the gasdynamic force in the subsonic, supersonic, and hypersonic cases are indicated. The reciprocal action of the electric field of the flow on the body is also analyzed, and a formula for the resultant electric force is given. The total force on the body is equal to the sum of the gasdynamic force and the electric force.

The negative potential acquired by a plane body is also calculated. Finally, the lack of validity of Debye's linearization in this case and the solution of the exterior nonlinear problem which characterize the electric potential and the electron distribution are discussed.

Introduction

WHEN A FINITE BODY moves rapidly through the ionosphere it can be inferred that the body becomes electrically charged because of the incident flux of electrons and ions. With the naturally or artificially charged body there will be electromagnetic interactions with the surrounding ionospheric gas. It can be conjectured that these interactions will affect the resulting force which the ionospheric gas exerts on the body and the electron density in its neighborhood. Naturally, to realize a concrete quantitative analysis it will be necessary to consider only those effects which are predominant, so that the formulation will be sufficiently simple to allow numerical solution and still describe the phenomena consistently.

An analysis of the resulting force has been given by Jastrow and Pearse[1] for a sphere moving in the upper ionosphere at about 400 km., in which region free molecule flow is assumed. For the lower ionosphere (Layers D and E) one can apply a macroscopic fluid-dynamic description by means of Maxwell's transfer equations coupled with Maxwell's electromagnetic field equations.

Received October 6, 1959. Revised and received February 20, 1960.

† This article is a revision of an earlier one that was completed while the author was at Convair.

* Formerly with Applied Mathematics Group, Physics Section. Presently, Senior Scientist, R.C.A., Systems Analysis, AFMTC, and Professor of Mathematical Physics, Brevard Engineering College, Melbourne, Fla.

The author wishes to acknowledge many valuable discussions with Mr. J. G. Wolfe and Dr. G. Plato.

The electron density at midday increases from a value of 1.5×10^4 electrons/cm.^{3} at 60 km. (D layer) to 1.5×10^6 electrons/cm.^{3} at 300 km. (F layer). In the E layer which is situated at about 100 km. altitude and is almost 20 km. thick, the density of electrons is about 1.5×10^5 electrons/cm.^{3} at midday and 10^4/cm.^{3} at midnight.[2]

The characteristic state of the ionosphere can be represented by ionized and quasi-neutral gas in which the negative particles are exclusively electrons with particle density N_e and the positively charged particles are ions with particle density N_i. This gas of charged particles is called a plasma. The characteristic property of the ionospheric plasma is quasi-neutrality (proposed by Shottky[3]), expressed by

$$N_e \sim N_i \sim N$$
$$|N_i - N_e| \ll N \tag{1}$$

This model in which the plasma has a strong electrostatic Coulomb interaction has certain similarities with the concentrated solutions of electrolytes in the Debye-Hückel[4] theory.

Boltzmann and Electromagnetic Field Equations for the Ionosphere Gas Model

We assume our model to be a homogeneous mixture of three types of particles. Each type will be macroscopically described by its distribution function

$$f_j(\mathbf{c}, \mathbf{r}, t), \qquad (j = 1, 2, 3) \tag{2}$$

where $\mathbf{c}$ is the actual velocity of a jth particle, $\mathbf{r}$ is the position vector of a cell in physical space, and t denotes the time. One defines $f_j(\mathbf{c}, \mathbf{r}, t)$ such that the probable number of particles located at time t in the neighborhood $d\mathbf{r}$ of the point $\mathbf{r}$ having velocity vectors ending in the neighborhood $d\mathbf{c}$ of $\mathbf{c}$ is equal to

$$f_j(\mathbf{c}, \mathbf{r}, t)\, d\mathbf{c}\, d\mathbf{r} \tag{3}$$

The probable number of particles of class j situated in the unit volume centered at $\mathbf{r}$ is

$$n_j = \int f_j(\mathbf{c}, \mathbf{r}, t)\, d\mathbf{c} \tag{4}$$

where the integration is extended over the whole $\mathbf{c}$ space. The quantity $n_j(\mathbf{r}, t)$ is called the number density function of the j-particles. The kinetic theory of a mixture of gases is based on the following system of Boltzmann integro-differential equations to be satisfied by the functions f_j:

$$\left\{\frac{\partial}{\partial t} + \mathbf{c}\cdot\nabla_{\mathbf{r}} + [\mathbf{F} + \epsilon_j(\mathbf{E} + \mathbf{c}\times\mathbf{H})]\cdot\nabla_{\mathbf{c}}\right\} f_j = \sum_k J_{jk},\ (j, k = 1, 2, 3), \quad \text{(e.m.u.)} \quad (5)$$

where

$\mathbf{F}$ = external gravitational field,
$\mathbf{E}$ = electric field,
$\mathbf{H}$ = magnetic field,
ϵ_j = ratio of charge e_j to mass m_j, and
J_{jk} = collision integrals over the velocity-impact parameter space.

The electromagnetic field $\mathbf{E}$, $\mathbf{H}$ will satisfy Maxwell's equations (c.g.s., e.m.u.)

$$\nabla\cdot\mathbf{E} = 4\pi\alpha^2 q$$

$$\nabla\times\mathbf{E} + \frac{\partial\mathbf{H}}{\partial t} = 0$$

$$\nabla\cdot\mathbf{H} = 0$$

$$\nabla\times\mathbf{H} - \alpha^{-2}\frac{\partial\mathbf{E}}{\partial t} = 4\pi\mathbf{J}$$

$$\alpha = 2.9979\times 10^{10}\ \text{cms}^{-1} \quad (6)$$

$$\mathbf{J} = \sum_{j=1}^{3} e_j n_j \overline{\mathbf{c}_j},\quad q = \sum_{j=1}^{3} e_j n_j,\quad \overline{\mathbf{c}_j}(\mathbf{r}, t) = \frac{1}{n_j}\int \mathbf{c}_j f_j d\mathbf{c}_j \quad (7)$$

where $\mathbf{J}$ and q are the electric current and charge densities, respectively.* In principle it should be possible to express the

$$\sum_{k=1}^{3} J_{jk}$$

which corresponds to distinct contributions, in an explicit form. To do this a detailed knowledge of the collision mechanisms and the clarification of the question of the legitimacy of considering only binary encounters between distant particles would be required. At present no such completely defined set of equations exists for mixtures of charges and neutral particles. It is also generally accepted that no mathematical model of the encounters for which approximate calculations have been effected gives a satisfactory description of all phenomena. Fortunately, there are two limiting cases which permit partial circumvention of these intrinsic difficulties. The first case concerns extreme rarefaction, in which the collision terms J_{jk} are essentially zero. In the second case one can apply the equations of transfer for the gas mixture together with additional hypotheses supported by indirect experimental information about the frequency of the different types of collisions, so that a consistent semiphenomenological and quantitative description of the observables related to the flow about bodies of reasonable and sufficient size is provided. It is the second case which is appropriate to our problem.

* Single charged ions and free-space constant inductive capacities $\epsilon = \alpha^{-2}$ and $\mu = 1$ are assumed.

Equations of Macroscopic Description for the Lower Ionosphere

As is known, by multiplying the Boltzmann equations by a particle property $\Phi_j(\mathbf{r}, \mathbf{c}, t)$ and integrating over $\mathbf{c}$ space, Maxwell's equations of transfer of that property Φ_j will follow.[5] In the case of a mixture it is convenient to specify Φ_j as a function $\Phi_j(\mathbf{C}_j)$ where $\mathbf{C}_j = \mathbf{c}_j - \mathbf{V}$ is the peculiar velocity relative to the mass motion of velocity $\mathbf{V}$ of the mixture. Adding the component transfer equation for $\Phi_j = m_j$, and since

$$\sum_{j=1}^{3} \rho_j \overline{\mathbf{C}_j} = 0$$

it follows that the equation of conservation of mass for the mixture is

$$\frac{\partial\rho}{\partial t} + \mathbf{V}\cdot\nabla_{\mathbf{r}}\rho + \rho\nabla_{\mathbf{r}}\cdot\mathbf{V} = 0 \quad (8)$$

where

$$\rho = \sum_{j=1}^{3}\rho_j \quad \text{and} \quad \rho_j = n_j m_j \quad (9)$$

The total transfer equations for $\Phi_j = m_j\mathbf{C}_j$ and $\Phi_j = 1/2 m_j|\mathbf{C}_j|^2$ are

$$\rho\left(\frac{\partial}{\partial t} + \mathbf{V}\cdot\nabla_{\mathbf{r}}\right)\mathbf{V} + \nabla_{\mathbf{r}}\cdot P = \rho\mathbf{F} + q\mathbf{E} + \mathbf{J}\times\mathbf{H} \quad \text{(e.m.u.)} \quad (10)$$

$$\rho\left(\frac{\partial}{\partial t} + \mathbf{V}\cdot\nabla_{\mathbf{r}}\right)U + \nabla_{\mathbf{r}}\cdot\mathbf{Q} + P:\nabla_{\mathbf{r}}\mathbf{V} = \mathbf{j}\cdot(\mathbf{E} + \mathbf{V}\times\mathbf{H}) \quad \text{(e.m.u.)} \quad (11)^*$$

where the conduction current $\mathbf{j}$ is the difference between the electric current $\mathbf{J}$ and the convection current $\mathbf{J}_c$,

$$\mathbf{j} = \mathbf{J} - \mathbf{V}\sum_{j=1}^{3} e_j n_j = \sum_{j=1}^{3} e_j n_j(\overline{\mathbf{c}_j} - \mathbf{V}) \quad (12)$$

and P, $\mathbf{Q}$, and U are identified with the stress tensor, heat flux vector, and intrinsic kinetic energy of the mixture, respectively.

The above transfer equations lead to a natural definition of kinetic temperature T of the mixture but do not imply thermal equilibrium which is a necessary condition for equipartition of energy. That is to say, when using Eqs. (10), (11), and (12) the kinetic temperatures of the components need not necessarily be equal. For ionospheric gas, experimental results indicate that the electronic temperature is much higher than the ionic and neutral particle temperature.

It is known that the energy required to ionize a molecule is much larger than the thermal energy. There-

* The colon written between two tensors indicates a double product in which a double sum is taken—i.e., $a:b$ denotes the sum

$$\sum_i\sum_j a_{ij}\,b_{ij}$$

fore, since it is quite probable that the ionizing agent will possess more energy than is necessary for ionization, this excess energy will add to the kinetic energy of the electron. If the electrons do not encounter too many molecules before recombination occurs, the mean electronic temperature should be larger than the molecular temperature. Since the ions are much more massive than the electrons, the electrons will accelerate more rapidly in an external field than the ions.

Therefore, the energy acquired from the field per unit time will be about $\sqrt{m_i/m_e}$ times larger for an electron than for an ion. According to the laws which hold for elastic collisions, only a small fraction of the electron energy, at most of order $4\,m_e/m_i$, can be transferred to a molecule.[6] Hence, in the neighborhood of the charged body where its electric field is sufficiently large, the mean temperature of the electrons should be larger than that of the ions and neutral particles. With decreasing density the number of collisions of electrons and neutral particles decreases; therefore, the electron temperature will increase. This behavior is supported by the comparison between the nearly "isothermal plasma" ($T_e = T$ = 5000 to 20,000°C.) of an electric arc burning in free air and the "nonisothermal" plasma of an electric discharge in mercury vapor at a low pressure of about 10^{-3} mm. of mercury. In the latter case, electron temperatures of 60,000 to 80,000°C. may appear while the ion and neutral-particle temperature remains the same as its surroundings. We then see that in the nonisothermal plasma of the ionosphere the thermal contact between the electron gas and the ion-neutral particle gas may be low even though they are uniformly mixed.

The results of the analysis made of the experimental results by the probe technique in gas discharge plasmas have indicated that the electrons follow a Maxwellian velocity distribution with great accuracy.[6] We will assume, therefore, that the electron gas of the ionospheric ternary mixture has a Maxwellian velocity distribution and a constant electron temperature $T_e \gg T$.*

In analogous fashion the ion gas will be considered to have a properly defined temperature by assuming that it is approximately isothermal with the neutral gas and the mixture; i.e., $T_i = T_n = T$. At an altitude of 100 km. the mean free path and collision time of the ions and neutral particles are about 10 cm. and 2.6×10^{-4} sec., respectively. For a body 5 m. long, the Knudsen number $K = 0.02 \ll 1$; therefore, a local Maxwellian distribution may be assumed and considered a sufficient approximation to the ion and neutral-particle distribution functions outside boundary or shock layer regions where large gradients occur.[7, 8] All three components then will be assumed to attain Maxwellian velocity distributions[5] given by

$$f_e = N(m_e/2\pi kT_e)^{3/2} \exp\,(-m_e C_e^2/2kT_e) \quad (13)$$

$$f_i = N(m_i/2\pi kT)^{3/2} \exp\,(-m_i C_i^2/2kT) \quad (14)$$

$$f_n = n(m_n/2\pi kT)^{3/2} \exp\,(-m_n C_n^2/2kT) \quad (15)$$

In the last equation the particle density $n(\mathbf{r})$ consequently must be a slowly varying function of $\mathbf{r}$. As is known, a magnetic field acting on each particle does not alter the number density for a uniform and stationary gas of charged particles, whereas an electric field potential ϕ will modify the density but the distribution will remain Maxwellian.[5] In Eq. (13) and (14) one should replace N by its product with the Maxwell-Boltzmann factors

$$n_e = N \exp\,(e\phi/kT_e) \quad (16)$$

$$n_i = N \exp\,(-e\phi/kT_i) \quad (17)$$

respectively.[5, 9] But the local application of these formulas will be legitimate only if, in the time that it takes for the particles in mass motion to pass from one small volume (in which the electric field can be considered uniform) to the next, the electrons and ions realize a sufficient number of collisions to adjust to the new local electric field equilibrium conditions. Furthermore, it is assumed implicitly that the macroscopic rotation of the gas of charged particles can be locally ignored. At a speed of 2700 m./sec. (about $M = 9.5$) the electrons and ions of the mixture realize 11 and 0.07 collisions, respectively, while passing massively through a 5-cm. distance. Then, if we define our small cubic volume (cell) to be of a size equal to 1/100 of the body's assumed 5-m. length we see that the ions do not accomplish the few collisions necessary to attain local equilibrium under the electric field within a cell. As a consequence, for the supersonic case, we take

$$n_i = N = \text{constant} \quad (18)$$

instead of Eq. (17) which is appropriate for a subsonic body.

Plausible Approximations and Final Equations

The following general simplifications will be introduced as suggested by heuristic and order-of-magnitude arguments:

(1) The gravitational potential is assumed to cause a negligible effect; therefore, $\mathbf{F} = 0$ is assumed in Eq. (10).

(2) The power dissipated by the forced diffusion of electrically charged particles acted upon by the Lorentz force is negligible with respect to the power required for the expansion or compression of the mixture during the motion of a fluid element. Therefore, the term

$$\mathbf{j}\cdot(\mathbf{E} + \mathbf{V} \times \mathbf{H}) = \sum_j e_j n_j(\bar{\mathbf{C}}_j - \mathbf{V})\cdot(\mathbf{E} + \mathbf{V} \times \mathbf{H}) \quad (19)$$

which expresses the ohmic heating of the gas, is set equal to zero in Eq. (11).

(3) Since the coordinate system $\mathbf{K}$ fixed in the body

* See footnote, p. 942. The subscripts i and e are relative to positive ions and electrons, and e will denote the charge of the electron.

will be assumed to move nonrelativistically with respect to the earth, a measurement of the earth's magnetic field taken at rest in **K** will yield $\mathbf{H}_0$ as determined at rest with respect to the earth. We can then write for **H** relative to **K**

$$\mathbf{H} = \mathbf{H}_0 + \mathbf{H}_1$$

where $\mathbf{H}_1$ is the field caused by the electric currents.

(4) The mass flow of the mixture is assumed to be steady relative to **K**. Then, we can write

$$\partial \mathbf{H}_1/\partial t = 0$$

and since $\mathbf{H}_0$ can be assumed uniform over large regions it follows that

$$\partial \mathbf{H}/\partial t = 0 \quad \text{and} \quad \nabla \times \mathbf{E} = 0$$

Since the electric potential of the body and the charge distribution is assumed steady, its electric field must be static. Also, since the convection and conduction currents in the surrounding gas will be steady, it follows that the magnetic field produced by the currents must be static. From the above considerations it can be seen that an electrostatic potential exists so that

$$\nabla^2\phi = -4\pi q \qquad q = e(n_i - n_e) \quad \text{(e.s.u.)} \quad (20)$$

(5) By an order-of-magnitude calculation it will be shown that

$$|\mathbf{J} \times \mathbf{H}| = \left|\left(\sum_j e_j n_j \bar{\mathbf{c}}_j\right) \times (\mathbf{H}_0 + \mathbf{H}_1)\right| \quad (21)$$

can be neglected with respect to $q|\mathbf{E}|$ and made equal to zero in Eq. (10).

The electric force $q\mathbf{E}$ acting upon a "fluid element" will then affect the mass velocity field **V**. The action of this electric field **E** on the mixture is accounted for by the collisions of the charged particles with the neutral particles. The study of the action of the electric field **E** on the ionospheric gas can be based on Eq. (10) as modified by the above assumptions and as will be modified further in special cases.

The Velocity Field and Its Dependence on the System of Electric Forces

In the cases of a subsonic body of regular shape or a slightly supersonic thin or slender body the following assumptions can be made:

(1) At sufficiently high Reynolds numbers ($Re \simeq 1.5\ MK^{-1}$) a hydrodynamic boundary layer with slip exists over the conductor.

(2) The viscosity is assumed zero in the outer region, i.e., the stress tensor P of the mixture is a scalar p and the term $P:\nabla_{\mathbf{r}}\mathbf{V}$ in Eq. (11) is equal to zero.

(3) The power transferred by heat conduction is assumed to be negligible in front of the power required for the expansion or compression so that the flux vector **Q** of intrinsic energy is essentially zero.

(4) Assumptions (2) and (3) and Eq. (15) imply the adiabatic law

$$p\rho^{-\kappa} = \text{constant} \quad (22)$$

while following the motion of a compressing or expanding fluid element.

(5) Since $\nabla \times \mathbf{E} = 0$,

$$\mathbf{V} = \text{grad}\ \psi \quad (23)$$

may be assumed, where ψ is a hydrodynamic potential. By Eqs. (8), (9), (10), (22), (23), and assumptions (1) preceding Eqs. (18) and (2) preceding Eq. (22), the nonlinear partial equation of motion follows as

$$\nabla\psi\cdot\nabla\left(\frac{|\nabla\psi|^2}{2}\right) = a\nabla^2\psi - \frac{(n_i - n_e)e}{\rho}\nabla\psi\cdot\nabla\phi \quad (24)$$

where $a^2 = \kappa p/\rho$ is the mixture's local speed of sound. Since

$$n_e/(n_i + n_e) \leq 10^{-7}$$

the exponent κ is essentially equal to C_p/C_v for the neutral gas.[10] Diffusion phenomena are thereby neglected.

On integrating over a streamline it might be assumed that the work of the force $(n_i - n_e)e\ \nabla\phi$ is negligible with respect to that of ∇p. As indicated in Eq. (19) this is tantamount to neglecting the ohmic heating caused by convection currents, to the approximate validity of Bernoulli's equation, and to the sound speed relation

$$a^2 = a_0^2 - \frac{\kappa - 1}{2}[V^2 - V_0^2] \quad (25)$$

where the subscript zero refers to conditions at great distance from the body.

In this form, Eq. (24) is reduced to the well-known nonlinear equation when no field $-\nabla\phi$ is present.

A procedure of the Oseen[11] type could probably be applied in some cases to calculate the perturbation on the velocity field $\nabla\psi$ caused by the known distribution of force $-q\nabla\phi$. It is plausible, therefore, to conjecture that in the subsonic case, and with the stated assumptions, an exception to the D'Alembert paradox[12] will occur as in the case of an incompressible flow under body forces.[13, 14]

For the subsonic or slightly supersonic thin plane or slender bodies a perturbation potential $V_0\Omega$,

$$\psi = V_0(X + \Omega) \quad (26)$$

can be introduced.[15]

By Eqs. (24), (25) and (26), and when **K** is a system of Cartesian coordinates x, y, z, the exact equation

$$\Omega_{yy} + \Omega_{zz} - \mu^2\Omega_{xx} = M^2D[\Omega] + \frac{(n_i - n_e)e}{\kappa a^2}[(1 + \Omega_x)\phi_x + \Omega_y\phi_y + \Omega_z\phi_z] \quad (27)$$

follows where $D[\Omega]$ is van Dyke's nonlinear term [reference 15, Eq. (4), p. 2],

$$\mu = \sqrt{M^2 - 1}, \qquad M = V_0/a_0$$

and where n_e and n_i are defined by Eqs. (16), (17), and (18).

By introducing the linearization assumption in a^2 as given by Eq. (25),

$$a^2 = a_0^2 - (\kappa - 1)\Omega_x V_0 \tag{28}$$

an extension of van Dyke's procedure can be visualized by considering the electric term in the perturbation scheme. The pressure distribution could then be finally calculated.

Similarly, the boundary layer analysis with slip-flow boundary conditions[16] may be generalized to include the electric force term. In this form the gas-dynamic lift and drag forces could be determined. However, near the body surface the mass velocity is much slower and the actual number of collisions should be much larger. The actual ion density may be between N and $N \exp(-e\phi/kT)$. Adequate estimates of the slip velocity may indicate the choice of Eq. (17) or (18) in the boundary layer analysis.

For hypersonic flow, Eq. (15) and assumptions (2), (3), (4) and (5) preceding Eq. (23) are no longer valid and the stress tensor P in Eqs. (10) and (11) can be taken as having the Navier-Stokes dependency. Recent hypersonic flow analyses based on the Navier-Stokes equations[17] may possibly be evolved to include the effect of $-q\nabla\phi$ on the flow field and transfer quantities.

We will now consider the probably less important reciprocal effect, that is, the action of the electric field on the charged particles bound to the conductor.

Potential Distribution and Electric Force Exerted on the Conducting Body

According to Eqs. (7), (16), (17) and (18), the charge density term in Eq. (20) is

$$-q = eN[\exp(e\phi/kT_e) - \exp(-e\phi/kT_i)] \tag{29a}$$

for subsonic speeds, and

$$-q = eN[\exp(e\phi/kT_e) - 1] \tag{29b}$$

for supersonic speeds. The steady plasma flow will realize a stationary space-charge density distribution in the infinite outer region bounded by the surface S of the charged body.

The space charge density $q = e(n_i - n_e)$ should vanish at infinity where the plasma is neutral. From a physical viewpoint the electric potential $\phi(x, y, z)$ which satisfies Eq. (20) and Eq. (29a) or (29b) must also be Newtonian and therefore representable by a convergent improper integral extended over the infinite outer region

$$\phi(x, y, z) = \iiint_{\infty} \frac{q(x', y', z')dv'}{\sqrt{(x - x')^2 + (y - y')^2 + (z - z')^2}} \tag{30}$$

As is known,[18] this representation is assured when ϕ is a twice continuously differentiable function satisfying the asymptotic conditions

$$\phi = 0(r^{-\nu})$$

$$\phi_x, \phi_y, \phi_z = 0(r^{-1-\nu})$$

$$\nabla^2\phi = -4\pi q = 0(r^{-2-\nu}), \quad 0 < \nu < 1$$

for $r = +(x^2 + y^2 + z^2)^{1/2} \to \infty$. This consideration leads to the formulation of the following exterior nonlinear Dirichlet problem:

$$\nabla^2\phi = -4\pi q[\phi], \text{ in the infinite outer region, where } q[\phi] \text{ is given by Eq. (29a) or (29b)} \tag{31a}$$

$$\phi = \phi_0, \text{ over the boundary } S \tag{31b}$$

$$\phi = 0(r^{-\nu}), \ |\nabla\phi| = 0(r^{-1-\nu}), \nabla^2\phi = 0(r^{-2-\nu}), \quad 0 < \nu < 1, r \to \infty \tag{31c}$$

If a unique twice continuously differentiable solution ϕ of this problem exists, then it has the integral representation of Eq. (30); therefore, it is the physically consistent distribution of electric potential which applies to Eqs. (24) and (27) through Eqs. (16) and (17).

The charge density over the surface S of the conductor is given by

$$\eta = -\frac{1}{4\pi}\left(\frac{\partial\phi}{\partial n}\right)_S \quad \text{(e.s.u.)} \tag{32}$$

where $\mathbf{n}$ is the normal vector toward the exterior of S. The resultant of the electric forces exerted on the charges bound to the body is therefore

$$\mathbf{T} = \frac{1}{8\pi}\int_S\int\left(\frac{\partial\phi}{\partial n}\right)^2 \mathbf{n}\, ds \quad \text{(e.s.u.)} \tag{33}$$

Calculation of the Electric Potential of a Thin Plane Body

Since the thermal velocity of the electrons is at least sixty times greater than that of the ions, the flux of electrons incident to the body surface S will be equal to the flux of ions only when part of the electrons are repelled by a negative charge over the body surface.

A steady body electric potential $\phi_0 < 0$ will be then characterized by the time-independent equality of the flux of ions to the flux of electrons with kinetic energy above $-e\phi_0$. This implies that photoejection of electrons at the body surface is not considered. We will denote by $\mathbf{c}$ the velocity of an electron with respect to the frame of reference $\mathbf{K}$ (Fig. 1).

According to the convention which directs the electric vector $\mathbf{E}$ toward a negatively charged body, the kinetic energy required of an electron to reach the body surface of potential $\phi_0 < 0$ is at least

$$\frac{1}{2}m_e|\mathbf{c}_0|^2 = -e\phi_0 > 0$$

We define the peculiar velocity of the electron at a point $\mathbf{r}$ of $\mathbf{K}$ by $\mathbf{C} = \mathbf{c} - \mathbf{V}(\mathbf{r})$ where $\mathbf{V}$ is the mass velocity at $\mathbf{r}$. The number of electrons per unit volume about

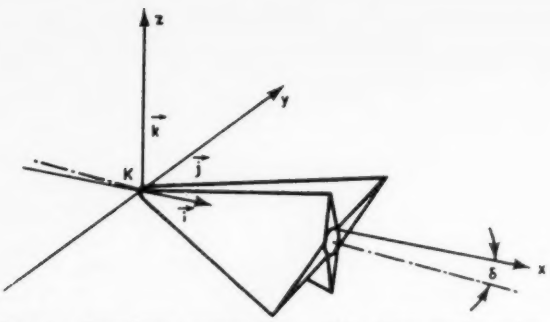

FIG. 1. Coordinate system for a thin plane configuration.

$\mathbf{r}$, with actual velocities in the range $\mathbf{c}$, $d\mathbf{c}$ is*

$$f[C(\mathbf{r})]d\mathbf{c} = n_e(m_e/2\pi kT_e)^{3/2} \exp(-m_e C^2/2kT_e)d\mathbf{c} \quad (34)$$

where
$$n_e = N \exp[e\phi(\mathbf{r})/kT_e] \quad (35)$$

In the neighborhood of the body we may assume also that

$$n_e = N \exp(e\phi_0/kT_e) \quad (36)$$

where ϕ_0 is the yet unknown body potential.

We denote by θ the angle of the electron velocity vector $\mathbf{c}$ with the outer normal unit vector $\mathbf{n}$, and find that only those electrons for which

$$(\pi/2) \leqq \theta \leqq (3\pi/2), \quad |\mathbf{c}| > c_0 = (-2e\phi_0/m_e)^{1/2} \quad (37)$$

can reach the surface. The number of electrons dN_e^* with velocities in the range $\mathbf{c}$, $d\mathbf{c}$ reaching in unit time a unit area of conducting surface are those encompassed by a cylinder of unit base and slant height c (as shown in Fig. 2):

$$dN_e^* = -f(C)\mathbf{c}\cdot\mathbf{n}\, d\mathbf{c} \quad (38)$$

Since $\mathbf{c} = \mathbf{C} + \mathbf{V}(\mathbf{r})$, we can assume

$$\mathbf{c}\cdot\mathbf{n} \cong C \cos\theta'$$

for a thin plane body at small angle of attack.

For every $\mathbf{r}$ of $\mathbf{K}$ we have

$$d\mathbf{c} = d\mathbf{C} = C^2 \sin\theta' dC d\theta' d\omega' \quad (39)$$

in velocity space of spherical coordinates C, θ', and ω'.

To obtain the total number N_e^* of electrons reaching the unit area in unit time we integrate over Γ, the lower half velocity space excised from a hemisphere of radius c_0.

$$\Gamma: \begin{cases} 0 \leqq \omega' \leqq 2\pi \\ \dfrac{\pi}{2} \leqq \theta' \leqq \dfrac{3\pi}{2} \\ c_0 \leqq C < +\infty \end{cases}$$

By Eqs. (34) and (36)–(39) we obtain

$$N_e^* = (kT_e/2\pi m_e)^{1/2} N e^{2\chi_0}(1 - \chi_0) \quad (40)$$

where

$$\chi_0 = e\phi_0/kT_e$$

For the ions, there is no barrier of potential and we will assume, as discussed for Eq. (18), that their local number density distribution is N. Hence,

$$N_i^* = -N\left(\frac{m_i}{2\pi kT_i}\right)^{3/2} \int_0^{2\pi} d\omega \times \int_{\pi/2}^{3\pi/2} \sin\theta\cos\theta\, d\theta \int_0^{\infty} C^3 \exp\left(\frac{-C^2}{2kT_i}\right) dC$$

$$= \left(\frac{kT_i}{2\pi m_i}\right)^{1/2} N \quad (41)$$

In the subsonic case we will replace N by n_i as given by Eq. (17) in terms of ϕ_0. By equating N_e^* to N_i^* in Eqs. (40) and (41), the value of ϕ_0 follows by solving the transcendental equation

$$e^{2\chi_0}[1 - \chi_0] = +\sqrt{(T_i/T_e)(m_e/m_i)} \quad (42)$$

If we take[1] $kT_e = 1$ ev $= 1.602 \times 10^{-12}$ erg, $T_e = 11{,}600°$K., $T_i = 200°$K., $(m_i/m_e) = 14 \times 1860$, for a model with atomic nitrogen atoms, by Eq. (42) we obtain

$$\chi_0 = -4.438, \quad \phi_0 = -4.438 \text{ volts}$$

Relative Order of Magnitude of the Gasdynamic, Electric, and Lorentz Forces

We will first determine the order of magnitude of the gasdynamic pressure increment Δp over a plane body by considering the simple limiting case of a flat plate at an angle of attack of $\delta = 0.05$ radian (about 3 degrees). The linear supersonic approximation gives, in dynes/cm.^{2},

$$\Delta p = 10\rho V_0^2 \delta (M^2 - 1)^{-1/2} \text{ for } \delta M < 1 \quad (43)$$

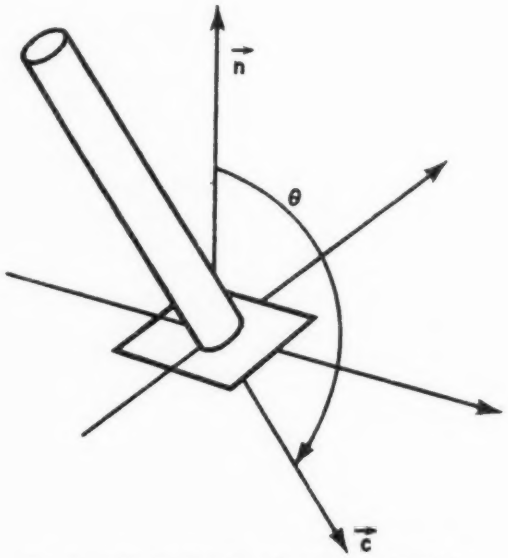

FIG. 2. Cylinder of unitary base and slant height c.

* Here we will assume that even in the close neighborhood of the body, Maxwellian distributions give a reasonable description of the actual distributions.

For an altitude of 100 km.,

$$\rho = 7.12 \times 10^{-7} \text{ m.}^{-4} \text{ Kp. sec.}^2$$

and if

$$V_0 = 2700 \text{ m. sec.}^{-1}, \quad M = 9.5$$

from Eq. (43) we obtain

$$\Delta p = 0.2754 \text{ dyne/cm.}^2$$

This value of Δp may be considered as a lower bound for a thin plane configuration at the same speed and altitude.

Since the knowledge of the electric pressure $(1/8\pi)(\partial\phi/\partial n)^2$ exerted on the conducting body would require the solution of Eq. (31) for a given three-dimensional closed surface S, we will consider here an infinite charged plate. This model will probably give a reasonable estimate of the electric attraction per unit area of a thin plane body.

If the infinite plate at negative potential ϕ_0 is orthogonal to the z axis, Eqs. (29b) and (31) imply

$$\phi''(z) = 4\pi Ne(e^{\beta\phi(z)} - 1), \quad \beta = e/kT_e \tag{44a}$$

$$\phi(0) = \phi_0(0) < 0 \tag{44b}$$

$$\lim_{z\to+\infty} \phi(z) = 0, \quad \lim_{z\to+\infty} \phi'(z) = 0 \tag{44c}$$

For this simple model a representation as given by Eq. (30) is impossible; therefore, the conditions of Eq. (31c) are weakened to those in Eq. (44c). From Eq. (44a) and by a quadrature we obtain

$$\phi'(z) = \pm[8\pi\, Ne(\beta^{-1}e^{\beta\phi} - \phi) + C_1]^{1/2} \tag{45}$$

where the constant C_1 is determined by condition of Eq. (44c),

$$C_1 = -8\pi N/kT_e \tag{46}$$

Since the potential $\phi(z)$ must be a negative, continuous, monotonically increasing function of z in $(0, \infty)$, the + sign in Eq. (45) is chosen. Then

$$\phi'(z) = +(8\pi NkT_e)^{1/2}(e^{\beta\phi} - \beta\phi - 1)^{1/2} \quad \text{(e.s.u.)} \tag{47}$$

is an ordinary differential equation which has a unique integral $\phi(z)$ satisfying the condition $\phi(0) = \phi_0 < 0$. If the plate is positively charged the + sign in Eq. (47) must be reversed.

The existence of a unique solution of the nonlinear asymptotic problem of Eqs. (44) is therefore assured. For $\chi(0) = \chi_0 = \beta\phi_0 = -4.438$

$$kT_e = 1 \text{ ev}, \quad N = 1.5 \times 10^5 \text{ cm.}^{-3}$$

and by Eq. (47)

$$\frac{1}{8\pi}[\phi'(0)]^2 = 8.29 \times 10^{-7} \text{ dyne/cm.}^2 \ll \Delta p = 2.75 \times 10^{-1} \text{ dyne/cm.}^2$$

We see that under these conditions of natural charge the electric stress is completely negligible.

In order to have a gasdynamic pressure increment of the same order as the electric pressure, the body potential should be about -10^6 volts or about $+14$ volts, as follows from the transcendental solution of Eq. (47).

The effect of the electric body force on the gas mixture might be important even for potentials ϕ_0 smaller than $+14$ volts. Constant potentials ϕ_0 which are lower or greater than the naturally acquired value could be maintained if the body surface S acts as an electrode and collects electric currents flowing in the interior of the body. We will now show that the part $\mathbf{J} \times \mathbf{H}$ of the Lorentz force can be neglected compared with the electrostatic term $q\mathbf{E}$.

As is known, the magnetic field induced by steady electric current densities $\mathbf{J}$ flowing through the whole space is given by[19]

$$\mathbf{H}(x, y, z) = \iiint_\infty (\mathbf{J} \times \mathbf{r}_0)[(x - x')^2 + (y - y')^2 + (z - z')^2]^{-1}\, dx'\, dy'\, dz' \quad \text{(e.m.u.)} \tag{48}$$

where

$$\mathbf{J} = \mathbf{J}_c + \mathbf{j}, \quad \mathbf{J}_c = e(n_i - n_e)\mathbf{V}, \quad \mathbf{j} = \sigma\mathbf{E} \tag{49}$$

and where $\mathbf{r}_0$ is a unit vector directed from the current element at (x', y', z') toward the field point (x, y, z). The electric conductivity σ of the mixture is nearly all caused by electrons, and for $T_e = 11{,}600°$K., it can be estimated as $\sigma = 1.2 \times 10^2$ mhos/m. at an altitude of 100 km.[5, 20]

For a thin plane configuration with three planes of symmetry $x = 0$, $y = 0$, and $z = 0$, the electric field $\mathbf{E}$ and the conduction current densities $\sigma\mathbf{E}$ which satisfy Eq. (31) should also be symmetrical with respect to the planes $x = 0$, $y = 0$, and $z = 0$. From Eq. (48) it then follows that the field $\mathbf{H}$ caused by the distribution of the conduction currents will vanish identically over the three planes of symmetry. For a thin plane symmetric configuration we may then assume that the field $\mathbf{H}$ caused by diverging or converging conduction currents $\mathbf{j}$ can be neglected compared with that caused by $\mathbf{J}_c$. This assumption may even apply to elongated thin bodies with one or two planes of symmetry. Let us find now a rough bound for the magnetic vector $\mathbf{H}$ at $r = 0$. The coordinate system $\mathbf{K}$ is now assumed to be at the centroid of a thin plane configuration as that shown in Fig. 1. Jastrow and Pearse[1] have obtained a numerical solution corresponding to Eq. (31) for a sphere of radius R.

The corresponding space charge distribution is essentially concentrated within a spherical sheath $R < r' < 1.4\ R$; for $r' > 1.4\ R$ it vanishes more strongly than $(1.4\ R/r')^2$. In considering a thin plane body of maximum length L we will now roughly assume that the space charge is constant within a sphere of radius $R = 0.7\ L$ around $r = 0$ and then decreases as $(R/r')^{5/2}$. Since we may assume $V < (4/3)V_0$, the convection current is bounded by

$$|\mathbf{J}_c(\mathbf{r}')| < J_0, \qquad r' \le R = 0.7\ L$$

$$|\mathbf{J}_c(\mathbf{r}')| < (R/r')^{5/2} J_0, \qquad r' \ge R = 0.7\ L$$

where

$$J_0 = \frac{4}{3} eN \left| e^{\beta\phi_0} - 1 \right| V_0 \qquad \text{(e.m.u.)} \qquad (50)$$

From Eq. (48) and the inequalities (50) there follows then a bound at $r = 0$ which is

$$H_1(0) \leq \frac{20}{3} \pi R J_0 \qquad \text{(e.m.u.)} \qquad (51)$$

From Eqs. (16) and (18) and the inequalities (50) and (51) the ratio

$$Z = \frac{\left| \mathbf{J}(0) \times (\mathbf{H}_0 + \mathbf{H}_1) \right|}{e \left| (n_i - n_e) \right| E_0} \leq \frac{4}{3} \frac{V_0 H_0}{E_0} + \left(\frac{320}{27} \right) \frac{\pi R\, eN \left| e^{\beta\phi_0} - 1 \right| V_0^2}{E_0} \qquad \text{(e.m.u.)} \qquad (52)$$

follows, where the earth's magnetic field intensity H_0 is taken to be equal to 0.7 gauss and

$$E_0 = \alpha (8\pi N k T_e)^{1/2} (e^{\beta\phi_0} - \beta\phi_0 - 1)^{1/2}$$

Taking $V_0 = 3.5 \times 10^5$ cm./sec., $H_0 = 0.7$, $e = 1.59 \times 10^{-20}$, $R = 350$ cm., $N = 1.5 \times 10^5$, $\beta = 1$, $T_e = 11{,}600°\text{K.}$,* we find

ϕ_0, volts	$Z \leqq$
-10^3	1.402×10^{-4}
-4.438	2.385×10^{-3}
$+13.992$	1.674×10^{-4}

Sharper bounds for $\mathbf{H}$ as defined by Eq. (48) should be developed to ascertain more generally the range of application of the approximation $\mathbf{J} \times \mathbf{H} \simeq 0$.

Conclusions

It has been indicated how to determine the electric field and its influence on the flow field. The flow field for a neutral gas will only be distorted by the action of the electric body forces with no basic changes in the features of Mach waves or shock layers. The electric potential is shielded and goes to zero very rapidly as one goes away from the body.

The negative potential acquired naturally by a plane, thin conducting body is of the order of -5 volts. It has been shown that the direct electric traction for this potential is negligible in comparison with the neutral gasdynamic pressure increment.

It appears to be possible to increase the electric potential artificially and thereby to increase the electric force exerted on the conducting body. For a positive body potential $\phi_0 = +14$ volts, the electric pressure over the body is of the order of the gasdynamic pressure increment. If $\phi_0 > 0$, the charge density of electrons in the neighborhood of the body is increased, and it would appear that the radar cross section would be modified.

To calculate the effect of the electric field on the flow field, it is first necessary to solve the exterior nonlinear boundary value problem of Eq. (31) for typical configurations. These exact solutions, which would also define the density of electrons around the body, are further necessary because the Debye approximation

$$e^{\chi} \cong 1 + \chi, \quad |\chi| \ll 1$$

is no longer valid since in all cases of interest $|\chi| \gg 1$. These exterior nonlinear Dirichlet problems have as yet no complete mathematical theory. Therefore, it seems worth while to investigate this problem further.

* Recent Langmuir probe measurements (R. L. Bogess, L. H. Brace, and N. W. Spencer, *J. Geophys. Research*, Vol. 64, p. 1628, 1959) indicate $T_e \backsimeq 2000°\text{K.}$ in the E layer.

References

[1] Jastrow, R., and Pearse, C. A., *Atmospheric Drag on the Satellite*, J. Geophys. Research, Vol. 62, No. 3, pp. 413–423, 1957.

[2] Mitra, S. K., *The Upper Atmosphere*, (2nd Rev. Ed.), Stechert-Hafner, Inc., New York, 1952.

[3] Shottky, W., *Wandströme und Theorie der positiven Säule*, Phys. Zeitschrift, Vol. 25, pp. 342–348, 1924.

[4] Debye, P., and Hückel, E., *Zür Theorie der Elektrolyte—I*, Phys. Zeitschrift, Vol. 24, pp. 185–206, 1923.

[5] Chapman, S., and Cowling, T. G., *The Mathematical Theory of Nonuniform Gases*, Cambridge Univ. Press, 1953.

[6] Rompe, R., and Steenbeck, M., *Der Plasmazustand der Gase*, Ergebn. Exakt. Naturwiss., Vol. 18, pp. 257–367, 1939.

[7] Hirschfelder, J. O., Curtiss, C. F., Bird, R. P., and Spotz, E. L., *The Kinetic Theory of Gases*, in *Thermodynamics and Physics of Matter*, Rossini, F. D. (Ed.), Princeton Univ. Press, 1955.

[8] Estermann, I., *Gases at Low Densities—I*, in *Thermodynamics and Physics of Matter*, Rossini, F. D. (Ed.), Princeton Univ. Press, 1955.

[9] Fowler, R. H., *Statistical Mechanics*, Cambridge Univ. Press, p. 586, 1936.

[10] Finkelnburg, W., and Maecker, H., *Elektrische Bögen und thermisches Plasma*, Handbuch der Physik, Vol. 22, Gasentladungen II, p. 344, Springer Verlag, Berlin, 1956.

[11] Oseen, C. W., *Neuere Methoden und Ergebnisse in der Hydrodynamik*, Akad.-Verlag, Leipzig, 1927.

[12] Finn, R. S., and Gilbarg, D., *Three-Dimensional Subsonic Flows and Asymptotic Estimates for Elliptic Partial Differential Equations*, Acta Math., Vol. 98, pp. 265–296, 1957.

[13] Lagally, M., *Berechnung der Kräfte und Momente die strömende Flüssigkeiten auf ihre Begrenzung ausüben*, Z. angew. Math. u. Mech., Vol. 2, No. 6, pp. 409–422.

[14] Hunziker, R. R., *Symposium on Naval Hydrodynamics*, National Research Council Publication No. 515, pp. 169–172, Washington, D.C., 1957.

[15] Van Dyke, M. D., *A Study of Second Order Supersonic Flow Theory*, NACA Report 1081, 1952.

[16] Maslen, S. H., *Second Approximation to Laminar Compressible Boundary Layer on Flat Plate in Slip Flow*, NASA TN 2818, 1952.

[17] Hayes, W. D., *Hypersonic Flow Theory*, Academic Press, New York and London, p. 388, 1959.

[18] Lichtenstein, L., *Grundlagen der Hydromechanik*, Julius Springer, Berlin, pp. 80–83, 1929.

[19] Stratton, J. A., *Electromagnetic Theory*, McGraw-Hill Publishers, Inc., New York, pp. 231–232, 1941.

[20] Spitzer, L., *Physics of Fully Ionized Gases*, Interscience Publishers, Inc., New York, pp. 81–84, 1956.

The Buckling of Circular Cylindrical Shells Under Purely Random External Pressures†

J. CLIFTON SAMUELS*
Purdue University

Summary

The mean-square stability theory of Samuels and Eringen is applied to the stability of circular cylindrical shells subjected to purely random external pressures. It is found that stability is determined by the character of the roots of a determinantal equation of the 36th degree. Nyquist's method of determining stability is applicable to this determinantal equation in numerical examples.

Explicit mean-square stability criteria are developed for a circular ring under purely random pressures. The study showed that all modes of vibration of the ring are unstable for sufficiently large spectral density of the pressure fluctuations.

(I) Introduction

THE STUDY OF the stability of shells under random external pressures leads to systems of linear differential equations with random functions as coefficients. A stability theory of equations with random coefficients has been developed by Samuels and Eringen[1] and Samuels.[2] It is appropriate, for such equations, to investigate the stability of the mean-square solution rather than the solution itself. Such stability is termed mean-square stability. Samuels and Eringen have applied the theory of mean-square stability to rods under random end loads and to *RLC* circuits with random capacity variations.

The object of the present paper is to apply the mean-square stability theory of Samuels and Eringen to the interesting problem of the stability of circular cylindrical shells under random external pressures. A slight generalization of the aforementioned stability theory is required as *systems* of equations with random parameters are involved in studying the stability of shells.

The shell is subjected to a uniform randomly time-varying pressure. The objective of the analysis is to find conditions for buckling in a mean-square sense.

(II) Equations for the Dynamical Buckling of Cylindrical Shells

The equations for the velocity-damped motion of a cylindrical shell under uniform radial time-varying loads are[3]

$$\left.\begin{aligned}
&a^2\frac{\partial^2 u}{\partial x^2}+\frac{1+\nu}{2}a\frac{\partial^2 v}{\partial x\partial\theta}-\nu a\frac{\partial w}{\partial x}+a\phi(t)\left(\frac{\partial^2 v}{\partial x\partial\theta}-\frac{\partial w}{\partial x}\right)+\frac{1-\nu}{2}\frac{\partial^2 u}{\partial\theta^2}=\left[\rho ah\frac{\partial^2 u}{\partial t^2}+\beta_u'\frac{\partial u}{\partial t}\right]\left(\frac{1-\nu^2}{Eh}\right)a\\
&\frac{1+\nu}{2}a\frac{\partial^2 u}{\partial x\partial\theta}+\frac{1-\nu}{2}a^2\frac{\partial^2 v}{\partial x^2}+\frac{\partial^2 v}{\partial\theta^2}-\frac{\partial w}{\partial\theta}+\alpha\left[\frac{\partial^2 v}{\partial\theta^2}+\frac{\partial^3 w}{\partial\theta^3}+a^2\frac{\partial^3 w}{\partial x^2\partial\theta}+a^2(1-\nu)\frac{\partial^2 v}{\partial x^2}\right]=\\
&\qquad\left[\rho ah\frac{\partial^2 v}{\partial t^2}+\beta_v'\frac{\partial v}{\partial t}\right]\left(\frac{1-\nu^2}{Eh}a\right)\\
&a\nu\frac{\partial u}{\partial x}+\frac{\partial v}{\partial\theta}-w-\alpha\left[\frac{\partial^3 v}{\partial\theta^3}+(2-\nu)a^2\frac{\partial^3 v}{\partial x^2\partial\theta}+a^4\frac{\partial^4 w}{\partial x^4}+\frac{\partial^4 w}{\partial\theta^4}+2a^2\frac{\partial^4 w}{\partial x^2\partial\theta^2}\right]-\\
&\qquad\phi(t)\left[w+\frac{\partial^2 w}{\partial\theta^2}\right]=\left[\rho ah\frac{\partial^2 w}{\partial t^2}+\beta_w'\frac{\partial w}{\partial t}\right]\left(\frac{1-\nu^2}{Eh}\right)a
\end{aligned}\right\}\qquad(1)$$

where u, v, and w are respectively the displacement of the middle surface in the x (longitudinal), θ (tangential and r (radial) directions; β_u, β_v, β_w are velocity damping constants; a denotes the radius of the middle surface of the shell and h its thickness; ρ, ν, and E are the mass density, Poisson's ratio, and Young's modulus respectively; $q(t)$ is the radial load; and

$$\left.\begin{aligned}
\phi(t)&\equiv[a(1-\nu^2)/Eh]q(t)\\
\alpha&\equiv h^2/12a^2
\end{aligned}\right\}\qquad(2)$$

(III) Equations for the Second Product Moments

We consider a simply supported shell as shown in Fig. 1. The boundary conditions to be satisfied at $x = 0$, l, are

$$\left.\begin{aligned}
v&=0 & N_x&=0\\
w&=0 & M_x&=0
\end{aligned}\right\}\qquad(3)$$

Received October 14, 1959. Revised and received April 4, 1960.

† Supported in part by a grant from the National Science Foundation.

* Associate Professor of Engineering Sciences.

where $$N_x = \frac{Eh}{1-\nu^2}\left[\frac{\partial u}{\partial x} + \nu\left(\frac{\partial v}{a\partial\theta} - \frac{w}{a}\right)\right]$$

is the axial stress resultant, and

$$M_x = -\frac{Eh^3}{12(1-\nu^2)}\left[\frac{\partial^2 w}{\partial x^2} + \frac{\nu}{a^2}\left(\frac{\partial v}{\partial\theta} + \frac{\partial^2 w}{\partial\theta^2}\right)\right]$$

is the bending moment due to axial stresses.

A solution satisfying these boundary conditions may be taken in the form

$$\left.\begin{aligned} u &= \sum_{n=0,\ m=1}^{\infty} u_{nm}(t)\sin n\theta\cos\frac{m\pi x}{l} \\ v &= \sum_{n=0,\ m=1}^{\infty} v_{nm}(t)\cos n\theta\sin\frac{m\pi x}{l} \\ w &= \sum_{n=0,\ m=1}^{\infty} w_{nm}(t)\sin n\theta\sin\frac{m\pi x}{l} \end{aligned}\right\} \qquad (4)$$

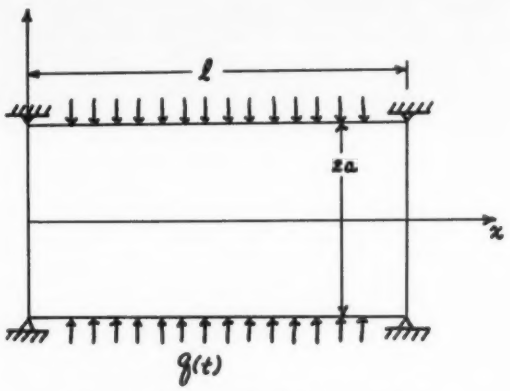

FIG. 1. Simply supported cylindrical shell.

Substituting (4) in (1) we obtain the following set of equations for u_{nm}, v_{nm}, and w_{nm}:

$$\left.\begin{aligned} &\ddot{u}_{nm}(t) + 2\beta_u\dot{u}_{nm}(t) + \frac{1}{M}\left(\lambda_m^2 + \frac{1-\nu}{2}n^2\right)u_{nm}(t) + \frac{1}{M}\left[\frac{1+\nu}{2}n\lambda_m + n\lambda_m\phi(t)\right]\times \\ &\qquad v_{nm}(t) + \frac{\lambda m}{M}[\nu+\phi(t)]w_{nm}(t) = 0 \\ &\ddot{v}_{nm}(t) + 2\beta_v\dot{v}_{nm}(t) + \left[\frac{1}{M}\left(\frac{1+\nu}{2}n\lambda_m\right)\right]u_{nm}(t) + \frac{1}{M}\left[\frac{1-\nu}{2}\lambda_m^2 + n^2 + n^2\alpha + \alpha(1-\nu)\lambda_m^2 n\right]\times \\ &\qquad v_{nm}(t) + \frac{1}{M}[n + \alpha n^3 + \alpha\lambda_m^2 n]w_{nm}(t) = 0 \\ &\ddot{w}_{nm}(t) + 2\beta_w\dot{w}_{nm} + \frac{\nu\lambda_m}{M}u_{nm} + \frac{1}{M}[n + \alpha n^3 + \alpha(2-\nu)\lambda_m^2 n]v_{nm} + \\ &\qquad \frac{1}{M}[\alpha\lambda_m^4 + \alpha n^4 + 2\alpha\lambda_m^2 n^2 + 1 + (1-n^2)\phi(t)]w_{nm}(t) = 0 \end{aligned}\right\} \qquad (5)$$

where $M = \rho a^2(1-\nu^2)/E$, $\lambda_m = m\pi a/l$, $2\beta_u = \beta_u'/\rho ah$, $2\beta_v = \beta_v'/\rho ah$, and $2\beta_w = \beta_w'/\rho ah$.

We suppose now that

$$\theta(t) = \phi_0 + p(t) \qquad (6)$$

where ϕ_0 is a constant and $p(t)$ will be taken as a stationary random function of time.[4] Using (6) in (5), we find

$$\left.\begin{aligned} &\ddot{u}_{nm} + 2\beta_u\dot{u}_{nm} + a_{uu}u_{nm} + a_{uv}u_{nm} + a_{uw}w_{nm} = \\ &\qquad -(n\lambda_m/M)p(t)v_{nm}(t) - (\lambda_m/M)p(t)w_{nm}(t) \\ &\ddot{v}_{nm} + 2\beta_v\dot{v}_{nm} + a_{vu}u_{nm} + a_{vv}v_{nm} + a_{vw}w_{nm} = 0 \\ &\ddot{w}_{nm} + 2\beta_w\dot{w}_{nm} + a_{wu}u_{nm} + a_{wv}v_{nm} + a_{ww}w_{nm} = \\ &\qquad [(1-n^2)p(t)/M]w_{nm}(t) \end{aligned}\right\} \qquad (7)$$

where

$$\left.\begin{aligned} a_{uu} &= (1/M)\left(\lambda_m^2 + \frac{1-\nu}{2}n^2\right) \\ a_{uv} &= (1/M)\left(\frac{1+\nu}{2}n\lambda_m + n\lambda_m\phi_0\right) \\ a_{uw} &= (\lambda_m/M)\ (\nu+\phi_0) \end{aligned}\right\} \qquad (8)$$

$$\left.\begin{aligned} a_{vu} &= (1/M)\frac{(1+\nu)}{2}n\lambda_m \\ a_{vv} &= (1/M)\left[\frac{1-\nu}{2}\lambda_m^2 + (1+\alpha)n^2 + \alpha(1-\nu)\lambda_m^2\right] \\ a_{vw} &= (1/M)[n + \alpha n^3 + \alpha\lambda_m^2 n] \\ a_{wu} &= \nu\lambda_m/M \\ a_{wv} &= (1/M)[n + \alpha n^3 + \alpha(2-\nu)\lambda_m^2 n] \\ a_{ww} &= (1/M)[\alpha\lambda_m^4 + \alpha n^4 + 2\alpha\lambda_m^2 n^2 + 1 + (1-n^2)\phi_0] \end{aligned}\right\} \qquad (8)$$

The system of differential equations (7) is converted to a system of integral equations on the infinite interval $(-\infty, \infty)$ by taking Fourier transforms, solving for $\bar{u}_{nm}$, $\bar{v}_{nm}$, and $\bar{w}_{nm}$ in terms of the transforms of the right-hand sides of (7), and then inverting. (A bar over

a quantity means Fourier transform, e.g.,

$$\bar{u}_{nm}(\zeta) = \mathfrak{F}\{u_{nm}(t)\} = \int_{-\infty}^{\infty} u_{nm}(t)e^{+i\zeta t}\,dt$$

with

$$u_{nm}(t) = \mathfrak{F}^{-1}\{\bar{u}_{nm}(\zeta)\} = \frac{1}{2\pi}\int_{-\infty}^{\infty} \bar{u}_{nm}(\zeta)e^{-it\zeta}\,d\zeta$$

as the inverse.) We find

$$\left.\begin{aligned} u_{nm}(t) &= \int_{-\infty}^{\infty} W_{uv}(t-\tau)p(\tau)v_{nm}(\tau)d\tau + \int_{-\infty}^{\infty} W_{uw}(t-\tau)p(\tau)w_{nm}(\tau)d\tau \\ v_{nm}(t) &= \int_{-\infty}^{\infty} W_{vv}(t-\tau)p(\tau)v_{nm}(\tau)d\tau + \int_{-\infty}^{\infty} W_{vw}(t-\tau)p(\tau)w_{nm}(\tau)d\tau \\ w_{nm}(t) &= \int_{-\infty}^{\infty} W_{wv}(t-\tau)p(\tau)v_{nm}(\tau)d\tau + \int_{-\infty}^{\infty} W_{ww}(t-\tau)p(\tau)w_{nm}(\tau)d\tau \end{aligned}\right\} \quad (9)$$

where

$$\left.\begin{aligned} W_{uv}(t) &= \mathfrak{F}^{-1}\left\{\frac{\Delta_{uv}}{\Delta}\left(-\frac{n\lambda_m}{M}\right)\right\} \\ W_{uw}(t) &= \mathfrak{F}^{-1}\left\{-\frac{\lambda_m\Delta_{uv} + (1-n^2)\Delta_{uw}}{M\Delta}\right\} \\ W_{vv}(t) &= \mathfrak{F}^{-1}\left\{\frac{n\lambda_m}{M}\frac{\Delta_{vv}}{\Delta}\right\} \\ W_{vw}(t) &= \mathfrak{F}^{-1}\left\{\frac{\lambda_m\Delta_{vv} + (1-n^2)\Delta_{vw}}{M\Delta}\right\} \\ W_{wv}(t) &= \mathfrak{F}^{-1}\left\{-\frac{n\lambda_m}{M}\frac{\Delta_{wv}}{\Delta}\right\} \\ W_{ww}(t) &= \mathfrak{F}^{-1}\left\{-\frac{\lambda_m\Delta_{wv} + (1-n^2)\Delta_{ww}}{M\Delta}\right\} \end{aligned}\right\} \quad (10)$$

in which

$$\left.\begin{aligned} \Delta_{uv} &= \zeta^4 + 2i(\beta_v+\beta_w)\zeta^3 - (a_{vv} + a_{ww} + 4\beta_v\beta_w)\zeta^2 - 2i(\beta_v a_{ww} + \beta a_{vvv})\zeta + a_{vv}a_{ww} + a_{vw}a_{wv} \\ \Delta_{uw} &= a_{uw}\zeta^2 + 2i\beta_v a_{uw}\zeta + a_{uv}a_{wv} - a_{uw}a_{vv} \\ \Delta_{vv} &= -a_{vv}\zeta^2 - 2i\beta_w a_{vv}\zeta + a_{vv}a_{ww} - a_{ww}a_{vw} \\ \Delta_{vw} &= -a_{vw}\zeta^2 - 2i\beta_u a_{vw}\zeta + a_{uv}a_{vw} - a_{vv}a_{uw} \\ \Delta_{wv} &= a_{ww}\zeta^2 + 2i\beta_v a_{ww}\zeta + a_{vv}a_{wv} - a_{ww}a_{vv} \\ \Delta_{ww} &= \zeta^4 + 2i(\beta_u+\beta_v)\zeta^3 - (a_{uu} + a_{vv} + 4\beta_u\beta_v)\zeta^2 - 2i(\beta_v a_{uu} + \beta_u a_{vv})\zeta + a_{uu}a_{vv} \end{aligned}\right\} \quad (11)$$

and $\Delta = -\zeta^6 - 2i(\beta_u+\beta_v+\beta_w)\zeta^5 + [a_{uu} + a_{ww} + 4\beta_w\beta_v + 4\beta_u\beta_v + 4\beta_u\beta_w]\zeta^4 + 2i[a_{uu}(\beta_v+\beta_w) + \beta_u(a_{vv} + a_{ww} + 4\beta_w\beta_v) + (\beta_v a_{ww} + \beta_w a_{vv})]\zeta^3 + [-a_{vv}a_{ww} - 4\beta_u(\beta_v a_{ww} + \beta_w a_{vv}) + a_{vw}a_{wv} + a_{ww}a_{uu} - a_{uu}(a_{vv} + a_{ww} + 4\beta_v\beta_w)]\zeta^2 + 2i[-\beta_u a_{vv}a_{ww} - a_{uu}(\beta_v a_{ww} + \beta_w a_{vv}) + \beta_w a_{vw}a_{wv} + \beta_v a_{ww}a_{uu}]\zeta + [a_{uu}a_{vv}a_{ww} - a_{vw}(a_{wv}a_{ww} - a_{uw}a_{wv}) + a_{ww}(a_{vw}a_{wv} - a_{uu}a_{vv})]$

In the conversion of (7) to integral equation form, no arbitrary constants of integration were introduced because we are interested only in solutions which are uninfluenced by initial conditions.

At this point in the analysis, we are ready to obtain integral equations for the determination of certain statistical averages. In order to do this, we must make certain assumptions about the statistical characteristics of the load $g(t)$ or, equivalently, about $p(t)$. We shall suppose that $p(t)$ is a *stationary ergodic* random process with mean zero. Then

$$\left.\begin{aligned} E[p(t+\tau)] &= E[p(t)] = 0 \\ E[p(t+\tau)p(t)] &= R_P(\tau) = \frac{1}{2\pi}\int_{-\infty}^{\infty} S_P(\omega)e^{-i\tau\omega}\,d\omega \end{aligned}\right\} \quad (12)$$

where E denotes ensemble average and $R_P(\tau)$ and $S_P(\omega)$ are respectively the *autocorrelation* and *spectral density* functions of $p(t)$. Because of the assumption of ergodicity these results are also given by the temporal averages

$$\left.\begin{aligned} \lim_{T\to\infty}\frac{1}{2T}\int_{-T}^{T} p(t+\tau)d\tau &= \lim_{T\to\infty}\frac{1}{2T}\int_{-T}^{T} p(t)dt = E[p(t)] = 0 \\ \lim_{T\to\infty}\frac{1}{2T}\int_{-T}^{T} p(t+\tau)p(t)dt &= E[p(t+\tau)p(t)] = R_P(\tau) \end{aligned}\right\} \quad (13)$$

Further, we shall suppose that $p(t)$ is an independent or white-noise process. This means that successive values of $p(t)$ are statistically independent. This assumption simplifies the analysis considerably and makes an exact derivation of the integral equations possible. Integral equations for certain statistical averages have been derived approximately when the random coefficients in the differential equations are not white-noise processes.[2]

For the white-noise process, the autocorrelation function takes the form

$$R_P(t_2 - t_1) = \langle p(t_1)p(t_2)\rangle = S\delta(t_2 - t_1) \quad (14)$$

where S is the constant spectral density of $p(t)$, $\delta(t)$ is the Dirac delta function, and $\langle\ \rangle$ denotes ensemble average.

To obtain equations for the mean square of u_{nm}, v_{nm}, w_{nm}, we square and average the equations in (9), which gives

$$\left.\begin{aligned}
\langle u_{nm}^2(t)\rangle &= S\int_{-\infty}^{\infty} W_{uv}^2(t-\tau)\langle v_{nm}^2(\tau)\rangle\,d\tau + \\
&\quad 2S\int_{-\infty}^{\infty} W_{uv}(t-\tau)W_{uw}(t-\tau)\langle v_{nm}(\tau)w_{nm}(\tau)\rangle\,d\tau + S\int_{-\infty}^{\infty} W_{uw}^2(t-\tau)\langle w_{nm}^2(\tau)\rangle\,d\tau \\
\langle v_{nm}^2(t)\rangle &= S\int_{-\infty}^{\infty} W_{vv}^2(t-\tau)\langle v_{nm}^2(\tau)\rangle\,d\tau + \\
&\quad 2S\int_{-\infty}^{\infty} W_{vv}(t-\tau)W_{vw}(t-\tau)\langle v_{nm}(\tau)w_{nm}(\tau)\rangle\,d\tau + S\int_{-\infty}^{\infty} W_{vw}^2(t-\tau)\langle w_{nm}^2(\tau)\rangle\,d\tau \\
\langle w_{nm}^2(t)\rangle &= S\int_{-\infty}^{\infty} W_{wv}^2(t-\tau)\langle v_{nm}^2(\tau)\rangle\,d\tau + \\
&\quad 2S\int_{-\infty}^{\infty} W_{wv}(t-\tau)W_{ww}(t-\tau)\langle v_{nm}(\tau)w_{nm}(\tau)\rangle\,d\tau + S\int_{-\infty}^{\infty} W_{ww}^2(t-\tau)\langle w_{nm}^2(\tau)\rangle\,d\tau
\end{aligned}\right\} \quad (15)$$

In getting (15) we used the result

$$\begin{aligned}
E\left\{\int_{-\infty}^{\infty}\int_{-\infty}^{\infty} W_1(t-\tau_1)W_2(t-\tau_2)p(\tau_1)p(\tau_2)g_1(\tau_1)g_2(\tau_2)d\tau_1 d\tau_2\right\} = \\
\int_{-\infty}^{\infty}\int_{-\infty}^{\infty} W_1(t-\tau_1)W_2(t-\tau_2)E\{p(\tau_1)p(\tau_2)g_1(\tau_1)g_2(\tau_2)\}d\tau_1\,d\tau_2 = \\
\int_{-\infty}^{\infty}\int_{-\infty}^{\infty} W_1(t-\tau_1)W_2(t-\tau_2)E\{p(\tau_1)p(\tau_2)\}E\{g_1(\tau_1)g_2(\tau_2)\}d\tau_1\,d\tau_2 = \\
\int_{-\infty}^{\infty}\int_{-\infty}^{\infty} W_1(t-\tau_1)W_2(t-\tau_2)S\delta(\tau_1-\tau_2)E\{g_1(\tau_1)g_2(\tau_2)\}d\tau_1\,d\tau_2 = \\
S\int_{-\infty}^{\infty} W_1(t-\tau)W_2(t-\tau)E\{g_1(\tau)g_2(\tau)\}d\tau \quad (16)
\end{aligned}$$

where g_1 or g_2 stands for v_{nm} or w_{nm}, and W_1 or W_2 stands for any of the weight functions in (10). For the validity of (16) see reference 5. In (15), we have four unknowns but only three equations. We can get another equation by multiplying the second and third of (9) with each other and averaging, which gives

$$\begin{aligned}
\langle v_{nm}(t)w_{nm}(t)\rangle = \\
S\int_{-\infty}^{\infty} W_{vv}(t-\tau)W_{wv}(t-\tau)\,\langle v_{nm}^2(\tau)\rangle\,d\tau + \\
S\int_{-\infty}^{\infty} W_{vw}(t-\tau)W_{ww}(t-\tau)\times \\
\langle v_{nm}(\tau)w_{nm}(\tau)\rangle\,d\tau + S\int_{-\infty}^{\infty} W_{vv}(t-\tau)\times \\
W_{ww}(t-\tau)\,\langle v_{nm}(\tau)w_{nm}(\tau)\rangle\,d\tau + \\
S\int_{-\infty}^{\infty} W_{vw}(t-\tau)W_{ww}(t-\tau)\,\langle w_{nm}^2(\tau)\rangle\,d\tau \quad (17)
\end{aligned}$$

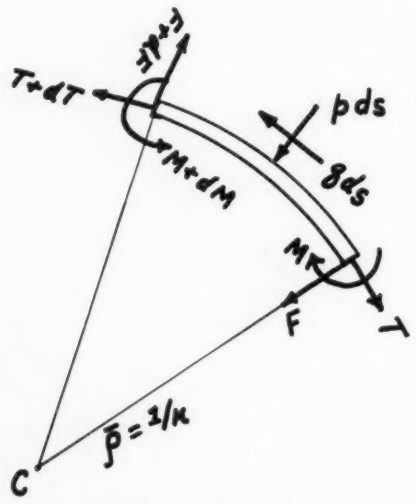

FIG. 2. Portion of a ring.

By transforming the last two equations of (15) and Eq. (17) we find

$$\left.\begin{aligned}
&(1 - S\overline{W_{vv}^2})\,\overline{\langle v_{nm}^2\rangle} - 2S\,\overline{W_{vv}W_{vw}}\,\overline{\langle v_{nm}w_{nm}\rangle} - \\
&\qquad S\,\overline{W_{vw}^2}\,\overline{\langle w_{nm}^2\rangle} = 0 \\
&-S\,\overline{W_{wv}^2}\,\overline{\langle v_{nm}^2\rangle} - 2S\,\overline{W_{wv}W_{ww}}\,\overline{\langle v_{nm}w_{nm}\rangle} + \\
&\qquad (1 - S\,\overline{W_{ww}^2})\,\overline{\langle w_{nm}^2\rangle} = 0 \\
&-S\,\overline{W_{uv}W_{wv}}\,\overline{\langle v_{nm}^2\rangle} + \\
&\qquad [1 - S(\overline{W_{vw}W_{wv}} + \overline{W_{vv}W_{ww}})]\,\overline{\langle v_{nm}w_{nm}\rangle} - \\
&\qquad S\,\overline{W_{vw}W_{ww}}\,\overline{\langle w_{nm}^2\rangle} = 0
\end{aligned}\right\} \quad (18)$$

Eq. (18) has a nontrivial solution if the determinant of the system is zero. In that case, we can write[7]

$$\left.\begin{aligned}\langle v_{nm}{}^2(t)\rangle &= \oint \frac{M(\zeta)D_v(\zeta)e^{-it\zeta}d\zeta}{D(\zeta)}\\ \langle w_{nm}{}^2(t)\rangle &= \oint \frac{M(\zeta)D_w(\zeta)e^{-it\zeta}d\zeta}{D(\zeta)}\\ \langle v_{nm}(t)w_{nm}(t)\rangle &= \oint \frac{M(\zeta)D_{vw}(\zeta)e^{-it\zeta}}{D(\zeta)}\end{aligned}\right\} \tag{19}$$

where $D_v(\zeta)$, $D_w(\zeta)$, and $D_{vw}(\zeta)$ are the cofactors of the elements of any row in the determinant

$$D(\zeta) = \begin{vmatrix} (1 - S\,\overline{W_{vv}{}^2}) & -2S\,\overline{W_{vv}W_{vw}} & -S\,\overline{W_{vw}{}^2} \\ -S\,\overline{W_{vw}{}^2} & -2S\,\overline{W_{wv}W_{ww}} & 1 - S\,\overline{W_{ww}{}^2} \\ -S\,\overline{W_{uv}W_{uv}} & 1 - S(\overline{W_{vw}W_{wv}} + \overline{W_{vv}W_{ww}}) & -S\,\overline{W_{vw}W_{ww}} \end{vmatrix} \tag{20}$$

$M(\zeta)$ is any analytic function in the domain of analyticity of the Fourier transforms of the products of the weighting functions, and $\mathscr{J}$ is a closed contour integral in that same domain.

Using (19) in the first of (15) we obtain

$$\langle u_{nm}{}^2(t)\rangle = S\int_{-\infty}^{\infty}\left[\frac{\overline{W_{vv}{}^2}MD_v + \overline{2W_{uv}W_{uw}}MD_{vw} + \overline{W_{uw}{}^2}MD_w}{D(\zeta)}\right]e^{-it\zeta}d\zeta \tag{21}$$

Eqs. (19) and (21) give us a formal solution for the mean-square displacements.

(IV) Mean-Square Stability

If $\langle u^2\rangle$, $\langle v^2\rangle$, and $\langle w^2\rangle$ are bounded as $t \to \infty$, we say that the shell is stable in the mean-square sense.

The mean-square stability of the buckled modes $u_{nm}(t)$, $v_{nm}(t)$, $w_{nm}(t)$ is determined by examining the roots of the determinantal equation

$$D(\zeta) = 0 \tag{22}$$

which lie in the domain of analyticity of the Fourier transform of the products of the weighting functions W_{uu}, W_{uv}, etc. As Eq. (22) is of very high degree in ζ, roots can be determined only by numerical methods. Nyquist's method[6] can also be employed to advantage here in determining stability. We have only to note whether the vector $D(i\omega)$ encircles the point zero as ω goes from $-\infty$ to $+\infty$.

Mean square stability of the total displacement further requires the sums for $\langle u^2\rangle$, $\langle v^2\rangle$, $\langle w^2\rangle$ to be convergent.

Explicit mean square stability criteria can be given when the shell is very long so that variations in the x-direction do not occur and the boundary conditions do not influence the results. In this case, the essential results can be obtained by studying the buckling of a circular ring under random external pressure.

(V) Equations for the Dynamical Buckling of a Circular Ring

The motion of a circular ring is governed by the following equations:

$$\left.\begin{aligned}(\partial T/\partial s) + \kappa F + q &= 0\\ (\partial F/\partial s) + \kappa T + p &= 0\\ (\partial M/\partial s) - F &= 0\end{aligned}\right\} \tag{23}$$

where M is the resultant bending moment at a section, F is the resultant shear force, T the resultant tension, p and q are respectively the normal and tangential loads acting on the ring per unit of length, and κ is the curvature of the element (see Fig. 2). If F is eliminated from (23) we get

$$\left.\begin{aligned}(\partial T/\partial s) + \kappa(\partial M/\partial s) + q &= 0\\ (\partial^2 M/\partial s^2) - \kappa T - p &= 0\end{aligned}\right\} \tag{24}$$

For dynamical buckling we suppose

$$\left.\begin{aligned} q &= \rho A(\partial^2 v/\partial t^2) - \beta_v(\partial v/\partial t)\\ p &= p' - \rho A(\partial^2 w/\partial t^2) - \beta_w(\partial w/\partial t)\\ T &= -p'a + \bar{l}(\theta, t)\\ M &= -\frac{EI}{a^2}\left(w + \frac{\partial^2 w}{\partial\theta^2}\right)\\ \kappa &= \frac{1}{a} - \frac{1}{a^2}\left(\frac{\partial^2 w}{\partial\theta^2} + w\right)\end{aligned}\right\} \tag{25}$$

where ρ is the mass density, A is the cross-sectional area, p' is uniform external pressure, a is the radius of the ring, EI is the flexural rigidity, v and w are respectively the tangential and radial displacements, $\bar{l}(\theta,t)$ is a small quantity of the order of v, w and their derivatives, θ is the polar angle, β_v and β_w are velocity damping factors. Inserting (25) in (24) and neglecting products of higher order, we obtain for the radial displacement

$$\frac{\partial^4 w}{\partial\theta^4} + \left(2 + \frac{p'a^3}{EI}\right)\frac{\partial^3 w}{\partial\theta^3} + \left(1 + \frac{p'a^3}{EI}\right)\frac{\partial w}{\partial\theta} = \frac{a^4}{EI}\left[-\rho A\frac{\partial^2 v}{\partial t^2} + \rho A\frac{\partial^3 w}{\partial t^2\partial\theta} - \beta_u\frac{\partial v}{\partial t} + \beta_w\frac{\partial v}{\partial t}\right] \tag{26}$$

This equation contains v, the tangential displacement.

From the condition of inextensional deformation, namely,

$$\partial v/\partial\theta = w \tag{27}$$

v can be eliminated from (26) to give

$$\frac{\partial^4 w}{\partial\theta^4} + \left(2 + \frac{p'a^3}{EI}\right)\frac{\partial^4 w}{\partial\theta^4} + \left(1 + \frac{a^2p'}{EI}\right)\frac{\partial^2 w}{\partial\theta^2} = \frac{A\rho a^4}{EI}\frac{\partial^2}{\partial t^2}\left(w - \frac{\partial^2 w}{\partial\theta^2}\right) + \beta_0\frac{a^4}{EI}\frac{\partial}{\partial t}\left[w - \frac{\partial^2 w}{\partial\theta^2}\right] \quad (28)$$

where we assumed $\beta_v = \beta_w = \beta_0$. Eq. (28) will be taken as the basic equation for the dynamical buckling of a circular ring.

Suppose

$$w(\theta,t) = \sum_{n=1}^{\infty} w_n(t)\cos n\theta \quad (29)$$

Then (28) is satisfied if $w_n(t)$ satisfies

$$\ddot{w}_n(t) + 2\beta\dot{w}_n(t) + {\omega'_n}^2 w(t) = 0 \quad (30)$$

where $2\beta = \beta_0/\rho A$ and

$${\omega'_n}^2 = \frac{EI}{\rho A a^4}\left[\frac{n^6}{1+n^2} - \left(2 + \frac{p'a^3}{EI}\right)\frac{n^4}{1+n^2} + \left(1 + \frac{p'a^3}{EI}\right)\frac{n^2}{1+n^2}\right] \quad (31)$$

Now we are interested in the situation where p' is a random function of time taken as

$$p'(t) = p_0 + \alpha(t) \quad (32)$$

where p_0 is a constant, the average value of $p'(t)$, and $\alpha(t)$ is a stationary independent stochastic process. If (32) is used in (31), ${\omega'_n}^2$ can be simplified to

$${\omega'_n}^2(t) = {\omega_n}^2 - (\lambda_n^2/\rho a)\alpha(t) \quad (33)$$

where

$${\omega_n}^2 = \frac{EI}{\rho A a^4}\frac{n^2(n^2-1)}{n^2+1}\left[n^2 - \left(1 + \frac{p_0 a^3}{EI}\right)\right]$$

and

$$\lambda_n^2 = n^2(n^2-1)/(n^2+1)a \quad (34)$$

(VI) Mean-Square Stability of the Ring

A ring is stable in the mean-square sense if $\langle w^2\rangle$ *and* $\langle v^2\rangle$ *are bounded as* $t \to \infty$. Using the inextensional deformation condition (27) and Eq. (29) for w it is easy to see that if $\langle w^2\rangle$ is stable in mean square, so is $\langle v^2\rangle$. Hence we can confine our study to the radial displacement.

From (29) we have

$$\langle w^2(\theta,t)\rangle = \sum_{n,\,m=1}^{\infty}\langle w_n(t)w_m(t)\rangle\cos n\theta\cos m\theta \quad (35)$$

For mean square stability of $w(\theta,t)$, the series on the right of (35) must converge for all t and θ, and be bounded for all t. A necessary condition for the latter is that $\langle w_n(t)w_m(t)\rangle$ should be bounded for all t. If, in addition, $\langle w(\theta,t)w(\theta',t)\rangle$ is initially convergent, then $\langle w(\theta,t)w(\theta',t)\rangle$ will be convergent for all t and θ, θ'. Hence $\langle w^2(\theta,t)\rangle$ will be convergent and bounded, and thus the ring will be stable in mean square. To show that $\langle w(\theta,t)w(\theta',t)\rangle$ is convergent for all θ, θ', and t when it is initially convergent and when $\langle w_n(t)w_m(t)\rangle$ is bounded for all t, we start by noting that

$$\langle w_n(t_0)w_m(t_0)\rangle = \frac{1}{4\pi^2}\int_0^{2\pi}\int_0^{2\pi}\langle w(\theta,t_0)w(\theta',t_0)\rangle \times \cos n\theta\cos m\theta'\,d\theta d\theta' \quad (36)$$

Eq. (36) assumes *only* that the series for $\langle w(\theta,t)w(\theta',t)\rangle$ is *initially* convergent. Initially,

$$\left|\langle w(\theta,t_0)w(\theta',t_0)\rangle\right| < M = \text{const.} < \infty \quad (37)$$

Hence from the theory of Fourier series[8] (36) gives

$$\langle w_n(t_0)w_m(t_0)\rangle < K/nm, \quad K = \text{const.} \quad (38)$$

Now since by hypothesis $\langle w_n(t)w_m(t)\rangle$ is bounded for all t, it is clear that there exists a constant K' such that*

$$\langle w_n(t)w_m(t)\rangle \leq K'/nm \quad (39)$$

Thus $\langle w_n(t)w_n(t)\rangle = 0(1/n, 1/m)$ and therefore

$$\langle w^2(\theta,t)\rangle = \sum_{n,\,m=1}^{\infty}\langle \dot{w}_n(t)w_m(t)\rangle\cos n\theta\cos m\theta \quad (40)$$

$$\leqq A\sum_{n,\,m}^{\infty}\frac{1}{nm}\cos n\theta\cos m\theta$$

The latter double series on the right is convergent by a theorem due to Hardy which extends Dirichlet's test to double series.

It remains now to establish the conditions under which $\langle w_n(t)w_m(t)\rangle$ is a bounded function of time. From (30), we readily obtain the integral equation.

$$w_n(t) = F_n(t) + (\lambda_n^2/\rho A)\int_{-\infty}^{\infty} W_n(t-\tau)\alpha(\tau)w_n(\tau)d\tau \quad (41)$$

where

$$F_n(t) = e^{-\beta t}[C_1\sin[(\omega_n^2 - \beta^2)^{1/2}t] + C_2\cos[(\omega_n^2 - \beta^2)^{1/2}t]$$

$$W_n(t) = \begin{cases}(\omega_n^2 - \beta^2)^{-1/2} \times \\ \quad e^{-\beta t}\sin[(\omega_n^2 - \beta^2)^{1/2}t], & \omega_n^2 > \beta^2,\ t > 0 \\ 0, & t < 0\end{cases} \quad (42)$$

In (42) we assumed that the system was underdamped for all modes. We will concern ourselves here only with this case. Also, mean-square stability can be studied without loss of generality by taking $F_n(t) \equiv 0$. The latter condition occurs when $\langle w_n(0)\rangle = \langle \dot{w}_n(0)\rangle = 0$.

From (41) with $F_n = 0$, we calculate

$$\langle w_n(t)w_n(t)\rangle = (\lambda_n^2\lambda_m^2/\rho^2A^2)\iint_{-\infty}^{\infty} W_n(t-\tau_1)W_m(t-\tau_2) \times \langle\alpha(\tau_1)\alpha(\tau_2)\rangle\langle w_n(\tau_1)w_m(\tau_2)\rangle d\tau_1 d\tau_2$$

For white noise, $\langle\alpha(\tau_1)\alpha(\tau_2)\rangle = S\delta(\tau_1 - \tau_2)$. Hence

* See Appendix.

$$\left.\begin{aligned}&\langle w_n(t)w_m(t)\rangle = \\ &S_{nm}\int_{-\infty}^{\infty} W_n(t-\tau)W_m(t-\tau)\langle w_n(\tau)w_m(\tau)\rangle d\tau \\ &S_{nm} = (S/\rho^2A^2)\lambda_n{}^2\lambda_m{}^2\end{aligned}\right\} \quad (43)$$

whose solution is[7]

$$\langle w_n(t)w_m(t)\rangle = \frac{1}{2\pi}\oint \frac{M(\zeta)e^{it\zeta}d\zeta}{1 - S_{nm}\mathfrak{F}\{W_n(t)W_m(t)\}} \quad (44)$$

where the integral is taken around a closed contour in the domain of analyticity of $\mathfrak{F}\{W_n(t)W_m(t)\}$ and $M(\zeta)$ is any analytic function in the same domain.

$$\left.\begin{aligned}&\mathfrak{F}\{W_n(t)W_m(t)\} = (1/4)i(\omega_n{}^2 - \beta^2)^{-1/2}\times \\ &\quad(\omega_m{}^2 - \beta^2)^{-1/2}\cdot[(\zeta - \tau_1)^{-1} - (\zeta - \tau_2)^{-1} - \\ &\qquad(\zeta + \tau_2{}^*)^{-1} + (\zeta + \tau_1{}^*)^{-1}] \\ &\tau_1 = 2i\beta + (\omega_n{}^2 - \beta^2)^{1/2} + (\omega_m{}^2 - \beta^2)^{1/2} \\ &\tau_2 = 2i\beta + (\omega_n{}^2 - \beta^2)^{1/2} - (\omega_m{}^2 - \beta^2)^{1/2}\end{aligned}\right\} \quad (45)$$

where an asterisk (*) denotes the conjugate complex. The frequency equation required for the evaluation of (44) is obtained by setting the denominator of the integrand equal to zero, i.e.,

$$\left.\begin{aligned}&s^4 + 4\beta s^3 + (12\beta^2 + a_{nm} + b_{nm})s^2 - \\ &\qquad 2[S_{nm} - 8\beta^3 - \beta(a_{nm}{}^2 + b_{nm}{}^2)]s + \\ &\qquad[(4\beta^2 + a_{nm}{}^2)(4\beta^2 + b_{nm}{}^2) - 4\beta S_{nm}] = 0 \\ &s = i\zeta \\ &a_{nm} = (\omega_n{}^2 - \beta^2)^{1/2} + (\omega_m{}^2 - \beta^2)^{1/2} \\ &b_{nm} = (\omega_n{}^2 - \beta^2)^{1/2} - (\omega_m{}^2 - \beta^2)^{1/2}\end{aligned}\right\} \quad (46)$$

Now $\langle w_n(t)w_m(t)\rangle$ will be a bounded function of time if the roots of (46) all have nonpositive real parts. By the Routh-Hurwitz criterion, the necessary and sufficient conditions for this are:

(a) All coefficients in (46) must be positive.

(b) The following inequality must be satisfied:

$$\begin{aligned}&-8\beta(12\beta^2 + a_{nm}{}^2 + b_{nm}{}^2)\times \\ &\qquad[S_{nm} - 8\beta^3 - \beta(a_{nm}{}^2 + b_{nm}{}^2)] > \\ &\qquad\{4[S_{nm} - 8\beta^3 - \beta(a_{nm}{}^2 + b_{nm}{}^2)]^2 + \\ &\qquad 16\beta^3[(4\beta^2 + a_{nm}{}^2)(4\beta^2 + b_{nm}{}^2) - 4\beta S_{nm}]\}\end{aligned} \quad (47)$$

For small damping and low spectral density of the pressure fluctuations, the condition for stability of $\langle w_n(t)w_m(t)\rangle$ is given approximately by

$$2\beta > \frac{S_{nm}}{2\omega_n\omega_m} = \frac{a^3S}{2\rho A(EI)}\cdot\frac{\lambda_n\lambda_m}{\sqrt{(n^2 - P_0)(m^2 - P_0)}} \quad (48)$$

where

$$P_0 \equiv 1 + (p_0a^3/EI) \quad (49)$$

Inequality (48) is obtained by explicitly solving for the roots of (46) by a perturbation technique[1] and requiring the real parts to be negative.

(VII) Discussion of Results

From Eq. (48) and inequality (47) we can come to the following conclusions about the *model* studied:

(1) If we exclude random fluctuations of the pressure but retain damping of the ring's motion, it will be stable, that is, the mean-square displacement will remain bounded with increasing time in the higher modes but may be unstable in the lower modes depending on the value of the *external* pressure p_0. If the pressure is *internal*, then the ring is stable in all modes.

(2) When damping is removed but random fluctuations of the radial pressure occur, the ring is unstable in all modes whether an external or internal pressure is applied.

(3) If a small amount of damping is present, the system is unstable for the higher modes for sufficiently high spectral density of the pressure fluctuations, whether the applied pressure is external or internal.

The system can be stable in all modes if the damping is sufficiently large and the spectral density is sufficiently small.

It is of interest to contrast the results of the statistically fluctuating external pressure applied to an undamped ring to those with a sinusoidally varying deterministic load. The latter case gives rise to a Mathieu differential equation for each mode $w_n(t)$. The stability of this mode depends on whether or not the point determined by two characteristic parameters lies in a stable region of the stability plot of Mathieu's differential equation.[9] We thus have regions of stability and instability in this case. When the external pressure is a purely random function, we do not get regions of stability; rather, the mode is unstable for any nonzero value of the spectral density of the pressure fluctuations. This is a curious result which has been shown to be true experimentally for simple second-order systems.[1]

It should be pointed out, however, that the results obtained in this study are for the linearized structural equations, for which the predictions of instability may not necessarily correspond to an instability for the more exact, nonlinear equations. The limitation imposed by the assumption that the pressure fluctuations form a white-noise process does not appear too severe for the predictions of the theory to be valid in practical cases. In particular, the instability phenomenon has been displayed in the laboratory for a noise process whose spectral density was far from flat out to infinite frequency.

Appendix: Remarks on Sufficient Conditions for Mean-Square Stability

Without further arguments, it is possible that the constant K' in (39) could depend on n and m, in which case (40) does not follow. Moreover, it has been pointed out that the series in (40) does not converge for $\theta = 0$.*

In order to circumvent these difficulties, another set of sufficiency conditions will be given here. For this

* Referee's comments.

purpose, we note that the solution (44) can be evaluated to read

$$\langle w_n(t)w_m(t)\rangle = \sum_{j=1}^{4} A_{nm}{}^{(j)} e^{-i\zeta_{nm}{}^{(j)}t} \tag{A1}$$

where the $A_{nm}{}^{(j)}$ are arbitrary constants and the $\zeta_{nm}{}^{(j)}$ are roots of (46) having the form

$$\begin{aligned} &\zeta_{nm}{}^{(j)} = i\beta_{nm}{}^{(j)} + \Omega_{nm}{}^{(j)} \\ &\beta_{nm}{}^{(j)} > 0,\ \beta_{nm}{}^{(j)} = 0(1),\ \Omega_{nm}{}^{(j)} = 0(n^2, m^2) \end{aligned} \tag{A2}$$

where 0 denotes *large of the order of*.

We now assert: If initially (at $t = 0$)

$$\sum_{n,\,m=1}^{\infty} \left(\sum_{j=1}^{4} \left| A_{nm}{}^{(j)} \right| \right) < \infty \tag{A3}$$

then (35) converges for all values of $t > 0$ and θ. To show this we have

$$\begin{aligned} \left| \langle w^2(\theta,t)\rangle \right| &= \left| \sum_{n,\,m=1}^{\infty} \langle w_n(t)w_m(t)\rangle \cos n\theta \cos m\theta \right| \\ &\leq \sum_{n,\,m}^{\infty} \left| \langle w_n(t)w_m(t)\rangle \right| \left|\cos n\theta\right| \left|\cos m\theta\right| \\ &\leq \sum_{n,\,m=1}^{\infty} \left| \langle w_n(t)w_m(t)\rangle \right| \end{aligned} \tag{A4}$$

Using (A1) in (A4) we get

$$\begin{aligned} \left| \langle w_2(\theta,t)\rangle \right| &\leq \sum_{n,\,m=1}^{\infty} \left(\sum_{j=1}^{4} \left| A_{nm}{}^{(j)} \right| \left| e^{i\zeta_{nm}{}^{(j)}t} \right| \right) \\ &\leq \sum_{n,\,m=1}^{\infty} \left(\sum_{j=1}^{4} \left| A_{nm}{}^{(j)} \right| \left| e^{-\beta_{nm}{}^{(j)}t} \right| \right) \\ &\leq \sum_{n,\,m=1}^{\infty} \left(\sum_{j=1}^{4} \left| A_{nm}{}^{(j)} \right| \right) < \infty \end{aligned} \tag{A5}$$

This establishes the desired result.

References

[1] Samuels, J. C., and Eringen, A. C., *On Stochastic Linear System*, J. Math. and Phys. (MIT), Vol. 38, July, 1959.

[2] Samuels, J. C., *On the Mean-Square Stability of Random Linear Systems*, Trans. IRE PGIT-5 (Special Supplement), June, 1959.

[3] Timoshenko, S., *Theory of Elastic Stability*, McGraw-Hill, New York, 1936.

[4] Laning, J. H., and Battin, R. H., *Random Processes in Automatic Control*, McGraw-Hill, New York, 1936.

[5] Samuels, J. C., *On the Stability of Random Systems and the Stabilization of Deterministic Systems with Random Noise*, J. Acoust. Soc. Amer., Vol. 32, May, 1960.

[6] Bode, H. W., *Network Analysis and Feedback Amplifier Design*, D. van Nostrand, New York, 1945.

[7] Titchmarsh, E. C., *Introduction to the Theory of Fourier Integrals*, 2nd Ed., Chap. XI; Oxford Univ. Press, 1948.

[8] Carslaw, H. S., *Introduction to the Theory of Fourier's Series and Integrals*, Chap. 8; Dover Publications, New York.

[9] Stoker, J. J., *Nonlinear Vibrations*, p. 205; Interscience Publishers, Inc., New York, 1950.

✦ ✦ ✦

Hypersonic Viscous Flow (*Continued from page 893*)

References

[1] Bush, W. B., *Magnetohydrodynamic-Hypersonic Flow Past a Blunt Body*, Journal of the Aero/Space Sciences, Vol. 25, No. 11, pp. 685–690, 728, November, 1958.

[2] Chu, B. T., *Thermodynamics of Electrically Conducting Fluids and Its Application to Magnetohydromechanics*, Brown University Report, WADC TN 57-350, 1957.

[3] Crocco, L., *Ein neue Stromfunktion fur die Erforschung der Beugung der Gase mit Rotation*, ZAMM, Vol. 17, pp. 1–7, 1937.

[4] Hayes, W. D., *The Vorticity Jump Across a Gas-Dynamic Discontinuity*, J. Fluid Mech., Vol. 2, pp. 595–600, 1957.

[5] Hayes, W. D., and Probstein, R. F., *Hypersonic Flow Theory*, Academic Press, New York, 1958.

[6] Lighthill, M. J., *Dynamics of a Dissociating Gas—Part 1*, J. Fluid Mech., Vol. 2, pp. 1–32, 1957.

[7] Kemp, N. H., *On Hypersonic Blunt-Body Flow with a Magnetic Field*, AVCO Report No. 19, 1958.

[8] Nisbet, I. C. T., *Interfacial Instability of Fluids of Arbitrary Electrical Conductivity in Uniform Magnetic Fields*, Cornell University Aero. Eng. Dept. Report, 1958.

[9] Probstein, R. F., *Continuous Theory and Rarefied Hypersonic Aerodynamics*, Brown University Report, WADC TN 58-145, 1958.

[10] Whitham, G. B., *A Note on the Standoff Distance of the Shock in High Speed Flow Past a Circular Cylinder*, Comm. Pure and Appl. Math., Vol. 10, pp. 531–535, 1957.

✦ ✦ ✦

Plastic Compressive Buckling (*Continued from page 893*)

lems may be obtained by a simple transformation or replotting of the results of the corresponding elastic problems. Because of the large number of parameters and the complex calculations, no attempt has been made at the present time to obtain numerical results for the fourth problem, a plate on point supports.

The solutions are based upon the deformation theory of plasticity advocated by Bijlaard and Stowell.

References

[1] Bijlaard, P. P., *Theory and Tests on the Plastic Stability of Plates and Shells*, Journal of the Aeronautical Sciences, Vol. 16, No. 9, pp. 529–541, September, 1949.

[2] Stowell, Elbridge Z., *A Unified Theory of Plastic Buckling of Columns and Plates*, NACA TR 898, 1948.

[3] Seide, Paul, and Stein, Manuel, *Compressive Buckling of Simply Supported Plates with Longitudinal Stiffeners*, NACA TN 1825, 1949.

[4] Anderson, Roger A., and Semonian, Joseph W., *Charts Relating the Compressive Buckling Stress of Longitudinally Supported Plates to the Effective Deflectional and Rotational Stiffness of the Supports*, NACA TN 2987, 1953.

[5] Budiansky, Bernard, and Seide, Paul, *Compressive Buckling of Simply Supported Plates with Transverse Stiffeners*, NACA TN 1557, 1948.

[6] Seide, Paul, and Barrett, Paul F., *The Stability of the Compression Cover of Box Beams Stiffened by Posts*, NACA TN 2153, 1950.

Readers' Forum

BRIEF REPORTS of investigations in the aerospace sciences and discussions of papers published in the JOURNAL are presented in this special department. Entries must be restricted to a maximum of 1,300 words or the equivalent of one JOURNAL page including formulas and illustrations. Publication is completed as soon as possible after receipt of the material. The Editorial Committee does not hold itself responsible for the opinions expressed by the correspondents.

Contents

Bending Stresses Due to Temperature in Hollow Circular Plates, Part III ..... MALCOLM NEWMAN AND MARVIN FORRAY 951

On Conical-Flow Upwash ..... JOSEPH L. SIMS 952

The Creep Deformation of Symmetrically Loaded Circular Cylindrical Shells ..... ANTHONY E. GEMMA 953

Aerodynamic Properties of Ring Airfoils in Supersonic Flight ..... CHARLES H. MURPHY AND MAYNARD J. PIDDINGTON 954

Comments on the Behavior of Sedov's Blast-Wave Solution as $\gamma \to 1$ ..... ERIC F. BROCHER 955

Author's Reply ..... N. C. FREEMAN 956

An Analogy Between Boundary-Layer Pressure Gradient and Chemical Reaction-Rate Effects ..... GEORGE R. INGER 956

A Simple Method of Estimating the Vortex Intensity ..... MILES J. BOBRIK 957

Comment on "Flow About an Unsteadily Rotating Disc." ..... PAU-CHANG LU 958

Calculation of Flow-Variable Gradients Behind Curved Shock Waves ..... NATHAN GERBER AND JOAN M. BARTOS 958

A Further Discussion of the Limiting Circulatory Lift of a Finite-Span Wing ..... FRANKLYN J. DAVENPORT 959

Further Studies on the Local Elastic Deformations of Honeycomb Faceplate Subjected to Uniaxial Compression ..... R. C. WEIKEL AND A. S. KOBAYASHI 961

Chordwise-Bending Effects on Wing-Vibration Modes ..... JOHN C. GLASGOW AND JAMES L. CRONIN, JR. 962

Note on Slow Viscous Flow Through the Space Between Two Coaxial Circular Cones With the Same Vertex ..... T. K. CHAUDHURY 963

Bending Stresses Due to Temperature in Hollow Circular Plates, Part III

Malcolm Newman and Marvin Forray

Principal Engineer and Design Specialist, Structures, Applied R & D Division, Republic Aviation Corporation, Farmingdale, L.I., N.Y.

June 10, 1960

IN PREVIOUS NOTES,[1, 2] formulas and curves have been presented for the nondimensional deflection, moments, and shears in a circular plate with a concentric hole subject to a linear thermal gradient through the thickness. This note will give formulas and design curves for the deflections and moments (shear is identically zero) for the following problems:

Outer Edge	Inner Edge	Configuration
Simple	Free	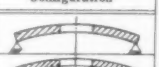
Free	Simple	
Free	Free	
Free	Clamped	
Simple	Freely Sliding And Restrained Against Rotation	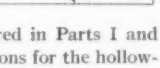
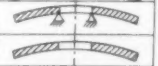
and these cases, in addition to those considered in Parts I and II, encompass the important boundary conditions for the hollow-circular-plate problem.

The first three problems (simple-free, free-simple, and free-free) are grouped together because they yield identical results within rigid-body displacements. The deflection relative to the inner boundary is

$$w/\alpha T_p b^2 = (1/2h)[(r^2/b^2) - 1] \qquad (1)$$

while the radial and tangential moments are

Contributors Please Note

Readers' Forum items must be confined to the equivalent of one page in the *Journal*. Contributions that exceed this limit will be returned to the authors for condensation and rewrite. To avoid inconvenience and delay, please adhere to the following specifications:

(1) Five, double-spaced, typewritten, manuscript pages (8½ by 11 in.), including wide margins, formulas, and headings, equal one printed page.

(2) For every illustration, deduct at least one-half or as much as one manuscript page, depending on the size of the illustration.

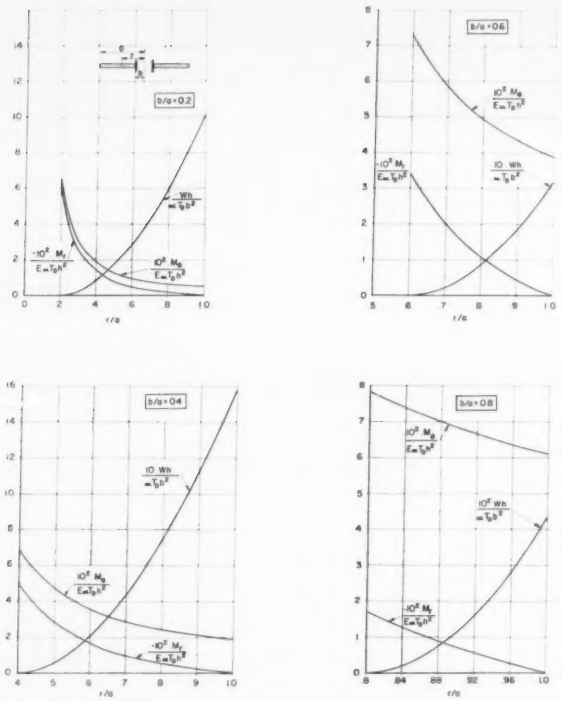

FIG. 1. Nondimensional deflection and moments for a plate with free outer boundary and clamped inner boundary.

$$M_r = M_\theta = 0 \tag{2}$$

where T_D is the temperature of the upper face minus the temperature of the lower face, w is positive downward, and α is the coefficient of linear expansion. The geometrical parameters are shown in Fig. 1.

The free-clamped and simple-freely sliding problems also yield identical results outside of a rigid-body displacement. The formulas for the deflection (relative to inner boundary) and moments in nondimensional form are

$$\frac{wh}{\alpha T_D b^2} = -(1+\nu)\frac{\{1/2[1-(r^2/b^2)]+\log(r/b)\}}{[(1+\nu)+(1-\nu)(b^2/a^2)]} \tag{3}$$

$$\frac{M_r}{E\alpha T_D h^2} = \frac{[1-(a^2/r^2)]}{12[(1-\nu)+(1+\nu)(a^2/b^2)]} \tag{4}$$

$$\frac{M_\theta}{E\alpha T_D h^2} = \frac{[1+(a^2/r^2)]}{12[(1-\nu)+(1+\nu)(a^2/b^2)]} \tag{5}$$

Fig. 1 shows these quantities versus r/a with $b/a = 0.2$, 0.4, 0.6, and 0.8 with Poisson's ratio $\nu = 0.3$.

REFERENCES

[1] Newman, M., and Forray, M., *Bending Stresses Due to Temperature in Hollow Circular Plates, Part I*, Journal of the Aero/Space Sciences, Vol. 27, No. 10, pp. 792–793, October, 1960.

[2] Forray, M., and Newman, M., *Bending Stresses Due to Temperature in Hollow Circular Plates, Part II*, Journal of the Aero/Space Sciences, Vol. 27, No. 11, pp. 870–871, November, 1960.

On Conical-Flow Upwash

Joseph L. Sims
Aeroballistics Laboratory, ABMA, Redstone Arsenal, Ala.

June 15, 1960

RECENTLY, a new group of solutions of supersonic flow fields about right circular cones has been[1,2] published. These solutions are for both zero angle of attack and for small angles of attack, and all results are presented in a body-fixed coordinate system. Additionally, all integrated velocity components are combined, in the manner outlined by Ferri[3] so that the total flow at any point in the field may be written as

$$\left.\begin{aligned} M^* &= M^*_1 + \alpha M^*_2 \cos\phi \\ \theta &= \theta_1 + \alpha\theta_2 \cos\phi \\ M^*_w &= \alpha M^*_{w_2} \sin\phi \end{aligned}\right\} \tag{1}$$

where

$M^* = v/a^*$, and a^* is the critical speed of sound
θ = the flow direction angle in radians
subscripts 1 denote zero-angle-of-attack quantities
subscripts 2 denote angle-of-attack quantities which are independent of the angle of attack, α, and the meridian plane, ϕ.
subscript w denotes a quantity in a normal direction to a meridian plane.

One flow-field quantity of interest that may be derived from these results is the upwash angle, which has a bearing on body-wing interference. Herein, the upwash factor will be reduced to the ratio of local angle of attack, α_l, to cone angle of attack, α. This can be done as follows:

$$\tan\alpha_l = \alpha M^*_{w_2}\sin\phi/(M^*_1 + \alpha M^*_2\cos\phi) \tag{2}$$

and if α is small, α_l is small and $\tan\alpha_l \approx \alpha_l$ so that

$$\alpha_l = \alpha M^*_{w_2}\sin\phi/(M_1{}^* + \alpha M^*_2\cos\phi) \tag{3}$$

Now, as α approaches zero

$$(\alpha_l/\alpha)_{\alpha\to 0} = (M^*_{w_2}/M^*_1)\sin\phi \tag{4}$$

where $\phi = 0$ is assumed to be at the windward meridian.

Some of the above-mentioned numerical results have been used in Eq. (4) to evaluate the ratio, α_l/α, in the $\pi/2$ meridian plane. Fig. 1 gives cone surface values of α_l/α as a function of free-stream Mach number for cone angles from 2.5 to 30.0 degrees, right outside of Ferri's entropy layer[4]. It is seen, for higher Mach numbers and larger cone angles, that the local angle of attack is less than the cone angle of attack. Thus, we see that for these cones the traditional upwash factor is actually a downwash factor. Fig. 2 presents the distribution of the factor α_l/α through the flow field for the various cone angles at a free-stream Mach number of 5. There data are plotted as a function of

$$\xi = (\varphi - \varphi_s)/(\varphi_w - \varphi_s)$$

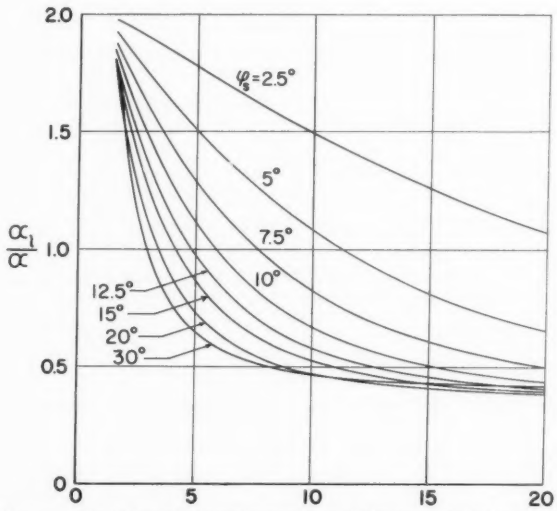

FIG. 1. Variation of the surface values of the upwash factor with free-stream Mach number.

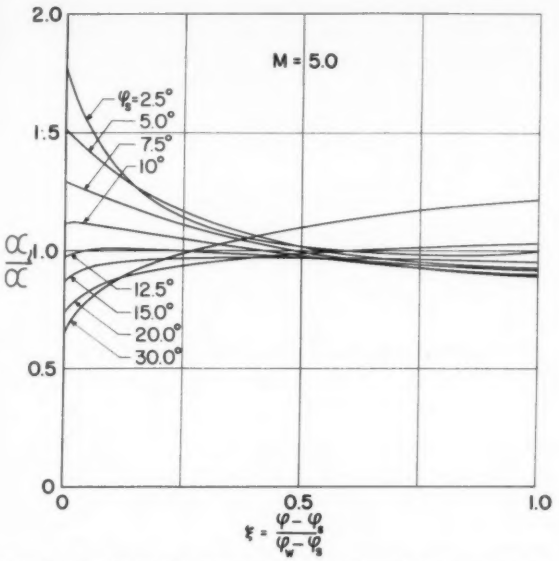

FIG. 2. Variation of the upwash factor through the conical flow fields at a free-stream Mach number of 5.

where

φ = conical-ray angle
s = surface value
w = shock-wave value

Here we see that the shape of the distribution curves is a very strong function of the cone angle. In general, the data in references 1 and 2 show that for low Mach numbers the upwash factors decrease as the flow field is traversed from cone to shock wave. For high Mach numbers the converse is generally true, and we get an increase in the upwash factor across the flow field.

REFERENCES

[1] Sims, Joseph L., *Supersonic Flow Around Right Circular Cones—Tables for Zero Angle of Attack*, ABMA Report DA-TR-11-60, March 1, 1960.

[2] Sims, Joseph L., *Supersonic Flow Around Right Circular Cones—Tables for Small Angle of Attack*, ABMA Report DA-TR-19-60, April 27, 1960.

[3] Ferri, Antonio, *The Method of Characteristics for the Determination of Supersonic Flow Over Bodies of Revolution at Small Angles of Attack*, NACA Report 1044, 1951.

[4] Ferri, Antonio, *Supersonic Flow Around Circular Cones at Angles of Attack*, NACA Report 1045, 1951.

The Creep Deformation of Symmetrically Loaded Circular Cylindrical Shells

Anthony E. Gemma
Assistant Project Engineer, Connecticut Operations–CANEL, Pratt & Whitney Aircraft, Middletown, Conn.

May 26, 1960

SYMBOLS

$\dot{\epsilon}_x, \dot{\epsilon}_\varphi$	= axial and circumferential strain rates, respectively
σ_x, σ_φ	= axial and circumferential stresses, respectively
B, n	= constants in power creep law
h	= shell thickness
N_x, N_φ	= axial and circumferential forces, respectively
$\dot{w}$	= radial displacement rate
a	= radius of cylinder
z	= thickness coordinate
κ_x, κ_φ	= curvature rates
M_x	= moment
β	= see Eq. (9)
α	= see Eq. (10)
c_1, c_2, c_3, c_4	= constants
$f(x)$	= see Eq. (11)
K_1, K_2, K_3, K_4	= constants
$\Phi(\eta)$	= see Eq. (13)
λ	= see Eq. (13)
ξ, η	= see Eq. (12)

THIS NOTE describes an approximate solution for circular cylindrical shells in steady creep. The problem is formulated using the Soderberg relationships,[1] together with a power creep law

$$\dot{\epsilon}_x = [\sigma_x - (1/2)\sigma_\varphi]\dot{e}/\sigma, \quad \dot{\epsilon}_\varphi = [\sigma_\varphi - (1/2)\sigma_x]\dot{e}/\sigma \qquad (1)$$

where

$$\sigma = (\sigma_x^2 + \sigma_\varphi^2 - \sigma_x\sigma_\varphi)^{1/2} \quad \dot{e} = B\sigma^n$$

From Eqs. (1) and since $N_i = h\sigma_i$, $(i = x,\varphi)$, the following expressions for the forces are obtained:

$$N_x = Ah(\dot{\epsilon}_\varphi + 2\dot{\epsilon}_x)K, \quad N_\varphi = Ah(\dot{\epsilon}_x + 2\dot{\epsilon}_\varphi)K \qquad (2)$$

where

$$A = (2/B)^{1/n}(1/\sqrt{3})^{(n+1)/n} \quad K = (\dot{\epsilon}_x^2 + \dot{\epsilon}_\varphi^2 + \dot{\epsilon}_x\dot{\epsilon}_\varphi)^{(1-n)/2n}$$

From the equilibrium equations for symmetrically loaded circular shells,[2] the forces N_x are constant, and for simplicity are assumed to be zero.

Then, from Eq. (2)

$$\dot{\epsilon}_\varphi = -2\dot{\epsilon}_x \qquad (3)$$

and the strain-displacement rates are

$$\dot{\epsilon}_\varphi = \dot{w}/a, \quad \dot{\epsilon}_x = -\dot{w}/2a \qquad (4)$$

Therefore,

$$N_\varphi = h(1/Ba)^{1/n}(\dot{w})^{1/n} \qquad (5)$$

Relationships for the curvature rates are (using the usual plate theory approximation)

$$\kappa_x = z(\partial^2\dot{w}/\partial x^2), \quad \kappa_\varphi = 0 \qquad (6)$$

Using expressions similar to Eqs. (2) with the strain rates replaced by curvature rates (i.e., Eqs. 6), and noting

$$M_i = 2\int_0^{h/2} (N_i/h)z\,dz, \quad i = x, \varphi$$

the axial moment is obtained

$$M_x = (n/1+2n)(1/\sqrt{3})^{(n+1)/n}(1/B)^{1/n}(h)^{(1+2n)/n} \times (\partial^2\dot{w}/\partial x^2)^{1/n} \qquad (7)$$

The equilibrium equation for a circular cylinder with no load is[3]

$$d^2(M_x)/dx^2 + (1/a)N_\varphi = 0 \qquad (8)$$

Using Eqs. (5) and (7) in Eq. (8), the governing differential equation for the creep deformation is

$$\partial^2[\partial^2\dot{w}/\partial x^2]^{1/n}/\partial x^2 + \beta(\dot{w})^{1/n} = 0 \qquad (9)$$

where

$$\beta = [(1+2n)/n](\sqrt{3}/ah)^{(n+1)/n}$$

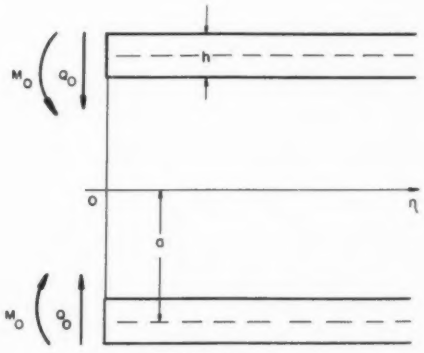

FIG. 1.

An approximate solution can be obtained if the assumption is made $n \gg 1$ (i.e., $1/n \to 0$). Indicating differentiation with respect to x by primes, Eq. (9) becomes

$$\dot{w}'^{v} - (\dot{w}''')^{2}(\dot{w}'')^{-1} + \alpha n \dot{w}'' = 0 \tag{10}$$

where $$\alpha = 2\sqrt{3}/ah$$

And the solution for Eq. (10) is

$$\dot{w} = c_1 \int\int f(x)dx\,dx + c_2 x + c_4$$
$$f(x) = \exp[(-\alpha n/2)(x + c_2)^2] \tag{11}$$

The solution can be conveniently stated by taking

$$\eta = x/a, \quad \dot{\xi} = \dot{w}/a \tag{12}$$

Then

$$\dot{\xi} = K_1 \int\int \Phi(\eta)d\eta\,d\eta + K_3\eta + K_4,$$
$$\Phi(\eta) = \exp[(-\lambda)(\eta + K_2)^2], \quad \lambda = \sqrt{3}n(a/h) \tag{13}$$

Special Case

Consider a semi-infinite cylinder with moments, M_0, and shears, Q_0, at $\eta = 0$, (Fig. 1). A suitable set of boundary conditions are

$$\left.\begin{aligned} &\text{at } \eta = \infty: \\ &\qquad \dot{\xi} = 0, \qquad (\partial\dot{\xi}/\partial\eta) = 0 \\ &\text{at } \eta = 0: \\ &M_\eta = (n/1 + 2n)(1/\sqrt{3})^{(n+1)/n}(h/Ba)^{1/n} \times \\ &\qquad h^2\,[\partial^2\dot{\xi}/\partial\eta^2]_{\eta=0}^{1/n} = M_0 \\ &Q_\eta = (1/n)(n/1 + 2n)(1/\sqrt{3})^{(n+1)/n}(h/Ba)^{1/n} \times \\ &\qquad h^2\left\{[\partial^2\dot{\xi}/\partial\eta^2]^{(1-n)/n}[\partial^3\dot{\xi}/\partial\eta^3]\right\}_{\eta=0} = Q_0 \end{aligned}\right\} \tag{14}$$

Relaxing the assumption $n \gg 1$, an approximate solution for a cylinder in second-stage creep with edge moments and shears is

$$\dot{\xi} = [(2\sqrt{3}/h^2)(Ba/h)^{1/n}M_0] \int\int \exp\,[-n\sqrt{3}(a/h)\eta^2 + (nQ_0/M_0)\eta]d\eta\,d\eta \tag{15}$$

Other cases of interest can be worked out using the general solution, Eqs. (11) or (13). Also, Eq. (15) can be used to get approximate solutions for various discontinuity problems.

References

[1] Soderberg, C. R., *Interpretation of Creep Tests on Tubes*, ASME Trans., Vol. 62, No. 3, pp. 738–748, 1940.

[2] Timoshenko, S., and Woinowsky-Krieger, S., *Theory of Plates and Shells*, 2nd Ed., Chapt. 15, McGraw-Hill Book Co., Inc., 1959.

[3] *Ibid.*

Aerodynamic Properties of Ring Airfoils in Supersonic Flight

Charles H. Murphy and Maynard J. Piddington

Aeronautical Research Engineers, Ballistic Research Laboratories, Aberdeen Proving Ground, Md.

May 17, 1960

THE LINEARIZED THEORY for supersonic flow over a thin ring airfoil with low-fineness ratio is quite similar to that for thin airfoils and was developed by H. Mirels[1] in 1948. According to this theory, the center of pressure is located at the midchord point and the lift coefficient C_{L_α} is $2/\beta$, where

$$\beta = \sqrt{M^2 - 1}$$

and the reference area is one half the wetted area.

A series of ring airfoils has been flight tested at the Transonic Range.[2] A drawing of these airfoils is shown in Fig. 1. For all models, the center of gravity was located at the midchord point and the maximum diameter, d, was 4.75 in. The other dimensions were

θ, deg.	c, in.	t/c
20	1.17	0.18
25	1.81	0.23
35	1.70	0.35

The models were tested at supersonic Mach numbers up to 3.7 and were found to be statistically stable for Mach numbers in excess of 1.7.[3]

In Fig. 2, the static-moment coefficient is plotted versus thickness ratio for $M = 3.1$. As can be seen from this plot, the moment coefficient is a linear function of (t/c). It should be noted that these values imply a fairly large static margin. If C_{L_α} is estimated to be 50 per cent greater than its thin-airfoil value, the 35° wedge would possess a static margin of almost 30 per cent.

For the models tested, the thin-airfoil theory predicts that the drag coefficient is

$$C_D = C_{D_f} + C_{L_\alpha}\alpha^2 + \frac{8}{\beta}\left[\frac{t}{c}\right]^2$$

where C_{D_f} is the skin-friction drag coefficient. Since C_{D_f} and α are usually quite small contributors to the total drag, this theory predicts $C_D/(t/c)^2$ to be a constant at fixed Mach number and to vary as β^{-1} with Mach number. Although models with wedge angles as large as 35° are not very thin, experimental values of $C_D/(t/c)^2$ were compared with theory. As can be seen from Fig. 3, this ratio is essentially constant but 15 per cent greater than its theoretical value. It was also found that its dependence on Mach number for $1.7 < M < 3.7$ is precisely that of the theory.

References

[1] Mirels, Harold, *Theoretical Wave Drag and Lift of Thin Supersonic Range Airfoils*, NACA TN 1678, August, 1948.

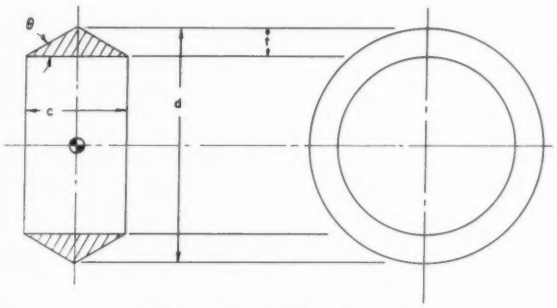

FIG. 1. Drawing of ring airfoil.

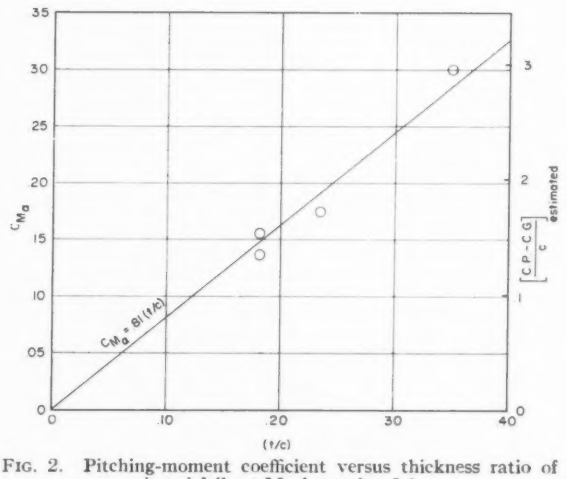

FIG. 2. Pitching-moment coefficient versus thickness ratio of ring airfoils at Mach number 3.1.

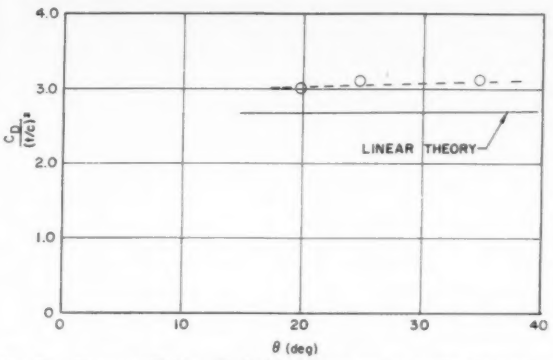

FIG. 3. Drag coefficient $C_D/(t/c)^2$ versus wedge angle of ring airfoils at Mach number 3.1.

[2] Rogers, Walter K., Jr., *The Transonic Free Flight Range*, BRL Rept. 1044, June, 1958.

[3] Piddington, Maynard J., and Murphy, Charles H., *The Drag and Stability of a Circular Wedge Airfoil in Supersonic Flight*, BRL Memo. Rept. 1245, January, 1960.

Comments on the Behavior of Sedov's Blast-Wave Solution as $\gamma \to 1$*

Eric F. Brocher
Research Assistant, Cornell University, Ithaca, N.Y.
June 1, 1960

IN A RECENT NOTE, Freeman[1] has studied the behavior of the blast-wave solution as $\gamma \to 1$ and compared it with the Newtonian theory of unsteady hypersonic flow. The order of approximation involved is not specified, and the formulas given for the similitude parameter and the radial velocity profile are not, in fact, uniformly valid in the limit of small radii. The purpose of the present note is to show how these restrictions can be removed, and to give a uniform approximation to Sedov's solution [neglecting $O(\epsilon^2)$, where $\epsilon = (\gamma - 1)/(\gamma + 1)$] for the planar, cylindrical, and spherical cases. An expansion procedure to get higher order approximations is demonstrated. In addition, it is shown that the range of validity of the blast-wave analogy with steady hypersonic flow tends to zero as $\gamma \to 1$.

In Sedov's exact solution, all physical quantities and the similitude parameter λ are expressed as functions of an auxiliary parameter V. If an inversion of $\lambda = \lambda(V)$ is made—i.e., if one can find $V = V(\lambda)$, it is possible to express quantities directly as functions of λ, giving a very clear picture of the structure of the shock layer. This inversion cannot be done exactly, but an expansion of $V = V(\lambda)$ in powers of ϵ can be found. Using the notation of reference 2, for $\omega = 0$ (uniform density in front of the shock wave), the similitude parameter λ is given (exactly) by

$$\lambda = (r/r_s) = [F_1(V)]^{-k}[F_3(V)]^{k(\gamma-1)/(2\gamma-\varphi)}\,[F_4(V)]^{-\Phi} \quad (1)$$

Setting

$$\alpha \equiv (2\gamma - \varphi)/[k(\gamma - 1)] = [(1 + j) + \epsilon(3 - j)]/2\epsilon \quad (2)$$

and

$$f \equiv F_1^{-k}F_4^{-\Phi} = \{[(\gamma + 1)/2k]V\}^{-k} \times \{[(\gamma + 1)/(\gamma + 1 - \varphi)][1 - (\varphi/2k)V]\}^{-\Phi} \quad (3)$$

Eq. (1) yields

$$V = (k/\gamma)\{1 + \epsilon\lambda^\alpha f(V)^{-\alpha}\} \quad (4)$$

One can show that $f(V)$ varies only slightly over the range of V.

* This research was supported by the USAF Office of Scientific Research under Contract AF 49(638)-544. The author is indebted to Dr. S. H. Lam for helpful discussions of the problem.

The variation of V itself is $O(\epsilon)$ because

$$V_s - V_b = (k/\gamma)\epsilon \quad (5)$$

The relation between the value of f at the origin of the blast (f_b) and at the shock (f_s) is found to be

$$f_s - f_b = [(3 - j)/(1 + j)^2]\epsilon^2 + O(\epsilon^3) \quad (6)$$

Moreover, f is monotonic over the range of V (for arbitrary γ in the cases $j = 1, 2$ and, for $1 \le \gamma \le 2$ in the case $j = 0$) and hence, the variation of f is $O(\epsilon^2)$.

f takes the value 1 immediately behind the shock, and thus can be written in the form

$$f = 1 + \epsilon^2 f_2(\lambda) + \epsilon^3 f_3(\lambda) + \ldots \quad (7)$$

Combining Eqs. (3) and (4), one gets

$$\left.\begin{aligned} f = \left\{\left(\frac{\gamma+1}{2\gamma}\right)[1 + \epsilon\lambda^\alpha f^{-\alpha}]\right\}^{-k} \left\{\left(\frac{\gamma+1}{\gamma+1-\varphi}\right) \times \left[1 - \frac{\varphi}{2\gamma}(1 + \epsilon\lambda^\alpha f^{-\alpha})\right]\right\}^{-\Phi} \\ = 1 - \epsilon^2\frac{(1 - \lambda^\alpha f^{-\alpha})}{(1 + j)}\left[\left(\frac{4}{1+j}\right) - (1 - \lambda^\alpha f^{-\alpha})\right] + \ldots \end{aligned}\right\} \quad (8)$$

Introducing the expansion of f in Eq. (8), one can determine the coefficients f_n by comparison. For instance, f_2 is found to be

$$f_2 = -\frac{(1 - \lambda^\alpha)}{(1 + j)}\left[\left(\frac{4}{1+j}\right) - (1 - \lambda^\alpha)\right] \quad (9)$$

Hence,

$$V = (k/\gamma)\{1 + \epsilon\lambda^\alpha + \epsilon^2\lambda^\alpha(1 - \lambda^\alpha) \times [(2/1 + j) - (1/2)(1 - \lambda^\alpha)] + O(\epsilon^3)\} \quad (10)$$

For the case $j = 1$, the first-order approximation [neglecting $O(\epsilon^2)$] is equivalent to that suggested by Einbinder.[2]

It is now possible to express all physical quantities as functions of λ. For instance, the radial velocity v and the Lagrangian coordinate r_0 are given by

$$(v/v_s) = [(\gamma + 1)/2k]\lambda V = \lambda\{1 - \epsilon(1 - \lambda^\alpha) + O(\epsilon^2)\} \quad (11)$$

$$\frac{r_0}{r_s} = \frac{\lambda^{(1+\epsilon)/2\epsilon}}{(2 - \lambda^\alpha)^{1/(1+j)}}\,[1 + O(\epsilon)] \quad (12)$$

Since the exponent α is $O(\epsilon^{-1})$, one notes that (a) the velocity profile tends to be linear in λ as $\epsilon \to 0$, and that (b) the velocity profiles are the same in the planar, cylindrical, and spherical cases, except in the neighborhood of the shock.

Using Eq. (12), one can express λ as a function of r_0:

$$\lambda = \left[\frac{2}{1 + (r_0/r_s)^{1+j}}\right]^{2\epsilon/(1+j)}\left(\frac{r_0}{r_s}\right)^{2\epsilon/(1+\epsilon)}[1 + O(\epsilon^2)] \quad (13)$$

It should be emphasized that higher order terms in the last exponent have to be kept in order for Eq. (13) to be uniformly valid.

Lower order approximations to Eqs. (13) and (11) are

$$\lambda = (r_0/r_s)^{2\epsilon/(1+\epsilon)}\,[1 + O(\epsilon)] \quad (14)$$

$$v/v_s = \lambda[1 + O(\epsilon)] = (r_0/r_s)^{2\epsilon/(1+\epsilon)}\,[1 + O(\epsilon)] \quad (15)$$

These constitute an improvement upon Eqs. (1) and (2) of reference 1. In the same reference, for the Newtonian theory of unsteady hypersonic flow, higher order terms in the exponent of the integrand of Eq. (12) should have been kept—i.e.,

$$\left(\frac{r}{r_s}\right)^2 = 2\epsilon\int_0^{r_s}\left(\frac{r_0}{r_s}\right)^{-2[(1-\epsilon)/(1+\epsilon)]+1} d\left(\frac{r_0}{r_s}\right)[1 + O(\epsilon)]$$

which yields

$$(r/r_s) = (r_0/r_s)^{2\epsilon/(1+\epsilon)}[1 + O(\epsilon)]$$

in accordance with Eq. (14) of the present note.

There is a point of interest concerning the shock growth as $\epsilon \to 0$. The relation between shock radius and blast energy E is given by

$$r_s = \text{const.} \left(\frac{E}{\rho_\infty I_j(\gamma)}\right)^{1/(3+j)} t^k \tag{16}$$

where

$$I_j(\gamma) = \int_0^1 \left(\frac{P}{\gamma - 1} + \frac{RV^2}{2}\right) \lambda^{2+j}\, d\lambda \tag{17}$$

Using Eq. (10), a straightforward but somewhat lengthy calculation yields

$$I_j(\gamma) = \frac{1 - \epsilon(2 \ln 2 - 1) + O(\epsilon^2)}{(3 + j)^2(j + 1)} \epsilon^{-1} \tag{18}$$

Hence, $r_s = O(\epsilon^{1/(3+j)})$, which means that the shock speed tends to zero as $\epsilon \to 0$. Thus, one has the paradoxical case of a strong shock which does not expand. In view of the analogy between the blast wave and steady hypersonic flow, it is of interest to see what this implies. In this analogy, $x = U_\infty t$ and one can show that

$$\left(\frac{r_s}{d}\right) = \left[\frac{C_D}{4^{1+j} I_j(\gamma)}\right]^{1/(3+j)} \left(\frac{x}{d}\right)^k \tag{19}$$

d denotes the leading-edge thickness or body diameter and C_D the nose-drag coefficient.

The range of validity R of the analogy is limited below by the small-shock-angle condition ($\tan^2 \sigma \leq 1/A$, where $A \gg 1$) and above by the strong-shock assumption. Using Eqs. (18) and (19), the range is found to be

$$AC\, \epsilon^{1/(1+j)} \leq (x/d) \leq C(M_\infty/M_s^*)^{(3+j)/(1+j)}\, \epsilon^{1/(1+j)} \tag{20}$$

where

$$C = (2C_D)^{1/(1+j)}/(3 + j) \tag{21}$$

and M_s^* is the shock Mach number below which the shock can no longer be regarded as strong.

Therefore, R gets closer to the nose as ϵ decreases and is $O(\epsilon^{1/(1+j)})$, which means that the analogy fails completely in the limit $\epsilon = 0$. Moreover, there is another reason that the analogy fails. The flow field can be divided into two regions: in one region the streamlines have crossed the shock at points where σ is not small, in the other, at points where σ is small. Using Eq. (13) the thickness of the shock layer δ_f in which the blast-wave analogy is valid is found to be

$$\delta_f = \text{const.}\ [2/(1 + j)]\epsilon + O(\epsilon^2) \tag{22}$$

Hence, this thickness tends to zero as $\gamma \to 1$ and is twice as large for $j = 0$ as for $j = 1$.

References

[1] Freeman, N. C., *A Note on the Explosion Solution of Sedov With Application to the Newtonian Theory of Unsteady Hypersonic Flow*, Journal of the Aero/Space Sciences, Vol. 27, No. 1, pp. 77–78, January, 1960.

[2] Hayes, W. D., and Probstein, R. F., *Hypersonic Flow Theory*, Academic Press, pp. 52–61, 1959.

[3] Einbinder, H. A., *A Note on Blast-Wave Theory*, Journal of the Aero/Space Sciences, Vol. 26, No. 3, pp. 191–192, March, 1959.

Author's Reply

N. C. Freeman
Aerodynamics Division, National Physical Laboratory, Teddington, Middlesex, England

August 8, 1960

MR. BROCHER, in the above note, appears to credit me in my previous note[1] with more than I had intended. The sole purpose of this note was to demonstrate that to derive a Newtonian solution in the explosion case, it was necessary to retain the first-order term in the exponent of Eq. (13) as is confirmed by the exact solution. Physically, this means that the process is required to be isentropic and not isothermal as Newtonian approach would suggest. The order of the approximation was not given in the note since, as Mr. Brocher demonstrates, the complete uniformly valid solution is more complicated. The terms neglected become significant, however, only in the region (r_0/r_s) of order e^{-1/ϵ^2}. Although it is undoubtedly true that the complete uniform behavior is given by retaining the complete form of the exponent in Eq. (12), it is difficult to see why the Newtonian theory would "demand" this.

I would also like to apologize to readers for an inexcusable error in my note which requires that ϵ should read 2ϵ in all equations except the exponent of Eq. (12). The following typographical errors should also be corrected:

Eqs. (6) and (7):
left-hand side should read p/ρ_∞

Sentence following Eq. (7):
insert factor ρ_∞ before parentheses

Eq. (9):
change p/p_s to read ρ/ρ_s

Eq. (10a):
change p_∞ to read ρ_∞

An Analogy Between Boundary-Layer Pressure Gradient and Chemical Reaction-Rate Effects

George R. Inger*
Department of Aeronautical Engineering, University of Michigan, Ann Arbor, Mich.

June 10, 1960

THE PURPOSE OF THIS NOTE is to point out a qualitative similarity between the effect of a pressure gradient on the boundary-layer velocity profile $u(Y)$ shape, and the effect of a homogeneous chemical reaction-rate term on the shapes of the corresponding thermodynamic-state profiles [fractional atom concentration $\alpha_A(Y)$ and temperature distribution $T(Y)$]. Consider the following boundary-layer equations governing a dissociated binary-mixture flow in the immediate vicinity of a mass-transfer-free surface $Y = 0 (u = v = 0)$:

Momentum

$$\left[\frac{\partial}{\partial Y}\left(\mu \frac{\partial u}{\partial Y}\right)\right]_{Y=0} = \frac{dp_e}{dX} \tag{1}$$

Atomic-Specie Mass

$$\left[\frac{\partial}{\partial Y}\left(\frac{\mu}{S_c}\frac{\partial \alpha_A}{\partial Y}\right)\right]_{Y=0} = -\left[\frac{\dot{W}_A}{\rho}\right]_{Y=0} \tag{2}$$

Energy

$$\left[\frac{\partial}{\partial Y}\left(\lambda \frac{\partial T}{\partial Y}\right)\right]_{Y=0} = \left[(h_A - h_M)\frac{\dot{W}_A}{\rho}\right]_{Y=0} - \left[\mu\left(\frac{\partial u}{\partial Y}\right)^2\right]_{Y=0} - \left[\frac{\mu}{S_c}(c_{P_A} - c_{P_M})\frac{\partial \alpha_A}{\partial Y}\frac{\partial T}{\partial Y}\right]_{Y=0} \tag{3}$$

where S_c is the Schmidt number, $\dot{W}_A$ the net rate of atomic mass production by chemical reaction, and the subscripts A, M refer to atomic and molecular species, respectively. Now, Eq. (1) illustrates the well-known fact that an unfavorable pressure gradient ($dp_e/dx > 0$) tends to cause an inflection point [$(\partial^2 u + \partial Y^2)(0) > 0$] in $u(Y)$ at some $Y > 0$. The net atomic-reaction rate at the wall plays a similar role in Eq. (2) regarding the shape of the atomic-specie profile. Recombination-dominated chemical nonequilibrium ($\dot{W}_A < 0$) in the gas near the wall acts like the unfavorable pressure gradient in the momentum equation, in that it tends to cause an inflection point in $\alpha_A(Y)$ at some $Y > 0$. This chemical-reaction effect holds true for either

* Graduate Student.

a catalytic $[\alpha_A(0) = 0]$ or noncatalytic $[(d\alpha_A/dY)(0) = 0]$ wall. While the values of $\alpha_A(0)$ and $(d\alpha_A/dY)(0)$ are determined by the degree of catalytic activity on the wall surface and the integrated effect of the gaseous-reaction rates across the entire boundary layer, the value of $(\partial^2\alpha_A/\partial Y^2)(0)$ is directly influenced by the gaseous-reaction rates in the vicinity of the wall. Furthermore, since $\dot{W}_A/\rho \sim p_e^2(T/300)^{\omega-2}$ for dissociation-recombination in air[1, 2] the tendency of $(\partial\alpha_A/\partial Y)$ to increase with Y for recombination-dominated reactions will be greater as the local pressure increases (being a maximum at the stagnation point), and will be most prominant at a given pressure for a recombination-rate temperature-dependence law that assumes $\omega > 2$ for $T_w > 300°K$.

The effect of the reaction-rate term on the temperature profile near the wall (Eq. 3) is opposite to the effect on $\alpha_A(Y)$; an inflection point in $T(Y)$ will appear in the presence of *dissociation-dominated* chemical nonequilibrium in the gas adjacent to the wall. This qualitative analogy with a pressure-gradient effect proves useful in the interpretation of the effects of dissociation-recombination reactions on the thermodynamic-state profile behavior in the boundary layer.

References

[1] Fay, J. A., and Riddell, F. R., *Theory of Stagnation Point Heat Transfer in Dissociated Air*, AVCO, Everett Research Report 1, April, 1957.

[2] Inger, G. R., *Chemical Non-Equilibrium in the Laminar Hypersonic Boundary Layer*, AF OSR TN-59-237, Report 7010-6 (ASTIA AD 212 007, Contract No. AF 49(638)-380), Bell Aircraft Corp., March, 1959.

A Simple Method of Estimating the Vortex Intensity

Miles J. Bobrik

Aerodynamics Department, De Havilland Aircraft of Canada, Downsview, Ontario

June 16, 1960

Symbols

$A(D)$	= calibration function
a_1a_2	= constants in equation (11)
c	= wing chord
D	= distance from the trailing vortex origin
k_1k_2	= constants of variation in equation (7)
n	= r.p.m.
p	= pressure
p_0	= pressure in the vortex-core center
$p_p(r)$	= total pressure in distance r
Δp_p	= $p_p(r_0) - p_p(0)$
r	= coordinate from the core center

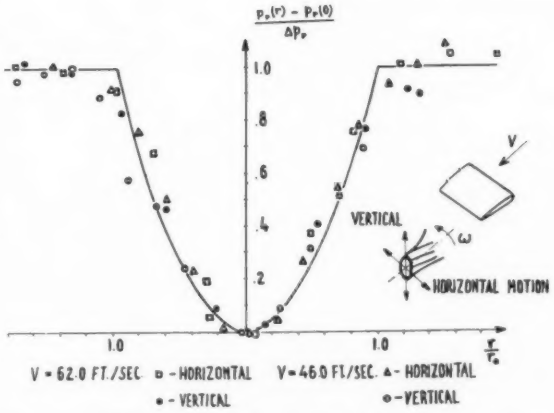

FIG. 1. Dimensionless total-pressure distribution in vortex. Comparison of Eq. (5) with experimental values.

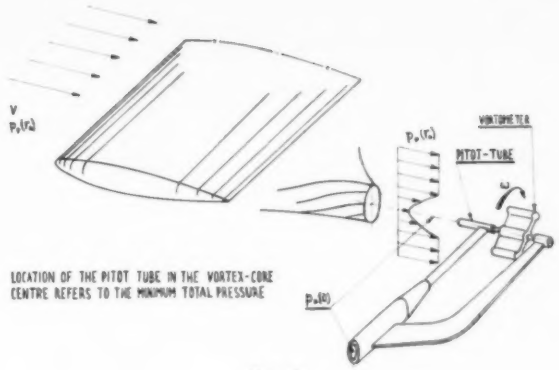

FIG. 2.

r_0	= radius of vortex core
t	= time
V	= free-stream velocity
V_i V_c	= velocity outside and inside the vortex core
Γ	= vortex intensity
$\gamma = \Gamma/Vc$	= nondimensional vortex intensity
ν	= kinematic viscosity
ρ	= density
σ	= surface bounded by integral curve
ω	= angular velocity

Introduction

TO DETERMINE THE PATTERN and intensity of a trailing vortex behind a wing or any other fairing body, the whole velocity field[1] or the angular velocity of the vortex field[2] has to be measured. These methods require much time. Therefore, they have no practical value in the verification of assumptions and theories based on the necessary simplifications of actual complex phenomena. The ideas set out below have been found very useful in overcoming this difficulty.

Principle of the Method

As shown in reference 2, a "core" is formed in the center of the potential vortex flow in a real fluid. From a mathematical viewpoint, this can be simulated by assuming the existence of a vortex sheet on the vortex core surface in the ideal fluid. According to reference 3, it can be said that the fluid inside the core behaves like a solid body rotating at a constant angular velocity while the fluid outside the vortex core has the characteristics of the ideal fluid. Thus the velocities, inside and outside the vortex core, can be expressed as

$$V_e = (\Gamma/2\pi r_0^2)r, \quad V_i = (\Gamma/2\pi r) \tag{1}$$

Assuming that the fluid in the vortex core is a rigid body, the equilibrium equation for the element of the core can be easily expressed. The tangent stress need not be taken into account because there is no relative radial motion of fluid inside the core. Considering the fact that velocities on the core surface should be equal, the static pressure in the core will be as follows:

$$p = p_0 + (\rho\omega^2/2)r^2 \tag{2}$$

The total pressure will be

$$p_p(r) = p + (\rho/2)(V^2 + r^2\omega^2) \tag{3}$$

By substituting Eq. (2) into Eq. (3), the following result is obtained:

$$p_p(r) = (\rho V^2/2) + \rho r^2\omega^2 + p_0 \tag{4}$$

The distribution of total pressure along the radius can be verified by measurements. For this purpose, the following nondimensional term has been found practical:

$$[p_p(r) - p_p(0)]/\Delta p_p = (r/r_0)^2 \tag{5}$$

It will be seen in Fig. 1 that, for practical purposes, the experimental data and the plot of term (5) are more or less identical.

Using the foregoing Eq. (4) and Stoke's theorem, the vortex intensity can be expressed as

$$\Gamma = \int_\sigma \text{curl } V \times d\sigma = 2\pi r_0^2\omega = (2\pi/\rho\omega)\Delta p_p \qquad (6)$$

For this, the difference between the total pressure in the vortex center and that in the free stream has to be measured, as well as the angular velocity of the core.

In Fig. 2 is shown a useful device for taking measurements. It can be easily designed and constructed. It should be noted that the measurements taken by this instrument have to be made at a suitable distance from the wing—i.e., where the trailing vortex sheet is completely rolled up into a single vortex line.[4] It has been proved[2] that in case of straight wings of linear lift curve the plots of rotational speed versus the free-stream velocity, as well as the total pressure in the vortex-core center versus the free-stream total pressure, are linear functions. Hence,

$$n = k_1 V_1 \quad p_p(0) = p_p(r_0)k_2 \qquad (7)$$

Expressing the vortex intensity in a nondimensional form, and using the terms (6) and (7)

$$\gamma = \frac{\Gamma}{Vc} = \frac{k}{k_1 V^2 \rho c}\, p_p(r_0)[1 - k_2] = \frac{A(D)[1 - k_2]}{k_1 c} \qquad (8)$$

It should be noted that the term $p_p(r_0)$ expresses the total pressure of the free stream. When measurements are taken in a wind tunnel with the test section open, it expresses the dynamic pressure. The function $A(D)$ represents the combined effect of fluid viscosity and distance upon the rate of dissipation of the vortex energy behind the wing.

Calibrating the Measurement Device

The dissipation of energy caused by the fluid viscosity can be expressed mathematically by damping the rotational motion as a function of time. As given in reference 3, that is

$$\omega(t) = \omega(0)[1 - \exp(-r_0^2/4\nu t)] \qquad (9)$$

For this particular purpose, time (t) should be taken as an approximate indication of the distance between the point of measurement and the trailing edge of the wing. Hence,

$$\omega(D) = \omega(0)[1 - \exp(-Vr_0^2/4\nu D)]$$

As the term Vr_0^2 means the volume of fluid inside the vortex tube, it may be considered to be a constant. Taking into consideration the above, as well as (8), the following equation is obtained

$$\gamma(D) = a_1[1 - k_2]/k_1 c = \gamma(0)[1 - \exp(-a_2/D)]$$

and

$$\gamma(0) = a_1/[1 - \exp(-a_2/D)][(1 - k_2)/k_1 c] \qquad (10)$$

Comparing the terms (8) and (10), it will be found that

$$A(D) = a_1/[1 - \exp(-a_2/D)] \qquad (11)$$

The above calibration constants, a_1 and a_2, can be obtained by comparing the values of the vortex intensity measured by the suggested instrument, and the vortex intensity computed on the basis of the lift of the wing.

References

[1] Popov, S. G., *Some Problems and Methods of the Experimental Aerodynamics*, Moscow, 1952.

[2] Hopkins, E. J., and Soresen, N. E., *A Device for Vortex-Core Measurements*, Journal of the Aeronautical Sciences, Vol. 23, No. 4, pp. 396–398, April, 1956.

[3] Kochin, J. R., Kybel, J. A., and Roze, N. V., *Theoretical Hydrodynamics*, Moscow, 1948.

[4] Spreiter, J. R., and Sachs, A. H., *The Rolling Up of the Trailing Vortex Sheet and Its Effects on the Downwash Behind Wings*, Journal of the Aeronautical Science, Vol. 18, No. 1, pp. 21–32, 72, January, 1951.

Comment on "Flow About an Unsteadily Rotating Disc"

Pau-Chang Lu
Graduate Assistant, Department of Mechanical Engineering, Case Institute of Technology, Cleveland, Ohio

June 15, 1960

A RECENT ARTICLE by Sparrow and Gregg[1] solves the unsteady flow about a rotating disc with varying angular speed by computing the deviations from the quasi-steady state. It would be of interest to compare their results with some cases where exact solutions are possible. One such case has been found and is described in the following.

If ω of the disc is described as

$$\omega = a_1(t + a_2)^{-1} \qquad (1)$$

where $a_2 > 0$, we can write

$$\eta = z(1/a_2\nu)^{1/2} \qquad (2a)$$

$$\tau = t/a_2 \qquad (2b)$$

$$V_r = rF(\eta, \tau)/a_2 \qquad (2c)$$

$$V_\varphi = rG(\eta, \tau)/a_2 \qquad (2d)$$

$$V_z = (\nu/a_2)^{1/2} H(\eta, \tau) \qquad (2e)$$

$$p = \mu P(\eta, \tau)/a_2 \qquad (2f)$$

and the system becomes, for sustained motion,

$$2H_{\eta\eta\eta} - 2H_{z\tau} - 2HH_{\eta\eta} + H_\eta^2 - 4G^2 = 0 \qquad (3a)$$

$$G_\tau - H_\tau G + HG_\eta - G_{\eta\eta} = 0 \qquad (3b)$$

$$\eta = \infty: \quad H_\eta = G = 0 \qquad (3c)$$

$$\eta = 0: \quad H = H_\eta = 0, \quad G = a_1(\tau + 1)^{-1} \qquad (3d)$$

$$P_\eta = H_{\eta\eta} - H_\tau - HH_\eta \qquad (3e)$$

$$F = -H_\eta/2 \qquad (3f)$$

where the subscripts indicate differentiations.

Now introduce the "similarity" parameter

$$\xi = \eta(\tau + 1)^{-1/2} \qquad (4a)$$

and write

$$H = (\tau + 1)^{-1/2} h(\xi) \qquad (4b)$$

$$G = a_1(\tau + 1)^{-1} g(\xi) \qquad (4c)$$

The system is then further reduced to

$$2h''' + \xi h'' + 2h' - 2hh'' + h'^2 - 4a_1^2 g^2 = 0 \qquad (5a)$$

$$2g'' + \xi g' + 2h'g - 2g'h + 2g = 0 \qquad (5b)$$

$$h(0) = h'(0) = h'(\infty) = 0 \qquad (5c)$$

$$g(0) = 1 \text{ and } g(\infty) = 0 \qquad (5d)$$

which can be solved numerically.

Reference

[1] Sparrow, E. M., and Gregg, J. L., *Flow About an Unsteadily Rotating Disc*, Journal of the Aero/Space Sciences, Vol. 27, No. 4, pp. 252–256, April, 1960.

Calculation of Flow-Variable Gradients Behind Curved Shock Waves

Nathan Gerber and Joan M. Bartos
Ballistic Research Laboratories, Aberdeen Proving Ground, Md.

June 16, 1960

KNOWLEDGE OF THE GRADIENTS and contour slopes of flow variables behind curved shock waves is useful in the investigation of a number of problems. (The flows are assumed to be steady, nonviscous, and isentropic along streamlines.) The determination of these quantities has been treated in pre-

vious papers —e.g., references 1, 2, and 3. Some tables for determining streamline curvature and pressure gradient along the streamline are available for two-dimensional flow[1, 2]; aside from these, no extensive calculations of shock-gradient functions have, to the authors' knowledge, been hitherto published.

Computation of the following quantities is considered in reference 4: (1) streamline curvature, (2) velocity gradient along streamline, (3) angle between streamline and density contour, and (4) angle between streamline and Mach number contour. These are found to have the following simplified forms (in the notation of Fig. 1):

$$\partial\theta/\partial s = F_1K_s + \epsilon F_2/r, \quad (1/q_1)(\partial q/\partial s) = F_3K_s + \epsilon F_4/r$$

$$\tan\zeta = \frac{F_4K_s + \epsilon F_4/r}{F_5K_s + \epsilon F_6/r}, \quad \tan\xi = \frac{F_7K_s + \epsilon F_4/r}{F_7K_s + \epsilon F_6/r}$$

where $\epsilon = 0$ for two dimensional, and $\epsilon = 1$ for axisymmetric flow, K_s is the shock-wave curvature, M_1 is the free-stream Mach number, and γ is the ratio of specific heats; F_1, F_2, . . . , F_7 are functions of M_1, β, and γ. It is seen that for axisymmetric flow the usefulness of the gradient functions is restricted because of the presence of the $1/r$ term; one can no longer, as in two-dimensional flow, obtain certain quantities (e.g., slope of sonic line) without having to specify the values of r and K_s.

The simple form of the above expressions suggests the practicability of a compilation of the coefficients of K_s and $1/r$. To this end, reference 4 provides a comprehensive series of tables of the functions F_1, F_2, . . . , F_7, θ, and M versus β for $\gamma = 1.4$, with the parameter M_1 ranging from 1.1 to 10.0. The listed values of M_1 and β were chosen so as to permit the determination of the functions to a reasonable degree of accuracy by means of graphical interpolation. It should be noted that these tables are applicable to both weak and strong shock waves in two-dimensional and axisymmetric flows.

Fig. 2 shows an example of results obtainable from these calculations. The right-hand curve shows the variation in slope of the constant-density lines along the shock wave of a supersonic sphere in nitrogen (shown at left) determined from shock-wave coordinate measurements and the appropriate shock-gradient functions. This information is useful in evaluating the flow fields about supersonic missiles from interferometer measurements.[5]

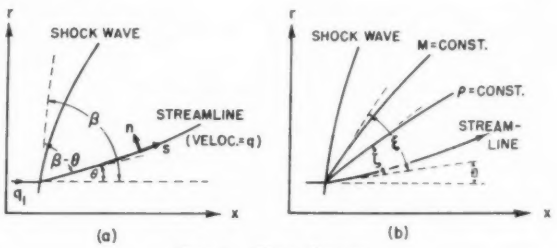

FIG. 1. Flow diagram.

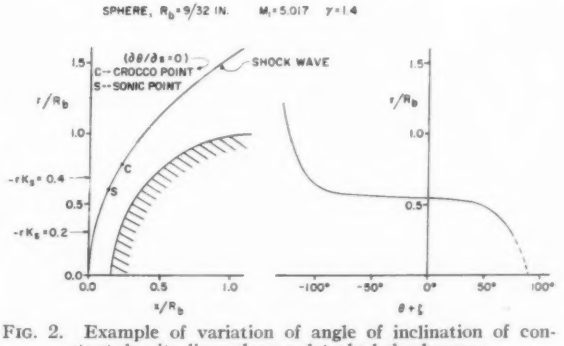

FIG. 2. Example of variation of angle of inclination of constant-density lines along a detached shock wave.

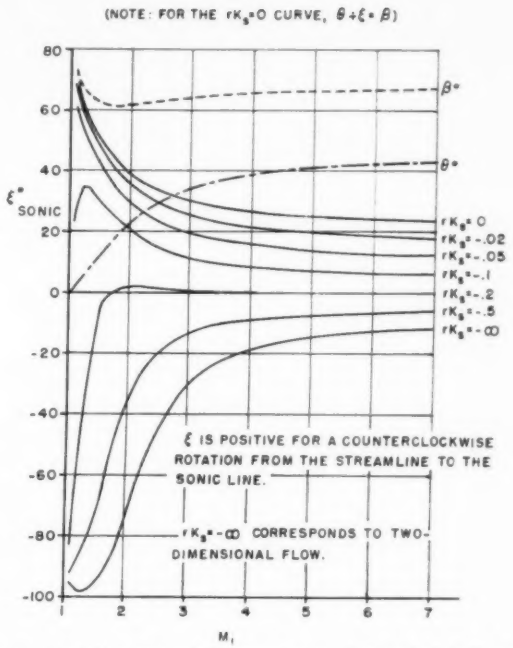

FIG. 3. Variation of angle between streamline and sonic line at shock wave.

Fig. 3 shows plots of the variation of ξ_{sonic}, the angle between the streamline and Mach number contour at the sonic point. For two-dimensional flow, the sonic line has a smaller slope than the streamline; for axisymmetric flow, the figure indicates the possibility of the sonic line having a slope greater than that of the streamline.

Additional applications for these tables can be found. For example, reference 4 contains a graph showing the geometrical conditions which must hold at the "Crocco point," the point where the streamline curvature is zero.

The functions F_1, F_2, . . . , F_7, θ, and M are programed for computation by the EDVAC in the Ballistic Research Laboratories, and they can be obtained quickly for any particular case of supersonic flow by specifying M_1 and γ in the computing-machine input.

REFERENCES

[1] Thomas, T. Y., *Calculation of the Curvature of Attached Shock Waves*, J. Math. & Phys., Vol. 27, p. 279, 1948.

[2] Eggers, A. J., Syvertson, C. A., and Kraus, S., *A Study of Inviscid Flow About Airfoils at High Supersonic Speeds*, NACA Rept. 1123, 1953.

[3] Wood, G. P., and Gooderum, P. B., *Method of Determining Initial Tangents of Contours of Flow Variables Behind a Curved, Axially Symmetric Shock Wave*, NACA TN 2411, July, 1951.

[4] Gerber, N., and Bartos, J. M., *Tables for Determination of Flow Variable Gradients Behind Curved Shock Waves*, Aberdeen Proving Ground, BRL R-1086, January, 1960.

[5] Sedney, R., and Kahl, G. H., *Interferometric Study of the Blunt Body Problem*, Aberdeen Proving Ground, BRL R-1100, April, 1960; also, to appear in Aeronautical Sciences and Space Flight series, Pergamon Press (given at 4th Symposium on Ballistic Missile and Space Technology, Los Angeles, August, 1959).

A Further Discussion of the Limiting Circulatory Lift of a Finite-Span Wing

Franklyn J. Davenport
Boeing Airplane Co., Transport Division, Renton, Wash.

June 20, 1960

THE JET FLAP'S ability to generate extremely large circulation lift coefficients has led to the exploration of limitations to

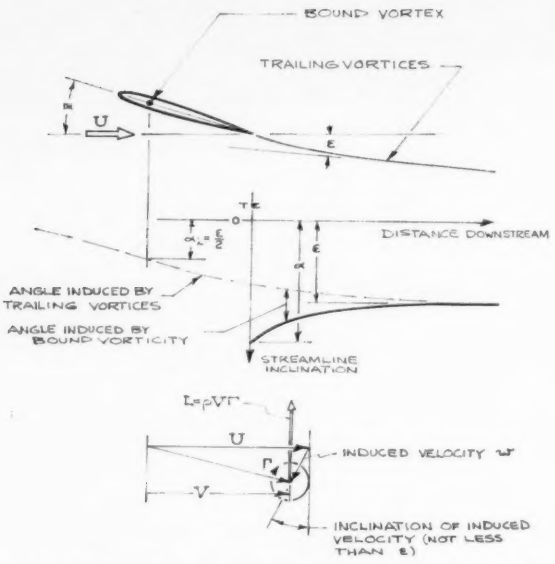

FIG. 1. Geometry of trailing vortex system and induced velocity.

circulation lift inherent in the nature of the finite-span vortex system. The key step in analyzing this problem is to discard the classical assumption that the vortex sheet may be considered to lie in the plane containing the lifting line and the free-stream velocity vector. It then becomes necessary to account for the reduction in velocity at the lifting line caused by the tilt of the induced velocity.

The most rigorous approach is to consider the flow in a Trefftz plane far downstream of the lifting line, through which the trailing-vortex system passes. If it is assumed that the lifting line is elliptically loaded and that the shed vortices remain in a sheet, it can be shown that

$$C_L = (\pi A/2) \sin \epsilon[1 - (\sin^2 \epsilon)/2] \tag{1}$$

where ϵ is the angle between the vortex sheet and the free-stream velocity at the Trefftz plane, and is equal to $\sin^{-1}(\Gamma_0/bU)$, where Γ_0 is the mid-span strength of the lifting vorticity. The limiting C_L is then

$$C_{L_{\text{lim}}} = (\pi A/3)\sqrt{2/3} = 0.855\,A \tag{2}$$

Helmbold[1] goes on to consider the more realistic case where the vortex sheet has rolled up into a pair of vortex cores, and shows that if the momentum and kinetic energy per unit length of the vortex system are conserved in the rolling-up process

$$C_L = (\pi^3 A/4) \sin \delta[1 - (\pi^2/4) \sin^2 \delta] \tag{3}$$

where δ is the angle of the axes of the vortex cores with respect to the free stream, and is equal to $\sin^{-1}(2\Gamma_0/\pi^2 bU)$.
This gives

$$C_{L_{\text{lim}}} = \pi^3 A/(3\sqrt{3}) = 1.90A \tag{4}$$

McCormick[2] approaches the problem by directly considering the induced flow at the lifting line. Making the assumption that the inclination of the vortex system (and, therefore, of the induced velocity) is equal to the downwash angle at the lifting line, it follows that

$$C_L = (\pi A/2) \sin \epsilon[1 - (\sin^2 \epsilon)/4] \tag{5}$$

which gives

$$C_{L_{\text{lim}}} = 2\pi A/(3\sqrt{3}) = 1.21A \tag{6}$$

Hancock[3] notes the discrepancy between the results of the Trefftz-plane approach and McCormick's method, and advances several possible explanations of the fact that circulation C_L's considerably greater than the limit according to Eq. (2), have been achieved in jet-flap tests,[4,5] but he does not challenge McCormick's analysis directly.

The results of an analysis based on the flow near the lifting line are quite sensitive to the assumptions concerning the inclination of the vortex sheet in the vicinity of the wing. In particular, the inclination chosen by McCormick is implausible because it neglects the effect of the bound vorticity on the streamline pattern just behind the wing. Fig. 1 indicates that the tilt of the induced-velocity vector should be at least as great as ϵ, the downwash angle far downstream, (or twice α_i, the induced angle at the wing).

Consider an elliptically-loaded lifting line having a mid-span circulation Γ_0. The magnitude of the downwash at the lifting line is

$$w = \Gamma_0/2b = (U \sin \epsilon)/2 \tag{7}$$

and its inclination is (at least)

$$\epsilon = 2\alpha_i = \sin^{-1}(\Gamma_0/bU) \tag{8}$$

Then the horizontal velocity at the lifting line is

$$V = U[1 - (\sin^2 \epsilon)/2] \tag{9}$$

The lift on the wing is

$$L = \rho V \Gamma_0(\pi b/4) \tag{10}$$

so

$$C_L = (\pi A/2) \sin \epsilon\,[1 - (\sin^2 \epsilon)/2] \tag{11}$$

This is identical to the result obtained by the Trefftz-plane approach (Eq. 1).

Next, consider the case when the vortex sheet has rolled up into a pair of vortex cores. For elliptical loading, the distance between the centers of these cores will be $\pi b/4$, and the downwash angle induced by each vortex at the other is

$$\delta = \sin^{-1}(2\Gamma_0/\pi^2 bU) \tag{12}$$

so

$$\sin \epsilon = (\pi^2/2) \sin \delta \tag{13}$$

If it is assumed that the average downwash velocity at the lifting line is still given by Eq. (7), but that the angle of inclination is now δ instead of ϵ, then

$$V = U[1 - (\pi^2/4) \sin^2 \delta] \tag{14}$$

which leads to

$$C_L = (\pi^3 A/4) \sin \delta[1 - (\pi^2/4) \sin^2 \delta] \tag{15}$$

This is identical to Helmbold's result (Eq. 3).

The highest value of circulation C_L observed by Lockwood, Turner, and Riebe[5] in their jet-flap investigations is roughly two times the aspect ratio of the wing tested, which tends to confirm Eqs. (3) and (4). It is, therefore, suggested that no discrepancy between the analysis based on conditions at the airfoil and that based on the flow far downstream should appear if the inclination of the induced velocity is properly specified.

REFERENCES

[1] Helmbold, H. B., *Limitations of Circulation Lift*, Journal of the Aeronautical Sciences, Vol. 24, No. 5, pp. 237–238, March, 1957.

[2] McCormick, B. W., *The Limiting Circulatory Lift of a Wing of Finite Aspect Ratio*, Journal of the Aero/Space Sciences, Vol. 26, No. 4, pp. 247–248, April, 1959.

[3] Hancock, G. J., *Comments on "Limiting Circulatory Lift of a Wing of Finite Aspect Ratio,"* Journal of the Aero/Space Sciences, Vol. 27, No. 1, pp. 65–66, January, 1960.

[4] Lowry, J. G., and Vogler, R. D., *Wind Tunnel Investigations to Determine the Effect of Aspect Ratio and End Plates on the Rectangular Wing with Jet Flaps Deflected 85°*, NACA TN 3863, December, 1956.

[5] Lockwood, V. E., Turner, T. R., and Riebe, J. M., *Wind Tunnel Investigation of Jet-Augmented Flaps on a Rectangular Wing to High Momentum Coefficients*, NACA TN 3865, December, 1956.

Further Studies on the Local Elastic Deformations of Honeycomb Faceplate Subjected to Uniaxial Compression

R. C. Weikel and A. S. Kobayashi
Research Specialist, Boeing Airplane Company, and Assistant Professor of Mechanical Engineering, University of Washington, respectively, Seattle, Wash.
June 27, 1960

Introduction

In constructing high-temperature honeycomb panels, the brazing process frequently leaves the honeycomb faceplate with permanent local deformations known as "intracell deformation." Such initial faceplate deformations in each honeycomb cell will affect the resultant local deformations of the honeycomb panel under compressive load, and reduce its load carrying capacity appreciably.

The objective of this note is to investigate these resultant deformations of a honeycomb panel under compressive load with such initial intracell deformations.

Method of Approach

The assumption made in this analysis are identical to those made in reference 1. In addition, the faceplate and honeycomb core are assumed to behave elastically at all times, thus eliminating the need for an elastic-plastic analysis. Marguerre's fundamental equations for the large deflection of thin plates with small initial curvature are used here with a slight modification in the lateral force equilibrium equation to account for the elastic spring-back forces due to wrinkling deformation of the honeycomb faceplate. These equations are (see reference 2)

$$\left.\begin{aligned}\nabla^4 F &= E[w_{,xy}{}^2 - w_{,xx}w_{,yy} + 2w_{,xy}{}^0w_{,xy} - w_{,xx}{}^0w_{,yy} - w_{,yy}{}^0w_{,xx}]\\ \nabla^4 w &= (h/D)[-(kw^w/h) + F_{,yy}(w + w^0)_{,xx} + F_{,xx}(w + w^0)_{,yy} - 2F_{,xy}(w + w^0)_{,xy}]\end{aligned}\right\} \quad (1)$$

where F is a stress function defined in terms of the plane-stress components as

$$\sigma_x = F_{,yy}, \qquad \sigma_y = F_{,xx}, \qquad \tau_{xy} = -F_{,xy} \quad (2)$$

and h, E, D are thickness, modulus of elasticity, flexural rigidity of the faceplate, respectively.

w, w^0, w^i, w^w are resultant lateral, initial intracell, intracell and wrinkling deformations of the faceplate, respectively.

The force boundary conditions to be satisfied for the uniaxial compressive loads of N per unit length, as shown in Fig. 1, are

$$\left.\begin{aligned}\frac{N}{\sqrt{2}} &= -\frac{h}{b}\int_{-b/2}^{b/2} F_{,yy}\Big]_{x=\pm b/2}\,dy\\ \frac{N}{\sqrt{2}} &= -\frac{h}{b}\int_{-b/2}^{b/2} F_{,xx}\Big]_{y=\pm b/2}\,dx\\ \frac{N}{\sqrt{2}} = \frac{h}{b}\int_{-b/2}^{b/2} F_{,xy}\Big]_{x=\pm b/2}\,dy &= \frac{h}{b}\int_{-b/2}^{b/2} F_{,xy}\Big]_{y\pm b/2}\,dx\end{aligned}\right\} \quad (3)$$

The displacement boundary conditions are satisfied by representing this lateral deformation by a double Fourier series in which all terms of the series satisfy the prescribed boundary conditions. As an approximation, only the first term in these Fourier's series are considered, and the following lateral deformations are obtained.

$$\left.\begin{aligned}w^0 &= A^0\cos(\pi x/b)\cos(\pi y/b),\quad w^w = A^w\cos[\pi(x-y)/2b]\\ w^i &= A^i\cos(\pi x/b)\cos(\pi y/b),\quad w = w^i + w^0\end{aligned}\right\} \quad (4)$$

where A^0 is the known amplitude of the initial intracell deformation, while A^i and A^w are the undetermined amplitudes of intracell and wrinkling deformations.

Substituting Eq. (4) into the first equation of Eq. (1) yields biharmonic equations in terms of A^0, A^i, and A^w. Representing a particular solution for the biharmonic equations as F_1, and a general solution of $\nabla^4 F = 0$ as F_2, then the general solution of $F = F_1 + F_2$ is obtained. This F must satisfy the force boundary conditions or Eq. (3), which allows the determination of the arbitrary constants in F_2 or F. Again taking only the first-order terms of the F_2 which is a product function of hyperbolic and trigonometric functions, the resultant F becomes

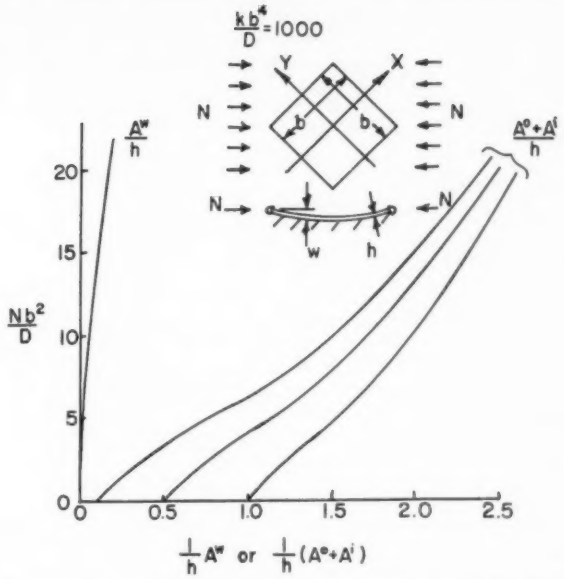

FIG. 1. Load coefficient versus amplitudes of deformation $kb^4/D = 1{,}000$.

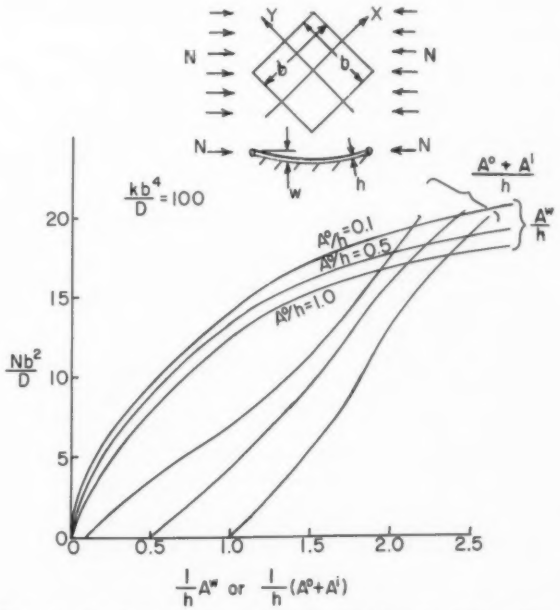

FIG. 2. Load coefficient versus amplitudes of deformation $kb^2/D = 100$.

$$F = -\frac{E}{25}\left\{A^w(A^i + A^0)\left[\cos\frac{\pi(x+3y)}{2b} + \cos\frac{\pi(3x+y)}{2b}\right] + A^i(A^i + A^0)\left[\cos\frac{2\pi x}{b} + \cos\frac{2\pi y}{b}\right]\right\} + \frac{Nb^2}{8\sqrt{2}\pi h \sinh\pi}\left[\cosh\frac{2\pi x}{b}\cos\frac{2\pi y}{b} + \cos\frac{2\pi x}{b}\cosh\frac{2\pi y}{b} + \sinh\frac{2\pi x}{b}\sin\frac{2\pi y}{b} + \sin\frac{2\pi x}{b}\sinh\frac{2\pi y}{b}\right] \quad (5)$$

Finally, for the determination of A^i and A^w, Galerkin's method is applied to the second equation of Eq. (1), after substituting Eqs. (4) and (5) into it. This requires that

$$\int_{-b/2}^{b/2}\int_{-b/2}^{b/2}\left\{\nabla^4 w - \frac{h}{D}\left[-\frac{kw^w}{h} + F_{,yy}(w+w^0)_{,xx} - F_{,xx}(w+w^0)_{,yy} - 2F_{,xy}(w+w^0)_{,xy}\right]\right\}\cos\frac{\pi x}{b}\cos\frac{\pi y}{b}\,dx\,dy = 0$$

$$\int_{-b/2}^{b/2}\int_{-b/2}^{b/2}\left\{\nabla^4 w - \frac{h}{D}\left[-\frac{kw^w}{h} + F_{,yy}(w+w^0)_{,xx} - F_{,xx}(w+w^0)_{,yy} - 2F_{,xy}(w+w^0)_{,xy}\right]\right\}\cos\frac{\pi(x-y)}{2b}\,dx\,dy = 0 \quad (6)$$

Eq. (6) then becomes two simultaneous equations involving the third powers of A^i and A^w and also the load coefficient, Nb^2/D, and the apparent coefficient, kb^4/D. Thus, for known kb^4/D and A^0, A^i and A^w can be computed from Eq. (6) for any given load N. The actual computation of A^i and A^w is lengthy and involves the use of a digital computer, and a reasonable judgment in detecting the correct solution among the multiple roots of A^i and A^w.

Results

The solutions of A^i and A^w of Eq. (6) are shown in graphical form in Figs. 1 and 2. It is noted that an increase in the initial deformation of $0.1h$ to $1.0h$ results in approximately 1/3 reduction in loads. Another interesting result is that for a low-apparent spring constant of $kb^4/D = 100$, the wrinkling deformation is lower than the intracell deformation at low loads. At high loads, however, the wrinkling deformation becomes larger than the intracell deformation, and thus the honeycomb panel will ultimately fail due to wrinkling deformation.

References

[1] Weikel, R. C., and Kobayashi, A. S., *On the Local Elastic Stability of Honeycomb Face Plate Subjected to Uniaxial Compression*, Journal of the Aero/Space Sciences, Vol. 26, No. 10, pp. 672–674, October, 1959.

[2] Yamaki, N., *Postbuckling Behavior of Rectangular Plates with Small Initial Curvature Loaded in Edge Compression*, J. Appl. Mech., Vol. 81, pp. 407–414, September, 1959.

Chordwise-Bending Effects on Wing-Vibration Modes

John C. Glasgow and James L. Cronin, Jr.
McDonnell Aircraft Corp., and Associate Professor, St. Louis University, St. Louis, Mo., respectively.

June 21, 1960

Symbol

- α_i = rotation in the vertical plane of the ith idealized wind section
- h_i = vertical motion of the ith idealized mass of the wing
- m_i = mass of the ith idealized wing section
- I_i = moment of inertia of the ith idealized wing section
- q_i = generalized coordinate describing the vertical displacement of point "i" on the structure
- ω = circular frequency of the vibrating system
- k_{ij} = stiffness influence coefficient of the wing expressing the force required at point "i" to produce a unit deflection at point "j"
- c_{ij} = flexibility influence coefficient expressing the deflection of point "j" due to a unit load applied at point "i"
- [ ] = rectangular matrix
- { } = column matrix
- [˜] = transpose of a rectangular matrix
- [\] = square diagonal matrix

Introduction

THE LOW-ASPECT-RATIO wing used on present-day aircraft has done much to alter the approach to the description of wing vibrations. The chordwise-bending parameter which has often been neglected in wing-vibration solutions can now become significant. Methods have been developed by Levy[1] and Turner[2] for the description of the stiffness properties of this type of structure by influence coefficients which include rib stiffness as a parameter. A method is proposed herein for the solution of this type of vibration problem including the effects of rotary inertia.

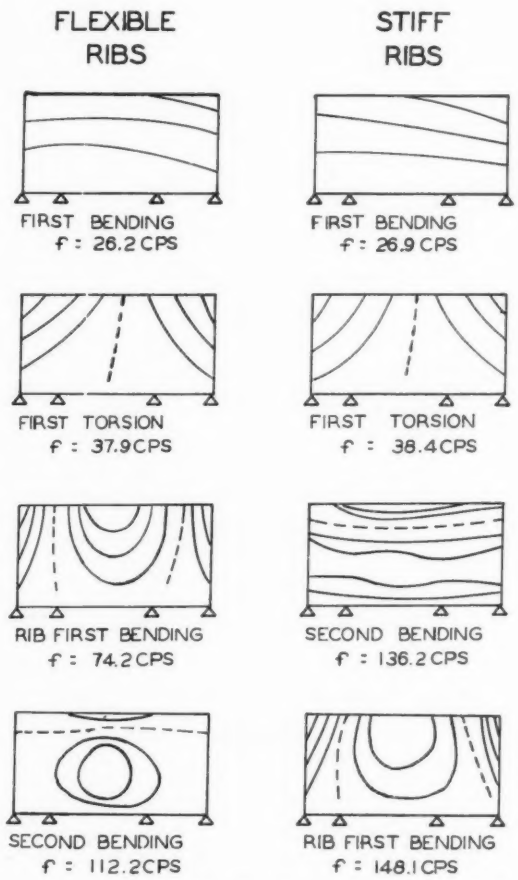

FIG. 1. Comparison of wing-vibration modes with two variations in rib stiffness.

Analysis

The wing or surface is idealized as being composed of rigid sections corresponding to the ribs or spars in the wing planform and hinged at the intersection points (rib-spar intersections). The weight of the surface being analyzed is considered to be distributed along these rib or spar sections, thus assigning a mass and moment of inertia to each idealized section of the wing. The hinged intersection points are considered to be restrained to act in accordance with the flexibility influence coefficients determined for the structure at these same intersection points.

Choosing a set of generalized coordinates to describe the vertical displacements of the intersection points will allow the description of the vertical translations and rotations of the idealized wing sections to be made in terms of these coordinates. Lagrange's equation for the vibrating system is now written in terms of the idealized section mass and moment of inertia, and the stiffness influence coefficients (which are the inverse of the flexibility influence coefficients) in the following matrix form:

$$\left[\left[\frac{\partial h}{\partial q}\right][\backslash m_i \backslash]\left[\frac{\partial h}{\partial q}\right]+\left[\frac{\partial \alpha}{\partial q}\right][\backslash I_i \backslash]\left[\frac{\partial \alpha}{\partial q}\right]\right]\left\{\ddot{q}\right\}+\left[k_{ij}\right]\left\{q\right\}=0$$

where

$$\left\{h_i\right\}=\left[\frac{\partial h}{\partial q}\right]\left\{q\right\}$$

$$\left\{\alpha_i\right\}=\left[\frac{\partial \alpha}{\partial q}\right]\left\{q\right\}$$

and h_i and α_i are the vertical translation and rotation, respectively, of the ith idealized mass and moment of inertia particle of the surface.

Employing the harmonic substitution and multiplying through by the flexibility-influence-coefficient matrix yields

$$\left[c_{ij}\right]\left[\left[\frac{\partial h}{\partial q}\right][\backslash m_i \backslash]\left[\frac{\partial h}{\partial q}\right]+\left[\frac{\partial \alpha}{\partial q}\right][\backslash I_i \backslash]\left[\frac{\partial \alpha}{\partial q}\right]\right]\left\{q\right\}=\frac{1}{\omega^2}\left\{q\right\}$$

which may be iterated to obtain the final result.

Conclusion

The above method was employed on a simplified surface of aspect ratio one. The rib stiffness was varied by a factor of 10 with the spars and skin held constant, and the resulting mode shapes and frequencies were compared. The third and fourth modes of vibration were found to vary considerably in shape and frequency, as shown in Fig. 1, indicating the effect of rib stiffness on the vibration characteristics. Solutions were obtained neglecting the effect of rotary inertia, and compared with those, including these effects. The frequency was found to increase by about 9 per cent in the third and fourth modes of vibration, when rotary-inertia effects were neglected.

References

[1] Levy, Samuel, *Structural Analysis and Influence Coefficients for Delta Wings*, Journal of the Aeronautical Sciences, Vol. 20, No. 7, pp. 449–454, July, 1953.

[2] Turner, M. J., Clough, R. W., Martin, H. C., and Topp, L. J., *Stiffness and Deflection Analysis of Complex Structures*, Journal of the Aeronautical Sciences, Vol. 23, No. 9, pp. 805–823, September, 1956.

Note on Slow Viscous Flow Through the Space Between Two Coaxial Circular Cones With the Same Vertex

T. K. Chaudhury*
Vidyasagar College, Calcutta, India
June 14, 1960

Slow viscous flow through cones has been considered by several authors (cf. Bond[1]), but it appears that the flow through a channel bounded by two coaxial cones has not yet been considered. It is the object of this paper to consider such flow.

Let the boundaries of the channel be $\theta = \alpha$ and $\theta = \beta$ $(\beta > \alpha)$ where (r, θ, φ) are polar coordinates. Firstly, it is assumed that the streamlines are straight lines diverging from the origin (i.e., the common vertex of the cones); so that

$$u = f(\theta)/r^2, \quad v = 0, \quad w = 0$$

(u, v, w) being the velocity components. Secondly, the motion is assumed to be slow, such that the inertia terms may be neglected.

Then the polar equations of motion reduce to

$$0 = -\frac{1}{\rho}\frac{\partial p}{\partial r}+\nu\left[\frac{\partial^2 u}{\partial r^2}+\frac{2}{r}\frac{\partial u}{\partial r}+\frac{\cot\theta}{r^2}\frac{\partial u}{\partial \theta}+\frac{1}{r^2}\frac{\partial^2 u}{\partial \theta^2}-\frac{2u}{r^2}\right] \quad (1)$$

$$0 = -\frac{1}{\rho}\frac{\partial p}{r\partial \theta}+\frac{2\nu}{r^2}\frac{\partial u}{\partial \theta} \quad (2)$$

$$0 = -\frac{1}{\rho}\frac{\partial p}{\partial \varphi} \quad (3)$$

Hence, substituting $u = f/r^2$ and eliminating p, we get from Eqs. (1) and (2)

$$f''' + f'' \cot\theta - f' \operatorname{cosec}^2\theta + 6f' = 0 \quad (4)$$

A first integral of this is

$$f'' + f' \cot\theta + 6f + c_1 = 0 \quad (5)$$

The general solution of Eq. (5) is

$$f(\theta) = AP_2(\cos\theta) + BQ_2(\cos\theta) - C \quad (6)$$

where $6C = C_1$ and $P_2(\cos\theta)$, $Q_2(\cos\theta)$ are Legendre functions of second degree and of first and second kinds, respectively.

Boundary conditions are $u = 0$, when $\theta = \alpha$ and $\theta = \beta$, i.e., $f(\cos\alpha) = 0$ and $f(\cos\beta) = 0$.
Thus, from Eq. (6),

$$AP_2(\cos\alpha) + BQ_2(\cos\alpha) - C = 0$$

and

$$AP_2(\cos\beta) + BQ_2(\cos\beta) - C = 0$$

which give $A = K_1C$, $B = K_2C$, where

$$\left.\begin{aligned} K_1 &= \frac{Q_2(\cos\beta) - Q_2(\cos\alpha)}{P_2(\cos\alpha)\,Q_2(\cos\beta) - Q_2(\cos\alpha)\,P_2(\cos\beta)} \\ K_2 &= \frac{P_2(\cos\alpha) - P_2(\cos\beta)}{P_2(\cos\alpha)\,Q_2(\cos\beta) - Q_2(\cos\alpha)\,P_2(\cos\beta)} \end{aligned}\right\} \quad (7)$$

Therefore,

$$f(\theta) = C[K_1P_2(\cos\theta) + K_2Q_2(\cos\theta) - 1] \quad (8)$$

Now if the volume of fluid passing per second radially outwards through the channel be denoted by Q

$$\begin{aligned} Q &= \int_\alpha^\beta 2\pi r \sin\theta\, r d\theta\, u \\ &= 2\pi C \int_\alpha^\beta \sin\theta [K_1P_2(\cos\theta) + K_2Q_2(\cos\theta) - 1]\, d\theta \\ &= 2\pi CK \end{aligned}$$

where

$$K = [(K_1/2)\cos\theta \sin^2\theta + (K_2/2) \times \{\cos\theta \sin^2\theta \log\cot(\theta/2) + \cos^2\theta\} + \cos\theta]_{\theta=\alpha}^{\theta=\beta} \quad (9)$$

Therefore, $$C = Q/2\pi K$$

Hence,

$$u = \frac{[K_1P_2(\cos\theta) + K_2Q_2(\cos\theta) - 1]}{2\pi K}\frac{Q}{r^2} \quad (10)$$

Now, from Eqs. (1), (5), and (8),

$$\begin{aligned} \partial p/\partial r &= (\mu/r^4)(f'' + f' \cot\theta) \\ &= (-6\mu/r^4)(f + c) \\ &= -(6\mu/r^4)[K_1P_2(\cos\theta) + K_2Q_2(\cos\theta)](Q/2\pi K) \end{aligned}$$

So

$$\frac{\partial p}{\partial r} = -\frac{3[K_1P_2(\cos\theta) + K_2Q_2(\cos\theta)]}{\pi K}\frac{\mu Q}{r^4} \quad (11)$$

* The author wishes to thank Professor B. B. Sen of Jadaupur University for his kind help in this work.

TABLE 1

	$\beta = 70°$				
	$\alpha = 5°$	$\alpha = 10°$	$\alpha = 20°$	$\alpha = 30°$	$\alpha = 40°$
K_1	0.6828	0.1397	−0.3123	−0.5755	−0.7864
K_2	−2.1693	−1.8562	−1.5958	−1.4441	−1.3226
K	0.3562	0.1154	0.0123	−0.0359	−0.0467

TABLE 2

	$\beta = 60°$					
	$\alpha = 3°$	$\alpha = 5°$	$\alpha = 10°$	$\alpha = 20°$	$\alpha = 30°$	$\alpha = 40°$
K_1	1.1179	0.7977	0.3897	−0.0112	−0.2673	−0.4828
K_2	−1.4616	−1.4103	−1.3449	−1.2805	−1.2395	−1.2052
K	0.1932	0.1179	0.0274	−0.0403	−0.0560	−0.0474

TABLE 3

	$\beta = 50°$			
	$\alpha = 5°$	$\alpha = 10°$	$\alpha = 20°$	$\alpha = 30°$
K_1	0.8645	0.5535	0.2043	−0.0368
K_2	−0.9696	−1.0099	−1.0553	−1.0864
K	0.0314	−0.0120	−0.0440	−0.0540

Tables 1, 2, and 3 show some calculated values of the constants K_1, K_2, K for different values of α and β.

DISCUSSION

The constant K_1 will be equal to zero for channels whose boundaries α and β are suitably chosen. But the constant K_2 will never be zero for any channel.

For the channels considered here, it can be seen by numerical calculations that the expression $K_1P_2(\cos\theta) + K_2Q_2(\cos\theta)$ is always positive and greater than 1. Therefore, $\partial p/\partial r$ will not be zero anywhere in the channels; furthermore, it can be seen that $\partial p/\partial r$ always has the sign opposite to the sign of u.

Again, from calculations, it is seen that in a channel for which the constant K is positive, u has the same sign as Q; but in a channel for which K is negative, u has the sign opposite to the sign of Q.

REFERENCES

[1] Bond, W. N., Philos. Mag., Vol. 50, pp. 1058, 1925.

[2] Harrison, W. J., Proc. Cambridge Philos. Soc., Vol. 19, p. 312, 1916–1919.

✦ ✦ ✦

INTERNATIONAL AEROSPACE ABSTRACTS

New IAS Periodical Beginning January, 1961

This new monthly will combine, in improved format, the abstracts and books sections formerly printed in *Aerospace Engineering*. For uninterrupted abstract service, enter your subscription now.

Turn to Inside Back Cover for Further Details.

Notice to Contributors

To expedite review, an additional copy of both the manuscript and figures should be submitted. The manuscript submitted for publication *must* be a double- or triple-spaced original. There should be wide margins on all sides of the sheets and triple spacing around formulas to allow for the marking of directions to the printer.

Original drawings (jet black India ink on white paper or tracing cloth) should accompany the manuscript. *(Blueprints are not acceptable.)* Photographs *must* be on glossy white paper. The smallest lettering on 8- by 10-in. figures should be no less than 1/4 in. high.

Formulas should be typewritten or carefully written in pen and ink. The difference between capital and lower-case letters and Greek symbols should be clearly distinguished.

Index to Volume 27

Journal of the Aerospace Sciences

Numbers 1–12, January–December, 1960

No. 1, January, pages 1–80
No. 2, February, pages 81–160
No. 3, March, pages 161–240
No. 4, April, pages 241–320
No. 5, May, pages 321–400
No. 6, June, pages 401–480
No. 7, July, pages 481–560
No. 8, August, pages 561–640
No. 9, September, pages 641–720
No. 10, October, pages 721–800
No. 11, November, pages 801–880
No. 12, December, pages 881–976

The material has been indexed in two sections: under a subject heading and by author.

* An asterisk following an item identifies it as having appeared in the Readers' Forum section.

Subject Index

AERODYNAMICS AND FLUID MECHANICS

Dimensionless Parameters for Viscous Similarity, Andrew G. Hammitt* ... 720
An Equivalence Principle for Water-Exit and -Entry Problems, John P. Moran* ... 876
An Exact Calculation of Some Steady, Diabatic, Two-Dimensional Fields of Compressible Flow, Bruce L. Hicks and Donald R. Chenoweth* ... 142
The Flow About a Charged Body Moving in the Lower Ionosphere, Raul R. Hunziker ... 935
Flow About an Unsteadily Rotating Disc, E. M. Sparrow and J. L. Gregg ... 252
Comment, Pau-Chang Lu* ... 958
The Hydraulic Analogy for External Flow, R. A. A. Bryant* 148
Influence Coefficients for Real Gases, Mario William Cardullo* ... 546
On Almost-Free-Molecule Flow Through an Orifice, V. C. Liu and G. R. Inger* ... 875
Note on the Turbulent Shear Stress Near a Wall, H. G. Elrod, Jr. (Vol. 24, p. 468)*
Erratum* ... 145
On an Exact Solution of Laminar Mixing of Two Different Gases, Luigi G. Napolitano* ... 144
Propagation of Weak Disturbances in a Gas Subject to Relaxation Effects, Franklin K. Moore and Walter E. Gibson ... 117
Rarefaction Effects in Low-Speed Turbulence, Harold S. Mickley and Anthony Turano, Jr.* ... 629
Remarks on the Eddy Viscosity in Compressible Mixing Flows, Lu Ting and Paul A. Libby* ... 797
Steady Performance Characteristics of Gas-Lubricated Journal Bearings With Slenderness Ratio $L/D = \pi$, W. A. Gross* ... 869

Bodies

An Approximate Solution of the Direct Supersonic Blunt-Body Problem for Arbitrary Axisymmetric Shapes, Stephen C. Traugott ... 361
Approximate Solutions for Supersonic Flow Over Wedges and Cones, A. G. Hammitt and K. R. A. Murthy* ... 71
Arc-Tangent Fits for Pressure and Pressure-Drag Coefficients of Axisymmetric Blunt Bodies at All Speeds, Ta Li* 309
A Comparison of Blunt-Body Flow-Field Results, Herbert W. Ridyard* ... 789
Computer Solution Techniques for Two-Dimensional Supersonic Flow Problems, William P. Harrison, Jr.* ... 315
The Effect of Thermal Radiation on the Inviscid Hypersonic Flow Over a Blunt Body, G. A. Bird* ... 713
Empirical Equation for the Wake-Spreading Limits Behind Three-Dimensional Bodies, W. J. Billerbeck, Jr.* ... 640
An Extension of the Linearized Characteristics Method for Calculating the Supersonic Flow Around Elliptic Cones, Anthony Martellucci ... 667
Fluctuating Lift and Drag Acting on a Cylinder in a Flow at Supercritical Reynolds Numbers, Y. C. Fung ... 801
Heat Transfer, Recovery Factor, and Pressure Distributions Around a Circular Cylinder Normal to a Supersonic Rarefied-Air Stream, O. K. Tewfik and W. H. Giedt ... 721
Inviscid Hypersonic Flow Over Unyawed Circular Cones, L. Pottsepp* ... 558
A Multiple Hot-Wire Array for Measurements of Downwash Integrals, Kent Kresa and Erik Mollö-Christensen* 141
On Conical-Flow Upwash, Joseph L. Sims* ... 952
On the Use of the Boundary-Layer Equations in the Hypersonic Viscous-Layer Regime, Robert A. Makofski* ... 468
Real Gas Effects in Flow Over Blunt Bodies at Hypersonic Speeds, H. T. Nagamatsu, R. E. Geiger, and R. E. Sheer, Jr. ... 241
Relation Between Transition Location and Pressure in Separated Shear Flows, J. Leith Potter and Jack D. Whitfield* ... 712
Second-Order Theory for Unsteady Supersonic Flow Past Slender, Pointed Bodies of Revolution, James D. Revell 730
A Simple Numerical Solution of the Supersonic Blunt-Body Problem for Real Gases, G. A. Bird* ... 151
Solution to the Flow About a Two-Dimensional Flat Plate at Infinite Mach Number, Donald L. Chubb* ... 68
Supersonic Flow at the Surface of a Circular Cone at Angle of Attack, Joseph E. Willett ... 907
Theoretical and Experimental Investigation of Second-Order Supersonic Wing-Body Interference, Mårten Landahl, Georg Drougge, and Beverly Beane ... 694
The Use of Rational Approximations in the Calculation of Flows With Detached Shocks, A. H. Van Tuyl* ... 559
Use of Reference Enthalpy in Specifying the Laminar Heat-Transfer Distribution Around Blunt Bodies in Dissociated Air, E. R. G. Eckert and O. E. Tewfik* ... 464
Viscous Aerodynamic Characteristics in Hypersonic Rarefied Gas Flow, Ronald F. Probstein and Nelson H. Kemp ... 174
Addendum and Errata* ... 554

Viscous and Leading-Edge Effects in Hypersonic Flow, Robert J. Whalen* ... 391

Boundary Layer

An Analogy Between Boundary-Layer Pressure Gradient and Chemical Reaction-Rate Effects, George R. Inger* 956
Analysis of Further Data on the Effect of Isolated Roughness on Boundary-Layer Transition in Supersonic Flow, Darwin W. Clutter and A. M. O. Smith* ... 70
An Approximate Investigation of the Effect of Boundary-Layer-Control Pumping on Powerplant Performance, T. F. Kirkwood* ... 799
Boundary-Layer Stabilization by Distributed Damping, Max O. Kramer* ... 69
Boundary-Layer Transition and Heat Transfer in Shock Tubes, R. A. Hartunian, A. L. Russo, and P. V. Marrone 587
Boundary-Layer Transition Measurements at Mach Numbers from 5.4 to 7.4, Fred Landis, Martin R. Fink, and Murray H. Rosenberg* ... 719
Boundary-Layer Transition on Blunt Bodies With Highly Cooled Boundary Layers, Kenneth F. Stetson ... 81
The Effect of Controlled Three-Dimensional Roughness on Boundary-Layer Transition at Supersonic Speeds, E. R. van Driest and W. D. McCauley ... 261
An Experiment on Oscillatory Shock-Wave Boundary-Layer Interaction, Wladyslaw Fiszdon and Erik Mollö-Christensen* ... 71
Experimental Evaluation of Heat Transfer With Transpiration Cooling in a Turbulent Boundary Layer at M = 3.2, E. Roy Bartle and Bernard M. Leadon* ... 78
First-Order Solution to the Compressible Laminar Boundary Layer in Slip Flow, Anthony Casaccio* ... 319
A Method of Calculating Velocity Distribution for Turbulent Boundary Layers in Adverse Pressure Distributions, Earl M. Uram ... 659
A Note on the Recovery and Reynolds-Analogy Factors in Laminar Flat-Plate Flow, D. A. Spence* ... 878
On a Solution to the Unsteady Laminar Boundary Layer, H. A. Hassan* ... 474
On Maximum Pressure Rise With Turbulent Boundary Layer, A. Mager and A. W. Goldstein* ... 234
On the Effects of Flow Obstructions on Free-Convection Boundary-Layer Oscillations, J. P. Holman, K. E. Stout, and E. E. Soehngen* ... 463
On the Response of the Laminar Boundary Layer to Small Fluctuations of the Free-Stream Velocity, Nicholas Rott and Martin L. Rosenzweig ... 741
On Three-Dimensional Boundary Layers Having Similar Solutions, M. G. Hall* ... 80
An Optical Boundary-Layer Probe, John W. Daiber ... 836
A Particular Solution to the Turbulent-Boundary-Layer Equations, George K. Walker* ... 715
Pitot-Probe Measurement of Local Skin-Friction Reduction Due to Transpiration in a Low-Speed, Turbulent Boundary Layer, Bernard M. Leadon and E. Roy Bartle* ... 235
A Rapid Method for Estimating the Shear Stress and the Separation Point in Laminar Incompressible Boundary-Layer Flows, Andreas Acrivos* ... 314
Reynolds-Analogy Parameter for the Laminar Boundary Layer With Blowing, Pr = 3/4, C. R. Faulders* ... 628
Skin-Friction Calculation for Turbulent Boundary Layers in Adverse Pressure Distributions, Earl M. Uram* ... 75
A Sublayer Theory for Fluid Injection Into the Incompressible Turbulent Boundary Layer, Donald L. Turcotte ... 675
Sweepback Effects in Turbulent Boundary-Layer Shock-Wave Interaction, R. J. Stalker ... 348
A Theoretical Investigation of the Interaction Between Shock Waves and Boundary Layers, M. Honda (Vol. 25, pp. 667–678)
Erratum* ... 76
Transition in a Separated Laminar Boundary Layer, B. H. Lochtenberg ... 92
Use of the Roughness Criterion to Refute Roughness as the Cause of Reported Transition Reversal, Jerold M. Bidwell* ... 622

Internal Flow

Derivation of an Analytical Expression for Supersonic Spillage of Single-Cone Inlets, Craig W. Hartsell* ... 788
Note on Slow Viscous Flow Through the Space Between Two Coaxial Circular Cones With the Same Vertex, T. K. Chaudhury* ... 963
The Piston-Driven Shock, Roy Gundersen* ... 467
Supersonic Inlet Dynamics, H. R. Fraiser ... 429

Nozzles, Orifices, and Jets

An Approximation for Subsonic Flow Through an Orifice, P. G. Morgan* ... 160
A Further Discussion of the Limiting Circulatory Lift of a Finite-Span Wing, Franklyn J. Davenport* ... 959
On Almost-Free-Molecule Flow Through an Orifice, V. C. Liu and G. R. Inger* ... 875
On the Thrust Hypothesis for the Jet Flap Including Jet-Mixing Effects, K. T. Yen ... 607
Remarks on a Study of Short, Flexible Nozzles, Edwin Pounder and John Copper* ... 73

Shock Waves

Calculation of Flow-Variable Gradients Behind Curved Shock Waves, Nathan Gerber and Joan M. Bartos* ... 958
An Experiment on Oscillatory Shock-Wave Boundary-Layer Interaction, Wladyslaw Fiszdon and Erik Mollö-Christensen* ... 71
A Graphical Solution for Normal Shock Waves in Real Gases, Charles E. Treanor* ... 158
Higher-Order Corrections to Taylor's Solution for Weak, Normal, Shock Waves, Martin Sichel* ... 635
A Note on the Explosion Solution of Sedov With Application to the Newtonian Theory of Unsteady Hypersonic Flow, N. C. Freeman* ... 77
Comments, Eric F. Brocher* ... 955
Author's Reply* ... 956
Note on the Sonic Freeze Concept, J. C. Gibbings* ... 874
On the Normal Shock Wave Attached to the Curved Surface, G. E. Gadd* ... 76
The Piston-Driven Shock, Roy Gundersen* ... 467
A Simple Numerical Solution of the Supersonic Blunt-Body Problem for Real Gases, G. A. Bird* ... 151
A Theoretical Investigation of the Interaction Between Shock Waves and Boundary Layers, M. Honda (Vol. 25, pp. 667–678)
Erratum* ... 76
A Three-Dimensional Linearized Analysis of the Forces Exerted on a Rigid Wing by a Shock Wave, F. Edward Ehlers and E. M. Shoemaker ... 257

Sloshing of Liquids

Sloshing of Liquids in Circular Canals and Spherical Tanks, Bernard Budiansky ... 161

Turbomachinery

An Approximate Equation for the "Choke-Line" of a Compressor, G. T. Csanady* ... 637
Effects of Flow Unsteadiness in Turbomachines, G. T. Csanady* ... 879
The Flow Field in the Diffuser of a Radial Compressor, Inge L. Ryhming* ... 798
Jet-Compressor Efficiencies as Influenced by the Nature of the Driving and Driven Gases, Suzanne S. Eichacker and Harold J. Hoge* ... 636

Vortices

Generalized Integral Relationship in Flow Fields With Vortex Sheets, Shinya Kobayakawa and Lu Ting* 872
On the Structure of Vortical Layers in Supersonic and Hypersonic Flows, Hsien K. Cheng* 155
A Simple Method of Estimating the Vortex Intensity, Miles J. Bobrik* 957
A Study of Vortex Cancellation, Allan Schaffer 193

Wings and Airfoils

Aerodynamic Properties of Ring Airfoils in Supersonic Flight, Charles H. Murphy and Maynard J. Piddington* 954
A Further Discussion of the Limiting Circulatory Lift of a Finite-Span Wing, Franklyn J. Davenport* 959
The Limiting Circulatory Lift of a Wing of Finite Aspect Ratio, Barnes W. McCormick, Jr. (Vol. 26, pp. 247–248)*
Comments, G. J. Hancock* 65
Author's Reply, Barnes W. McCormick, Jr.* 66
Minimum Wing Wave Drag With Volume Constraint, T. Strand 615
On Supersonic Flow Past Thick Airfoils, Abraham Kogan. 504
On the Prediction of Mixed Subsonic/Supersonic Pressure Distributions, Colin S. Sinnott 767
On the Thrust Hypothesis for the Jet Flap Including Jet-Mixing Effects, K. T. Yen 607
On the Unsteady Motion of a Delta Wing in Supersonic Flight, M. M. Stanišić* 399
Sweepback Effects in Turbulent Boundary-Layer Shock-Wave Interaction, R. J. Stalker 348
A Three-Dimensional Linearized Analysis of the Forces Exerted on a Rigid Wing by a Shock Wave, F. Edward Ehlers and E. M. Shoemaker 257
Theoretical and Experimental Investigation of Second-Order Supersonic Wing-Body Interference, Mårten Landahl, Georg Drougge, and Beverly Beane 694
Wings With Minimum Drag Due to Lift in Supersonic Flow, Ingeborg Ginzel and Hans Multhopp 13

AEROELASTICITY

Application of Power Spectral Methods in Airplane and Missile Design, Kenneth R. Thorson and Quentin R. Bohne 107
Chordwise-Bending Effects on Wing-Vibration Modes, John C. Glasgow and James L. Cronin, Jr.* 962
Dynamic Effects in Fatigue Testing, Richard M. Rowland and James L. Cronin* 390
Dynamic Response of Beams With Large Amplitudes, Thein Wah* 877
The Effect of Thrust and Drag Load on the Aeroelastic Behavior of Booster Systems, John E. Stevens* 639
The Equation of Energy Balance for Fluttering Systems With Some Applications in the Supersonic Regime, John D. C. Crisp (Vol. 26, pp. 703–716, 738)
Errata* 73
Flexural Vibrations of a Thick-Walled Circular Cylinder According to the Exact Theory of Elasticity, Joshua E. Greenspon 37
Flexural Vibrations of Elastic Sandwich Plates, Yi-Yuan Yu 272
High-Frequency Oscillation of Slender Bodies and Wings, Meir Hanin* 544
Inertia Effects on Some Static Aeroelastic Problems, D. J. Johns* 237
The Influence of Panel Deformations on Wing Flutter, D. J. Johns* 137
A Method of Reducing Aeroelastic Effects of Highly Swept Wings, Edward J. Hopkins, Don W. Jillie, and Raymond M. Hicks* 634
Natural Frequency of Beams With Variable Moments of Inertia, Ming L. Pei* 304
A Note for Finding Complex Roots of a Special Kind of Quartic Equation, F. A. Lee* 714
On Supersonic Flutter of Long Panels, John W. Miles* 476
On the Bernoulli-Euler Beam Theory With Random Excitation, J. L. Bogdanoff and J. E. Goldberg 371
On the Estimation of Structural Damping From Aircraft Resonance Tests, Ronald D. Milne 339
Optimization of the Flight-Control, Airframe System, I. L. Ashkenas and D. T. McRuer 197
Oscillatory Aerodynamic Coefficients for a Unified Supersonic-Hypersonic Strip Theory, William P. Rodden and James D. Revell 451
Real Gas Effects in Flow Over Blunt Bodies at Hypersonic Speeds, H. T. Nagamatsu, R. E. Geiger, and R. E. Sheer, Jr. 241
A Simplified Expression for the Period of Nonlinear Oscillations of Curved and Flat Panels, Joshua E. Greenspon*. 138
Comment, Robert E. Kelley* 621
Simplified Vibration Analysis of Elastic Sandwich Plates, Yi-Yuan Yu 894
Traveling-Gust Method for Airfoils in Strong Blast Waves, J. Ray Ruetenik* 795

AEROTHERMODYNAMICS AND ABLATION

Ablation of Reinforced Plastics in Supersonic Flow, George W. Sutton 377
An Analogy Between Boundary-Layer Pressure Gradient and Chemical Reaction-Rate Effects, George R. Inger*. 956
Calculation of Hypersonic Shock-Layer Flow Parameters, Knowing Shock-Layer Ratio of Specific Heats, Alfred B. C. Anderson* 873
A Comparison of Transient and Quasi-Steady Performance of Melting-Type Re-Entry Shields, Ernst Wilhelm Adams* 791
Differential Equation of Compressible Turbulent Skin-Friction Coefficient Around an Arbitrary Body of Revolution at High Speed, Paul K. Chang* 466
Dynamics and Thermodynamics of Re-Entry, W. H. T. Loh 748
The Effect of a Deceleration Force on a Melting Boundary Layer, Simon Ostrach, Arthur W. Goldstein, and Jesse Hamman* 626
The Effect of Shock-Generated Vorticity, Surface Slip, and Temperature Jump on Stagnation-Point Heat-Transfer Rates, H. Hoshizaki* 135
The Effect of Thermal Radiation on the Inviscid Hypersonic Flow Over a Blunt Body, G. A. Bird* 713
An Experimental and Theoretical Study of Quartz Ablation at the Stagnation Point, Mac C. Adams, William E. Powers, and Steven Georgiev 535
Experimental Study of an Ablating Sphere With Hydromagnetic Effect Included, John H. Boynton* 306
Heat Conduction in a Melting Slab, Stephen J. Citron 219
Heat Transfer, Recovery Factor, and Pressure Distributions Around a Circular Cylinder Normal to a Supersonic Rarefied-Air Stream, O. K. Tewfik and W. H. Giedt 721
An Investigation of Laminar, Transitional, and Turbulent Heat Transfer on Blunt-Nosed Bodies in Hypersonic Flow, Robert J. Cresci, Donald A. MacKenzie, and Paul A. Libby 401
Inviscid Flow With Nonequilibrium Molecular Dissociation for Pressure Distributions Encountered in Hypersonic Flight, Martin H. Bloom and Martin H. Steiger 821
Mach-Line Determination for Air in Dissociation Equilibrium, Roy J. Heyman* 311
Comments, Eldon L. Knuth* 796
Mass-Transfer Cooling in a Turbulent Boundary Layer, J. P. Hartnett, D. J. Masson, J. F. Gross, and Carl Gazley, Jr.* 623
Measurements of Skin Friction of the Compressible Turbulent Boundary Layer on a Cone With Foreign Gas Injection, Constantine C. Pappas and Arthur F. Okuno 321
A New Concept for Calculating Thermal Boundary Layers, Ernst Wilhelm Adams* 549

Pitot-Probe Measurement of Local Skin-Friction Reduction Due to Transpiration in a Low-Speed, Turbulent Boundary Layer, Bernard M. Leadon and E. Roy Bartle* 235
Propagation of Weak Disturbances in a Gas Subject to Relaxation Effects, Franklin K. Moore and Walter E. Gibson 117
Radiation Versus Mass-Transfer Effects for Ablating Re-Entry Shields of a Nonlifting Satellite, Ernst Wilhelm Adams* 868
Skin-Friction Calculation for Turbulent Boundary Layers in Adverse Pressure Distributions, Earl M. Uram* 75
Some Mass-Transfer Results With External-Flow Pressure Gradients, J. R. Baron and P. E. Scott* 625
Some Real-Gas Flow Parameters for Air, Wayne D. Erickson* 716
The Stagnation-Point Ablation of Teflon During Hypersonic Flight, S. M. Scala and N. S. Diaconis* 140
Stagnation-Point Heat-Transfer Measurements in Hypersonic, Low-Density Flow, S. E. Neice, R. W. Rutowski, and K. K. Chan* 387
Steady-State Melting of a Semi-Infinite Medium With Temperature-Dependent Properties, Stephen J. Citron* 470
Sublimation in a Hypersonic Environment, Sinclaire M. Scala 1
Temperature Profiles in a Finite Solid With Moving Boundary, C. Forbes Dewey, Jr., Stewart I. Schlesinger, and Lawrence Sashkin 59
The Thickness of a Melting Ablation-Type Heat Shield, Ernst Wilhelm Adams* 620
Turbulent Heat Transfer on Blunt-Nosed Bodies in Two-Dimensional and General Three-Dimensional Hypersonic Flow, Roberto Vaglio-Laurin 27
Use of Reference Enthalpy in Specifying the Laminar Heat-Transfer Distribution Around Blunt Bodies in Dissociated Air, E. R. G. Eckert and O. E. Tewfil.* 464
Viscous Hypersonic Similitude for a Dissociating Gas, Robert J. Whalen* 550

COMPUTERS AND ANALOGY

An Analogy Between Magnetohydrodynamics and Heat Transfer, D. C. Leigh and G. W. Sutton* 469
The Analysis of Redundant Structures by the Use of High-Speed Digital Computers, Walter J. Crichlow and Gernot W. Haggenmacher 595
Computer Solution Techniques for Two-Dimensional Supersonic Flow Problems, William P. Harrison, Jr.* 315
The Epicycle Method for the Reduction of Flight-Test Data Using a Digital Computer, R. P. Danis 913
Shear Lag Solutions for Sheet-Stringer Panels by Means of a Hydrodynamic Analogy, Martin Goland 291

CONTROL

Closed-Loop Flip-Flop Control Systems, Milton Rogers and George Shapiro 841
Multicondition Terminal Control Systems for Aircraft, Richard V. Morris and Carl W. Steeg, Jr. 703
Optimization of the Flight-Control, Airframe System, I. L. Ashkenas and D. T. McRuer 197
The Response of Linear Systems to Non-Gaussian Random Inputs, Stephen H. Crandall, William H. Siebert, and Bernard P. Hoquetis* 154
A Statistically Averaged Error Criterion for Feedback-System Synthesis, John Zaborszky and John W. Diesel. 128
The Transfer Function of a Spring-Tab Control. Malcolm J. Abzug* 307

FLIGHT DYNAMICS AND PERFORMANCE

The Approximate Solution of the Equations of Motion of an Airplane Moving in a Vertical Plane, E. F. Trombley* .. 394
An Axis System for Five and Six Degree of Freedom Airplane Dynamic Problems, William L. Wynn* 473
Minimum Time-to-Climb of an Airplane, John Carstoiu* .. 311

INSTRUMENTS

Foucault Pendulum Effect in a Schuler-Tuned System, Charles Broxmeyer 343
Multicondition Terminal Control Systems for Aircraft, Richard V. Morris and Carl W. Steeg, Jr. 703
The Pitot and Static Tubes—Condensed Sources of General Fundamentals and Applications, Jay W. Stuart, Jr.* 136

LANDING GEAR

Slip Coefficient for a Tire, John E. Stevens* 305

MAGNETOHYDRODYNAMICS

An Analogy Between Magnetohydrodynamics and Heat Transfer, D. C. Leigh and G. W. Sutton* 469
Compressible Flat-Plate Boundary-Layer Flow With an Applied Magnetic Field, William B. Bush 49
Compressibility Effects in Magnetoaerodynamic Flows Past Thin Bodies, J. E. McCune and E. L. Resler, Jr. 493
Constant-Temperature Magneto-Gasdynamic Channel Flow, Jack L. Kerrebrock and Frank E. Marble* 78
Electrogasdynamic Motion of a Charged Body in a Plasma, L. Kraus and H. Yoshihara 229
Experimental Study of an Ablating Sphere With Hydromagnetic Effect Included, John H. Boynton* 306
The Flow About a Charged Body Moving in the Lower Ionosphere, Raul R. Hunziker 935
Hydromagnetic Effects on Heating and Shear at a Three-Dimensional Stagnation Point in Hypersonic Flow, Nelson H. Kemp* 553
Hypersonic Viscous Flow Near the Stagnation Point in the Presence of Magnetic Field, Ching-Sheng Wu 882
Incompressible Wedge Flows of an Electrically Conducting Viscous Fluid in the Presence of a Magnetic Field, K. T. Yen 74
Magnetohydrodynamic Effects on Exothermal Waves, R. A. Gross, W. Chinitz, and T. J. Rivlin 283
Magnetohydrodynamic Effects on the Formation of Couette Flow, L. N. Tao 334
On Magnetohydrodynamic Channel Flow, J. E. McCune and W. R. Sears* 139
On the High-Speed Flow of a Compressible Conductive Fluid Past a Slender Body, Ken-ichi Kusukawa* 551
A Phenomenon in Unsteady Magnetohydrodynamic Flow Theory, S. F. Borg* 472
A Possible "Fully Developed" Hydromagnetic Pipe Flow, A. Demetriades* 388
Similar Solutions for Boundary Layers in Constant-Temperature Magneto-Gasdynamic Channel Flow, Jack L. Kerrebrock* 156

MATERIALS

Ablation of Reinforced Plastics in Supersonic Flow, George W. Sutton 377
A Comparison of Transient and Quasi-Steady Performance of Melting-Type Re-Entry Shields, Ernst Wilhelm Adams* 791
An Experimental and Theoretical Study of Quartz Ablation at the Stagnation Point, Mac C. Adams, William E. Powers, and Steven Georgiev 535
On Theoretical Considerations of Plastic-Flow Criteria, W. Komkov* 477
Radiation Versus Mass-Transfer Effects for Ablating Re-Entry Shields of a Nonlifting Satellite, Ernst Wilhelm Adams* 868
The Stagnation-Point Ablation of Teflon During Hypersonic Flight, S. M. Scala and N. S. Diaconis* 140
Steady-State Melting of a Semi-Infinite Medium With Temperature-Dependent Properties, Stephen J. Citron* 470
Sublimation in a Hypersonic Environment, Sinclaire M. Scala 1
The Thickness of a Melting Ablation-Type Heat Shield, Ernst Wilhelm Adams* 620

MATHEMATICS

A Further Extension of the Routh-Hurwitz Stability Criteria for Quintic and Sextic Equations, Herbert Saunders* 396
A Note for Finding Complex Roots of a Special Kind of Quartic Equation, F. A. Lee* 714

POWER PLANTS

An Approximate Investigation of the Effect of Boundary-Layer-Control Pumping on Powerplant Performance, T. F. Kirkwood* 799
A Method of Estimating the Environmental Damping Coefficient of a Rotating Disc, P. Srinivasan* 312
Performance of Nuclear Rocket for Large-Payload, Earth-Satellite Booster, Eldon W. Sams 481
The Strain Analysis of Solid Propellant Rocket Grains, M. L. Williams 574
Variable-Thrust Rocket Engines and Their Modes of Operation, Mario William Cardullo* 793

PROPELLERS

Theory of Supersonic-Propeller Aerodynamics, Donald Earl Ordway and Richard W. Hale 437

SPACECRAFT

Analytical and Numerical Studies of Three-Dimensional Trajectories to the Moon, A. B. Mickelwait and R. C. Booton, Jr. 561
A Class of Optimum Trajectory Problems in Gravitational Fields, E. W. Graham 296
Closed-Loop Flip-Flop Control Systems, Milton Rogers and George Shapiro 841
Dynamics and Thermodynamics of Re-Entry, W. H. T. Loh 748
The Effect of Thrust and Drag Load on the Aeroelastic Behavior of Booster Systems, John E. Stevens* 639
The Epicycle Method for the Reduction of Flight-Test Data Using a Digital Computer, R. P. Danis 913
An Equivalence Principle for Water-Exit and -Entry Problems, John P. Moran* 876
A Graphical Approach to the Determination of the Eccentricity and the Perigee Angle, Wayne Tempelman* 630
Minor Circle Flight at Large Angles of Inclination, W. H. T. Loh* 397
On a Class of Variational Problems in Rocket Flight, G. Leitmann (Vol. 26, p. 586)
Comment, G. Leitmann* 153
Performance of Nuclear Rocket for Large-Payload, Earth-Satellite Booster, Eldon W. Sams 481
Terminal Guidance System for Satellite Rendezvous, W. H. Clohessy and R. S. Wiltshire 653
Two Analytical Results of Fin-Stabilized Rocket Trajectory Under Quadratic Drag Law, K. S. Sung and C. Park* 388

STRUCTURES

Analysis of Low-Aspect-Ratio Aircraft Structures, Charles H. Samson, Jr., and Heinrich W. Bergmann 679
The Analysis of Redundant Structures by the Use of High-Speed Digital Computers, Walter J. Crichlow and Gernot W. Haggenmacher 595
An Approximation to the Deflections and Strains in a Uniformly Loaded, Clamped, Rectangular Panel Subjected to Very Large Plastic Deformations, Joshua E. Greenspon* 392
Bending of an Orthotropic Plate Clamped on the Boundary of a Conic Section, Y. Ōhasi and T. Suzuki* 386
The Buckling of Circular Cylindrical Shells Under Purely Random External Pressures, J. Clifton Samuels 943
Concerning the Torsion of Prismatic Bars Having a Hexagonal Cross-Section, M. M. Stanišić, C. A. Hauck, and R. A. Mathias* 631
Creep Deformation and Stresses in Pressurized, Long Cylindrical Shells, M. P. Bieniek and A. M. Freudenthal 763
The Creep Deformation of Symmetrically Loaded Circular Cylindrical Shells, Anthony E. Gemma* 953
The Divergence of Supersonic Linear Viscoelastic Lifting Surfaces Including Chordwise Bending, Harry H. Hilton 926
Elastic Instability of a Cylindrical Shell Under Arbitrary Circumferential Variation of Axial Stress, P. P. Bijlaard and R. H. Gallagher 854
Further Studies on the Local Elastic Deformations of Honeycomb Faceplate Subjected to Uniaxial Compression, R. C. Weikel and A. S. Kobayashi* 961
Initially Warped Sandwich Panel Under Combined Loadings, Chieh C. Chang and Bertrand T. Fang 779
Limit Analysis of Multicell Boxes Submitted to Pure Torque, Fernando Venancio Filho* 236
Matrix Solution of the *n*-Section Column, W. T. Thomson (Vol. 16, pp. 623–624)*
Comments, M. Gololobov* 474
Author's Reply, William T. Thomson* 474
A Method of Transforming Concentrated Surface Forces Into Continuous Surface Forces, William Zuk and Mohammed Abdul Majeed* 478
Minimum Weight Analysis Based on Structural Reliability, Harry H. Hilton and Morris Feigen 641
Minimum Weight Analysis of Orthotropic Plates Under Compressive Loading, George Gerard 21
On Axisymmetrical Buckling of Clamped, Shallow, Spherical Shells, Bernard Budiansky and Hubertus Weinitschke* 545
Plastic Bending of a Work-Hardening Circular Plate With Clamped Edge, Chintsun Hwang 815
Plastic Compressive Buckling of Simply Supported Plates on Interior Elastic Supports, Paul Seide 921
Ring With Edge Moments, Anthony E. Gemma* 867
Shear Lag Solutions for Sheet-Stringer Panels by Means of a Hydrodynamic Analogy, Martin Goland 291
A Simple Method of Matric Structural Analysis: Part V—Structures Containing Plate Elements of Arbitrary Shape and Thickness, Bertram Klein 859
Stability of Flat, Simply Supported Corrugated-Core Sandwich Plates Under Combined Loads, Leonard A. Harris and Richard R. Auelmann 525
Strain-Energy Expressions in Nonlinear Shell Analyses, D. O. Brush* 555
Stress Functions for Plates Bounded by Piecewise Analytic Curves, Ming M. Chen and P. T. Hsu* 240
Tangent-Modulus Column Theory, George Gerard* 627
Torsion Analysis of Multicell Tubes, F. W. Niedenfuhr* 308
Torsion of an Elliptical Shaft With Diametrically Opposite Flat Sides, M. M. Stanišić and B. A. Sherwood* 462

Thermal Stresses

Axisymmetric Bending Stresses in Solid Circular Plates With Thermal Gradients, Marvin Forray and Malcolm Newman* 717
Bending Stresses Due to Temperature in Hollow Circular Plates, Part I, Malcolm Newman and Marvin Forray* 792
Bending Stresses Due to Temperature in Hollow Circular Plates, Part II, Marvin Forray and Malcolm Newman* 870
Bending Stresses Due to Temperature in Hollow Circular Plates, Part III, Malcolm Newman and Marvin Forray* 951
Formulas for the Determination of Thermal Stresses in Rings, Marvin Forray* 238
Large Deflections of Structures Subjected to Heating and External Loads, M. J. Turner, E. H. Dill, H. C. Martin, and R. J. Melosh 97
The Problem of Strain Accumulation Under Thermal Cycling, B. E. Gatewood* 461
Table for Thermal Stresses in Rings, Marvin Forray* 478
Thermal Stresses in a Long Circular Shell With Axial Temperature Variation, D. J. Johns* 393

THERMODYNAMICS

An Additional Note on Equilibrium Skin Temperatures, B. Saelman* ... 320
An Analogy Between Magnetohydrodynamics and Heat Transfer, D. C. Leigh and G. W. Sutton* ... 469
Boundary-Layer Transition and Heat Transfer in Shock Tubes, R. A. Hartunian, A. L. Russo, and P. V. Marrone ... 587
Combustion in the Boundary Layer on a Porous Surface, Alan Q. Eschenroeder ... 901
Effectiveness of Radiation as a Structural Cooling Technique for Hypersonic Vehicles, Roger A. Anderson and William A. Brooks, Jr. ... 41
Experimental Evaluation of Heat Transfer With Transpiration Cooling in a Turbulent Boundary Layer at $M = 3.2$, E. Roy Bartle and Bernard M. Leadon* ... 78
Heat Conduction in a Melting Slab, Stephen J. Citron ... 219
Heat Transfer at a Corner, Victor Zakkay* ... 157
An Investigation of Laminar, Transitional, and Turbulent Heat Transfer on Blunt-Nosed Bodies in Hypersonic Flow, Robert J. Cresci, Donald A. MacKenzie, and Paul A. Libby ... 401
Minimizing the Mass of Thin Radiating Fins, J. Ernest Wilkins, Jr.* ... 145
The Minimum-Weight Straight Fin of Triangular Profile Radiating to Space, Edwin N. Nilson and Richard Curry* ... 146
A Note on the Relation of Biot's Method in Heat Conduction to a Least-Squares Procedure, Stephen J. Citron* ... 317
On Minimum-Weight Rectangular Radiating Fins, Chen-Ya Liu* ... 871
On the Use of Normal Coordinates for the Solution of Lumped Parameter Transient Heat-Transfer Problems, M. E. Gurtin ... 357
Periodic Temperature Distribution in a Two-Layer Composite Slab, W. F. Campbell* ... 633
Periodic Temperature Distribution in a Two-Layer Composite Slab, Thomas E. Stonecypher* ... 152
Radiation Cooling of Finite Heat-Conducting Solids, P. J. Schneider* ... 546
Stable Combustion of a High-Velocity Gas in a Heated Boundary Layer, Donald L. Turcotte ... 509
A Study of Supersonic Combustion, Robert A. Gross and Wallace Chinitz ... 517
Temperature Profiles in a Finite Solid With Moving Boundary, C. Forbes Dewey, Jr., Stewart I. Schlesinger, and Lawrence Sashkin ... 59

WATER-BASED AIRCRAFT

A Study of Spray Generated by Seaplane Hulls, Shizuo Kikuhara ... 415

WIND TUNNELS AND EQUIPMENT

Boundary-Layer Transition and Heat Transfer in Shock Tubes, R. A. Hartunian, A. L. Russo, and P. V. Marrone ... 587
Boundary-Layer Transition on Blunt Bodies With Highly Cooled Boundary Layers, Kenneth F. Stetson ... 81
Determination of Pitch and Yaw Rates of Models in Free-Flight Ranges by Magnetic Induction, Bernard S. Golosman* ... 638
A Heated Hypersonic Stagnation-Temperature Probe, Richard D. Wood* ... 556
Improvement of a Pressure Pickup for the Measurements of Turbulence Characteristics, Y. Kobashi, N. Kono, and T. Nishi* ... 149
A Multiple Hot-Wire Array for Measurements of Downwash Integrals, Kent Kresa and Erik Mollö-Christensen* ... 141
On the Maximum Attainable Temperature in Resonance Tubes, Ascher H. Shapiro* ... 66
An Optical Boundary-Layer Probe, John W. Daiber ... 836
Pitot-Probe Measurement of Local Skin-Friction Reduction Due to Transpiration in a Low-Speed, Turbulent Boundary Layer, Bernard M. Leadon and E. Roy Bartle* ... 235
Real Gas Effects in Flow Over Blunt Bodies at Hypersonic Speeds, H. T. Nagamatsu, R. E. Geiger, and R. E. Sheer, Jr. ... 241
Relaxation Effects on the Interpretation of Impact-Probe Measurements, William F. Van Tassell and Eugene E. Covert* ... 147
Errata* ... 549
Remarks on a Study of Short, Flexible Nozzles, Edwin Pounder and John Copper* ... 73

Author Index

ABZUG, MALCOLM J. The Transfer Function of a Spring-Tab Control* ... 307
ACRIVOS, ANDREAS. A Rapid Method for Estimating the Shear Stress and the Separation Point in Laminar Incompressible Boundary-Layer Flows* ... 314
ADAMS, ERNST WILHELM. A Comparison of Transient and Quasi-Steady Performance of Melting-Type Re-Entry Shields* ... 791
ADAMS, ERNST WILHELM. A New Concept for Calculating Thermal Boundary Layers* ... 549
ADAMS, ERNST WILHELM. Radiation Versus Mass-Transfer Effects for Ablating Re-Entry Shields of a Nonlifting Satellite* ... 868
ADAMS, ERNST WILHELM. The Thickness of a Melting Ablation-Type Heat Shield* ... 620
ADAMS, MAC C., WILLIAM E. POWERS, AND STEVEN GEORGIEV. An Experimental and Theoretical Study of Quartz Ablation at the Stagnation Point ... 535
ANDERSON, ALFRED B. C. Calculation of Hypersonic Shock-Layer Flow Parameters, Knowing Shock-Layer Ratio of Specific Heats* ... 873
ANDERSON, ROGER A., AND WILLIAM A. BROOKS, JR. Effectiveness of Radiation as a Structural Cooling Technique for Hypersonic Vehicles ... 41
ASHKENAS, I. L., AND D. T. MCRUER. Optimization of the Flight-Control, Airframe System ... 197
AUELMANN, RICHARD R., AND LEONARD A. HARRIS. Stability of Flat, Simply Supported Corrugated-Core Sandwich Plates Under Combined Loads ... 525
BARON, J. R., AND P. E. SCOTT. Some Mass-Transfer Results With External-Flow Pressure Gradients* ... 625
BARTLE, E. ROY, AND BERNARD M. LEADON. Experimental Evaluation of Heat Transfer With Transpiration Cooling in a Turbulent Boundary Layer at $M = 3.2$* ... 78
BARTLE, E. ROY, AND BERNARD M. LEADON. Pitot-Probe Measurement of Local Skin-Friction Reduction Due to Transpiration in a Low-Speed, Turbulent Boundary Layer* ... 235
BARTOS, JOAN M., AND NATHAN GERBER. Calculation of Flow-Variable Gradients Behind Curved Shock Waves* ... 958
BEANE, BEVERLY, MÅRTEN LANDAHL, AND GEORG DROUGGE. Theoretical and Experimental Investigation of Second-Order Supersonic Wing-Body Interference ... 694
BERGMANN, HEINRICH W., AND CHARLES H. SAMSON, JR. Analysis of Low-Aspect-Ratio Aircraft Structures ... 679
BIDWELL, JEROLD M. Use of the Roughness Criterion to Refute Roughness as the Cause of Reported Transition Reversal* ... 622
BIENIEK, M. P., AND A. M. FREUDENTHAL. Creep Deformation and Stresses in Pressurized, Long Cylindrical Shells ... 763

BIJLAARD, P. P., AND R. H. GALLAGHER. Elastic Instability of a Cylindrical Shell Under Arbitrary Circumferential Variation of Axial Stress 854
BILLERBECK, W. J., JR. Empirical Equation for the Wake-Spreading Limits Behind Three-Dimensional Bodies* 640
BIRD, G. A. The Effect of Thermal Radiation on the Inviscid Hypersonic Flow Over a Blunt Body* 713
BIRD, G. A. A Simple Numerical Solution of the Supersonic Blunt-Body Problem for Real Gases* 151
BLOOM, MARTIN H., AND MARTIN H. STEIGER. Inviscid Flow With Nonequilibrium Molecular Dissociation for Pressure Distributions Encountered in Hypersonic Flight 821
BOBRIK, MILES J. A Simple Method of Estimating the Vortex Intensity* 957
BOGDANOFF, J. L., AND J. E. GOLDBERG. On the Bernoulli-Euler Beam Theory With Random Excitation 371
BOHNE, QUENTIN R., AND KENNETH R. THORSON. Application of Power Spectral Methods in Airplane and Missile Design 107
BOOTON, R. C., JR., and A. B. MICKELWAIT. Analytical and Numerical Studies of Three-Dimensional Trajectories to the Moon 561
Borg, S. F. A Phenomenon in Unsteady Magnetohydrodynamic Flow Theory* 472
BOYNTON, JOHN H. Experimental Study of an Ablating Sphere With Hydromagnetic Effect Included* 306
BROCHER, ERIC F. Comments on: A Note on the Explosion Solution of Sedov With Application to the Newtonian Theory of Unsteady Hypersonic Flow, N. C. Freeman (p. 77)* 955
AUTHOR'S Reply, N. C. FREEMAN 956
BROOKS, WILLIAM A., JR., AND ROGER A. ANDERSON. Effectiveness of Radiation as a Structural Cooling Technique for Hypersonic Vehicles 41
BROXMEYER, CHARLES. Foucault Pendulum Effect in a Schuler-Tuned System 343
BRUSH, D. O. Strain-Energy Expressions in Nonlinear Shell Analyses* 555
BRYANT, R. A. A. The Hydraulic Analogy for External Flow* 148
BUDIANSKY, BERNARD. Sloshing of Liquids in Circular Canals and Spherical Tanks 161
BUDIANSKY, BERNARD, AND HUBERTUS WEINITSCHKE. On Axisymmetrical Buckling of Clamped, Shallow, Spherical Shells* 545
BUSH, WILLIAM B. Compressible Flat-Plate Boundary-Layer Flow With an Applied Magnetic Field 49

CAMPBELL, W. F. Periodic Temperature Distribution in a Two-Layer Composite Slab* 633
CARDULLO, MARIO WILLIAM. Influence Coefficients for Real Gases* 546
CARDULLO, MARIO WILLIAM. Variable-Thrust Rocket Engines and Their Modes of Operation* 793
CARSTOIU, JOHN. Minimum Time-to-Climb of an Airplane* 311
CASACCIO, ANTHONY. First-Order Solution to the Compressible Laminar Boundary Layer in Slip Flow* 319
CHAN, K. K., S. E. NEICE, AND R. W. RUTOWSKI. Stagnation-Point Heat-Transfer Measurements in Hypersonic, Low-Density Flow* 387
CHANG, CHIEH C., AND BERTRAND T. FANG. Initially Warped Sandwich Panel Under Combined Loadings 779
CHANG, PAUL K. Differential Equation of Compressible Turbulent Skin-Friction Coefficient Around an Arbitrary Body of Revolution at High Speed* 466
CHAUDHURY, T. K. Note on Slow Viscous Flow Through the Space Between Two Coaxial Circular Cones With the Same Vertex* 963
CHEN, MING M., AND P. T. HSU. Stress Functions for Plates Bounded by Piecewise Analytic Curves* 240
CHENG, HSIEN K. On the Structure of Vortical Layers in Supersonic and Hypersonic Flows* 155
CHENOWETH, DONALD R., AND BRUCE L. HICKS. An Exact Calculation of Some Steady, Diabatic, Two-Dimensional Fields of Compressible Flow* 142
CHINITZ, W., R. A. GROSS, AND T. J. RIVLIN. Magnetohydrodynamic Effects on Exothermal Waves 283
CHINITZ, WALLACE, AND ROBERT A. GROSS. A Study of Supersonic Combustion 517
CHUBB, DONALD L. Solution to the Flow About a Two-Dimensional Flat Plate at Infinite Mach Number* 68
CITRON, STEPHEN J. Heat Conduction in a Melting Slab 219
CITRON, STEPHEN J. A Note on the Relation of Biot's Method in Heat Conduction to a Least-Squares Procedure* 317
CITRON, STEPHEN J. Steady-State Melting of a Semi-Infinite Medium With Temperature-Dependent Properties* 470
CLOHESSY, W. H., AND R. S. WILTSHIRE. Terminal Guidance System for Satellite Rendezvous 653
CLUTTER, DARWIN W., AND A. M. O. SMITH. Analysis of Further Data on the Effect of Isolated Roughness on Boundary-Layer Transition in Supersonic Flow* 70
COPPER, JOHN, AND EDWIN POUNDER. Remarks on a Study of Short, Flexible Nozzles* 73
COVERT, EUGENE E., AND WILLIAM F. VAN TASSELL. Relaxation Effects on the Interpretation of Impact-Probe Measurements* 147
Errata* 549
CRANDALL, STEPHEN H., WILLIAM H. SIEBERT, AND BERNARD P. HOQUETIS. The Response of Linear Systems to Non-Gaussian Random Inputs* 154
CRESCI, ROBERT J., DONALD A. MACKENZIE, AND PAUL A. LIBBY. An Investigation of Laminar, Transitional, and Turbulent Heat Transfer on Blunt-Nosed Bodies in Hypersonic Flow 401
CRICHLOW, WALTER J., AND GERNOT W. HAGGENMACHER. The Analysis of Redundant Structures by the Use of High-Speed Digital Computers 595
CRISP, JOHN D. C. The Equation of Energy Balance for Fluttering Systems With Some Applications in the Supersonic Regime (Vol. 26, pp. 703–716, 738)
Errata* 73
CRONIN, JAMES L., JR., and JOHN C. GLASGOW. Chordwise Bending Effects on Wing-Vibration Modes 962
CRONIN, JAMES L., AND RICHARD M. ROWLAND. Dynamic Effects in Fatigue Testing* 390
CSANADY, G. T. An Approximate Equation for the "Choke-Line" of a Compressor* 637
CSANADY, G. T. Effects of Flow Unsteadiness in Turbomachines* 879
CURRY, RICHARD, AND EDWIN N. NILSON. The Minimum-Weight Straight Fin of Triangular Profile Radiating to Space* 146

Daiber, John W. An Optical Boundary-Layer Probe 836
DANIS, R. P. The Epicycle Method for the Reduction of Flight-Test Data Using a Digital Computer 913
DAVENPORT, FRANKLYN J. A Further Discussion of the Limiting Circulatory Lift of a Finite-Span Wing* 959
DEMETRIADES, A. A Possible "Fully Developed" Hydromagnetic Pipe Flow* 388
DEWEY, C. FORBES, JR., STEWART I. SCHLESINGER, AND LAWRENCE SASHKIN. Temperature Profiles in a Finite Solid With Moving Boundary 59
DIACONIS, N. S., AND S. M. SCALA. The Stagnation-Point Ablation of Teflon During Hypersonic Flight* 140
DIESEL, JOHN W., AND JOHN ZABORSZKY. A Statistically Averaged Error Criterion for Feedback-System Synthesis 128
DILL, E. H., M. J. TURNER, H. C. MARTIN, AND R. J. MELOSH. Large Deflections of Structures Subjected to Heating and External Loads 97
DROUGGE, GEORG, MÅRTEN LANDAHL, AND BEVERLY BEANE. Theoretical and Experimental Investigation of Second-Order Supersonic Wing-Body Interference 469

ECKERT, E. R. G., AND O. E. TEWFIK. Use of Reference Enthalpy in Specifying the Laminar Heat-Transfer Distribution Around Blunt Bodies in Dissociated Air* 464
EHLERS, F. EDWARD, AND E. M. SHOEMAKER. A Three-Dimensional Linearized Analysis of the Forces Exerted on a Rigid Wing by a Shock Wave 257
EICHACKER, SUZANNE S., AND HAROLD J. HOGE. Jet-Compressor Efficiencies as Influenced by the Nature of the Driving and Driven Gases* 636
ELROD, H. G., JR. Note on the Turbulent Shear Stress Near a Wall (Vol. 24, p. 468)* Erratum* 145
ERICKSON, WAYNE D. Some Real-Gas Flow Parameters for Air* 716
ESCHENROEDER, ALAN Q. Combustion in the Boundary Layer on a Porous Surface 901

FANG, BERTRAND T., AND CHIEH C. CHANG. Initially Warped Sandwich Panel Under Combined Loadings 779
FAULDERS, C. R. Reynolds-Analogy Parameter for the Laminar Boundary Layer With Blowing, $Pr = 3/4$* 628
FEIGEN, MORRIS, AND HARRY H. HILTON. Minimum Weight Analysis Based on Structural Reliability 641
FILHO, FERNANDO VENANCIO. Limit Analysis of Multicell Boxes Submitted to Pure Torque* 236
FINK, MARTIN R., FRED LANDIS, AND MURRAY H. ROSENBERG. Boundary-Layer Transition Measurements at Mach Numbers from 5.4 to 7.4* 719
FISZDON, WLADYSLAW, AND ERIK MOLLÖ-CHRISTENSEN. An Experiment on Oscillatory Shock-Wave Boundary-Layer Interaction* 71
FORRAY, MARVIN. Formulas for the Determination of Thermal Stresses in Rings* 238
FORRAY, MARVIN. Table for Thermal Stresses in Rings* .. 478
FORRAY, MARVIN, AND MALCOLM NEWMAN. Axisymmetric Bending Stresses in Solid Circular Plates With Thermal Gradients* 717
FORRAY, MARVIN, AND MALCOLM NEWMAN. Bending Stresses Due to Temperature in Hollow Circular Plates, Part I* 792
FORRAY, MARVIN, AND MALCOLM NEWMAN. Bending Stresses Due to Temperature in Hollow Circular Plates, Part II* 870
FORRAY, MARVIN, AND MALCOLM NEWMAN. Bending Stresses Due to Temperature in Hollow Circular Plates, Part III* 951
FRAISER, H. R. Supersonic Inlet Dynamics 429
FREEMAN, N. C. A Note on the Explosion Solution of Sedov With Application to the Newtonian Theory of Unsteady Hypersonic Flow* 77
Comments, Eric F. Brocher* 955
Author's Reply, N. C. Freeman* 956
FREUDENTHAL, A. M., AND M. P. BIENIEK. Creep Deformation and Stresses in Pressurized, Long Cylindrical Shells 763
FUNG, Y. C. Fluctuating Lift and Drag Acting on a Cylinder in a Flow at Supercritical Reynolds Numbers 801

GADD, G. E. On the Normal Shock Wave Attached to the Curved Surface* 76
GALLAGHER, R. H., AND P. P. BIJLAARD. Elastic Instability of a Cylindrical Shell Under Arbitrary Circumferential Variation of Axial Stress 854
GATEWOOD, B. E. The Problem of Strain Accumulation Under Thermal Cycling* 461
GAZLEY, CARL, JR., J. P. HARTNETT, D. J. MASSON, AND J. F. GROSS. Mass-Transfer Cooling in a Turbulent Boundary Layer* 623
GEIGER, R. E., H. T. NAGAMATSU, AND R. E. SHEER, JR. Real Gas Effects in Flow Over Blunt Bodies at Hypersonic Speeds 241
GEMMA, ANTHONY E. The Creep Deformation of Symmetrically Loaded Circular Cylindrical Shells* 953
GEMMA, ANTHONY E. Ring With Edge Moments* 867
GEORGIEV, STEVEN, MAC C. ADAMS, AND WILLIAM E. POWERS. An Experimental and Theoretical Study of Quartz Ablation at the Stagnation Point 535
GERARD, GEORGE. Minimum Weight Analysis of Orthotropic Plates Under Compressive Loading 21
GERARD, GEORGE. Tangent-Modulus Column Theory* ... 627
GERBER, NATHAN, AND JOAN M. BARTOS. Calculation of Flow-Variable Gradients Behind Curved Shock Waves* .. 958
GIBBINGS, J. C. Note on the Sonic Freeze Concept* 874
GIBSON, WALTER E., AND FRANKLIN K. MOORE. Propagation of Weak Disturbances in a Gas Subject to Relaxation Effects 117
GIEDT, W. H., AND O. K. TEWFIK. Heat Transfer, Recovery Factor, and Pressure Distributions Around a Circular Cylinder Normal to a Supersonic Rarefied-Air Stream 721
GINZEL, INGEBORG, AND HANS MULTHOPP. Wings With Minimum Drag Due to Lift in Supersonic Flow 13
GLASGOW, JOHN C., AND JAMES L. CRONIN, JR. Chordwise-Bending Effects on Wing-Vibration Modes* 962
GOLAND, MARTIN. Shear Lag Solutions for Sheet-Stringer Panels by Means of a Hydrodynamic Analogy 291
GOLDBERG, J. E., AND J. L. BOGDANOFF. On the Bernoulli-Euler Beam Theory With Random Excitation 371
GOLDSTEIN, A. W., AND A. MAGER. On Maximum Pressure Rise With Turbulent Boundary Layer* 234
GOLDSTEIN, ARTHUR W., SIMON OSTRACH, AND JESSE HAMMAN. The Effect of a Deceleration Force on a Melting Boundary Layer* 626
GOLOLOBOV, M. Comments on: Matrix Solution of the n-Section Column, W. T. Thomson (Vol. 16, pp. 623–624)* 474
Author's Reply, William T. Thomson* 474
GOLOSMAN, BERNARD S. Determination of Pitch and Yaw Rates of Models in Free-Flight Ranges by Magnetic Induction* 638
GRAHAM, E. W. A Class of Optimum Trajectory Problems in Gravitational Fields 296
GREENSPON, JOSHUA E. An Approximation to the Deflections and Strains in a Uniformly Loaded, Clamped, Rectangular Panel Subjected to Very Large Plastic Deformations* 392
GREENSPON, JOSHUA E. Flexural Vibrations of a Thick-Walled Circular Cylinder According to the Exact Theory of Elasticity 37
GREENSPON, JOSHUA E. A Simplified Expression for the Period of Nonlinear Oscillations of Curved and Flat Panels* 138
Comment, Robert E. Kelley* 621
GREGG, J. L., AND E. M. SPARROW. Flow About an Unsteadily Rotating Disc 252
GROSS, J. F., J. P. HARTNETT, D. J. MASSON, AND CARL GAZLEY, JR. Mass-Transfer Cooling in a Turbulent Boundary Layer* 623
GROSS, R. A., W. CHINITZ, AND T. J. RIVLIN. Magneto-hydrodynamic Effects on Exothermal Waves 283
GROSS, ROBERT A., AND WALLACE CHINITZ. A Study of Supersonic Combustion 517
GROSS, W. A. Steady Performance Characteristics of Gas-Lubricated Journal Bearings With Slenderness Ratio $L/D = \pi$* 869
GUNDERSEN, ROY. The Piston-Driven Shock* 467
GURTIN, M. E. On the Use of Normal Coordinates for the Solution of Lumped Parameter Transient Heat-Transfer Problems 357

HAGGENMACHER, GERNOT W., AND WALTER J. CRICHLOW. The Analysis of Redundant Structures by the Use of High-Speed Digital Computers 595

HALE, RICHARD W., AND DONALD EARL ORDWAY. Theory of Supersonic-Propeller Aerodynamics ... 437
HALL, M. G. On Three-Dimensional Boundary Layers Having Similar Solutions* ... 80
HAMMAN, JESSE, SIMON OSTRACH, AND ARTHUR W. GOLDSTEIN. The Effect of a Deceleration Force on a Melting Boundary Layer* ... 626
HAMMITT, A. G., AND K. R. A. MURTHY. Approximate Solutions for Supersonic Flow Over Wedges and Cones* ... 71
HAMMITT, ANDREW G. Dimensionless Parameters for Viscous Similarity* ... 720
HANCOCK, G. J. Comment on: The Limiting Circulatory Lift of a Wing of Finite Aspect Ratio, Barnes W. McCormick, Jr. (Vol. 26, pp. 247–248)* ... 65
Author's Reply, Barnes W. McCormick, Jr.* ... 66
HANIN, MEIR. High-Frequency Oscillation of Slender Bodies and Wings* ... 544
HARRIS, LEONARD A., AND RICHARD R. AUELMANN. Stability of Flat, Simply Supported Corrugated-Core Sandwich Plates Under Combined Loads ... 525
HARRISON, WILLIAM P., JR. Computer Solution Techniques for Two-Dimensional Supersonic Flow Problems* ... 315
HARTNETT, J. P., D. J. MASSON, J. F. GROSS, AND CARL GAZLEY, JR. Mass-Transfer Cooling in a Turbulent Boundary Layer* ... 623
HARTSELL, CRAIG W. Derivation of an Analytical Expression for Supersonic Spillage of Single-Cone Inlets* ... 788
HARTUNIAN, R. A., A. L. RUSSO, AND P. V. MARRONE. Boundary-Layer Transition and Heat Transfer in Shock Tubes ... 587
Hassan, H. A. On a Solution to the Unsteady Laminar Boundary Layer* ... 474
HAUCK, C. A., M. M. STANIŠIĆ, AND R. A. MATHIAS. Concerning the Torsion of Prismatic Bars Having a Hexagonal Cross-Section* ... 631
HEYMAN, ROY J. Mach-Line Determination for Air in Dissociation Equilibrium* ... 311
HICKS, BRUCE L., AND DONALD R. CHENOWETH. An Exact Calculation of Some Steady, Diabatic, Two-Dimensional Fields of Compressible Flow* ... 142
HICKS, RAYMOND M., EDWARD J. HOPKINS, AND DON W. JILLIE. A Method of Reducing Aeroelastic Effects of Highly Swept Wings* ... 634
HILTON, HARRY H. The Divergence of Supersonic Linear Viscoelastic Lifting Surfaces Including Chordwise Bending ... 926
HILTON, HARRY H., AND MORRIS FEIGEN. Minimum Weight Analysis Based on Structural Reliability ... 641
HOGE, HAROLD J., AND SUZANNE S. EICHACKER. Jet-Compressor Efficiencies as Influenced by the Nature of the Driving and Driven Gases* ... 636
HOLMAN, J. P., K. E. STOUT, AND E. E. SOEHNGEN. On the Effects of Flow Obstructions on Free-Convection Boundary-Layer Oscillations* ... 463
HONDA, M. A Theoretical Investigation of the Interaction Between Shock Waves and Boundary Layers (Vol. 25, pp. 667–678)
Erratum* ... 76
HOPKINS, EDWARD J., DON W. JILLIE, AND RAYMOND M. HICKS. A Method of Reducing Aeroelastic Effects of Highly Swept Wings* ... 634
HOQUETIS, BERNARD P., STEPHEN H. CRANDALL, AND WILLIAM H. SIEBERT. The Response of Linear Systems to Non-Gaussian Random Inputs* ... 154
HOSHIZAKI, H. The Effect of Shock-Generated Vorticity, Surface Slip, and Temperature Jump on Stagnation-Point Heat-Transfer Rates* ... 135
HSU, P. T., AND MING M. CHEN. Stress Functions for Plates Bounded by Piecewise Analytic Curves* ... 240
HUNZIKER, RAUL R. The Flow About a Charged Body Moving in the Lower Ionosphere ... 935
HWANG, CHINTSUN. Plastic Bending of a Work-Hardening Circular Plate With Clamped Edge ... 815
INGER, G. R., AND V. C. LIU. On Almost-Free-Molecule Flow Through an Orifice* ... 875
INGER, GEORGE R. An Analogy Between Boundary-Layer Pressure Gradient and Chemical Reaction-Rate Effects* 956

JILLIE, DON W., EDWARD J. HOPKINS, AND RAYMOND M. HICKS. A Method of Reducing Aeroelastic Effects of Highly Swept Wings* ... 634
JOHNS, D. J. Inertia Effects on Some Static Aeroelastic Problems* ... 237
JOHNS, D. J. The Influence of Panel Deformations on Wing Flutter* ... 137
JOHNS, D. J. Thermal Stresses in a Long Circular Shell With Axial Temperature Variation* ... 393

KELLEY, ROBERT E. Comment on: A Simplified Expression for the Period of Nonlinear Oscillations of Curved and Flat Panels, J. E. Greenspon (Vol. 27, p. 138)* ... 621
KEMP, NELSON H. Hydromagnetic Effects on Heating and Shear at a Three-Dimensional Stagnation Point in Hypersonic Flow* ... 553
KEMP, NELSON H., AND RONALD F. PROBSTEIN. Viscous Aerodynamic Characteristics in Hypersonic Rarefied Gas Flow ... 174
Addendum and Errata* ... 554
KERREBROCK, JACK L. Similar Solutions for Boundary Layers in Constant-Temperature Magneto-Gasdynamic Channel Flow* ... 156
KERREBROCK, JACK L., AND FRANK E. MARBLE. Constant-Temperature Magneto-Gasdynamic Channel Flow* 78
KIKUHARA, SHIZUO. A Study of Spray Generated by Seaplane Hulls ... 415
KIRKWOOD, T. F. An Approximate Investigation of the Effect of Boundary-Layer-Control Pumping on Powerplant Performance* ... 799
KLEIN, BERTRAM. A Simple Method of Matric Structural Analysis: Part V—Structures Containing Plate Elements of Arbitrary Shape and Thickness ... 859
KNUTH, ELDON L. Comments on: "Mach-Line Determination for Air in Dissociation Equilibrium"* ... 796
KOBASHI, Y., N. KONO, AND T. NISHI. Improvement of a Pressure Pickup for the Measurements of Turbulence Characteristics* ... 149
KOBAYAKAWA, SHINYA, AND LU TING. Generalized Integral Relationship in Flow Fields With Vortex Sheets* ... 872
KOBAYASHI, A. S., AND R. C. WEIKEL. Further Studies on the Local Elastic Deformations of Honeycomb Faceplate Subjected to Uniaxial Compression* ... 961
KOGAN, ABRAHAM. On Supersonic Flow Past Thick Airfoils ... 504
KOMKOV, W. On Theoretical Considerations of Plastic-Flow Criteria* ... 477
KONO, N., Y. KOBASHI, AND T. NISHI. Improvement of a Pressure Pickup for the Measurements of Turbulence Characteristics* ... 149
KRAMER, MAX O. Boundary-Layer Stabilization by Distributed Damping* ... 69
KRAUS, L., AND H. YOSHIHARA. Electrogasdynamic Motion of a Charged Body in a Plasma ... 229
KRESA, KENT, AND ERIK MOLLÖ-CHRISTENSEN. A Multiple Hot-Wire Array for Measurements of Downwash Integrals* ... 141
KUSUKAWA, KEN-ICHI. On the High-Speed Flow of a Compressible Conductive Fluid Past a Slender Body* ... 551

LANDAHL, MÅRTEN, GEORG DROUGGE, AND BEVERLY BEANE. Theoretical and Experimental Investigation of Second-Order Supersonic Wing-Body Interference ... 694
LANDIS, FRED, MARTIN R. FINK, AND MURRAY H. ROSENBERG. Boundary-Layer Transition Measurements at Mach Numbers from 5.4 to 7.4* ... 719

LEADON, BERNARD M., AND E. ROY BARTLE. Experimental Evaluation of Heat Transfer With Transpiration Cooling in a Turbulent Boundary Layer at $M = 3.2$*.... 78

LEADON, BERNARD M., AND E. ROY BARTLE. Pitot-Probe Measurement of Local Skin-Friction Reduction Due to Transpiration in a Low-Speed, Turbulent Boundary Layer*.... 235

LEE, F. A. A Note for Finding Complex Roots of a Special Kind of Quartic Equation*.... 714

LEIGH, D. C., AND G. W. SUTTON. An Analogy Between Magnetohydrodynamics and Heat Transfer*.... 469

LEITMANN, G. Comment on: On a Class of Variational Problems in Rocket Flight (Vol. 26, p. 586)*.... 153

LI, TA. Arc-Tangent Fits for Pressure and Pressure-Drag Coefficients of Axisymmetric Blunt Bodies at All Speeds* 309

LIBBY, PAUL A., ROBERT J. CRESCI, AND DONALD A. MACKENZIE. An Investigation of Laminar, Transitional, and Turbulent Heat Transfer on Blunt-Nosed Bodies in Hypersonic Flow.... 401

LIBBY, PAUL A., AND LU TING. Remarks on the Eddy Viscosity in Compressible Mixing Flows*.... 797

LIU, CHEN-YA. On Minimum-Weight Rectangular Radiating Fins*.... 871

LIU, V. C., AND G. R. INGER. On Almost-Free-Molecule Flow Through an Orifice*.... 875

LOCHTENBERG, B. H. Transition in a Separated Laminar Boundary Layer.... 92

LOH, W. H. T. Dynamics and Thermodynamics of Re-Entry.... 748

LOH, W. H. T. Minor Circle Flight at Large Angles of Inclination*.... 397

LU, PAU-CHANG. Comment on: Flow About an Unsteadily Rotating Disc, E. M. Sparrow and J. L. Gregg (p. 252)*.... 958

MCCAULEY, W. D., AND E. R. VAN DRIEST. The Effect of Controlled Three-Dimensional Roughness on Boundary-Layer Transition at Supersonic Speeds.... 261

MCCUNE, J. E., AND E. L. RESLER, JR. Compressibility Effects in Magnetoaerodynamic Flows Past Thin Bodies. 493

MCCUNE, J. E., AND W. R. SEARS. On Magnetohydrodynamic Channel Flow*.... 139

MCRUER, D. T., AND I. L. ASHKENAS. Optimization of the Flight-Control, Airframe System.... 197

MACKENZIE, DONALD A., ROBERT J. CRESCI, AND PAUL A. LIBBY. An Investigation of Laminar, Transitional, and Turbulent Heat Transfer on Blunt-Nosed Bodies in Hypersonic Flow.... 401

MAGER, A., AND A. W. GOLDSTEIN. On Maximum Pressure Rise With Turbulent Boundary Layer*.... 234

MAJEED, MOHAMMED ABDUL, AND WILLIAM ZUK. A Method of Transforming Concentrated Surface Forces Into Continuous Surface Forces*.... 478

MAKOFSKI, ROBERT A. On the Use of the Boundary-Layer Equations in the Hypersonic Viscous-Layer Regime*.... 468

MARBLE, FRANK E., AND JACK L. KERREBROCK. Constant-Temperature Magneto-Gasdynamic Channel Flow* 78

MARRONE, P. V., R. A. HARTUNIAN, AND A. L. RUSSO. Boundary-Layer Transition and Heat Transfer in Shock Tubes.... 587

MARTELLUCCI, ANTHONY. An Extension of the Linearized Characteristics Method for Calculating the Supersonic Flow Around Elliptic Cones.... 667

MARTIN, H. C., M. J. TURNER, E. H. DILL, AND R. J. MELOSH. Large Deflections of Structures Subjected to Heating and External Loads.... 97

MASSON, D. J., J. P. HARTNETT, J. F. GROSS, AND CARL GAZLEY, JR. Mass-Transfer Cooling in a Turbulent Boundary Layer*.... 623

MATHIAS, R. A., M. M. STANIŠIĆ, AND C. A. HAUCK. Concerning the Torsion of Prismatic Bars Having a Hexaonal Cross-Section*.... 631

MELOSH, R. J., M. J. TURNER, E. H. DILL, AND H. C. MARTIN. Large Deflections of Structures Subject to Heating and External Loads.... 97

MICKELWAIT, A. B., AND R. C. BOONTON, JR. Analytical and Numerical Studies of Three-Dimensional Trajectories to the Moon.... 561

MICKLEY, HAROLD S., AND ANTHONY TURANO, JR. Rarefaction Effects in Low-Speed Turbulence*.... 629

MILES, JOHN W. On Supersonic Flutter of Long Panels*.. 476

MILNE, RONALD D. On the Estimation of Structural Damping From Aircraft Resonance Tests.... 339

MOLLÖ-CHRISTENSEN, ERIK, AND KENT KRESA. A Multiple Hot-Wire Array for Measurements of Downwash Integrals*.... 141

MOLLÖ-CHRISTENSEN, ERIK, AND WLADYSLAW FISZDON. An Experiment on Oscillatory Shock-Wave Boundary-Layer Interaction*.... 71

MOORE, FRANKLIN K., AND WALTER E. GIBSON. Propagation of Weak Disturbances in a Gas Subject to Relaxation Effects.... 117

MORAN, JOHN P. An Equivalence Principle for Water-Exit and -Entry Problems*.... 876

MORGAN, P. G. An Approximation for Subsonic Flow Through An Orifice*.... 160

MORRIS, RICHARD V., AND CARL W. STEEG, JR. Multicondition Terminal Control Systems for Aircraft.... 703

MULTHOPP, HANS, AND INGEBORG GINZEL. Wings With Minimum Drag Due to Lift in Supersonic Flow.... 13

MURPHY, CHARLES H., AND MAYNARD J. PIDDINGTON. Aerodynamic Properties of Ring Airfoils in Supersonic Flight*.... 954

MURTHY, K. R. A., AND A. G. HAMMITT. Approximate Solutions for Supersonic Flow Over Wedges and Cones*.. 71

NAGAMATSU, H. T., R. E. GEIGER, AND R. E. SHEER, JR. Real Gas Effects in Flow Over Blunt Bodies at Hypersonic Speeds.... 241

NAPOLITANO, LUIGI G. On an Exact Solution of Laminar Mixing of Two Different Gases*.... 144

NEICE, S. E., R. W. RUTOWSKI, AND K. K. CHAN. Stagnation-Point Heat-Transfer Measurements in Hypersonic, Low-Density Flow*.... 387

NEWMAN, MALCOLM, AND MARVIN FORRAY. Axisymmetric Bending Stresses in Solid Circular Plates With Thermal Gradients*.... 717

NEWMAN, MALCOLM, AND MARVIN FORRAY. Bending Stresses Due to Temperature in Hollow Circular Plates, Part I*.... 792

NEWMAN, MALCOLM, AND MARVIN FORRAY. Bending Stresses Due to Temperature in Hollow Circular Plates, Part II*.... 870

NEWMAN, MALCOLM, AND MARVIN FORRAY. Bending Stresses Due to Temperature in Hollow Circular Plates, Part III*.... 951

NIEDENFUHR, F. W. Torsion Analysis of Multicell Tubes* 308

NILES, ALFRED S. Beam-Columns With Elastically Restrained Ends*.... 316

NILSON, EDWIN N., AND RICHARD CURRY. The Minimum-Weight Straight Fin of Triangular Profile Radiating to Space*.... 146

NISHI, T., Y. KOBASHI, AND N. KONO. Improvement of a Pressure Pickup for the Measurements of Turbulence Characteristics*.... 149

ŌHASI, Y., AND T. SUZUKI. Bending of an Orthotropic Plate Clamped on the Boundary of a Conic Section*.... 386

OKUNO, ARTHUR F., AND CONSTANTINE C. PAPPAS. Measurements of Skin Friction of the Compressible Turbulent Boundary Layer on a Cone With Foreign Gas Injection... 321

ORDWAY, DONALD EARL, AND RICHARD W. HALE. Theory of Supersonic-Propeller Aerodynamics.... 437

OSTRACH, SIMON, ARTHUR W. GOLDSTEIN, AND JESSE HAMMAN. The Effect of a Deceleration Force on a Melting Boundary Layer*.... 626

PAPPAS, CONSTANTINE C., AND ARTHUR F. OKUNO. Measurements of Skin Friction of the Compressible Turbulent Boundary Layer on a Cone With Foreign Gas Injection ... 321
PARK, C., AND K. S. SUNG. Two Analytical Results of Fin-Stabilized Rocket Trajectory Under Quadratic Drag Law* ... 388
PEI, MING L. Natural Frequency of Beams With Variable Moments of Inertia* ... 304
PIDDINGTON, MAYNARD J., AND CHARLES H. MURPHY. Aerodynamic Properties of Ring Airfoils in Supersonic Flight* ... 954
POTTER, J. LEITH, AND JACK D. WHITFIELD. Relation Between Transition Location and Pressure in Separated Shear Flows* ... 712
POTTSEPP, L. Inviscid Hypersonic Flow Over Unyawed Circular Cones* ... 558
POUNDER, EDWIN, AND JOHN COPPER. Remarks on a Study of Short, Flexible Nozzles* ... 73
POWERS, WILLIAM E., MAC C. ADAMS, AND STEVEN GEORGIEV. An Experimental and Theoretical Study of Quartz Ablation at the Stagnation Point ... 535
PROBSTEIN, RONALD F., AND NELSON H. KEMP. Viscous Aerodynamic Characteristics in Hypersonic Rarefied Gas Flow ... 174
Addendum and Errata* ... 554

RESLER, E. L., JR., AND J. E. MCCUNE. Compressibility Effects in Magnetoaerodynamic Flows Past Thin Bodies 493
REVELL, JAMES D. Second-Order Theory for Unsteady Supersonic Flow Past Slender, Pointed Bodies of Revolution ... 730
REVELL, JAMES D., AND WILLIAM P. RODDEN. Oscillatory Aerodynamic Coefficients for a Unified Supersonic-Hypersonic Strip Theory ... 451
RIBNER, H. S. Further Comments on: The Limiting Circulatory Lift of a Wing of Finite Aspect Ratio, Barnes W. McCormick (Vol. 26, pp. 247–248)* ... 460
Comment, G. J. Hancock (Vol. 27, pp. 65–66)*
RIDYARD, HERBERT W. A Comparison of Blunt-Body Flow-Field Results* ... 789
RIVLIN, T. J., R. A. GROSS, AND W. CHINITZ. Magnetohydrodynamic Effects on Exothermal Waves ... 283
RODDEN, WILLIAM P., AND JAMES D. REVELL. Oscillatory Aerodynamic Coefficients for a Unified Supersonic-Hypersonic Strip Theory ... 451
ROGERS, MILTON, AND GEORGE SHAPIRO. Closed-Loop Flip-Flop Control Systems ... 841
ROSENBERG, MURRAY H., FRED LANDIS, AND MARTIN R. FINK. Boundary-Layer Transition Measurements at Mach Numbers from 5.4 to 7.4* ... 719
ROSENZWEIG, MARTIN L., AND NICHOLAS ROTT. On the Response of the Laminar Boundary Layer to Small Fluctuations of the Free-Stream Velocity ... 741
ROTT, NICHOLAS, AND MARTIN L. ROSENZWEIG. On the Response of the Laminar Boundary Layer to Small Fluctuations of the Free-Stream Velocity ... 741
ROWLAND, RICHARD M., AND JAMES L. CRONIN. Dynamic Effects in Fatigue Testing* ... 390
RUETENIK, J. RAY. Traveling-Gust Method for Airfoils in Strong Blast Waves* ... 795
RUSSO, A. L., R. A. HARTUNIAN, AND P. V. MARRONE. Boundary-Layer Transition and Heat Transfer in Shock Tubes ... 587
RUTOWSKI, R. W., S. E. NEICE, AND K. K. CHAN. Stagnation-Point Heat-Transfer Measurements in Hypersonic, Low-Density Flow* ... 387
RYHMING, INGE L. The Flow Field in the Diffuser of a Radial Compressor* ... 798

SAELMAN, B. An Additional Note on Equilibrium Skin Temperatures* ... 320
SAMS, ELDON W. Performance of Nuclear Rocket for Large-Payload, Earth-Satellite Booster ... 481
SAMSON, CHARLES H., JR., AND HEINRICH W. BERGMANN. Analysis of Low-Aspect-Ratio Aircraft Structures ... 679
SAMUELS, J. CLIFTON. The Buckling of Circular Cylindrical Shells Under Purely Random External Pressures ... 943
SASHKIN, LAWRENCE, C. FORBES DEWEY, JR., AND STEWART I. SCHLESINGER. Temperature Profiles in a Finite Solid With Moving Boundary ... 59
SAUNDERS, HERBERT. A Further Extension of the Routh-Hurwitz Stability Criteria for Quintic and Sextic Equations* ... 396
SCALA, S. M., AND N. S. DIACONIS. The Stagnation-Point Ablation of Teflon During Hypersonic Flight* ... 140
SCALA, SINCLAIRE M. Sublimation in a Hypersonic Environment ... 1
SCHAFFER, ALLAN. A Study of Vortex Cancellation ... 193
SCHLESINGER, STEWART I., C. FORBES DEWEY, JR., AND LAWRENCE SASHKIN. Temperature Profiles in a Finite Solid With Moving Boundary ... 59
SCHNEIDER, P. J. Radiation Cooling of Finite Heat-Conducting Solids* ... 546
SCOTT, P. E., AND J. R. BARON. Some Mass-Transfer Results With External-Flow Pressure Gradients* ... 625
SEARS, W. R., AND J. E. MCCUNE. On Magnetohydrodynamic Channel Flow* ... 139
SEIDE, PAUL. Plastic Compressive Buckling of Simply Supported Plates on Interior Elastic Supports ... 921
SHAPIRO, ASCHER H. On the Maximum Attainable Temperature in Resonance Tubes* ... 66
SHAPIRO, GEORGE, AND MILTON ROGERS. Closed-Loop Flip-Flop Control Systems ... 841
SHEER, R. E., JR., H. T. NAGAMATSU, AND R. E. GEIGER. Real Gas Effects in Flow Over Blunt Bodies at Hypersonic Speeds ... 241
SHERWOOD, B. A., AND M. M. STANIŠIĆ. Torsion of an Elliptical Shaft With Diametrically Opposite Flat Sides* ... 462
SHOEMAKER, E. M., AND F. EDWARD EHLERS. A Three-Dimensional Linearized Analysis of the Forces Exerted on a Rigid Wing by a Shock Wave ... 257
SICHEL, MARTIN. Higher-Order Corrections to Taylor's Solution for Weak, Normal, Shock Waves* ... 635
SIEBERT, WILLIAM H., STEPHEN H. CRANDALL, AND BERNARD P. HOQUETIS. The Response of Linear Systems to Non-Gaussian Random Inputs* ... 154
SIMS, JOSEPH L. On Conical-Flow Upwash* ... 952
SINNOTT, COLIN S. On the Prediction of Mixed Subsonic/Supersonic Pressure Distributions ... 767
SMITH, A. M. O., AND DARWIN W. CLUTTER. Analysis of Further Data on the Effect of Isolated Roughness on Boundary-Layer Transition in Supersonic Flow* ... 70
SOEHNGEN, E. E., J. P. HOLMAN, AND K. E. STOUT. On the Effects of Flow Obstructions on Free-Convection Boundary-Layer Oscillations* ... 463
SPARROW, E. M., AND J. L. GREGG. Flow About an Unsteadily Rotating Disc ... 252
SPENCE, D. A. A Note on the Recovery and Reynolds-Analogy Factors in Laminar Flat-Plate Flow* ... 878
SRINIVASAN, P. A Method of Estimating the Environmental Damping Coefficient of a Rotating Disc* ... 312
STALKER, R. J. Sweepback Effects in Turbulent Boundary-Layer Shock-Wave Interaction ... 348
STANIŠIĆ, M. M. On the Unsteady Motion of a Delta Wing in Supersonic Flight* ... 399
STANIŠIĆ, M. M., C. A. HAUCK, AND R. A. MATHIAS. Concerning the Torsion of Prismatic Bars Having a Hexagonal Cross-Section* ... 631
STANIŠIĆ, M. M., AND B. A. SHERWOOD. Torsion of an Elliptical Shaft With Diametrically Opposite Flat Sides* ... 462
STEEG, CARL W., JR., AND RICHARD V. MORRIS. Multicondition Terminal Control Systems for Aircraft ... 703

Steiger, Martin H., and Martin H. Bloom. Inviscid Flow With Nonequilibrium Molecular Dissociation for Pressure Distributions Encountered in Hypersonic Flight ... 821

Stetson, Kenneth F. Boundary-Layer Transition on Blunt Bodies With Highly Cooled Boundary Layers ... 81

Stevens, John E. The Effect of Thrust and Drag Load on the Aeroelastic Behavior of Booster Systems* ... 639

Stevens, John E. Slip Coefficient for a Tire* ... 305

Stonecypher, Thomas E. Periodic Temperature Distribution in a Two-Layer Composite Slab* ... 152

Stout, K. E., J. P. Holman, and E. E. Soehngen. On the Effects of Flow Obstructions on Free-Convection Boundary-Layer Oscillations* ... 463

Strand, T. Minimum Wing Wave Drag With Volume Constraint ... 615

Stuart, Jay W., Jr. The Pitot and Static Tubes—Condensed Sources of General Fundamentals and Applications* ... 136

Sung, K. S., and C. Park. Two Analytical Results of Fin-Stabilized Rocket Trajectory Under Quadratic Drag Law* ... 388

Sutton, G. W., and D. C. Leigh. An Analogy Between Magnetohydrodynamics and Heat Transfer* ... 469

Sutton, George W. Ablation of Reinforced Plastics in Supersonic Flow ... 377

Suzuki, T., and Y. Ōhasi. Bending of an Orthotropic Plate Clamped on the Boundary of a Conic Section* ... 386

Tao, L. N. Magnetohydrodynamic Effects on the Formation of Couette Flow ... 334

Tempelman, Wayne. A Graphical Approach to the Determination of the Eccentricity and the Perigee Angle* ... 630

Tewfik, O. E., and E. R. G. Eckert. Use of Reference Enthalpy in Specifying the Laminar Heat-Transfer Distribution Around Blunt Bodies in Dissociated Air* ... 464

Tewfik, O. K., and W. H. Giedt. Heat Transfer, Recovery Factor, and Pressure Distributions Around a Circular Cylinder Normal to a Supersonic Rarefied-Air Stream ... 721

Thorson, Kenneth R., and Quentin R. Bohne. Application of Power Spectral Methods in Airplane and Missile Design ... 107

Ting, Lu, and Shinya Kobayakawa. Generalized Integral Relationship in Flow Fields With Vortex Sheets* ... 872

Ting, Lu, and Paul A. Libby. Remarks on the Eddy Viscosity in Compressible Mixing Flows* ... 797

Traugott, Stephen C. An Approximate Solution of the Direct Supersonic Blunt-Body Problem for Arbitrary Axisymmetric Shapes ... 361

Treanor, Charles E. A Graphical Solution for Normal Shock Waves in Real Gases* ... 158

Trombley, E. F. The Approximate Solution of the Equations of Motion of an Airplane Moving in a Vertical Plane* ... 394

Turano, Anthony, Jr., and Harold S. Mickley. Rarefaction Effects in Low-Speed Turbulence* ... 629

Turcotte, Donald L. Stable Combustion of a High-Velocity Gas in a Heated Boundary Layer ... 509

Turcotte, Donald L. A Sublayer Theory for Fluid Injection Into the Incompressible Turbulent Boundary Layer ... 675

Turner, M. J., E. H. Dill, H. C. Martin, and R. J. Melosh. Large Deflections of Structures Subjected to Heating and External Loads ... 97

Uram, Earl M. A Method of Calculating Velocity Distribution for Turbulent Boundary Layers in Adverse Pressure Distributions ... 659

Uram, Earl M. Skin-Friction Calculation for Turbulent Boundary Layers in Adverse Pressure Distributions* ... 75

Vaglio-Laurin, Roberto. Turbulent Heat Transfer on Blunt-Nosed Bodies in Two-Dimensional and General Three-Dimensional Hypersonic Flow ... 27

van Driest, E. R., and W. D. McCauley. The Effect of Controlled Three-Dimensional Roughness on Boundary-Layer Transition at Supersonic Speeds ... 261

Van Tassell, William F., and Eugene E. Covert. Relaxation Effects on the Interpretation of Impact-Probe Measurements* ... 147

Errata* ... 549

Van Tuyl, A. H. The Use of Rational Approximations in the Calculation of Flows With Detached Shocks* ... 559

Wah, Thein. Dynamic Response of Beams With Large Amplitudes* ... 877

Walker, George K. A Particular Solution to the Turbulent-Boundary-Layer Equations* ... 715

Weikel, R. C., and A. S. Kobayashi. Further Studies on the Local Elastic Deformations of Honeycomb Faceplate Subjected to Uniaxial Compression* ... 961

Weinitschke, Hubertus, and Bernard Budiansky. On Axisymmetrical Buckling of Clamped, Shallow, Spherical Shells* ... 545

Whalen, Robert J. Viscous and Leading-Edge Effects in Hypersonic Flow* ... 391

Whalen, Robert J. Viscous Hypersonic Similitude for a Dissociating Gas* ... 550

Whitfield, Jack D., and J. Leith Potter. Relation Between Transition Location and Pressure in Separated Shear Flows* ... 712

Wilkins, J. Ernest, Jr. Minimizing the Mass of Thin Radiating Fins* ... 145

Willett, Joseph E. Supersonic Flow at the Surface of a Circular Cone at Angle of Attack ... 907

Williams, M. L. The Strain Analysis of Solid Propellant Rocket Grains ... 574

Wiltshire, R. S., and W. H. Clohessy. Terminal Guidance System for Satellite Rendezvous ... 653

Wood, Richard D. A Heated Hypersonic Stagnation-Temperature Probe* ... 556

Wu, Ching-Sheng. Hypersonic Viscous Flow Near the Stagnation Point in the Presence of Magnetic Field ... 882

Wynn, William L. An Axis System for Five and Six Degree of Freedom Airplane Dynamic Problems* ... 473

Yen, K. T. Incompressible Wedge Flows of an Electrically Conducting Viscous Fluid in the Presence of a Magnetic Field* ... 74

Yen, K. T. On the Thrust Hypothesis for the Jet Flap Including Jet-Mixing Effects ... 607

Yoshihara, H., and L. Kraus. Electrogasdynamic Motion of a Charged Body in a Plasma ... 229

Yu, Yi-Yuan. Flexural Vibrations of Elastic Sandwich Plates ... 272

Yu, Yi-Yuan. Simplified Vibration Analysis of Elastic Sandwich Plates ... 894

Zaborszky, John, and John W. Diesel. A Statistically Averaged Error Criterion for Feedback-System Synthesis ... 128

Zakkay, Victor. Heat Transfer at a Corner* ... 157

Zuk, William, and Mohammed Abdul Majeed. A Method of Transforming Concentrated Surface Forces Into Continuous Surface Forces* ... 478

75

27

261

147
549

559

877

715

961

545

391

550

712

145

907

574

553

556

382

373

74

07

29

72

94

8
7

8

Announcing . . .

INTERNATIONAL AEROSPACE ABSTRACTS

First issue
January 1961

A monthly service providing fast, comprehensive coverage of the world's aerospace literature

Each monthly issue of *International Aerospace Abstracts* will bring you abstracts of hundreds of the latest reports, periodical articles, meeting papers, and books—selected on the basis of their importance to aerospace technology. Coverage will be world-wide. Convenient subject arrangement will permit rapid location of topics of interest, and an author index in each issue will give further access. This new monthly will combine, in improved format, the abstracts and book sections formerly carried in *Aerospace Engineering*.

SUPPORTED by the NATIONAL SCIENCE FOUNDATION and the AIR FORCE OFFICE OF SCIENTIFIC RESEARCH

DESIGNED EXPRESSLY FOR THE ENGINEER AND SCIENTIST

PROMPT ☆ SELECTIVE ☆ INFORMATIVE ☆ TIME-SAVING ☆ EXPANDED COVERAGE

Access to original publications will be provided through the facilities of The IAS Library at National Headquarters in New York.

A separate index volume is being planned for yearly publication.

Subscription Information (Domestic and Foreign)

Basic Rate:	$60 per year
IAS Corporate Member Rate:	$40 per year
Individual IAS Member Rate:	$20 per year

An Individual IAS Member may subscribe at the special rate of $20 per year only if he signs an agreement certifying that the copies are for his personal use.

(Subscriptions will be written on a calendar year basis.)

Prices of the Annual Index Volume will be announced later.

For uninterrupted abstract service,

SEND IN YOUR SUBSCRIPTION ORDER NOW

INSTITUTE OF THE AEROSPACE SCIENCES **2 East 64th Street / New York 21, N.Y.**

CORPORATE MEMBERS

OF THE

INSTITUTE OF THE AEROSPACE SCIENCES

AC SPARK PLUG DIVISION, GENERAL MOTORS CORPORATION

ACADEMY OF AERONAUTICS

AEROJET-GENERAL CORPORATION

AEROLAB DEVELOPMENT COMPANY

AERONCA MANUFACTURING CORPORATION

AERONUTRONIC, DIVISION OF FORD MOTOR COMPANY

AEROQUIP CORPORATION

AGAWAM AIRCRAFT PRODUCTS, INC.

ALLIED RESEARCH ASSOCIATES, INC.

ALLISON DIVISION, GENERAL MOTORS CORPORATION

ALUMINUM COMPANY OF AMERICA

AMERICAN AIRLINES, INC.

AMERICAN BOSCH ARMA CORPORATION

AMERICAN STEEL & WIRE DIVISION, UNITED STATES STEEL CORPORATION

AMOCO CHEMICALS CORPORATION

AMPHENOL-BORG ELECTRONICS CORPORATION

ARDE ASSOCIATES

ASSOCIATED AVIATION UNDERWRITERS

ASTRO-ELECTRONIC PRODUCTS DIVISION, RADIO CORPORATION OF AMERICA

AUTOMATION INDUSTRIES, INCORPORATED

AVCO-EVERETT RESEARCH LABORATORY

AVIEN, INC.

BEECH AIRCRAFT CORPORATION

BELL AEROSPACE CORPORATION

THE BENDIX CORPORATION

BOEING AIRPLANE COMPANY

BOOZ, ALLEN APPLIED RESEARCH, INC.

BULOVA RESEARCH AND DEVELOPMENT LABORATORIES, INC.

CANADAIR, LTD.

CESSNA AIRCRAFT COMPANY

CHANCE VOUGHT AIRCRAFT, INCORPORATED

THE CHASE MANHATTAN BANK

CHICAGO AERIAL INDUSTRIES, INC.

THE CLEVELAND PNEUMATIC INDUSTRIES, INC.

CLIFFORD MANUFACTURING DIVISION, STANDARD-THOMSON CORPORATION

CONTINENTAL MOTORS CORPORATION

CORNELL AERONAUTICAL LABORATORY, INC.

COX & COMPANY, INC.

CURTISS-WRIGHT CORPORATION

DANIEL, MANN, JOHNSON, & MENDENHALL

THE DECKER CORPORATION

DEFENSE ELECTRONIC PRODUCTS DIVISION, RADIO CORPORATION OF AMERICA

DEFENSE SYSTEMS DIVISION, GENERAL MOTORS CORPORATION

DEL MAR ENGINEERING LABORATORIES

DELCO-RADIO DIVISION, GENERAL MOTORS CORPORATION

DELCO-REMY DIVISION, GENERAL MOTORS CORPORATION

DOAK AIRCRAFT COMPANY, INC.

DOUGLAS AIRCRAFT COMPANY, INC.

DZUS FASTENER COMPANY, INC

EASTERN AIR LINES, INC.

EATON MANUFACTURING COMPANY

EDO CORPORATION

ELASTIC STOP NUT CORPORATION OF AMERICA

ENGINEERING SUPERVISION COMPANY

FAIRCHILD CAMERA AND INSTRUMENT CORPORATION

FAIRCHILD ENGINE AND AIRPLANE CORPORATION

THE GARRETT CORPORATION

GENERAL APPLIED SCIENCE LABORATORIES, INC.

GENERAL DYNAMICS CORPORATION

GENERAL ELECTRIC COMPANY

GENERAL PRECISION EQUIPMENT CORPORATION

GIANNINI CONTROLS CORPORATION

THE B. F. GOODRICH COMPANY

GOODYEAR AIRCRAFT CORPORATION

GRUMMAN AIRCRAFT ENGINEERING CORPORATION

HUGHES AIRCRAFT COMPANY

INSURANCE COMPANY OF NORTH AMERICA COMPANIES

INTERNATIONAL BUSINESS MACHINES CORPORATION FEDERAL SYSTEMS DIVISION

THE INTERNATIONAL NICKEL COMPANY, INC.

ITT LABORATORIES, DIVISION OF INTERNATIONAL TELEPHONE AND TELEGRAPH CORPORATION

JANITROL AIRCRAFT DIVISION, MIDLAND-ROSS CORPORATION

JOHNS-MANVILLE SALES CORPORATION

WALTER KIDDE & COMPANY, INC.

KOLLSMAN INSTRUMENT CORPORATION

LAVELLE AIRCRAFT CORPORATION

LEAR, INCORPORATED

C. W. LEMMERMAN, INC.

THE LIQUIDOMETER CORPORATION

ARTHUR D. LITTLE, INC.

LOCKHEED AIRCRAFT CORPORATION

THE MARQUARDT CORPORATION

THE MARTIN COMPANY

McDONNELL AIRCRAFT CORPORATION

MELETRON CORPORATION

MINNEAPOLIS-HONEYWELL REGULATOR COMPANY

MOBIL OIL COMPANY

NATIONAL CREDIT OFFICE, INC.

NORTH AMERICAN AVIATION, INC.

NORTHROP CORPORATION

NUCLEAR DEVELOPMENT CORPORATION OF AMERICA

PAN AMERICAN WORLD AIRWAYS, INC.

THE RALPH M. PARSONS COMPANY

PESCO PRODUCTS DIVISION, BORG-WARNER CORPORATION

PHILLIPS PETROLEUM COMPANY

PIASECKI AIRCRAFT CORPORATION

POLY INDUSTRIES, INC.

RAMO-WOOLDRIDGE DIVISION, THOMPSON RAMO WOOLDRIDGE INC.

REPUBLIC AVIATION CORPORATION

ROHR AIRCRAFT CORPORATION

PAUL ROSENBERG ASSOCIATES

RYAN AERONAUTICAL COMPANY

SANDBERG-SERRELL CORPORATION

SHAFER BEARING DIVISION, CHAIN BELT COMPANY

SHELL OIL COMPANY

SIMMONDS PRECISION PRODUCTS, INC.

SOLAR AIRCRAFT COMPANY

SOUTHWEST PRODUCTS COMPANY

SPACE TECHNOLOGY LABORATORIES, INC.

R. DIXON SPEAS ASSOCIATES

SPERRY GYROSCOPE COMPANY, DIVISION OF SPERRY RAND CORPORATION

STANDARD OIL COMPANY OF CALIFORNIA

STANDARD OIL COMPANY (INDIANA)

STANLEY AVIATION CORPORATION

THERM, INCORPORATED

THIOKOL CHEMICAL CORPORATION

TRANS WORLD AIRLINES, INC.

UNION CARBIDE METALS COMPANY, DIVISION OF UNION CARBIDE CORPORATION

UNITED AIR LINES, INC.

UNITED AIRCRAFT CORPORATION

UNITED STATES AVIATION UNDERWRITERS, INC.

VITRO CORPORATION OF AMERICA

WESTERN GEAR CORPORATION

WESTINGHOUSE ELECTRIC CORPORATION

WYMAN-GORDON COMPANY
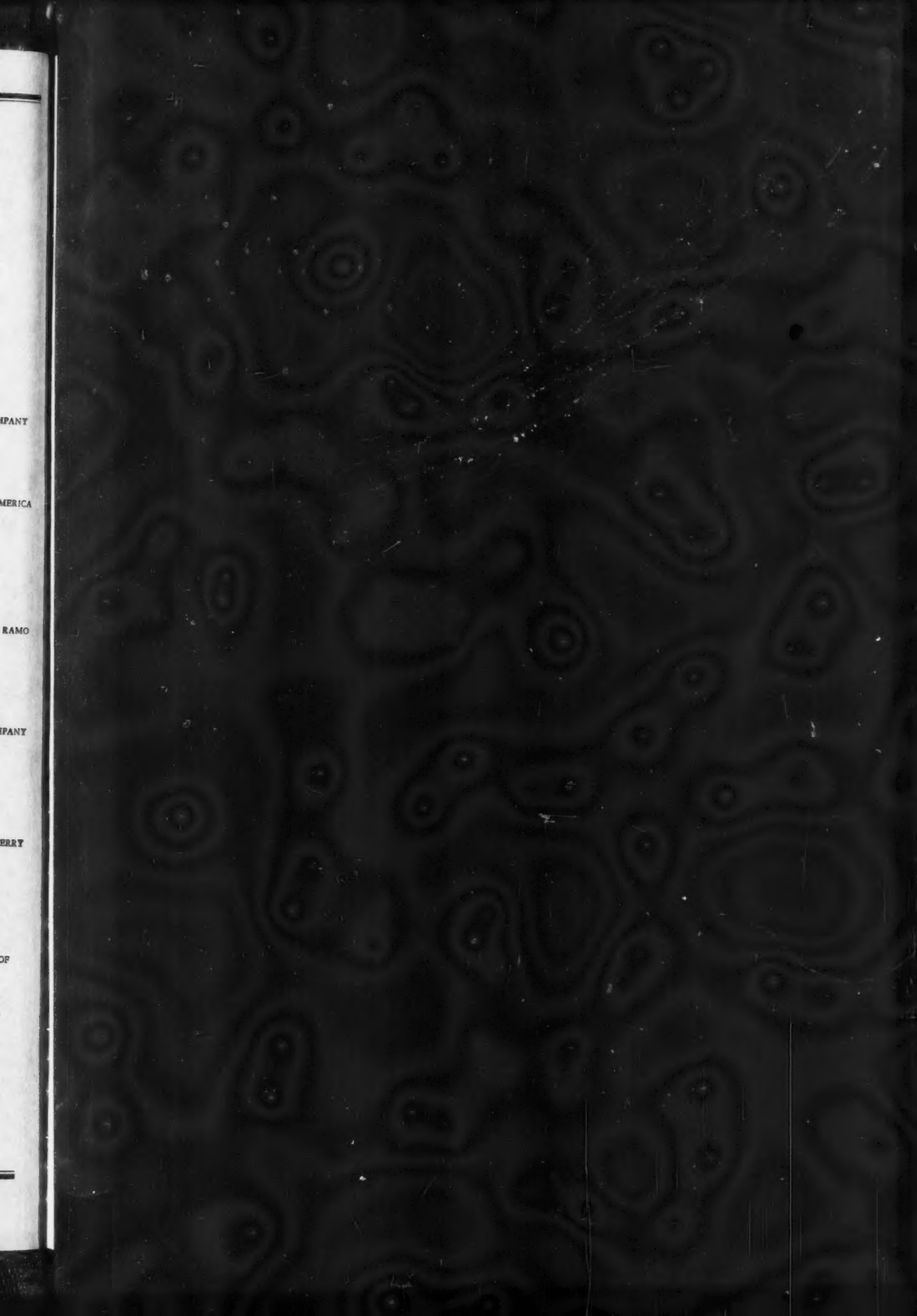
YOUNG RADIATOR COMPANY